



**LAKE MAUREPAS MONITORING (PHASE III)
Annual Report: Year 2 (Nov 1, 2023-Nov 1, 2024)**

**Prepared by:
Kyle Piller, Chris Murray, Gary Shaffer, Fereshteh Emami,
and Robert Moreau**

SUBMITTED DECEMBER 29 2024

Table of Contents

Executive Summary 3

Aquatics Monitoring..... 4-51

Aquatic Physiology Monitoring..... 52-80

Wetlands Monitoring 81-92

Chemical Monitoring..... 93-208

Education/Outreach..... 209-216

Executive Summary

The overall goal of this project is to conduct a monitoring study including the Lake Maurepas ecosystem and its surrounding watershed, specifically monitoring the abiotic and biotic components of this region. Southeastern Louisiana University is gathering biological data within the aquatic and wetland realms to provide baseline abiotic and biotic data regarding the condition of Lake Maurepas prior to the initiation of the Air Products Carbon Sequestration Project. In particular, the aquatics team is monitoring fish, crab, and shrimp populations to assess spatial and temporal variation throughout the lake. Scientific buoys also have been deployed to monitor real-time water quality throughout the lake. The wetlands team is monitoring wetland vegetation, elevation change, and updating habitat maps depicting ecosystem health of the Lake Maurepas wetland area. The physiology team is conducting an ecotoxicological assessment and monitoring survey to develop baseline levels of a variety of physiological parameters for a suite of target species. The chemical monitoring team is examining the impacts of dredging in Lake Maurepas and is monitoring chemical particulates from both the water column and benthos. These chemical monitoring programs have been tasked with understanding the fate and transport of possible toxic chemicals in the environment. Finally, Southeastern has developed a project website that highlights Southeastern's role as the independent monitoring entity. Southeastern's Turtle Cove Environmental Field station is supporting the project researchers by providing access and transportation to the lake and wetland regions and is responsible for the design, development, and implementation of education/outreach activities that combine our traditional transfer of ecosystem knowledge in the area with that of the scientific bio-monitoring findings from our research.

I. Aquatics Monitoring

Kyle R. Piller, PhD

Southeastern Louisiana University, Dept. of Biological Sciences

Hammond, LA 70402

kyle.piller@selu.edu

Report prepared by: Wray Gabel, Tyler Steven Coleman, Alexander Mott, David Camak, Camden Oathout, Corwyn Hall, and Kyle R. Piller

Overview

During Year 2 of the project, the aquatics team continued executing their sampling protocol to assess spatial and temporal variation of the aquatic biotic community in Lake Maurepas. Quarterly surveys were conducted across six lake sectors using various gear types, including gillnets, trawls, electrofishing, crab traps, and dredges, to target fish, shrimp, crabs, and other invertebrates. During sampling, species abundance and total lengths were quantified, and weights of economically relevant species were recorded. The team also continued environmental DNA (eDNA) sampling as part of two projects: one focused on detecting fish species in open water and the other on invertebrate species in sediment. In January 2024, four YSI monitoring buoys were deployed to collect real-time data on aquatic parameters such as water temperature, dissolved oxygen, pH, carbon dioxide, and turbidity. One buoy is equipped with a weather station to record atmospheric conditions, including air temperature, relative humidity, barometric pressure, absolute humidity, wind speed, and wind direction. All data are recorded every 30 minutes and are available on the [project website](#). Summary data from fish and crab field sampling (species, quantities, and total counts) are also publicly accessible via the [project website](#).

Currently, the team is conducting Sampling Period 3b (11/01/2024-01/31/2025, Table 1). To date, aquatic biota data in Lake Maurepas related to the Lake Maurepas Monitoring Program has been collected from 08/01/2023 (Period 1a) through 12/16/2024 (Period 3b).

Table 1. Quarterly sampling period divisions.

Sampling Period	Start	End
Period 1	8/1/2023	1/31/2024
1a	8/1/2023	10/31/2023
1b	11/1/2023	1/31/2024
Period 2	2/1/2024	7/31/2024
2a	2/1/2024	4/30/2024
2b	5/1/2024	7/31/2024
Period 3	8/1/2024	1/31/2025
3a	8/1/2024	10/31/2024
3b	11/1/2024	1/31/2025
Period 4	2/1/2025	7/31/2025
4a	2/1/2025	4/30/2025
4b	5/1/2025	7/31/2025

Sampling Period	Start	End
Period 5	8/1/2025	1/31/2026
5a	8/1/2025	10/31/2025
5b	11/1/2025	1/31/2026
Period 6	2/1/2026	7/31/2026
6a	2/1/2026	4/30/2026
6b	5/1/2026	7/31/2026
Period 7	8/1/2026	1/31/2027
7a	8/1/2026	10/31/2026
7b	11/1/2026	1/31/2027

Project Objectives

1. To monitor the aquatic biotic components of Lake Maurepas from a spatial and temporal perspective.
 - Fish diversity and abundance
 - Invertebrate diversity and abundance
 - Environmental DNA monitoring
 - Genetic monitoring of select groups of fishes (new addition since last year)

2. To utilize YSI buoys to monitor a suite of abiotic parameters in Lake Maurepas to help inform any changes we detect in the aquatic biodiversity component of the project.

Methods/Study Design

We sampled the aquatic biota (vertebrate and invertebrate organisms) of Lake Maurepas. The sampling protocol and sampling objectives varied based on the gear type and sampling design employed. These methodologies are discussed in detail in the following sections of this report.

Random Sampling Site Selection

Lake Maurepas was divided into six sectors (Figure 1a) based on zones from previous seismic testing (Figure 1b). These original sectors were adjusted to ensure more uniform surface areas between sectors (Table 2).



(a) Created Sectors

(b) Original Sectors

Figure 1. Created sectors (a) used for the aquatics sampling design, and (b) the seismic testing zones used by Exodus during the seismic surveys in 2023.

Table 2. Surface area of each created sector (a).

Sector	Area (km ²)
1	39
2	37
3	39
4	43
5	38
6	38

An 800-m² spatial grid was overlaid on the lake shapefile using ArcGIS Pro software (version 3.1.2, Environmental Systems Research Institute, Redlands, California), and a centroid for each grid cell was generated (Figure 2). This grid resulted in 313 centroid points across Lake Maurepas. Additionally, three separate series of points were created for shoreline and inshore sampling (Figure 2):

1. Shoreline Points (SH): Points along the lake shoreline spaced every 100-m (n=652).
2. Electrofishing Shoreline Points (ESH): Points spaced every 500-m along the shoreline designated specifically for electrofishing (n=130).

3. Inshore Points (IN): Points located 50-m inshore from the defined lake shoreline spaced every 100-m (n=601).
 - a. From the inshore points, 12 points were selected every 5.4-km to serve as eDNA inshore sampling points.

This systematic grid and point selection approach ensures comprehensive spatial coverage for both lake-wide and targeted sampling efforts.

Each series of points (grid centroids, shoreline points, electrofishing shoreline points, and inshore points) is used to randomly select sampling locations across the lake for various gear types. The objective is to sample all randomly selected points within each sector during each sampling period (Table 3). The number of random points selected per sector varies by sampling method.

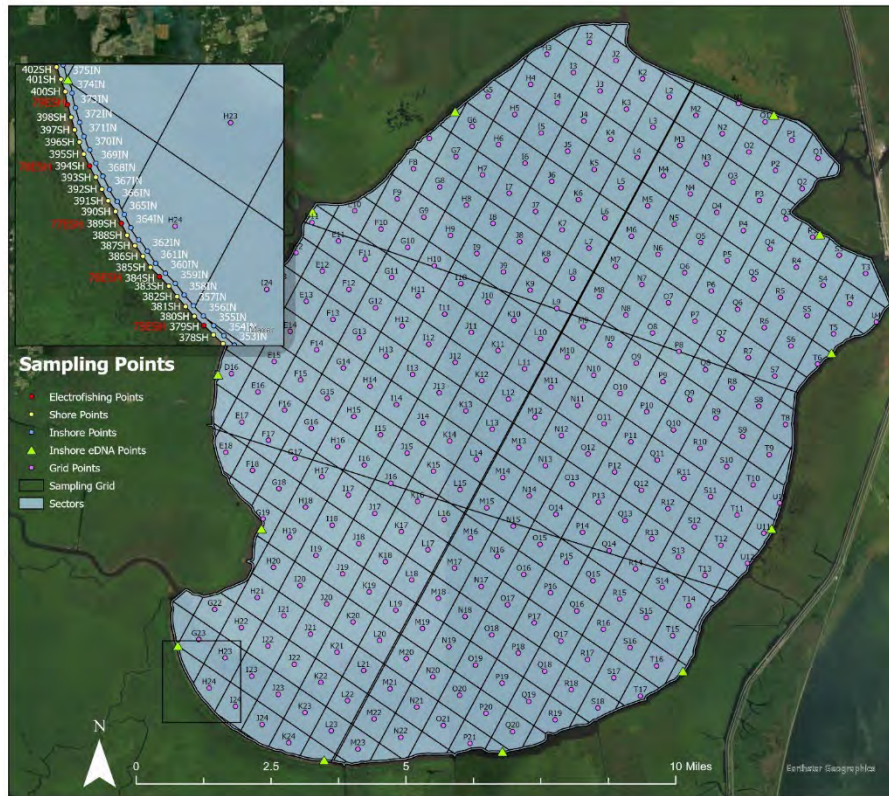
An exception to this randomized sampling design is the inshore eDNA points, which consist of 12 standardized (not random), equidistant points around the lake’s boundary. For open water eDNA sampling, two random grid points are selected per sector. For methods such as gillnets and electrofishing, a percentage of available points within each sector is randomly chosen rather than a fixed number (Table 3). Similarly, there is a variable number of predefined inshore eDNA points per sector, and the number of predefined inshore eDNA points varies by sector due to differences in shoreline area (Table 3).

To further ensure unbiased sampling, a random cardinal direction was assigned for trawl pulls.

Additionally, for all sampling methods, at least three extra random points were selected as alternates to address obstacles (e.g., shipwrecks, dredge pipes, or machinery) that might prevent sampling at the originally chosen location.

Table 3. Total number or proportion of points sampled per sector and the type of point used for the sampling design of each gear type.

Gear Type	Number of Points Per Sector	Type of Point
Dredge	3	Grid Centroid
Crab Traps	10	Grid Centroid
Gillnets	2.5%	Inshore Point (IN)
Otter Trawl	3	Grid Centroid
Bottom Trawl	3	Grid Centroid



Electrofishing	25%	Electrofishing Shoreline Point (ESH)
eDNA Inshore	2	Inshore Point (IN)
eDNA Open Water	1-3	Grid Centroid

Figure 2. All points used to randomly select locations for sampling, including the grid cells with centroid points (letters D–U), inshore points (IN), inshore eDNA points, shoreline points (SH), and electrofishing shoreline points (ESH).

Fishes

Fishes were collected using three methods (otter trawl, gillnets, and boat electrofishing) in Year 2. A modified mini-Missouri bottom trawl (Herzog et al. 2009) was used to collect fishes in sampling period 1b, before being replaced by a flat otter trawl. A 16-ft flat otter trawl with a 12.7-mm bar mesh nylon body and 6.35-mm bar mesh tail was pulled at three sampling sites in each sector (Table 3), which amounted to 18 trawl pulls in each sampling period. The otter trawl was used to sample the nekton community, which includes fish, portunid crabs, and penaeid shrimp (Correia et al. 2024). This differed from Year 1, in which a modified mini-Missouri bottom trawl was employed to sample the fish community, and the flat otter trawl was used to sample for shrimp. These methodologies are now combined and considered to be a single sample of the nekton community assemblage. The methodologies for both trawls are the same. Trawl sampling began in the center of a selected grid if water was at least 1.0-m deep. If the center of the grid was not suitable for sampling (e.g., large coverage of vegetation, submerged structure), then a clockwise or counterclockwise direction was randomly selected and traveled until the grid was possible to sample. If the entire grid could not be sampled, a predefined extra randomly selected grid was sampled. Trawls were pulled in 3-minute intervals at

approximately 2.23-mph into the wind; if wind was absent, trawls were pulled in a predefined randomly selected direction (Coleman 2023). The trawl was manually pulled from the water and the contents were placed into a live well where fishes would be sorted to minimize mortality. Fish were identified to species and total length was recorded. For species where large quantities were captured, total length of the first 50 individuals were recorded and the rest were then counted. Game fish and protected species (defined in Section 5.1: Table 7) were weighed when total length exceeded 150-mm.

Gillnets were used to sample areas close to shore. Gillnets were set out perpendicular to the shoreline at approximately 50 meters from the shore (i.e., inshore points). Two and a half percent of the shoreline was sampled in each sector of the lake, resulting in three sets in sectors 1, 3, 4, and 6, and two sets in sectors 2 and 5. Gillnets soaked overnight (for an average of 13.15 hours) and were then pulled. Data were collected on each fish as stated above for trawl sampling. Three methodological changes were made to the gillnet sampling since Year 1 in order to increase catch rate and improve logistics. First, the amount of available inshore points sampled per sector was reduced from 5% to 2.5%. Second, we originally deployed two 30-ft x 6-ft nets, with 10-ft panels of varying mesh size, one large mesh (76.2-mm, 88.9-mm, 101.6-mm) and one small mesh (9.5-mm, 12.7-mm, 15.9-mm). Nets were set parallel to each other at each point. We now use a single 80-ft x 6-ft net consisting of 8 10-ft panels of varying mesh size (38.1-mm, 57.15-mm, 25.4-mm, 44.45-mm, 19.05-mm, 63.5-mm, 6.35-mm, 50.8-mm). Third, nets are now soaked overnight, as opposed to only being set for an hour in Year 1.

An 18-ft aluminum pulsed-DC Smith-Root electrofishing boat (SR18HX Model) was used to sample 25% of the shoreline in each sector (Table 3), which amounted to 32 transects in each sampling period. Starting at the randomly selected electrofishing shoreline point and proceeding clockwise, a 15-minute (900-second) electrofishing transect was driven along the shoreline in a zig-zag pattern at an average speed of 2-mph. Pulse frequency (\bar{x} = 29 Hz, [2029]), voltage (\bar{x} = 219 V, [125-300]), and amperage (\bar{x} = 64 A, [30-70]) settings varied based on water conductivity. Two dippers with 10-ft long net poles (4.76-mm net mesh) captured stunned fish from the bow and deposited them in a live well until the end of the transect. Data were collected on each fish as stated above for trawl sampling. There was no electrofishing done in Year 1.

During sampling for fishes, a small clip of the adipose fin was taken from any Blue Catfish (*Ictalurus furcatus*) and Channel Catfish (*Ictalurus punctatus*) to assess the levels of potential hybridization between these species by DNA metabarcoding. Collections of Blue and Channel Catfish occurred in each designated sector (1–6) and in each major river (Tickfaw, Amite, and Blind rivers) flowing into Lake Maurepas. Fin clips were taken (either caudal or adipose) and preserved in 95% EtOH within 15-mL vials. To account for an outgroup needed in future analyses, a total of 12 Flathead Catfish (*Pylodictis olivaris*) fin clips were also collected

from sectors 1–5 and the Tickfaw River. Total length (mm) and mass (g) were measured for each individual when applicable. Individuals were released after tissue samples and measurements were taken. Samples were collected between July–November 2024.

Invertebrates

Invertebrates were collected using three methods (crab traps, dredges, and otter trawls) in Year 2. Blue crabs (*Callinectes sapidus*) were collected using a 0.42x0.61x0.61-m crab trap consisting of four open funnels for entry. One crab trap was deployed at each randomly selected grid point (10 points per sector; Table 3) for a total of 60 crab traps in each sampling period. This differs from Year 1, where 15 crab traps were deployed per sector. Traps were baited with whole frozen Gulf Menhaden (*Brevoortia patronus*) and dropped to the bottom of the lake. After approximately 48 hours, traps were pulled and crab carapace length, width, height (depth), and weight were recorded. Crab sex, gravid status of female crabs, and overall health condition data were also collected. Crabs were then released.

Dredges were used to collect benthic aquatic invertebrates such as insects, polychaetes, snails, and of particular interest, *Rangia* clams (*Rangia cuneata*). Dredges utilized the standard Petite Ponar Grab with a volume of 8.2 liters. Dredges were deployed at three points in each sector, with three replicates at each point, for a total of 57 benthic samples collected in each sampling period. This methodology was changed from 5 points per sector per sampling period in Year 1 to three points per sector in Year 2. Samples were processed in the field first, mixing with water and straining through a 12-inch 500 μ m sieve. All remaining organisms and sediment were placed into a jar with 95% ethanol. In the laboratory, each sample was stained with Rose Bengal to stain and assist with sorting of the invertebrates within the sample. All aquatic invertebrates were removed from the sample, identified to the lowest taxonomic level, and recorded. All *Rangia* clams were also measured by total weight (g), wet weight of their internal tissue (g), shell weight (g), and sexed if able.

Shrimp were included in the nekton community sampling done with the otter trawl (see above for relevant methods). Any shrimp caught in the otter trawl were stored on ice with identifying information. In the lab, specimens were identified to species and the weight (g), total length (mm), carapace length (mm), and sex (if possible) were recorded (Mace and Rozas 2015; Beukema 1992; DeLancey, Wenner, and Jenkins 2008).

Water Quality

Four YSI buoys (Amite, Tickfaw, Blind, and Maurepas Buoys) were deployed on January 31, 2024 (Figure 3) to monitor and report water quality and weather data, and to make those data available to the public. Each buoy is affixed with an Exo1 YSI sensor and a CO2Pro™ Submersible pCO2 Sensor. In addition, the Blind Buoy is affixed with a MaxiMet Compact Weather Station. The water quality parameters monitored by these buoys

include CO₂, temperature, turbidity, specific conductivity, salinity, dissolved oxygen concentration (mg/L and % saturation), and pH (Table 4). The weather station monitors atmospheric conditions in addition to water quality. This includes air temperature, rain total, rain intensity, dew point, barometric pressure, relative humidity, wind speed, wind gust speed, and wind direction (Table 4). All water quality and meteorological parameters are measured every 30 minutes, 7 days a week, starting on the date of deployment. Data for relevant parameters (those reported here) collected by these buoys is available on the [project website](#).

After deployment, the buoys had a considerable adjustment period in which the water quality data collected by the buoys was inconsistent and unreliable for much of Year 2 due to manufacturing design and quality control issues with the buoys. After working with YSI to implement a new and improved canister design for housing the buoy electronics, we anticipate an improvement in the performance and reliability of the water quality readings in subsequent years. The new canisters were installed in early November 2024.

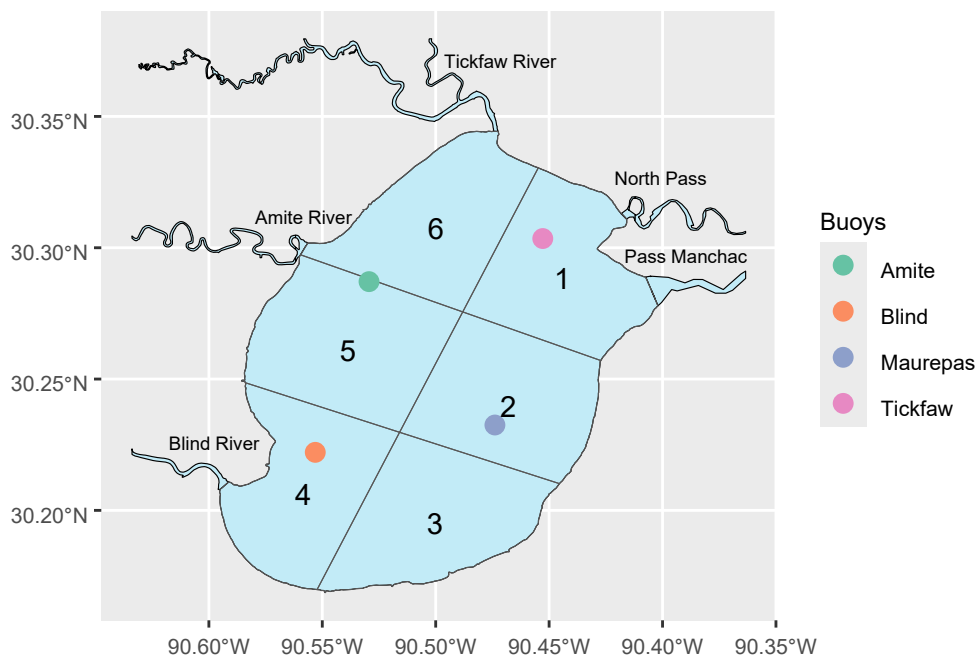


Figure 3. Locations of Amite, Tickfaw, Blind, and Maurepas Buoys on Lake Maurepas.

Table 4. Units of measurement and definitions for relevant parameters monitored by YSI water quality and meteorological monitoring buoys.

Parameter	Units	Description
CO2	Parts per million by volume (ppmV)	CO2
Temperature	Fahrenheit (F)	Exo
Turbidity	Nephelometric Turbidity Unit (NTU)	Exo
Specific Conductivity	Microsiemens per centimeter (mS/cm)	Exo
Salinity	Parts per thousand (ppt)	Exo
DO Concentration	Milligrams per liter (mg/L)	Exo
DO Concentration	Percent Saturation (%)	Exo
pH	None	Exo
Air Temperature	Fahrenheit (F)	Weather Station
Rain Total	Millimeters (mm)	Weather Station
Rain Intensity	Millimeters per hour (mm/hr)	Weather Station
Dew Point	Fahrenheit (F)	Weather Station
Barometric Pressure	Millibar (mbar)	Weather Station
Relative Humidity	Percent (%)	Weather Station
Wind Speed	Miles per hour (mph)	Weather Station
Wind Gust Speed	Miles per hour (mph)	Weather Station

In addition to the four buoys, water quality data is collected on a more localized scale at each sampling location throughout the lake for all gear types and sampling events. We use a handheld YSI Pro DSS to record the dissolved oxygen, conductivity, salinity, total dissolved solids, pH, turbidity, and temperature of the water at the surface (top 3-ft). Starting in the next year, we will also be measuring the water transparency using a secchi disc at each sampling location.

Environmental DNA (eDNA)

A Smith-Root eDNA Backpack Sampler was used to collect environmental DNA samples from water samples at 12 inshore sites and 12 open water sites, which amounts to 24 sites sampled total per sampling period. As described above, the open water points will be randomized for each sampling event and the 12 inshore points remain consistent throughout the sampling duration (Figure 2). Sediment samples for invertebrate eDNA analysis will also be taken during each sampling event at 6 inshore and 6 open water points using Petite Ponar Grab with a volume of 8.2-L. At each point, an eDNA sample is collected using the backpack sampler with a target flow rate of 0.5-L/min with a 1.5-mm glass fiber filter. At the time of sampling, the cardinal direction of the wind is noted as well as the presence of any potentially baited crab traps in the vicinity. All field samples

are kept on ice for transport to the lab where they are subsequently stored in a freezer at -20°C until processing. Additional parameters are recorded by the backpack sampler including pressure, flow, rate, sample duration, and volume. The concentrations (ng/μL) of DNA in water samples and sediment samples are processed separately in the lab, quantified using Qubit High Sensitivity dsDNA Assays. Polymerase Chain Reaction (PCR) is used to amplify the target DNA sequences to track what species are where in the lake.

Results

Below are results for fishes, invertebrates, and water quality from Year 2.

Fishes

As stated above, data on fish biodiversity and assemblage structure of fishes in Lake Maurepas was collected using gillnets, otter trawls, bottom trawls, and a boat electrofisher, and sampling objectives vary based on gear type. The bottom trawl was used for a single sampling period (1b) in Year 2, before being replaced by the otter trawl. See Section 4 for more information.

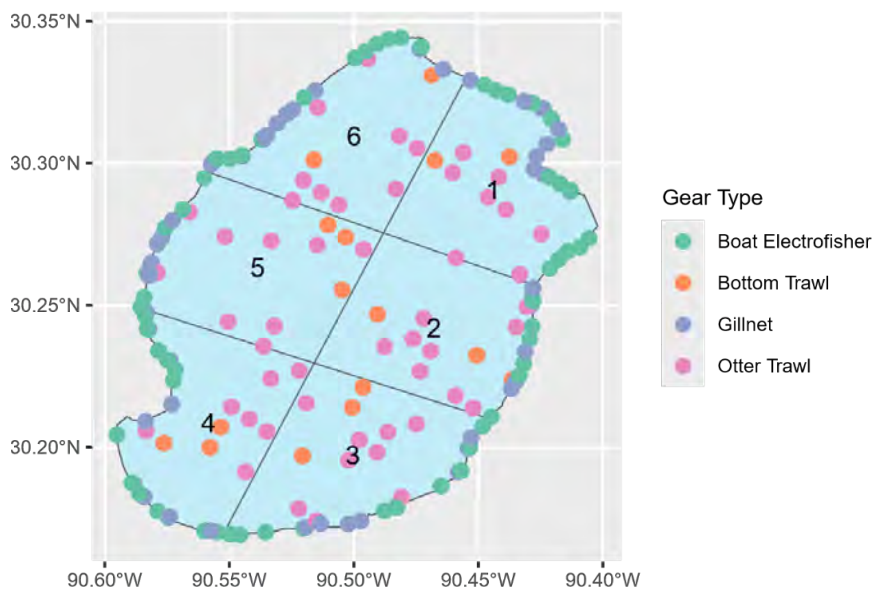


Figure 4. Locations of sampling events on Lake Maurepas with a boat electrofisher, otter trawl, bottom trawl, and gillnets in the current year.

Table 5. Number of sampling events with each gear type, total number of fish collected, and total number of species collected per sector for the current year.

Sector	Bottom Trawls	Gillnets	Electrofishing	Otter Trawls	Number Species	Number Fish
1	3	12	21	9	41	19667
2	3	6	6	9	27	11618
3	3	9	12	9	25	16741
4	3	9	14	9	32	17645
5	3	6	6	9	24	12057
6	3	12	12	9	38	7532
Total	18	54	71	54	187	85231

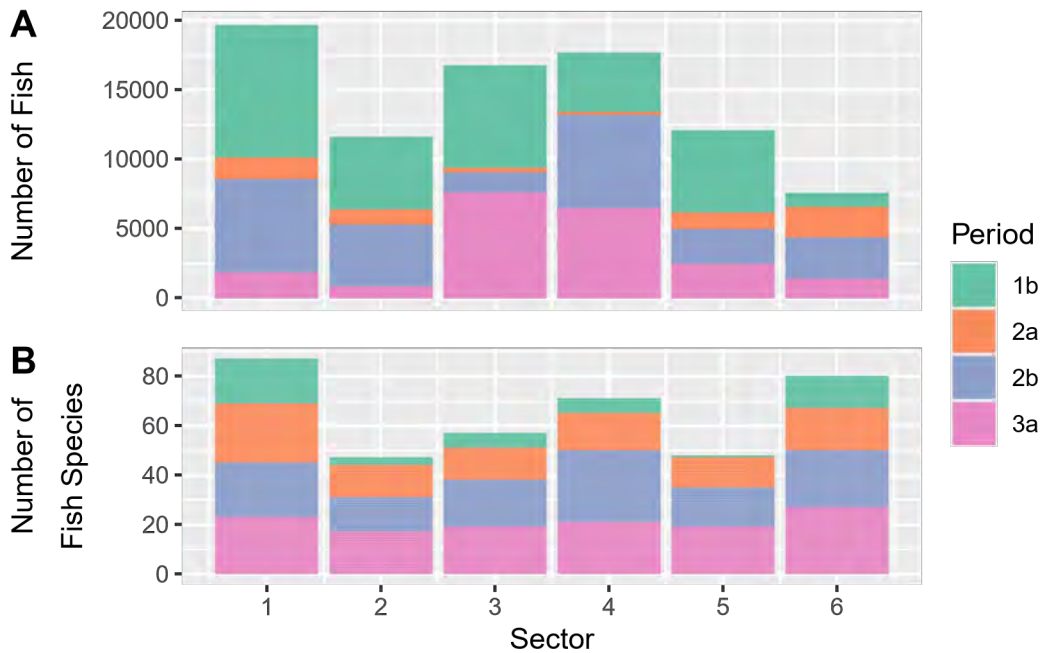


Figure 5. Number of fish (A) and number of fish species (B) sampled in each sector during each sampling period for the current year.

In Year 2, the greatest number of fish were caught in sector 1, with a total of 19,667, while the fewest were caught in sector 6, with 7,532 individuals (Table 5, Figure 5). Sector 1 also recorded the highest species richness, with 41 species, whereas sector 5 had the lowest, with 24 species (Table 5, Figure 5). Across all sectors, a total of 18 bottom trawls, 54 gillnets, 71 electrofishing transects, and 54 otter trawls were conducted, amounting to 197 sampling events in Year 2 (Table 5, Figure 4). A more accurate comparison of catch rates accounting for these differences is presented below in the Catch Per Unit Effort (CPUE) analysis.

All sampling objectives for Year 2 were met, with the exception of electrofishing, which was not initiated until partway through Sampling Period 2a.

Catch per Unit Effort (CPUE) was calculated on a gear-specific basis as the mean number of fish and fish species per sampling trip. Effort was defined according to the sampling gear and the habitat being targeted (Hubert and Fabrizio 2007). For both trawl types (bottom and otter), CPUE was defined as the mean number of fish or fish species per trawl. For gillnets, CPUE was defined as the mean number of fish or fish species per net-night. For electrofishing, CPUE was defined as the mean number of fish or fish species per 15-minute transect. Table 6 provides a summary of the number of fish of each species caught using each gear type in Year 2, presented as the mean number of fish and the mean number of fish species.

Table 6. Quantity of each fish species caught in each gear type for the current year.

Species	Gear Type				Total Number of Fish
	Bottom Trawls	Gillnets	Electrofishing	Otter Trawls	
Alligator Gar	0	13	0	0	13
American Eel	0	0	12	0	12
Atlantic Croaker	0	4	0	0	4
Atlantic Needlefish	0	0	3	0	3
Atlantic Stingray	0	1	0	0	1
Atlantic Tarpon	0	1	0	0	1
Bay Anchovy	32644	0	0	42138	74782
Bigmouth Buffalo	0	0	1	0	1
Black Bullhead	0	1	0	0	1
Black Crappie	0	16	1	0	17
Black Drum	0	1	0	0	1
Blue Catfish	39	190	161	580	970
Bluegill	3	4	19	9	35
Chain Pipefish	0	0	0	2	2
Channel Catfish	5	600	17	310	932
Clown Goby	10	0	0	236	246
Flathead Catfish	0	4	390	0	394
Freshwater Drum	0	8	16	1050	1074
Freshwater Goby	0	0	0	25	25

Gafftopsail Catfish	0	4	0	0	4
Gizzard Shad	0	249	299	0	548
Gulf Killifish	0	0	1	0	1
Gulf Menhaden	1	103	342	448	894
Gulf Pipefish	0	0	0	10	10
Gulf Sturgeon	0	2	0	0	2
Hardhead Catfish	0	1	0	0	1
Hogchoker	17	0	0	961	978
Inland Silverside	1	0	70	0	71
Ladyfish	0	2	9	0	11
Largemouth Bass	0	0	76	0	76
Lepomis Sp.	0	0	2	0	2
Longear Sunfish	0	1	6	0	7
Longnose Gar	0	20	6	0	26
Naked Goby	1	0	0	429	430
Orangespotted Sunfish	0	0	2	0	2
Red Drum	0	9	6	0	15
Redear Sunfish	0	5	13	0	18
Redspotted Sunfish	0	8	15	1	24
Sand Seatrout	0	0	0	4	4
Sheepshead	0	1	0	0	1
Silver Carp	0	1	0	0	1
Skipjack Herring	0	56	0	0	56
Smallmouth Buffalo	0	0	34	0	34
Southern Flounder	0	1	0	3	4
Spot	0	4	0	0	4
Spotted Gar	0	138	319	2	459
Striped Mullet	0	35	2767	0	2802
Threadfin Shad	0	130	61	0	191
White Bass	0	12	0	0	12
White Crappie	0	1	0	0	1
Yellow Bass	0	26	0	0	26
Yellow Bullhead	0	0	2	0	2
Totals	32721	1652	4650	46208	85231

CPUE: Number of Fish	1817.833	32.392	75.016	906.588	
CPUE: Number of Species	2.333	6.902	5.081	5.118	

Note: Binomial nomenclature for all species referenced in this table can be found in Table 7 below.

Collectively, 85,231 fish representing 52 species (Table 6) were sampled across all sectors of Lake Maurepas during Year 2 using bottom trawls (32,721), gillnets (1,652), electrofishing (4,650), and otter trawls (46,208). Bottom trawls produced 9 distinct species, none of which were unique to that gear type, however, bottom trawls were only utilized for a single sampling period (1b) during Year 2. Electrofishing caught 28 distinct species (9 exclusively: American Eel, Atlantic Needlefish, Bigmouth Buffalo, Gulf Killifish, Largemouth Bass, *Lepomis* sp., Orangespotted Sunfish, Smallmouth Buffalo, Yellow Bullhead), gillnets caught 35 distinct species (16 exclusively: Alligator Gar, Atlantic Croaker, Atlantic Stingray, Atlantic Tarpon, Black Bullhead, Black Drum, Gafftopsail Catfish, Gulf Sturgeon, Hardhead Catfish, Sheepshead, Silver Carp, Skipjack Herring, Spot, White Bass, White Crappie, Yellow Bass), and otter trawls caught 17 distinct species (4 exclusively: Chain Pipefish, Freshwater Goby, Gulf Pipefish, Sand Seatrout; Table 6).

Gillnets were the least effective in terms of catching high quantities of fish (CPUE: number of fish=32.392), but were the most effective at catching the greatest diversity of fishes (CPUE: number of fish species=6.902). This included species of fish that were exclusively sampled by gillnets, of which the most notable are the Gulf Sturgeon and the Atlantic Tarpon. Alternatively, otter trawls caught the highest quantity of fish (CPUE: number of fish=906.588), but caught a less diverse array of fishes than gillnets (CPUE: number of species=5.118), where a majority of the catch consisted of Bay Anchovies. Bay Anchovies accounted for 88% of the total catch for all gear types. Electrofishing had a similar species CPUE to that of otter trawls (5.081), and a CPUE for the number of fish of 75.016 (Table 6).

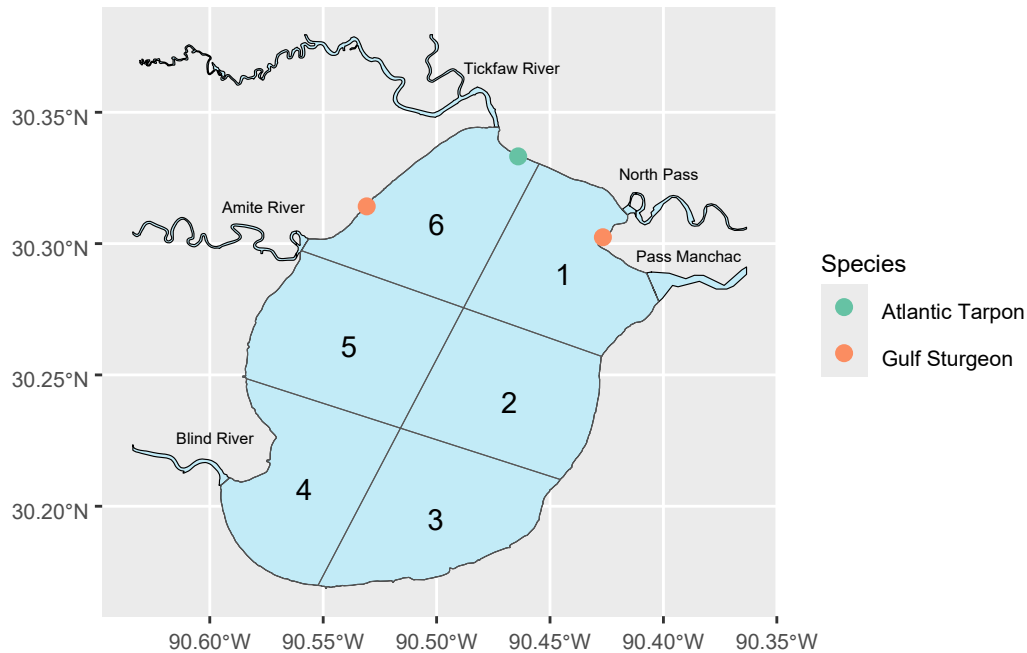


Figure 6. Locations where Gulf Sturgeon and Atlantic Tarpon were caught in Lake Maurepas in the current year.

One young-of-year (YOY) Atlantic Tarpon (TL=316-mm) was collected on October 23, 2024 (Crabtree et al. 1997; Stein 2013), which we believe to be the first documented record in Lake Maurepas (Figure 6). Adult and juvenile Atlantic Tarpon are not commonly reported any further west than Lake Borgne in the Pontchartrain Basin (Drymon et al. 2021; Luo et al. 2020; Stephens et al. 2024; Stein 2013). Little is known about Tarpon spawning, but it is believed to take place offshore in May and August, with eggs and larvae drifting inshore being subjected to environmental conditions (Crabtree et al. 1997). It is likely that this YOY Tarpon drifted into the Pontchartrain Basin, and then traveled inland due to water moving into Lake Maurepas from Lake Pontchartrain due to drought conditions in August, September, and October of that year. Storms also have the potential to blow juvenile tarpon into new habitats (Ault et al. 2007), another potential cause for its presence in the lake.

Two juvenile Gulf Sturgeon (TL=840mm and 890mm) were collected on April 25, 2024 (Figure 6). These represent the first documented records of this species in Lake Maurepas (Brogdon et al. 2024; Parauka, Duncan, and Lang 2011). Gulf Sturgeon have been considered a threatened species since their listing in 1991 (Hightower et al. 2002). Gulf Sturgeon are known to spawn in rivers (Wilber, Peterson, and Slack 2019; Brogdon 2022), and juvenal and adult Gulf Sturgeon spend time in estuarine and freshwater habitats (Parauka, Duncan, and Lang 2011; Wilber, Peterson, and Slack 2019; Fox, Hightower, and Parauka 2002; Edwards et al. 2003), including in the nearby Lake Pontchartrain (Brogdon et al. 2024). However, no effort has been made to sample for Gulf

sturgeon west of the Lake Pontchartrain Causeway (Baer et al. 2024; Brogdon 2022; Morrow et al. 1998), and therefore, little is known about their populations or potential breeding in Lake Maurepas and its rivers (Tickfaw, Amite, and Blind).

Table 7. Common name, binomial name, family, trophic class, and species type for all fish species caught during monitoring in the current year, and for all fish species historically documented in Lake Maurepas.

Common Name	Binomial Name	Family	Trophic Class	Species Type
Alligator Gar	<i>Atractosteus spatula</i>	Lepisosteidae	C	NG
American Eel	<i>Anguilla rostrata</i>	Anguillidae	I/C	NG
Atlantic Croaker	<i>Micropogonias undulatus</i>	Sciaenidae	P	G
Atlantic Needlefish	<i>Strongylura marina</i>	Belonidae	I/C	NG
Atlantic Stingray	<i>Dasyatis sabina</i>	Dasyatidae	I	NG
Atlantic Tarpon	<i>Megalops atlanticus</i>	Megalopidae	C	G
Bay Anchovy	<i>Anchoa mitchilli</i>	Engraulidae	P/I	B
Bigmouth Buffalo	<i>Ictiobus cyprinellus</i>	Catostomidae	I	NG
Black Bullhead	<i>Ameiurus melas</i>	Ictaluridae	I/C	NG
Black Crappie	<i>Pomoxis nigromaculatus</i>	Centrarchidae	I/C	G
Black Drum	<i>Pogonias cromis</i>	Sciaenidae	I	G
Blue Catfish	<i>Ictalurus furcatus</i>	Ictaluridae	I/C	G
Bluegill	<i>Lepomis macrochirus</i>	Centrarchidae	I	G
Chain Pipefish	<i>Syngnathus louisianae</i>	Syngnathidae	I	NG
Channel Catfish	<i>Ictalurus punctatus</i>	Ictaluridae	I/C	G
Clown Goby	<i>Microgobius gulosus</i>	Gobiidae	I	NG
Flathead Catfish	<i>Pylodictis olivaris</i>	Ictaluridae	I/C	G
Freshwater Drum	<i>Aplodinotus grunniens</i>	Sciaenidae	I/C	G
Freshwater Goby	<i>Ctenogobius shufeldti</i>	Gobiidae	I	NG
Gafftopsail Catfish	<i>Bagre marinus</i>	Ariidae	I/C	G
Gizzard Shad	<i>Dorosoma cepedianum</i>	Clupeidae	D	B
Gulf Killifish	<i>Fundulus grandis</i>	Fundulidae	C/I	NG
Gulf Menhaden	<i>Brevoortia patronus</i>	Clupeidae	P/D	B
Gulf Pipefish	<i>Syngnathus scovelli</i>	Syngnathidae	I	NG
Gulf Sturgeon	<i>Acipenser oxyrhynchus</i>	Acipenseridae	I	P
Hardhead Catfish	<i>Ariopsis felis</i>	Ariidae	I/C	G
Hogchoker	<i>Trinectes maculatus</i>	Paralichthyidae	D/I	NG
Inland Silverside	<i>Menidia beryllina</i>	Atherinopsidae	I/P	B

Ladyfish	<i>Elops saurus</i>	Elopidae	C	NG
Largemouth Bass	<i>Micropterus salmoides</i>	Centrarchidae	I/C	G
Longear Sunfish	<i>Lepomis megalotis</i>	Centrarchidae	I	G
Longnose Gar	<i>Lepisosteus osseus</i>	Lepisosteidae	C	NG
Naked Goby	<i>Gobiosoma bosc</i>	Gobiidae	I	NG
Orangespotted Sunfish	<i>Lepomis humilis</i>	Centrarchidae	I	G
Red Drum	<i>Sciaenops ocellatus</i>	Sciaenidae	I/C	G
Redear Sunfish	<i>Lepomis microlophus</i>	Centrarchidae	I	G
Redspotted Sunfish	<i>Lepomis miniatus</i>	Centrarchidae	I	G
Sand Seatrout	<i>Cynoscion arenarius</i>	Sciaenidae	P	G
Sheepshead	<i>Archosargus probatocephalus</i>	Sparidae	H/I	G
Silver Carp	<i>Hypophthalmichthys molitrix</i>	Cyprinidae	P	NG
Skipjack Herring	<i>Alosa chrysochloris</i>	Clupeidae	P	B
Smallmouth Buffalo	<i>Ictiobus bubalus</i>	Catostomidae	I/D	NG
Southern Flounder	<i>Paralichthys lethostigma</i>	Paralichthyidae	C	G
Spot	<i>Leiostomus xanthurus</i>	Sciaenidae	D/I	G
Spotted Gar	<i>Lepisosteus oculatus</i>	Lepisosteidae	C	NG
Striped Mullet	<i>Mugil cephalus</i>	Mugilidae	D/H	B
Threadfin Shad	<i>Dorosoma petenense</i>	Clupeidae	P	B
White Bass	<i>Morone chrysops</i>	Moronidae	I/C	G
White Crappie	<i>Pomoxis annularis</i>	Centrarchidae	I/C	G
Yellow Bass	<i>Morone mississippiensis</i>	Moronidae	I/C	G
Yellow Bullhead	<i>Ameiurus natalis</i>	Ictaluridae	I/C	NG

We designated each species in Table 7 with a trophic class and a species type. Trophic classes include invertivores (I), carnivores (C), planktivores (P), herbivores (H), and detritivores (D). When a species belonged to more than one trophic classification, their food habits were denoted by the appropriate combination of major trophic classes. Trophic classification followed Miranda, Habrat, and Miyazono (2008), Darnell (1958), and Parker et al. (2023). Species types include bait (B), game (G), non-game (NG), and protected (P) species.

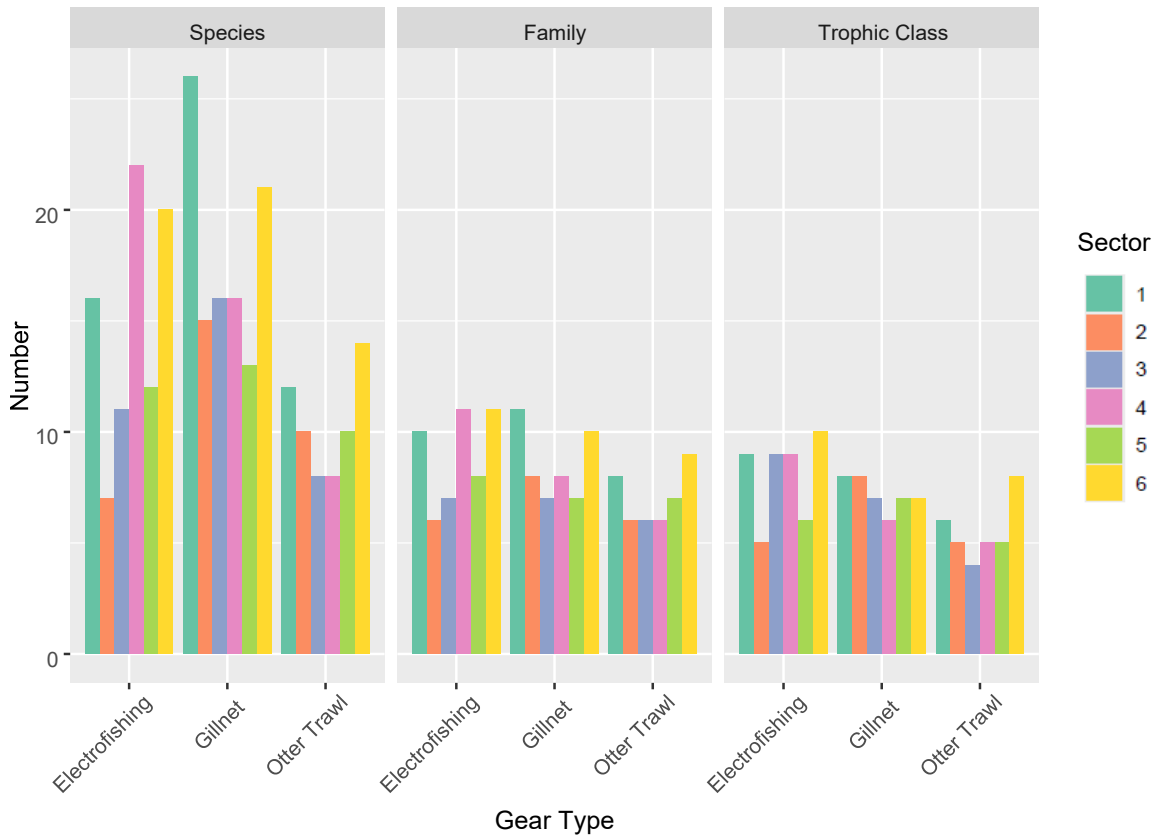


Figure 7. Number of fish species, families, and trophic classes caught between sectors by electrofishing, gillnets, and otter trawls.

To summarize fish assemblage among sectors, differences in species, family, and trophic richness were examined between gear types. Trophic classifications followed Miranda, Habrat, and Miyazono (2008), Darnell (1958), and Parker et al. (2023). A detailed list of trophic class designations for each species is provided in Table 7.

Sector 1 exhibited the highest species richness (40), and was tied with sector 6 for the highest family richness (19; Figure 7). Sector 6 also had the second highest number of species (38; Figure 7). Sectors 1, 2, and 6 had the highest number of distinct trophic classes (12; Figure 7). These sectors are influenced by freshwater inputs from the Tickfaw and Amite rivers, while also experiencing saline water inflow from Lake Pontchartrain through North Pass and Pass Manchac (Figure 3). In contrast, sector 5 exhibited the lowest diversity, with only 24 distinct species, 12 families, and 10 trophic classes (Figure 7), reflecting its location farther south and away from the influence of these freshwater inflows (Figure 3).

Gillnets caught the highest number of distinct species (34), followed by boat electrofishers (28), and otter trawls (17). Gillnets also caught the greatest number of families (15) followed by boat electrofishers (13), and otter trawls (10). The greatest

number of distinct trophic classes of fishes were caught using boat electrofishers (11; Figure 7). These results emphasize the influence of gear specificity on the observed patterns of fish assemblages in Lake Maurepas.

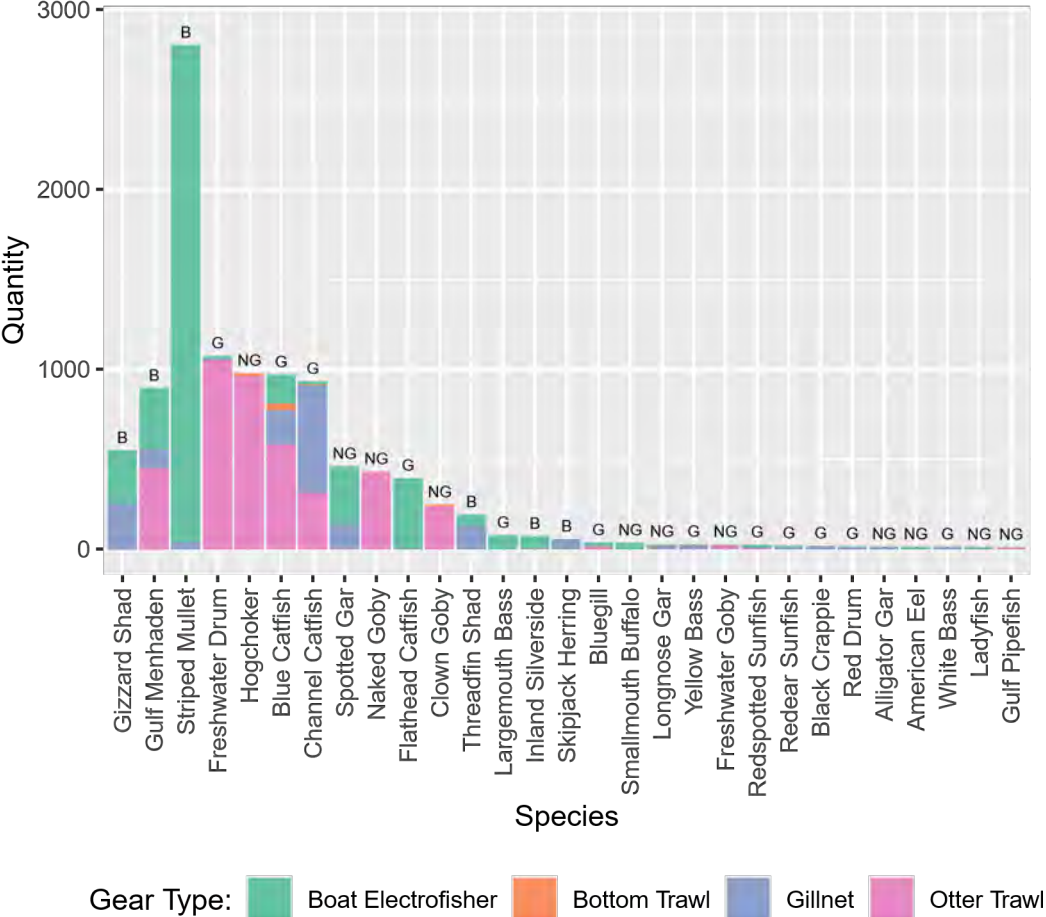


Figure 8. Quantity of fish of each species caught with boat electrofishers, bottom trawls, otter trawls, and gillnets, where the total number caught was greater than 10 individuals for the current year. Each bar is labeled with the species type, including bait (B), game (G), and non-game (NG) species. Bay Anchovies (a bait species) were excluded from this figure because of the exceptionally large quantity of individuals (74,782).

Aside from Bay Anchovies, which dominated the total catch, the most abundant fish species (with a total catch quantity of at least 100 individuals) across all gear types were (in descending quantity): Blue Catfish, Channel Catfish, Clown Goby, Flathead Catfish, Freshwater Drum, Gizzard Shad, Gulf Menhaden, Hogchoker, Naked Goby, Spotted Gar, Striped Mullet, and Threadfin Shad—all of which were caught using more than two gear types (Figure 8).

Among species where >10 individuals were caught, bait fish (6 species) constituted 44% (n=4,562) of the total catch, while game species (12 species) constituted 35% (n=3,593) of the total catch, when Bay Anchovies were excluded (Figure 8). Non-game fish (11 species) constituted 22% (n=2,244) of the total catch when Bay Anchovies were excluded (Figure 8). Including Bay Anchovies, bait fish accounted for 93% (n=79,344) of the total catch, game fish represented only 4% (n=3,593), and non-game fish constituted 3% (n=2,244) of the total catch.

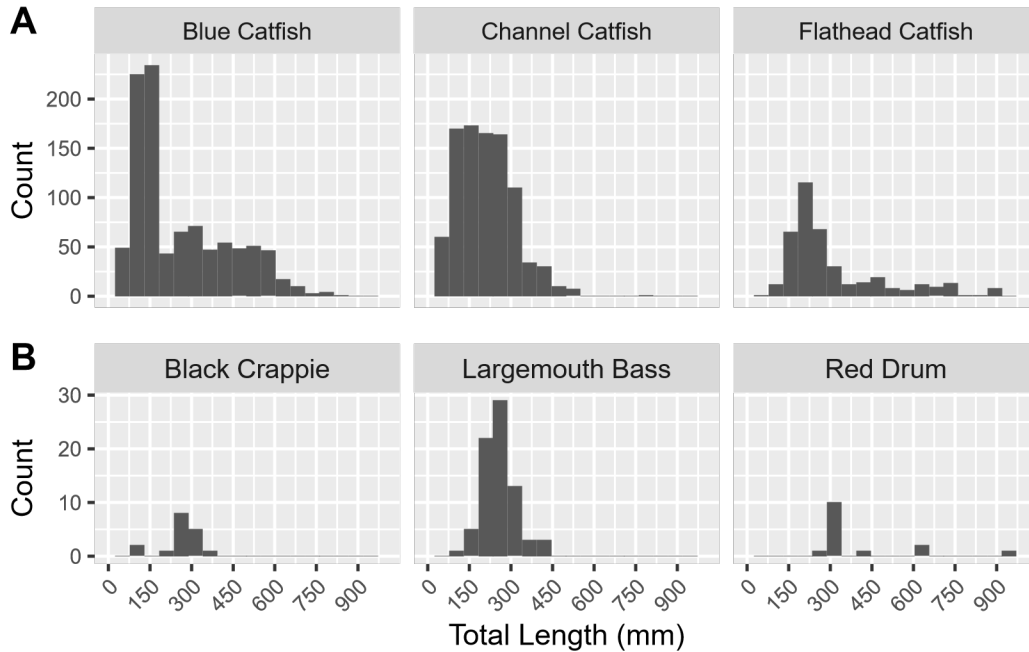


Figure 9. Count of individuals of major game species caught in Lake Maurepas, including (A) catfish and (B) other game species.

The size distributions of Blue Catfish, Channel Catfish, Flathead Catfish, and Largemouth Bass revealed distinct peaks in specific size classes. For Blue Catfish, the majority of individuals (30%, n=295) were observed in the 100-150-mm range (\bar{x} =259.75 [26-821]; Figure 9), representing a common size class evident from our sampling of Lake Maurepas, despite an apparent positive skew in the distribution of sizes observed. Similarly, Channel Catfish were predominantly within the 200-250-mm size class, comprising 19% (n=177) of all measured individuals (\bar{x} =211.24 [20-808]; Figure 9). Largemouth Bass also showed a peak size range of 200-250-mm, accounting for 30% (n=23) of recorded lengths (\bar{x} =258.25 [20-414]; Figure 9). These findings reflect key length frequencies within the surveyed habitats.

Genomics

Overall, 192 tissue samples were taken and preserved (*i.e.* equivalent to two 96-well sequencing plates) (Figs. 10A-C, Table 8). Genomic DNA was isolated from tissue using the DNeasy Blood and Tissue following manufacturer's instructions (QIAGEN). DNA quantity was assessed using a NanoDrop™ One^C Microvolume UV-Vis Spectrophotometer (Thermo Fisher Scientific). The quality of DNA was verified by electrophoresis using a 1.5% agarose gel stained with ethidium bromide, as well as light wavelength absorbance ratios (260/280 and 260/230) from the NanoDrop. Mean DNA quantity was 85.7 ng/μL for Blue Catfish, 151.9 ng/μL for Channel Catfish, and 143.9 ng/μL for Flathead Catfish. Ideal per-sample DNA quantity for sequencing is 50–100 ng/μL.

Samples will be sequenced at Diversity Arrays Technology (<https://www.diversityarrays.com>) in Bruce, Australian Capital Territory. Diversity Array Technology sequencing (DArTseq) is a proprietary sequencing technology that reduces the complexity of genomes by targeting predominately active (*i.e.* low copy sequence) genomic regions using a cocktail of restriction enzymes to fragment DNA in a highly reproducible manner. These genomic regions typically contain the most useful genetic information. Sequencing will produce thousands of SilicoDArT and single nucleotide polymorphic (SNP) markers. SilicoDArT are dominant (presence/absence) markers, while SNPs are co-dominant markers (variation in nucleotides).

Genomic markers will be utilized in downstream population genetic and bioinformatic analyses. We will examine if there are genetically distinct (*i.e.*, structured) populations of Blue and Channel catfish within Lake Maurepas or each is a single, panmictic population (*i.e.*, extensive gene flow). We will also calculate basic diversity statistics (*e.g.*, expected and observed heterozygosities), as well as levels of gene flow among populations. We will also test for genomic introgression between Blue and Channel catfish individuals. Hybrids between Channel Catfish (females) and Blue Catfish (males) are artificially produced in hatcheries to enhance traits such as growth rates (*e.g.*, Dunham and Argue 2000; Jiang et al. 2008; Fantini-Hoag et al. 2022; Wang et al. 2022). However, there is limited investigations into the extent of hybridization in the wild.

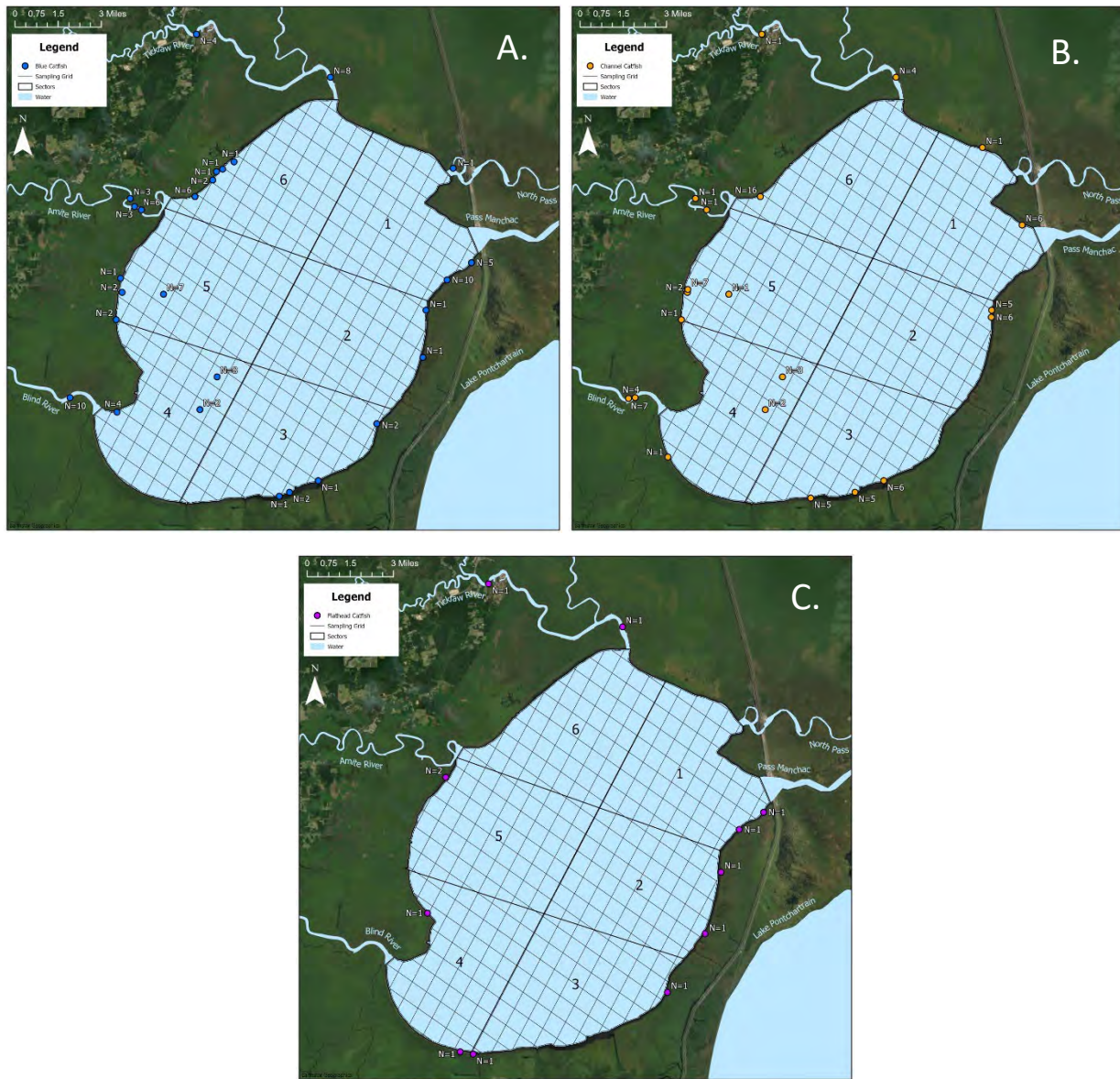


Figure 10. Collection localities of genetic samples across Lake Maurepas, and the Tickfaw, Amite, and Blind rivers for A. Blue Catfish (*Ictalurus furcatus*) (Blue points, n=95), B. Channel Catfish (*Ictalurus punctatus*) (orange points, n=85) and C. Flathead Catfish (*Pylodictis olivaris*) (purple points, n=12). All individuals were collected across the six lake sectors, as well as the Tickfaw, Amite, and Blind rivers.

Table 8. Sample size (N), mean DNA quantity (Qty_{DNA}), mean total length (TL), and mean mass (Mass) per catfish species (Blue, Channel, and Flathead catfish), per sector (Sectors 1–6; Tickfaw, Amite, and Blind rivers).

Species	Sector	N	Qty _{DNA} (ng/μL)	TL (mm)	Mass (g)
Blue Catfish (<i>Ictalurus furcatus</i>)	1	16	83.7	592	2443
	2	2	62.6	491	1275
	3	6	140.4	497	1284
	4	16	91.1	420	923
	5	10	79.3	503	1146
	6	11	123.4	526	1458
	Tickfaw	12	53.0	307	287
	Amite	12	83.0	287	231
	Blind	10	60.0	119	12
	Subtotal	95	85.7	388	990
Channel Catfish (<i>Ictalurus punctatus</i>)	1	7	124.8	384	490
	2	11	255.7	---	---
	3	16	156.4	---	---
	4	7	84.2	148	---
	5	10	59.6	241	150
	6	16	245.9	---	---
	Tickfaw	5	93.4	164	33
	Amite	2	104.3	189	62
	Blind	11	84.3	144	33
	Subtotal	85	151.9	188	89
Flathead Catfish (<i>Pylodictis olivaris</i>)	1	2	234.3	700	4085
	2	2	150.6	454	1220
	3	2	112.5	444	2305
	4	2	139.5	350	605
	5	2	97.3	620	3667
	Tickfaw	2	129.5	492	2359
	Subtotal	12	143.9	510	2373
TOTAL	192	118.7	347	910	

Invertebrates

Data on invertebrates in Lake Maurepas was collected using crab traps (crabs), otter trawls (shrimp), and ponar dredges (clams and benthic invertebrates), and sampling objectives vary based on gear type (Fig. 11). See Section 4 for more information.

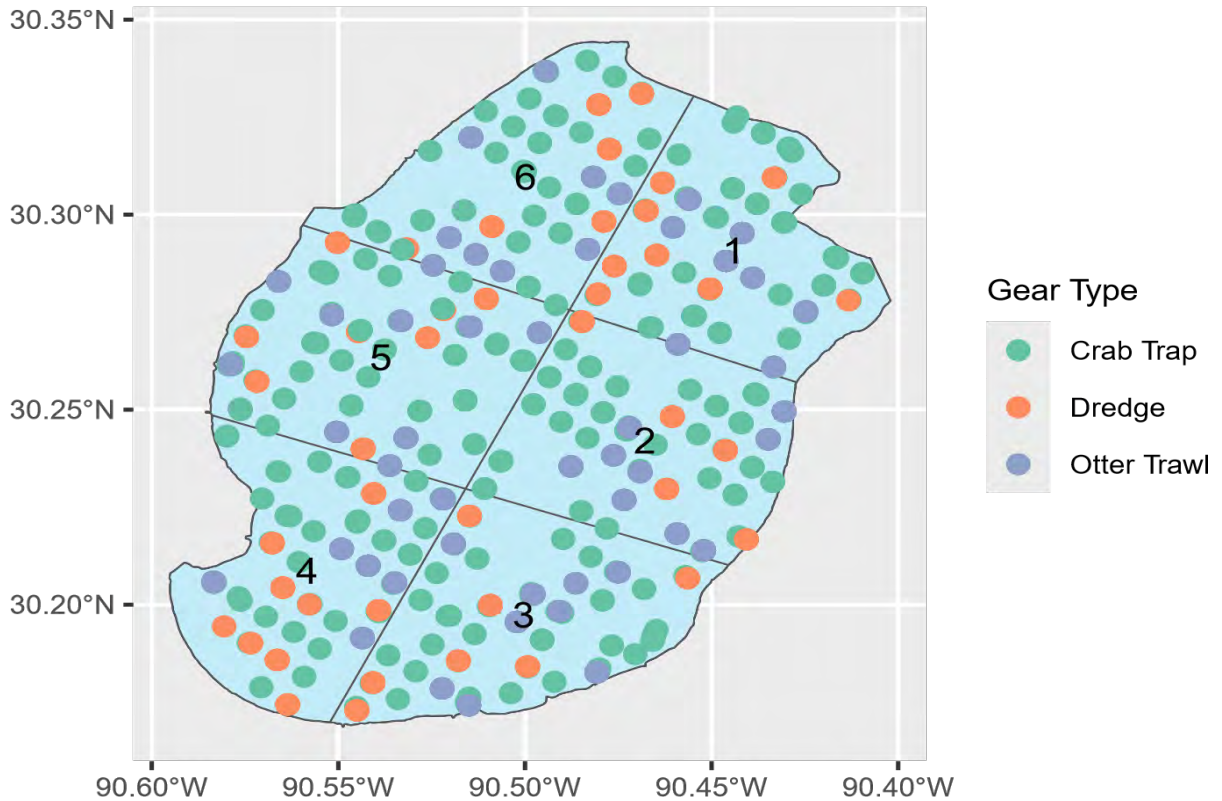


Figure 11. Locations of sampling events targeting invertebrates on Lake Maurepas in the current year, using ponar dredges, crab traps, and otter trawls.

In our 240 set crab traps (Table 9), we collected a total of 398 crabs over the course of all four sampling periods of Year 2, with the majority of blue crabs being found in Sector 1 at 103 individuals, and the fewest found in Sectors 3 and 4 at 44 individuals (Figure 12). We found the most crabs ($n=160$) during Period 2b, which is in line with their typical breeding season, while we found the fewest crabs ($n=65$) during Period 3a as temperatures began to decrease, and when blue crabs generally migrate towards saltwater (Darnell 1958).

Table 9. Number of sampling events with each gear type, total number of crabs, benthic invertebrates, shrimp, and clams collected per sector for the current year.

Sector	Dredges	Crab Traps	Otter Trawls	Number Crabs	Number Benthic Inverts	Number Clams	Number Shrimp
1	15	40	9	103	2954	111	2
2	16	40	9	84	3244	28	4
3	18	40	9	44	3226	5	48
4	16	40	9	44	2333	2	80
5	15	40	9	68	1333	8	13
6	15	40	9	55	2441	15	16

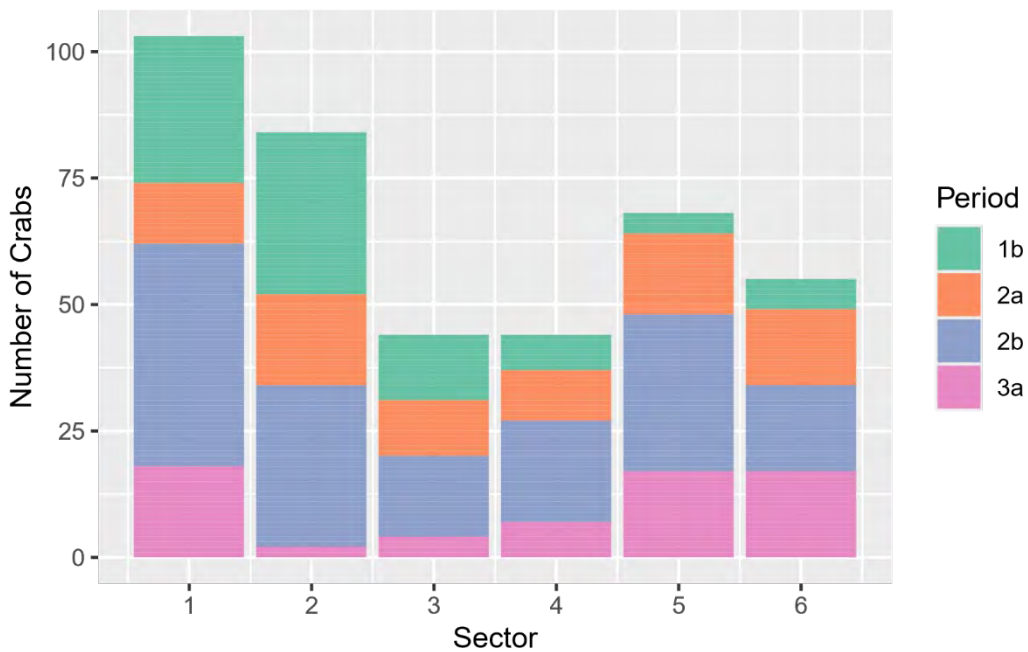


Figure 12. Number of crabs caught in each sector during each sampling period for the current year.

Generally, we find higher densities of blue crabs in Sectors 1, 2, and 6 depending on the sampling period, all of which are relatively close to Pass Manchac; a source of saline water and the migratory path the crabs use to travel to and from the Gulf of Mexico (Figure 13). Despite being able to tolerate lower salinity levels, the highest densities of blue crabs we estimated based on our collections occurred in sectors of higher salinity, though they can be found throughout Lake Maurepas depending on the time of year. Blue crabs will utilize different salinities throughout their juvenile stages (Archambault, Wenner, and Whitaker 1990), and even as adults will often partition habitats along the salinity gradient by sex (Hines, Lipcius, and Haddon 1987).

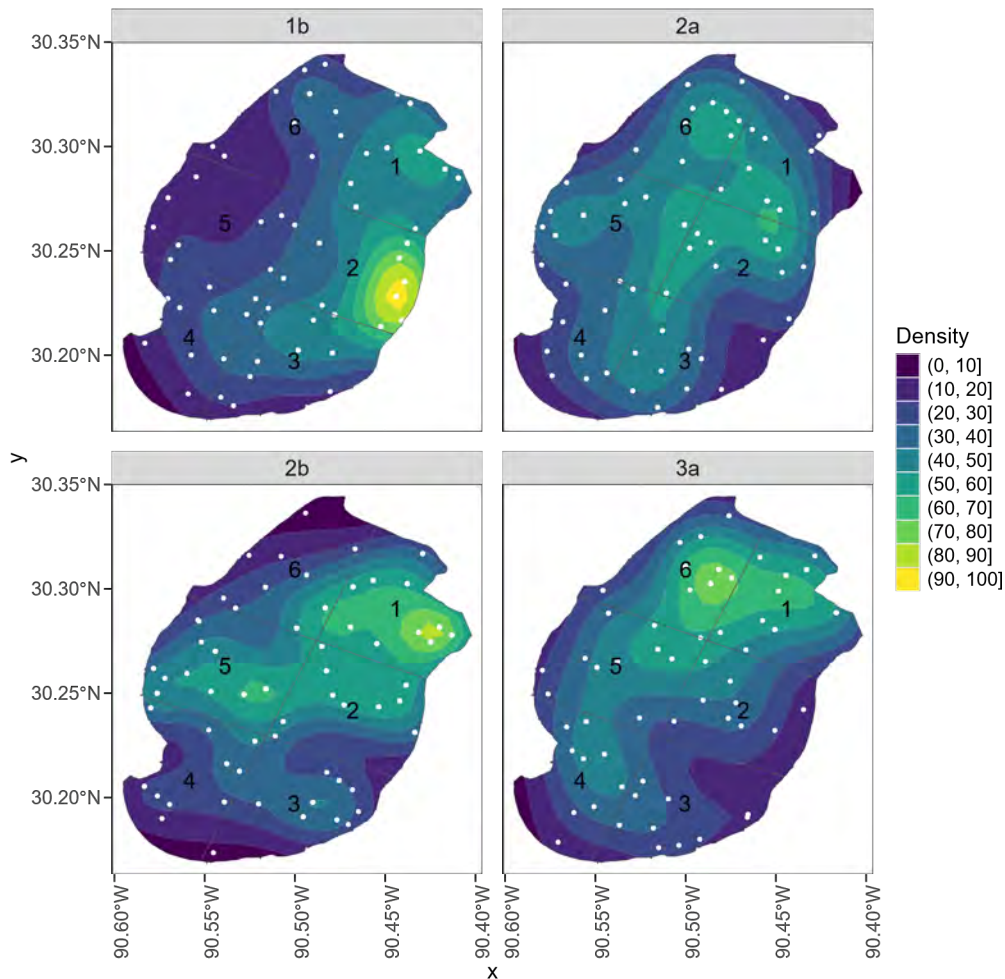


Figure 13. Crab trap locations (white points) and estimated seasonal probability density of crabs caught in Lake Maurepas for the current year. All density plots were created using kernel density estimation (KDE), where the density values (z) represent the estimated probability density.

In total we found 359 male blue crabs and 36 female blue crabs. Male and female crabs had a similar average carapace width at 154.37-mm for males and 156.94-mm for females, while male crabs on average weighed more than female crabs at 187.7-g for males and 153.61-g for females (Figure 14). Both of these measurements are influenced by the much lower female sample size, especially in sectors 4 and 6. This sample size difference between sexes is expected, since crab pot-based sampling for blue crabs is often male-biased (Brunson et al. 2024). To compound this, other studies in estuarine systems at lower latitudes report that male blue crabs are found more often in less saline locations compared to female crabs, which tend to occupy saltier habitats in order to

better incubate their eggs (Epifanio 2019). Our data corroborates this, as the majority of the specimens we find in the relatively freshwater Lake Maurepas are male. We see no trend between size, sex and spatial distribution. At the time of this report, only samples from periods 1b, 2a, and 2b have been fully processed, while samples from period 3a are still being sorted through. Therefore, these results will be focused on the former 3 periods.

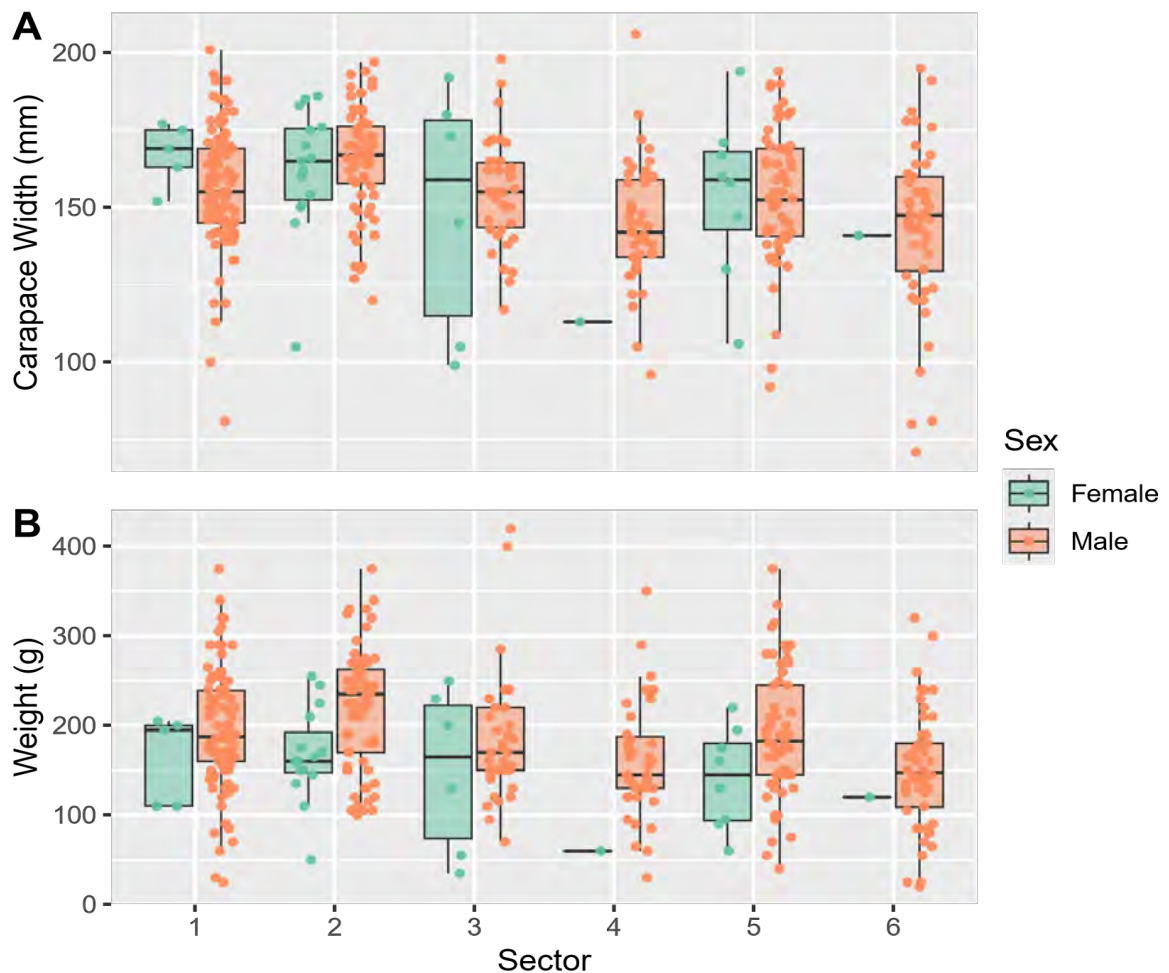


Figure 14 Blue crab carapace width (A) and weight (B) of female and male crabs caught in Lake Maurepas for the current year in each sector.

We found a total of 21 different taxa in all of our samples (Table 10), 12 of which have more than 10 specimens (Figure 15). The most common taxa observed was the Mud Snail (*Probythinella protera*) at 4,516 individuals, while Oligochaete earthworms were the 2nd most common taxa at 3,964 individuals. Other organisms that we found in much smaller quantities include water mites (*Hydrachnidia*), possum shrimp (*Taphromysis louisianae*), caddisfly larvae (*Oecetis cinerascens*), biting midge larvae (*Ceratopogonidae*),

and mayfly larvae (*Ephemeroptera*). Many of these were found in the southern sectors of the lake away from both saltwater inflow and the majority of boating traffic, making this a possible location to target for future additions to sampling protocol. We are likely under-sampling water mites, which are small enough to fit through the current mesh size that we use ($500\mu m$). We have seen greater presence of caddisfly larvae in the lake from the shelters they leave behind, but we have only collected a few with residents inside. Larval insects may be more abundant closer to the shoreline, and our current sampling methods are not capturing those communities well. Finally, animals like possum shrimp may be quick enough to escape our dredge before being captured, which could mean that they are more common at these sites than what is indicated in our samples.

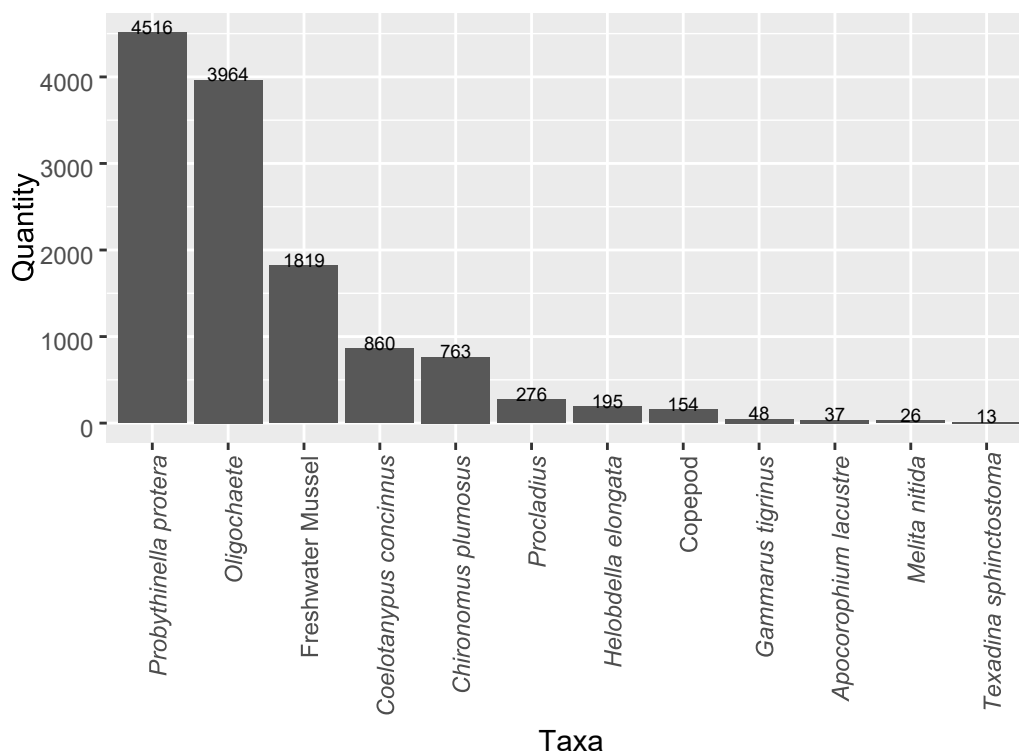


Figure 15. Count of each distinct taxa of benthic invertebrate (for taxa with >10 individuals) collected and identified in lake Maurepas for the current year.

Table 10. Number of taxa collected in each sector during the current year.

Taxa	Sector 1	Sector 2	Sector 3	Sector 4	Sector 5	Sector 6
<i>Apocorophium lacustre</i>	5	19	13	0	0	0
<i>Ceratopogonidae</i>	0	0	0	4	0	0
<i>Chironomus plumosus</i>	61	88	170	72	65	307
<i>Coelotanypus concinnus</i>	127	154	172	147	145	115
Copepod	8	40	28	4	10	64
<i>Ephemeroptera</i>	0	1	0	1	0	0
Freshwater Mussel	273	914	309	76	109	138
<i>Gammarus tigrinus</i>	1	10	10	16	5	6
<i>Helobdella elongata</i>	22	0	55	36	33	49
<i>Hydrachnidia</i>	0	0	8	0	1	0
<i>Melita nitida</i>	4	12	5	2	3	0
<i>Oecetis cinerascens</i>	0	1	0	0	1	0
<i>Oligochaete</i>	536	525	1117	981	242	563
<i>Probythinella protera</i>	1207	1089	734	425	471	590
<i>Procladius</i>	36	33	66	68	38	35
<i>Quadrula quadrula</i>	0	0	0	1	0	0
Spider	0	0	0	1	0	0
<i>Taphromysis louisianae</i>	0	1	4	0	0	0
<i>Texadina sphinctostoma</i>	5	2	1	2	3	0
Unknown Chironomid	0	0	1	0	0	0
Unknown Tanypis	0	0	2	0	0	0
Total in Sector	2285	2889	2695	1836	1126	1867

The average species richness in any particular quadrant is about 6 species, the highest number of species in a quadrant was 9, and the lowest number of species was 4. Overall, species richness does not seem to be different across sectors or sampling periods (Figure 16a). The average species abundance in a single quadrant was 230 invertebrates, the highest number of invertebrates in a single quadrant was 705, and the lowest was 31.

Overall, we see three different patterns of species abundance when looking between sectors and periods. In the sectors 1 and 2 (sectors close to Pass Manchac), we see an increase in species abundance from 1b to 2b, coinciding with general increase in temperature. In sectors 4 and 5, those closest to the Blind and Amite Rivers, we see a relatively stable number of species regardless of sampling period. Finally, in Sectors 3 and 6, we see a decrease in species abundance in sampling period 2a, followed by a recovery in sampling period 2b (Figure 16b). This could be caused by different species occupying

these sectors in the winter and summer with a turnover period during the spring for organisms in these sectors to acclimatization.

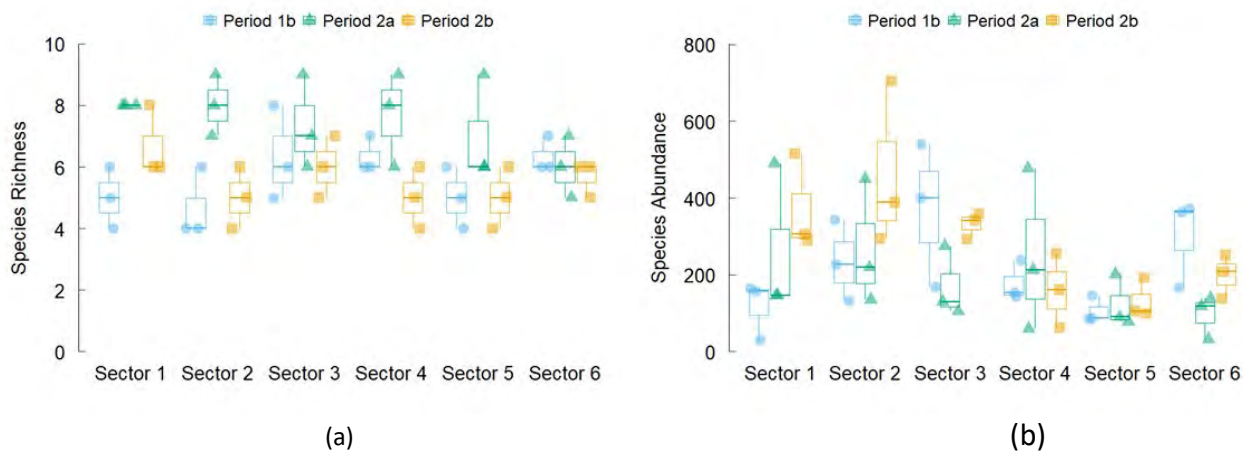


Figure 16. Species richness (a) and abundance (b) of aquatic invertebrates in Lake Maurepas across each sector and period.

We saw no spatial difference among invertebrate communities across each sector (Figure 17). While there could be differences in invertebrate community structure between Sectors 4 and 6, the southwestern and northwestern regions of Lake Maurepas respectively, all samples are still clustered together closely, and a similarity percentage analysis (SIMPER) did not indicate any differences in species composition between those communities.

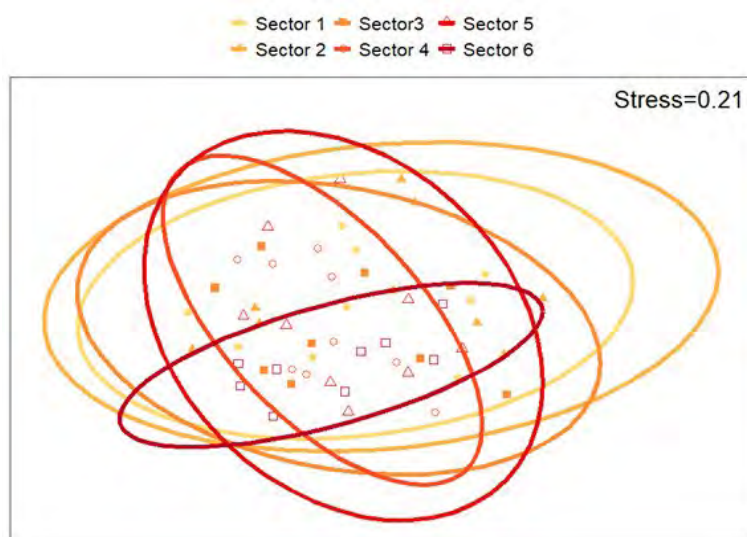


Figure 17. Non-metric Multidimensional Scaling plot of macroinvertebrate abundance collected from Lake Maurepas comparing each sector during sampling periods 1b, 2a, and 2b. Ovals represent 95% confidence intervals.

We noticed a strong seasonal difference of invertebrate communities between sampling periods 1b and 2b (Figure 18). According to a SIMPER analysis, the four most influential organisms driving the differences in these communities were earthworms (*Oligochaetes*), non-biting midge larvae (*Chironomus plumosus*), freshwater mussels, and mud snails (*Probythinella protera*). Earthworms and midge larvae were more abundant in period 1a during the colder months, while the gastropods (mud snails and freshwater mussels) were more abundant in period 2b during the warmer months. These species may be driving some of the abundance patterns seen in Figure 18, especially those in Sectors 3 and 6 which have a decrease of species abundance in the spring, followed by an increase during the summer. This abundance pattern is likely caused by these organisms being highly dominant during their respective period while being absent outside of them, and few other species being present during the interim, unlike in other sectors.

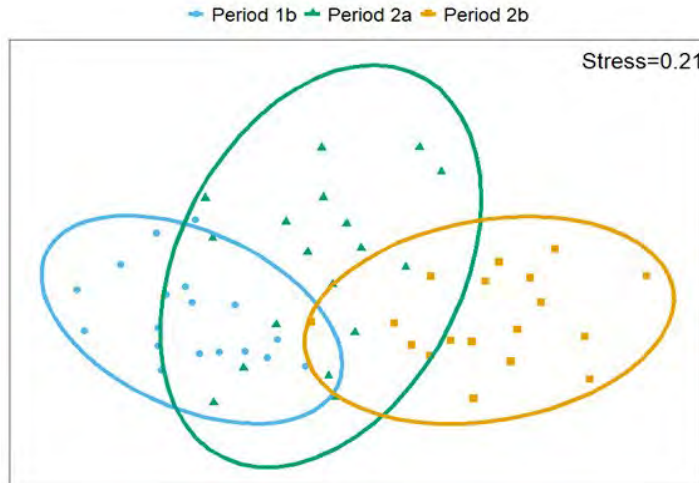


Figure 18. Non-metric Multidimensional Scaling plot of macroinvertebrate abundance collected from Lake Maurepas comparing three out of the four sampling periods. Ovals represent 95% confidence intervals.

In total, we caught 7 brown shrimp (*Farfantepenaeus aztecus*), 2 white shrimp (*Litopenaeus setiferus*), and 180 marsh grass shrimp (*Macrobrachium ohione*). The former two species were found in the northern portion of the lake, while the latter species was abundant throughout the southern portion of Lake Maurepas, as well as at the mouths of the freshwater rivers (Figure 19A). Both brown shrimp (Li and Clarke 2005) and white shrimp (Peterson and Turner 1994; Howe, Wallace, and Rikard 1999) utilize estuaries during their juvenile stages at different times of the year before returning to the ocean for their adult stage. Juvenile brown shrimp show better growth in salinities no lower than 4-ppt, which Lake Maurepas is always under, and juvenile white shrimp are

able to osmoregulate even at salinities as low a 1-ppt (Jaffer et al. 2020). While these conditions should be tolerable to both shrimp, the location of Lake Maurepas may be too distant from the Gulf of Mexico for many brown and white shrimps to migrate to, while Lake Pontchartrain could provide a more suitable habitat. The most common shrimp collected during our sampling was *Macrobrachium ohione*, a widespread freshwater species which requires increased salinity for reproduction; in particular for stage-1 larvae to moult into stage-2 (Rome, Conner, and Bauer 2009). It is possible the *Macrobrachium ohione* migrate out of Lake Maurepas in order to deliver their offspring into more saline waters, but this would require sampling outside of the lake to confirm, and seems unlikely considering most specimens were found away from Pass Manchac.

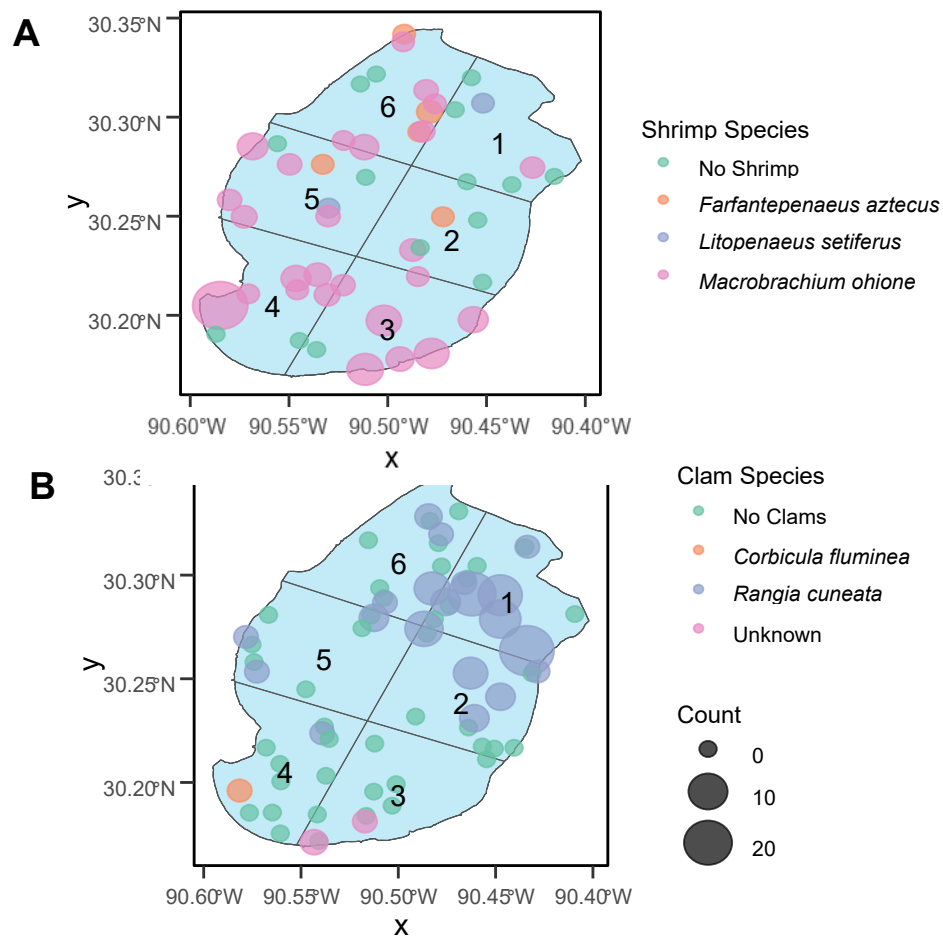


Figure 19. Locations and counts of shrimp (A) and clam (B) species collected on Lake Maurepas in the current year.

Similar to the benthic invertebrates, only periods 1b, 2a, and 2b have been fully processed at this time, so results will be focused on those sampling periods. We caught

and measured 119 clams for this current year. The majority of *Rangia cuneata* caught were in Sector 1, with large populations in Sector 2, smaller populations in Sectors 5 and 6, and occasional samples in Sector 4 (Figure 19B). This is in line with expected population distributions favoring the saline side of Lake Maurepas. There may be a slight increase in total weight of *Rangia* clams between periods 1b and 2a, and no apparent differences between those collected during period 2b and every other period (Figure 20), coinciding with warmer temperatures.

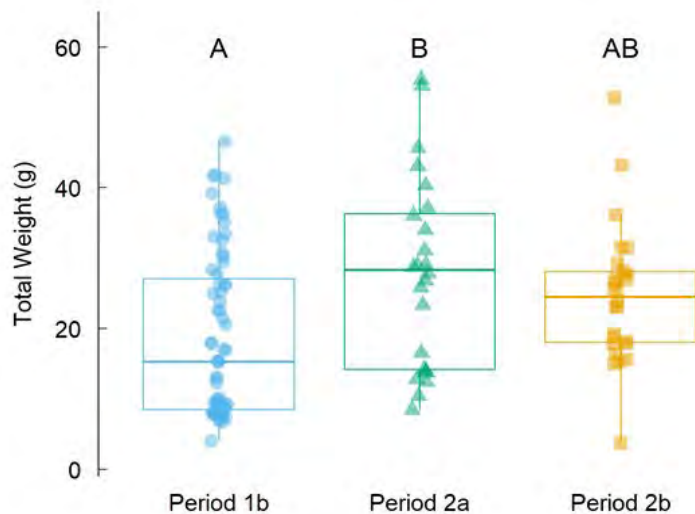


Figure 20. Total weight (grams) of all *Rangia* clams (n=118) sampled in Lake Maurepas throughout the current year.

Water Quality

Water quality data collected by the buoys in Year 2 proved unreliable due to engineering challenges with the buoy design. As a result, data from the buoys from the past year will not be reported here. However, water quality data was also collected using a handheld YSI ProDSS during routine aquatic sampling throughout Lake Maurepas and within the Tickfaw, Amite, and Blind Rivers in Year 2 (Figure 21).

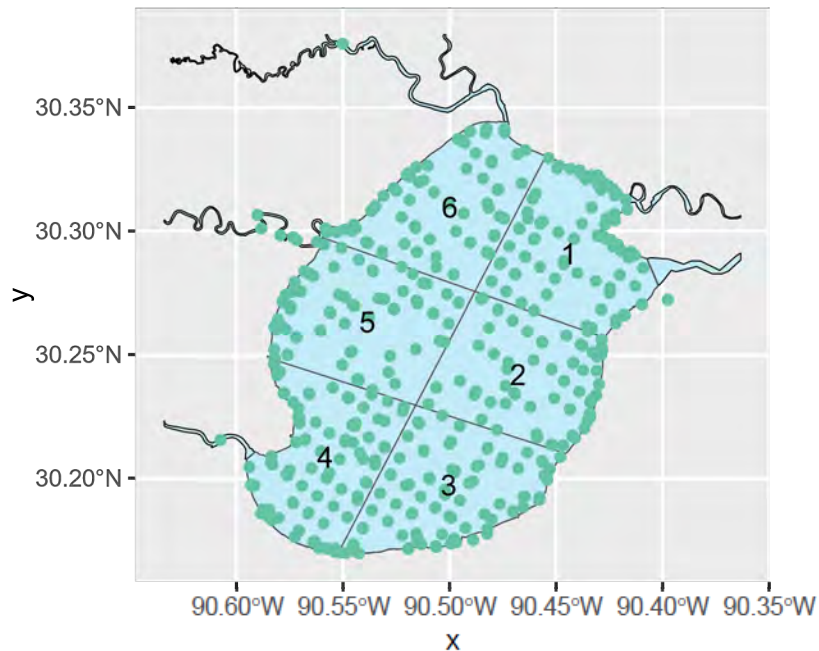


Figure 21. Locations of YSI water quality samples collected on Lake Maurepas and the surrounding watershed in the current year.

We collected 524 water quality samples across Lake Maurepas and the surrounding watershed in Year 2 (Figure 20). On Lake Maurepas, salinity levels were highest in Sectors 1, 2, and 6 (1: $\bar{x}=1.01 \pm 0.4$ ppt, 2: $\bar{x}=0.94 \pm 0.27$ ppt, 6: $\bar{x}=0.86 \pm 0.41$ ppt; Figure 22). These sectors are closest to Pass Manchac, which connects Lake Maurepas to the more saline waters of Lake Pontchartrain (Figure 21). Conductivity exhibited a similar trend (1: $\bar{x}=1964.09 \pm 711.02$ $\mu\text{mhos/cm}$, 2: $\bar{x}=1825.38 \pm 470.1$ $\mu\text{mhos/cm}$, 6: $\bar{x}=1616.12 \pm 624.4$ $\mu\text{mhos/cm}$; Figure 22), as did total dissolved solids (1: $\bar{x}=1286.52 \pm 479.46$ mg/L, 2: $\bar{x}=1209.87 \pm 329.07$ mg/L, 6: $\bar{x}=1091.38 \pm 491.08$ mg/L; Figure 22; Figure 21). In contrast, turbidity was greatest in Sectors 4 and 3 (4: $\bar{x}=13.23 \pm 7.88$ NTU, 3: $\bar{x}=9.42 \pm 6.47$ NTU; Figure 22). These sectors are located farthest from Pass Manchac and nearest to the Blind River (Figure 22). Dissolved oxygen was generally higher in the northern sectors (1: $\bar{x}=7.95 \pm 1.31$ mg/L, 2: $\bar{x}=7.67 \pm 1.32$ mg/L, 5: $\bar{x}=7.99 \pm 0.87$ mg/L, and 6: $\bar{x}=7.94 \pm 1.45$ mg/L; Figure 22), however this was a relatively weak spatial pattern (Figure 22). Water temperature showed no clear spatial variation across the lake (Figure 23).

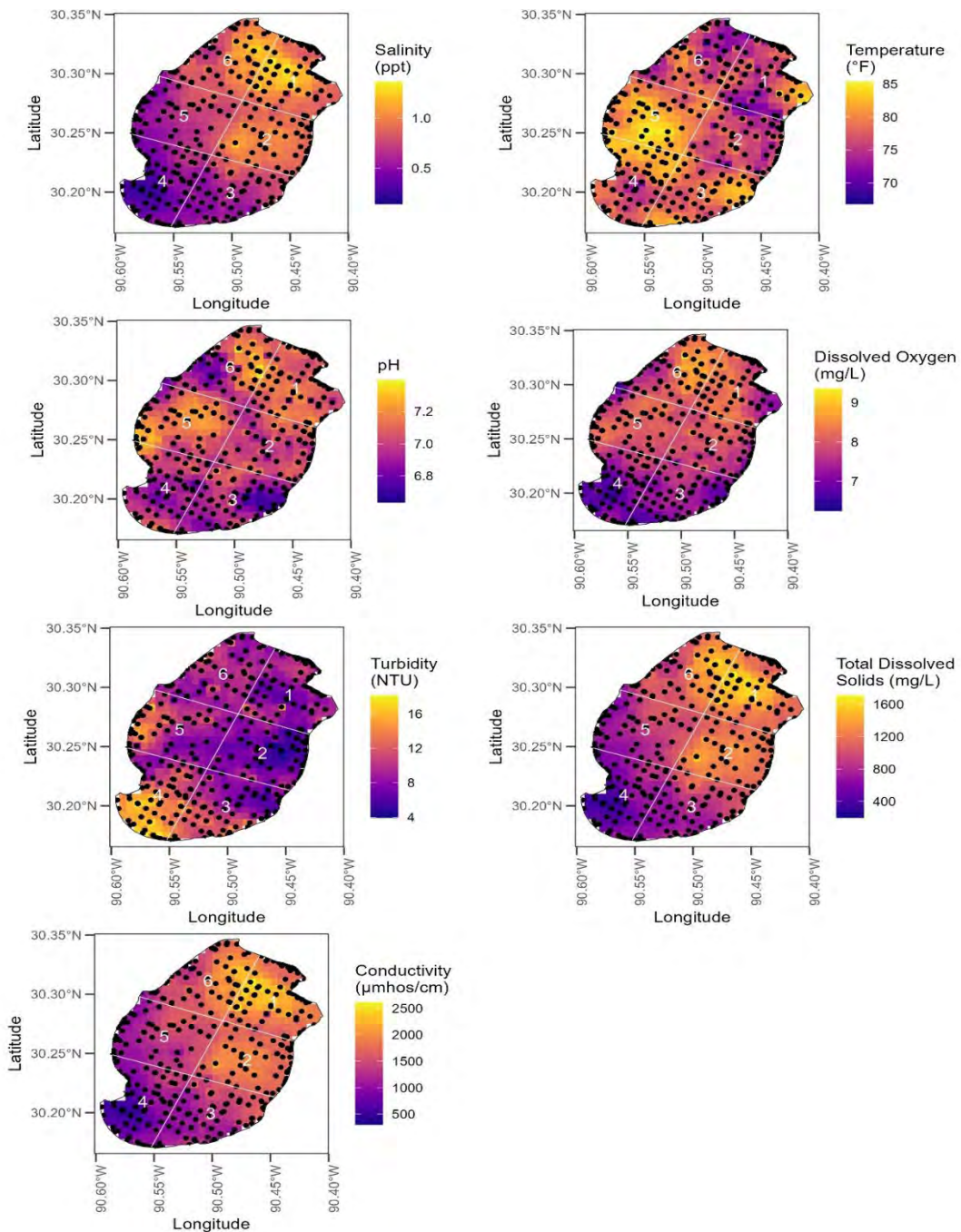


Figure 22. Inverse distance weighting (IDW) interpolations for water quality parameters sampled using handheld YSI unit. Each plot represents a separate parameter, where lighter colors represent higher values and darker colors represent lower values. All interpolations were generated with an inverse distance power (beta) parameter of 1 and a 600-meter grid cell size.

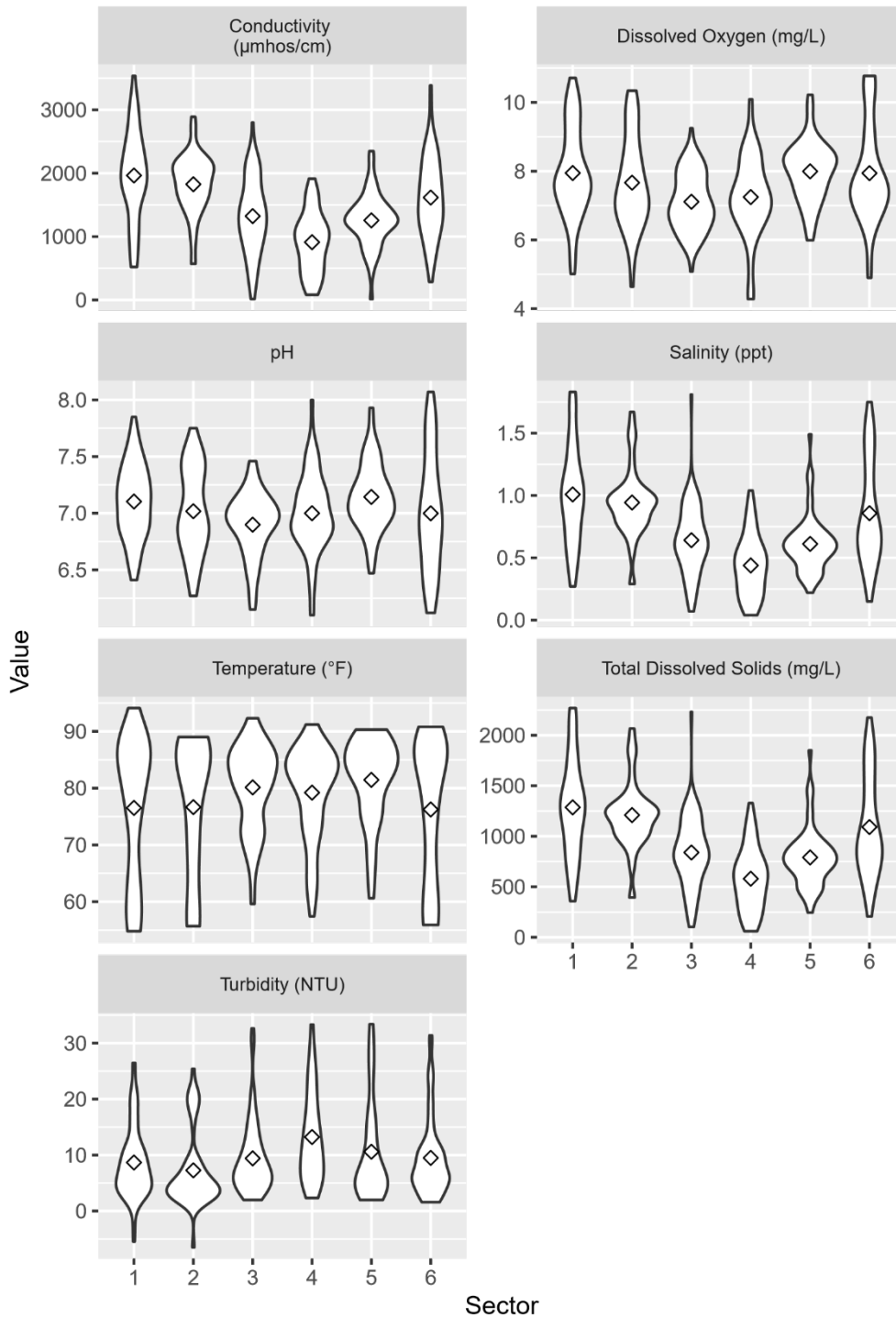


Figure 23. Water quality variables measured by YSI by sector, collected from Lake Maurepas in the current year. The mean value for each variable in each sector is represented by a hollow diamond shape.

Calculated mean values and standard deviations for each water quality variable in each sector for Year 2 can be found in the Appendix: Table A1.

Environmental DNA (eDNA)

A total of 95 water eDNA samples and were collected in Year 2, of which 95 have been extracted (100%): 24 from sampling period 1b, 24 from sampling period 2a, 23 from sampling period 2b, and 24 from sampling period 3a. The average DNA concentration for water samples was 9.85ng/μL, which amounts to 10.19ng/μL in sampling period 1b, 3.78ng/μL in sampling period 2a, and 15.59ng/μL in sampling period 2b (Figure 24). Concentrations of DNA in water samples from period 3a have not yet been calculated. A total of 70 sediment eDNA samples were collected in Year 2, of which 69 have been extracted (99%): 16 from sampling period 1b, 18 from sampling period 2a, 18 from sampling period 2b, and 18 from sampling period 3a. The average DNA concentration for the sediment samples was 11.27ng/μL, which amounts to 7.26ng/μL in sampling period 1b, 16.83ng/μL in sampling period 2a, 18.11ng/μL in sampling period 2b, and 2.89ng/μL in sampling period 2b (Figure 24).

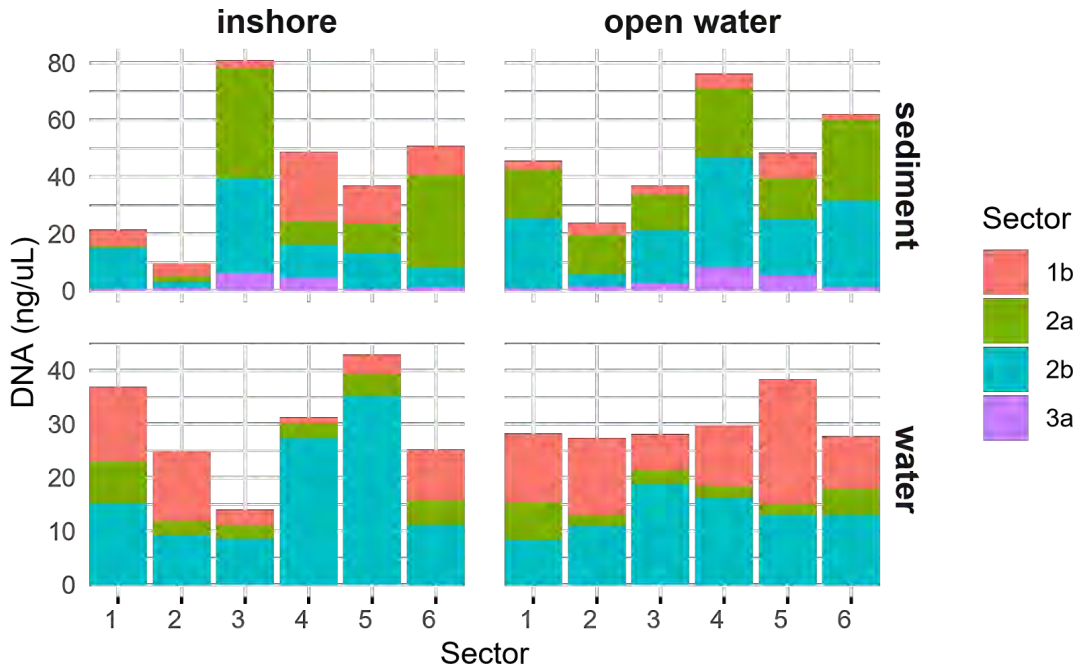


Figure 24. Extracted DNA concentrations (ng/μL) for sample each sampling type (sediment, top and water, bottom) at different site types (inshore, left and open water, right) from each sector during each sampling period in the current year.

Samples of eDNA from water and sediment have only been processed in full through sampling period 1b in Year 2. The following results report only on these samples. In total, water samples had 469 total fish detections in sampling period 1b across open water and inshore sites—representing 30 families, 57 genera, and 64 detected species. Of these detections, 259 came from open water sites, representing 58 species, and 210 came from inshore sites,

representing 55 species, with 49 species shared between sites (Table 11; Figure 25). Of these detected species, 6 are believed to come from DNA originating from crab trap bait: Blue Runner, Barred Grunt, Pigfish, Corocoro Grunt, Cobia, and Vermillion Snapper, as there are no historic or current records of these species in the lake. All detections reported in Table 11 can be located in Lake Maurepas in Figure 26.

There were 25 total species detected by eDNA in Lake Maurepas that were also seen while field sampling using gillnets, otter trawls, bottom trawls, or electrofishing (Table 12). There were 38 species that were only detected by eDNA, and 27 species that were only seen while field sampling. Of the 12 most abundant fish species seen while field sampling (Blue Catfish, Channel Catfish, Clown Goby, Flathead Catfish, Freshwater Drum, Gizzard Shad, Gulf Menhaden, Hogchoker, Naked Goby, Spotted Gar, Striped Mullet, and Threadfin Shad), 9 were also detected by eDNA, including Channel Catfish, Blue Catfish, Flathead Catfish, Freshwater Drum, Gulf Menhaden, Threadfin Shad, Naked Goby, Spotted Gar, and Striped Mullet (Table 12). Binomial names for all species detected by eDNA in Lake Maurepas can be found in Table 11.

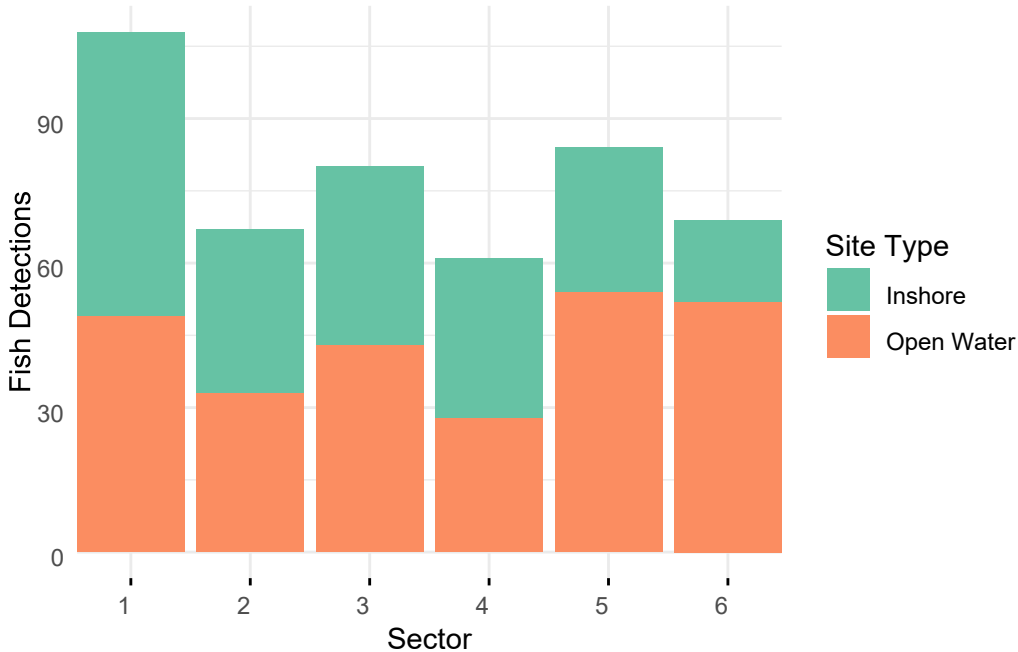


Figure 25. Total fish detections during period 1b from water samples taken in the current year.

Table 11. Fish detections made by water samples taken during period 1b.

Binomial Name	Common Name	Open Water Detections	Inshore Detections
<i>Ambloplites ariommus</i>	Shadow Bass	375IN	S6, I3, G11, L12, M23
<i>Ammocrypta beanii</i>	Naked Sand Darter	227IN, 48IN	S6, G11, K23, M23
<i>Anchoa mitchilli</i>	Bay Anchovy	96IN, 227IN, 186IN, 141IN, 48IN, 553IN, 507IN, 461IN, 420IN	S6, M16, S11, O9, M4, I3, G8, G11, L12, I17, K23, M23
<i>Aplodinotus grunniens</i>	Freshwater Drum	227IN, 461IN, 420IN, 326IN	S6, I3, G8, L12, K23
<i>Archosargus probatocephalus</i>	Sheepshead	96IN	S6, I3, G8
<i>Ariopsis felis</i>	Hardhead Catfish	96IN	G8, G11, I17
<i>Atractosteus spatula</i>	Alligator Gar	553IN	I3, M23
<i>Bagre marinus</i>	Gaftopsail Catfish	96IN	O9, L12, M23
<i>Bairdiella chrysoura</i>	Silver Perch	96IN	S6, L12
<i>Brevoortia patronus</i>	Gulf Menhaden	96IN, 227IN, 186IN, 141IN, 48IN, 553IN, 507IN, 461IN, 420IN, 375IN, 279IN	S6, M16, S11, O9, M4, I3, G8, G11, L12, I17, K23, M23
<i>Caranx crysos</i>	Blue Runner		G8
<i>Carpionodes carpio</i>	River Carpsucker	227IN, 461IN, 420IN	S6, O9, M23
<i>Centropomus undecimalis</i>	Common Snook	96IN	S6
<i>Citharichthys spilopterus</i>	Bay Whiff		M23
<i>Conodon nobilis</i>	Barred Grunt	96IN	
<i>Ctenogobius shufeldti</i>	Freshwater Goby	96IN, 461IN	S6, M23
<i>Cynoscion nothus</i>	Silver Seatrout	96IN, 186IN, 141IN, 48IN, 553IN, 461IN, 420IN, 279IN	S6, M4, I3, G8, G11, L12, I17, K23, M23

<i>Cyprinella venusta</i>	Blacktail Shiner	227IN, 186IN, 553IN, 507IN, 461IN, 420IN, 375IN, 326IN, 279IN	S6, M16, O9, I3, G8, G11, L12, I17, K23, M23
<i>Dorosoma cepedianum</i>	Threadfin Shad	227IN, 141IN, 48IN	M16, S11, O9, G8, K23, M23
<i>Dorosoma petenense</i>	Threadfin Shad	96IN, 227IN, 186IN, 141IN, 48IN, 553IN, 507IN, 461IN, 420IN, 375IN, 326IN	S6, S11, O9, I3, G8, I17, K23, M23
<i>Erimyzon tenuis</i>	Sharpfin Chubsucker	96IN, 141IN	S6, O9, G8, K23, M23
<i>Etheostoma swaini</i>	Gulf Darter	96IN	
<i>Fundulus chrysotus</i>	Golden Topminnow	96IN, 186IN, 553IN, 507IN, 461IN	L12
<i>Fundulus olivaceus</i>	Blackspotted Topminnow	48IN, 420IN	S6
<i>Gambusia affinis</i>	Western Mosquitofish	96IN	
<i>Gobiesox strumosus</i>	Skilletfish	96IN, 186IN, 553IN, 279IN	S6, M16, S11, I3, G8, G11, L12, K23, M23
<i>Gobiosoma bosc</i>	Naked Goby	96IN, 186IN, 141IN, 420IN	S6, M16, G8, G11, L12, K23, M23
<i>Harengula jaguana</i>	Scaled Sardine	141IN	
<i>Hypentelium nigricans</i>	Northern Hog Sucker	227IN, 186IN, 420IN	S6, I3, G8, L12
<i>Ictalurus furcatus</i>	Blue Catfish	96IN, 227IN, 141IN, 420IN	S6, M16, O9, G8, G11, K23, M23
<i>Ictalurus punctatus</i>	Channel Catfish	553IN, 279IN	M4, L12
<i>Ictiobus cyprinellus</i>	Bigmouth Buffalo	96IN, 186IN, 48IN, 553IN, 507IN, 461IN, 279IN	S6, O9, M4, I3, G8, G11, L12, K23, M23
<i>Lagodon rhomboides</i>	Pinfish	96IN, 227IN, 141IN, 461IN, 420IN	S6, M16, G8, G11, L12, K23, M23

<i>Leiostomus xanthurus</i>	Spot	96IN, 186IN, 141IN, 48IN, 553IN, 461IN, 420IN	S6, O9, I3, G8, L12
<i>Lepisosteus oculatus</i>	Spotted Gar	96IN, 227IN, 48IN, 507IN, 420IN	S6, M16, O9, G8, G11, L12, K23
<i>Lepomis gulosus</i>	Warmouth	96IN, 141IN, 48IN, 420IN	S6, M16, G11, L12, M23
<i>Lepomis macrochirus</i>	Bluegill	96IN, 227IN, 186IN, 141IN, 553IN, 507IN, 461IN, 420IN, 326IN, 279IN	S6, M16, S11, M4, I3, G8, G11, L12, M23
<i>Lepomis megalotis</i>	Longear Sunfish	96IN, 227IN, 141IN, 48IN, 553IN, 507IN, 279IN	S6, S11, G8, G11, L12, K23, M23
<i>Menidia beryllina</i>	Inland Silverside	96IN, 186IN, 48IN, 553IN, 507IN, 461IN, 420IN, 326IN, 279IN	S6, S11, I3, G8, L12, I17, K23, M23
<i>Menticirrhus americanus</i>	Southern Kingfish	96IN	O9
<i>Micropogonias undulatus</i>	Atlantic Croaker	96IN	
<i>Micropterus punctulatus</i>	Spotted Bass	96IN, 227IN, 48IN	S6, S11, O9, L12, M23
<i>Minytrema melanops</i>	Spotted Sucker	96IN, 553IN, 507IN	S6
<i>Moxostoma poecilurum</i>	Black Redhorse	96IN, 227IN, 186IN, 48IN, 553IN, 461IN, 420IN, 279IN	S6, S11, O9, M4, L12, K23, M23
<i>Mugil cephalus</i>	Striped Mullet	96IN, 48IN, 553IN, 507IN, 420IN	S6, M16, S11, O9, M4, I3, G8, G11, L12, K23, M23
<i>Myrophis punctatus</i>	Speckled Worm Eel	96IN	
<i>Notropis texanus</i>	Weed Shiner		S6

<i>Orthopristis chrysoptera</i>	Pigfish	96IN, 186IN, 48IN, 553IN, 507IN, 461IN, 420IN	S6, S11, O9, M4, G8, G11, L12, M23
<i>Orthopristis ruber</i>	Corocoro Grunt		M23
<i>Paralichthys lethostigma</i>	Southern Flounder	96IN, 420IN	S6, I3, G8
<i>Percina sciera</i>	Inshore Lizardfish	186IN, 420IN	G11, L12
<i>Percina vigil</i>	Saddleback Darter		S6, G8
<i>Pimephales vigilax</i>	Bullhead Minnow		O9
<i>Pogonias cromis</i>	Black Drum	96IN, 186IN	S6, L12
<i>Pomoxis annularis</i>	White Crappie	96IN	S6
<i>Pylodictis olivaris</i>	Flathead Catfish	507IN, 461IN	I3, G8
<i>Rachycentron canadum</i>	Cobia	96IN, 227IN, 186IN, 141IN, 48IN, 553IN, 507IN, 461IN, 420IN, 375IN, 326IN, 279IN	S6, M16, S11, O9, M4, I3, G8, G11, K23, M23
<i>Rhomboplites aurorubens</i>	Vermillion Snapper	96IN, 186IN, 420IN	S6, O9, G11, M23
<i>Sciaenops ocellatus</i>	Red Drum	96IN	G8, G11, L12
<i>Sphoeroides parvus</i>	Least Puffer	96IN, 420IN	I3, G11, L12
<i>Strongylura marina</i>	Atlantic Needlefish	96IN	I3, G8
<i>Synodus foetens</i>	Gulf Toadfish		G8, L12

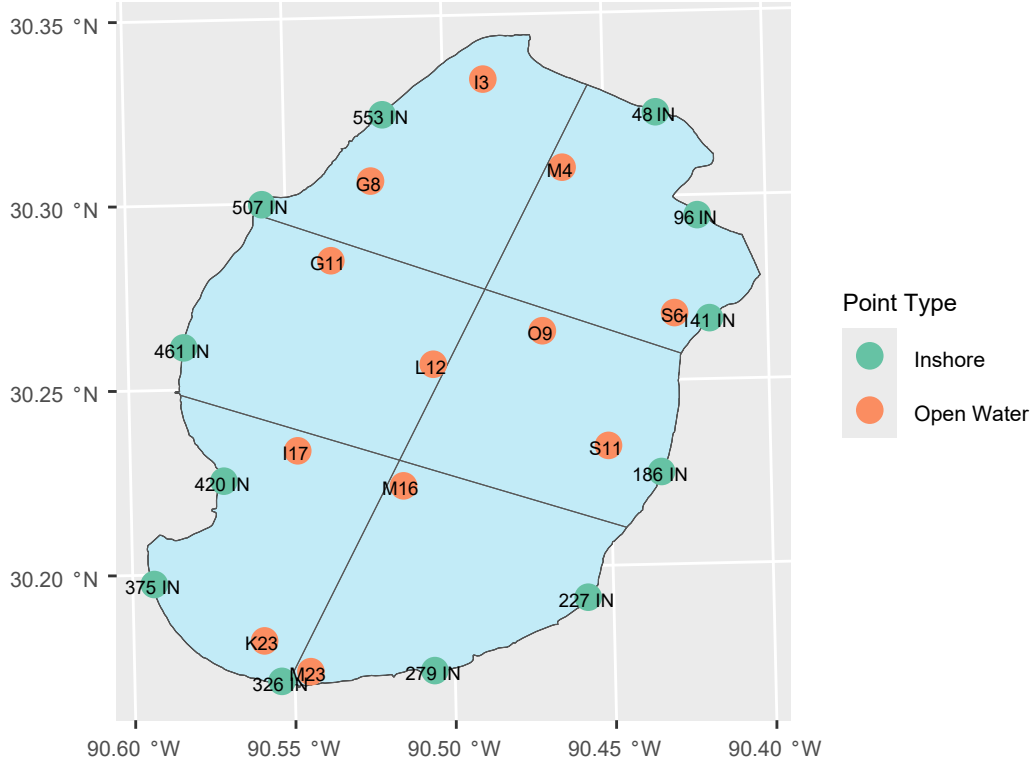


Figure 26. Points sampled in Lake Maurepas for eDNA in sampling period 1b of the current year.

Table 12. Fish detections made by eDNA sampling and fish species identified from field sampling.

eDNA	Both	Field
Speckled Worm Eel	Alligator Gar	American Eel
Bay Whiff	Atlantic Croaker	Largemouth Bass
Barred Grunt	Atlantic Needlefish	Smallmouth Buffalo
Black Redhorse	Bay Anchovy	Gizzard Shad
Blacktail Shiner	Bigmouth Buffalo	Ladyfish
Blue Runner	Black Drum	Redear Sunfish
Bullhead Minnow	Channel Catfish	Longnose Gar
Cobia	Bluegill	Hogchoker
Common Snook	Blue Catfish	Gulf Pipefish
Gaftsailsail Catfish	Flathead Catfish	Clown Goby
Golden Topminnow	Freshwater Drum	Sand Seatrout
Inshore Lizardfish	Gulf Menhaden	Chain Pipefish
Gulf Toadfish	Hardhead Catfish	Skipjack Herring
Pigfish	Threadfin Shad	White Bass
Naked Sand Darter	Inland Silverside	Yellow Bass

Least Puffer	Longear Sunfish	Black Crappie
Sharpfin Chubsucker	Naked Goby	Gulf Sturgeon
Western Mosquitofish	Sheepshead	Atlantic Stingray
Northern Hog Sucker	Freshwater Goby	Redspotted Sunfish
Blackspotted Topminnow	Southern Flounder	Gulf Killifish
Pinfish	Spot	Silver Carp
Corocoro Grunt	Spotted Gar	Gafftopsail Catfish
Dwarf Goatfish	Red Drum	Black Bullhead
Shadow Bass	Striped Mullet	Yellow Bullhead
River Carpsucker	White Crappie	Lepomis Sp.
Silver Seatrout		Orangespotted Sunfish
Scaled Sardine		Atlantic Tarpon
Silver Perch		
Southern Kingfish		
Spotted Bass		
Spotted Sucker		
Orangespotted Blenny		
Skilletfish		
Gulf Darter		
Weed Shiner		
Warmouth		
Saddleback Darter		
Vermillion Snapper		

Literature Cited

- Archambault, A., E. L. Wenner, and D. Whitaker. 1990. Life History and Abundance of Blue Crab, *Callinectes sapidus* Rathbun, at Charleston Harbor, South Carolina. *Bulletin of Marine Science* 46: 145–58.
- Ault, J., N. Zurcher, N. Farmer, E. Perusquia, J. Luo, J. Ault, J. Posada, et al. 2007. Population Dynamics and Resource Ecology of Atlantic Tarpon and Bonefish. In, 20074112:217–58. CRC Press. <http://www.crcnetbase.com/doi/abs/10.1201/9781420004250.sec3>.
- Baer, Ashley M., G. C. Constant, K. D. Kimmel, M. A. Dance, and J. N. Brogdon. 2024. Spatial and Temporal Distribution of Juvenile Gulf Sturgeon in the Pearl River, Louisiana, and Adjacent Estuaries of the Gulf of Mexico. *North American Journal of Fisheries Management* 44: 551–71. <https://doi.org/https://doi.org/10.1002/nafm.10984>.

- Beukema, J. 1992. Dynamics of Juvenile Shrimp *Crangon crangon* in a Tidal-Flat Nursery of the Wadden Sea After Mild and Cold Winters. *Marine Ecology Progress Series* 83: 157–65.
<https://doi.org/10.3354/meps083157>.
- Brogdon, J. 2022. Characterizing Habitat Suitability for Gulf Sturgeon (*Acipenser oxyrinchus desotoi*) in Southern Louisiana. PhD thesis, Louisiana State University.
https://doi.org/10.31390/gradschool_theses.5650.
- Brogdon, J. N., A. Baer, G. Constant, C. N. Glaspie, M. D. Miner, L. Y. Georgiou, and M. A. Dance. 2024. Variability in Estuarine Habitat Use of a Threatened Species in the Northern Gulf of Mexico: Implications for Coastal Restoration. *Global Ecology and Conservation* 49 (January): e02766. <https://doi.org/10.1016/j.gecco.2023.e02766>.
- Brunson, J. F., K. A. Sitta, M. R. Kendrick, and P. R. Kingsley-Smith. 2024. Evidence for a Male Bias in Atlantic Blue Crab Pot-Based Sampling. *North American Journal of Fisheries Management* 44: 101–12. <https://doi.org/https://doi.org/10.1002/nafm.10962>.
- Correia, K. M., S. B. Alford, B. A. Belgrad, K. M. Darnell, M. Z. Darnell, B. T. Furman, M. O. Hall, et al. 2024. Hurricane Effects on Seagrass and Associated Nekton Communities in the Northern Gulf of Mexico. *Estuaries and Coasts* 47: 162–75.
<https://doi.org/10.1007/s12237-023-01276-w>.
- Crabtree, R. E., E. C. Cyr, D. C. Chaverri, W. O. McLarney, and J. M. Dean. 1997. Reproduction of Tarpon, *Megalops atlanticus*, From Florida and Costa Rican Waters and Notes on Their Age and Growth. *Bulletin of Marine Science*. 61:271-285.
- Darnell, R. M. 1958. Food Habits of Fishes and Larger Invertebrate of Lake Pontchartrain, Louisiana, and Estuarine Community. *Publ. Inst. Mar. Sci. Univ. Texas* 5:353-416.
- DeLancey, L., E. Wenner, and J. Jenkins. 2008. Long-Term Trawl Monitoring of White Shrimp, *Litopenaeus setiferus* (Linnaeus), Stocks Within the ACE Basin National Estuarine Research Reserve, South Carolina. *Journal of Coastal Research* 10055 (November): 193–99.
<https://doi.org/10.2112/SI55-007.1>.
- Drymon, J. M., M. B. Jargowsky, M. A. Dance, M. Lovell, C. Lou Allen Hightower, A. E. Jefferson, A. M. Kroetz, and S. P. Powers. 2021. Documentation of Atlantic Tarpon (*Megalops atlanticus*) Space Use and Move Persistence in the Northern Gulf of Mexico Facilitated by Angler Advocates. *Conservation Science and Practice* 3: e331.
<https://doi.org/10.1111/csp2.331>.
- Edwards, R. E., K. J. Sulak, M. T. Randall, and C. B. Grimes. 2003. Movements of Gulf Sturgeon

- (*Acipenser oxyrinchus desotoi*) in Nearshore Habitat as Determined by Acoustic Telemetry. *Gulf of Mexico Science* 21 (1). <https://doi.org/10.18785/goms.2101.05>.
- Epifanio, C. E. 2019. Early Life History of the Blue Crab *Callinectes sapidus*: A Review. *Journal of Shellfish Research* 38 (1): 1. <https://doi.org/10.2983/035.038.0101>.
- Fox, D. A., J. E. Hightower, and F. M. Parauka. 2002. Estuarine and Nearshore Marine Habitat Use by Gulf Sturgeon from the Choctawhatchee River System, Florida. *American Fisheries Society Symposium*, 28: 111-126.
- Herzog, D. P., D. E. Ostendorf, R. A. Hrabik, and V. A. Barko. 2009. The Mini-Missouri Trawl: A Useful Methodology for Sampling Small-Bodied Fishes in Small and Large River Systems. *Journal of Freshwater Ecology* 24: 103-108. [10.1080/02705060.2009.9664270](https://doi.org/10.1080/02705060.2009.9664270)
- Hightower, J.E., K. P. Zehfuss, D. A. Fox, and F. M. Parauka. 2002. Summer Habitat Use by Gulf Sturgeon in the Choctawhatchee River, Florida. *Journal of Applied Ichthyology* 18:595-600.
- Hines, A., R. Lipcius, and A. Haddon. 1987. Population Dynamics and Habitat Partitioning by Size, Sex, and Molt Stage of Blue Crabs *Callinectes sapidus* in a Sub-Estuary of Central Chesapeake Bay. *Marine Ecology Progress Series* 36: 55–64. <https://doi.org/10.3354/meps036055>.
- Howe, J. C., R. K. Wallace, and F. S. Rikard. 1999. Habitat Utilization by Postlarval and Juvenile Penaeid Shrimps in Mobile Bay, Alabama. *Estuaries* 22: 971. <https://doi.org/10.2307/1353076>.
- Hubert, W. A., and M. C. Fabrizio. 2007. Relative Abundance and Catch Per Unit Effort. In, 279–325. Bethesda, Maryland: American Fisheries Society.
- Jaffer, Y. D., R. Saraswathy, M. Ishfaq, Jose Antony, D. S. Bundela, and P. C. Sharma. 2020. Effect of Low Salinity on the Growth and Survival of Juvenile Pacific White Shrimp, *Penaeus vannamei*: A Revival. *Aquaculture* 515:734561. <https://doi.org/10.1016/j.aquaculture.2019.734561>.
- Li, J., and A. J. Clarke. 2005. Sea Surface Temperature and the Brown Shrimp (*Farfantepenaeus Aztecus*) Population on the Alabama, Mississippi, Louisiana and Texas Continental Shelves. *Estuarine, Coastal and Shelf Science* 64: 261–66. <https://doi.org/10.1016/j.ecss.2005.02.019>.

- Luo, J., J. S. Ault, B. T. Ungar, S. G. Smith, M. F. Larkin, T. N. Davidson, D. R. Bryan, et al. 2020. Migrations and Movements of Atlantic Tarpon Revealed by Two Decades of Satellite Tagging. *Fish and Fisheries* 21: 290–318. <https://doi.org/10.1111/faf.12430>.
- Mace, M. M., and L. P. Rozas. 2015. Estimating Natural Mortality Rates of Juvenile White Shrimp *Litopenaeus setiferus*. *Estuaries and Coasts* 38: 1580–92. <https://doi.org/10.1007/s12237-014-9901-7>.
- Miranda, L. E., M. D. Habrat, and S. Miyazono. 2008. Longitudinal Gradients Along a Reservoir Cascade. *Transactions of the American Fisheries Society* 137: 1851–65. <https://doi.org/10.1577/T07-262.1>.
- Morrow, J. V, J. P. Kirk, K. J. Killgore, H. Rogillio, and C. Knight. 1998. Status and Recovery Potential of Gulf Sturgeon in the Pearl River System, Louisiana– Mississippi. *North American Journal of Fisheries Management* 18: 798–808.
- Parauka, F. M., M. S. Duncan, and P. A. Lang. 2011. Winter Coastal Movement of Gulf of Mexico Sturgeon Throughout Northwest Florida and Southeast Alabama. *Journal of Applied Ichthyology* 27 (2): 343–50. <https://doi.org/https://doi.org/10.1111/j.1439-0426.2011.01671.x>.
- Parker, S. W., T. S. Coleman, A. K. Carlson, and J. R. Fischer. 2023. Characterization of Fish Assemblages in Eleven Multi-Use Reservoirs from North Carolina, USA. *Journal of Freshwater Ecology* 38: 2241494. <https://doi.org/10.1080/02705060.2023.2241494>.
- Peterson, G. W., and R. E. Turner. 1994. The Value of Salt Marsh Edge Vs Interior as a Habitat for Fish and Decapod Crustaceans in a Louisiana Tidal Marsh. *Estuaries* 17: 235. <https://doi.org/10.2307/1352573>.
- Rome, N. E., S. L. Conner, and R. T. Bauer. 2009. Delivery of Hatching Larvae to Estuaries by an Amphidromous River Shrimp: Tests of Hypotheses Based on Larval Molting and Distribution. *Freshwater Biology* 54:1924–32.
- Stein, W. 2013. Fish and Decapod Community Structure in Estuarine Habitats of the New Orleans Land Bridge, Including a Description of the Life Cycle of Tarpon (*Megalops atlanticus*) in Southeastern Louisiana. *University of New Orleans Theses and Dissertations*.
- Stephens, S. A., M. A. Dance, M. Zapp Sluis, R. J. Kline, M. K. Streich, G. W. Stunz, A. J. Adams, R. J. D. Wells, and J. R. Rooker. 2024. Spatial Distribution and Movement of Atlantic Tarpon (*Megalops atlanticus*) in the Northern Gulf of Mexico. *PLOS ONE* 19 (3): e0298394. <https://doi.org/10.1371/journal.pone.0298394>.

Wilber, D. H., M. S. Peterson, and W. T. Slack. 2019. Cross-Site Comparisons of Gulf Sturgeon Prey Assemblages Throughout the Northern Gulf of Mexico Reveal Regional Differences. *Fisheries Research* 211 (March): 121–30. <https://doi.org/10.1016/j.fishres.2018.11.005>.

Appendix

Table A1: Average values and standard deviations for water quality parameters measured by handheld YSI on Lake Maurepas in the current year.

Sector	Sal (ppt)	Temp (F)	pH	DO (mg/L)	Turbidity (NTU)	TDS (mg/L)	Conductivity (μmhos/cm)
1	1.01 ± 0.4	76.52 ± 12.22	7.1 ± 0.32	7.95 ± 1.31	8.68 ± 6.28	1286.52 ± 479.46	1964.09 ± 711.02
2	0.94 ± 0.27	76.66 ± 12.01	7.02 ± 0.38	7.67 ± 1.32	7.27 ± 6.75	1209.87 ± 329.07	1825.38 ± 470.1
3	0.64 ± 0.28	80.14 ± 7.4	6.9 ± 0.29	7.11 ± 0.84	9.42 ± 6.47	839.45 ± 352.67	1322.42 ± 590.88
4	0.44 ± 0.24	79.21 ± 8.13	7 ± 0.35	7.25 ± 1.18	13.23 ± 7.88	579.82 ± 307.27	911.35 ± 469.97
5	0.61 ± 0.23	81.46 ± 7.4	7.14 ± 0.3	7.99 ± 0.87	10.6 ± 8.81	790.49 ± 288.94	1255.78 ± 421.94
6	0.86 ± 0.41	76.24 ± 12.35	7 ± 0.52	7.94 ± 1.45	9.5 ± 6.91	1091.38 ± 491.08	1616.12 ± 624.4

II. Aquatic Physiology Monitoring

Chris Murray, PhD

Southeastern Louisiana University, Dept. of Biological Sciences

Hammond, LA 70402

christopher.murray@selu.edu

Report prepared by: Tyler Steven Coleman, Wray Gabel, Anthony Johnson, Maggie McGreal, Christopher M. Murray

1. Overview

This report details the methodologies and outcomes of monitoring organismal physiological health in relation to anthropogenic influence and conservation objectives of biota in Lake Maurepas during the field sampling seasons of the Lake Maurepas Monitoring Program. Physiological stress indicators, endocrine disruption biomarkers, heavy metal concentrations, and organismal gas gradients were systematically monitored biannually in blue crabs (*Callinectes sapidus*), catfishes (*Ictalurus furcatus* and *I. punctatus*), bullfrogs (*Lithobates spp.*), and alligators (*Alligator mississippiensis*) across six designated seismic testing quadrats within the lake. The previously listed organisms are utilized as representative model species for the broader ecological community present within the system, as their physiological and biochemical responses provide insights that are broadly applicable to other taxa. The selected metrics enable the assessment of population-level risks with a resolution that surpasses the binary limitations of presence/absence data, population demography or environmental heavy metal or synthetic toxin detection from abiotic media, offering a more nuanced and predictive understanding of ecosystem health. In the near future, collected data will be analyzed spatially, temporally, and spatiotemporally to elucidate patterns and trends in organismal and environmental responses in the form of journal publications.

During Year 2 of the program, the team successfully captured blue crabs, catfishes, bullfrogs, and alligators throughout Lake Maurepas. Overall, the team has quantified [1] physiological stress using leukocyte profiling (catfishes, bullfrogs, alligators) and hemolymph density (blue crabs), [2] endocrine disruptor exposure using sex steroid concentrations and gonadal histopathology (catfishes, bullfrogs, alligators), [3] fecundity as a proxy for reproductive energy allocation (blue crabs), [4] heavy metal exposure using histopathological metrics (hepatopancreas and gill hyperplasia in blue crabs, liver hyperplasia in catfishes, bullfrogs, and alligators), [5] blood (catfishes, bullfrogs, alligators) or hemolymph (blue crabs) pH for osmotic gas gradient stress, [6] alligator nest survival and hatching success, and [7] alligator population demographics (e.g., size, growth rate, survival) with mark-recapture (Table 1).

Currently, the team is capturing blue crabs and catfishes for the new sampling period (from 01 November 2024 to 30 April 2025). Sampling for bullfrogs and alligators will resume

when the weather begins to warm (i.e., nighttime low temperature > 13°C [~55°F]) in early spring—sampling is limited due to the life history patterns of these animals.

Table 1. Total number of samples collected (Samples) for each data type (Data) from 01 November 2023 to 31 October 2024 for the monitoring program by group (Animal).

Animal	Data	Samples
<i>Blue Crabs</i>		
	Hemolymph density	91
	Fecundity	5
	Hepatopancreas histopathology	15
	Gill histopathology	14
	Hemolymph pH	30
<i>Catfishes</i>		
	Leukocyte profile	120
	Testosterone concentration	18
	Estradiol concentration	10
	Liver histopathology	15
	Gonad histopathology	14
	Hepatosomatic index	120
	Gonadosomatic index	120
	Blood pH	23
<i>Bullfrogs</i>		
	Leukocyte profile	11
	Testosterone concentration	<i>In progress</i>
	Estradiol concentration	<i>In progress</i>
	Liver histopathology	<i>In progress</i>
	Gonad histopathology	<i>In progress</i>
	Hepatosomatic index	10
	Gonadosomatic index	10
	Blood pH	0
<i>Alligator</i>		
	Leukocyte profile	95
	Testosterone concentration	15
	Estradiol concentration	22
	Blood pH	32
	Nest survivorship	<i>assessed</i>
	Population demography	<i>In progress</i>

2. Objectives

- Physiological stress using contemporary leukocyte profiling (bullfrog, catfishes, and alligator) and hemolymph density (blue crab).
- Endocrine disruptor exposure quantified using sex steroid concentration [testosterone (T) and 17 β -estradiol(E₂)] monitoring and gonadal histopathology.
- Fecundity as a proxy for reproductive energy allocation (blue crab).
- Heavy metal exposure using histopathological metrics quantifying liver hyperplasia and cirrhosis/fibrosis (bullfrog, catfishes, and alligator), hepatopancreas hyperplasia and cirrhosis/fibrosis, and gill histopathology (blue crab).
- Blood or hemolymph pH monitored to quantify osmotic gas gradient stress.
- Alligator population viability using nest counts, egg viability, and hatching success annually.
- Lastly, the Lake Maurepas alligator population will be monitored demographically (population size, growth rate, survivorship) with mark-recapture analysis.

3. Methods

3.1 Blue crabs

Blue crabs were captured via passive trapping in collaboration with the aquatics team (for exact sampling design, see Aquatics Team Report, Section 4.3). The first 10 crabs caught in each sector were collected and marked with a Floy tag, and hemolymph was drawn from the body cavity using a heparinized 1.5" 27-gauge needle and 1CC syringe. Each crab sampled was brought back to the laboratory. Crabs were euthanized using ganglia puncture followed by freezing (Hatfield Science Center SOP) and dissected for gill and hepatopancreas tissue samples. Tissues were fixed in neutral buffered formalin for histological analysis. Hepatopancreas and gill samples were histologically processed by the Louisiana Animal Disease Diagnostic Laboratory. Assessment of histopathology and gill malformations was performed by CMM and TSC. Hemolymph pH was quantified using an Orion Star A211 benchtop pH meter (Thermo Scientific). Hemolymph density was calculated by centrifuging whole hemolymph at 5,000 g for 5 minutes and cellular volume compared to the remaining substrate volume. Females collected were checked for eggs. Egg samples were divided into 1-gram subsets and counted at that weight. The entire egg mass was weighed, and 1g count was multiplied by the total weight. All weights were obtained on a digital Thermo Fisher analytic balance (Fisher Brand™).

3.2 Catfishes

Catfishes were captured in each sector using otter trawl and boat electrofishing sampling in collaboration with the aquatics team (for exact sampling design, see Aquatics Team Report, Section 4.4). The first 10 catfishes from each sector were sampled for the physiology team. A few (<20 total) larger catfishes (>40 cm) caught were also sampled for hypothesis-driven testing outside the specific focus of the Lake Maurepas Monitoring Program Report but are included herein. Whole blood was drawn from the caudal vein using a heparinized 23-gauge needle and 3CC syringe within five minutes of capture (Murray et al. 2013). Each animal was measured for total body mass (g), individually marked with a Floy tag (Floy Tag Inc.), and placed on ice for collection. In the laboratory, all catfish were dissected for sexing and hepatosomatic and gonadosomatic indices. Leukocyte profiles, blood pH, and plasma steroid samples were prepared and quantified as follows: For leukocyte profiles, whole blood was smeared one cell layer thick on a microscope slide, fixed in methanol, and stained using Geimsa Wright stain (VWR). The first 100 leukocytes were counted, and the ratio of heterophils to leukocytes was calculated (Murray et al., 2013). The remaining whole blood was used to quantify blood pH using an Orion Star A211 benchtop pH meter (Thermo Scientific), which was centrifuged, and plasma supernatant was removed for steroid hormone (T and E₂) concentration. Plasma samples were extracted for T using a methanol extraction protocol (Han and Liu. 2019), while E₂ samples were extracted using a 3:2 vol: vol ethyl acetate to hexane protocol (Murray et al., 2017). Samples were analyzed for T and E₂ concentrations using independent low-detection ELISA kits (Enzo Life Sciences) in duplicate with randomized pools. Liver and gonad samples were fixed in neutral buffered formalin and histologically processed by the Louisiana Animal Disease Diagnostic Laboratory. Assessment of histopathology hepatic and gonadal malformations were performed by CMM and TSC with assistance from D. Siegel (Southeast Missouri State University).

3.3 Bullfrogs

Bullfrogs were opportunistically sampled in all six sectors during the summer and fall of 2024. Whole blood was drawn from the caudal vein using a heparinized 3.81 cm 23 or 27-gauge needle and 1CC syringe within five minutes of capture (Murray et al. 2013). Back in the laboratory, all frogs were euthanized using a 300mg/L concentration of MS-222 (AVMA 2020) and dissected for sexing and hepatosomatic and gonadosomatic indices. Leukocyte profiles, blood pH, and plasma steroid samples were prepared and quantified as follows: For leukocyte profiles, whole blood was smeared one cell layer thick on a microscope slide, fixed in methanol, and stained using Geimsa Wright stain (VWR). The first 100 leukocytes were counted, and the ratio of heterophils to leukocytes was calculated (Murray et al. 2013). The remaining whole blood was used to quantify blood pH using an Orion Star A211 benchtop pH meter (Thermo Scientific), which was centrifuged, and plasma supernatant was removed for steroid hormone

(T and E₂) concentration. Plasma samples were extracted for T using a methanol extraction protocol (Han and Liu. 2019), while E₂ samples were extracted using a 3:2 vol: vol ethyl acetate to hexane protocol (Murray et al. 2017). Samples are undergoing analysis for T and E₂ concentrations using independent low-detection ELISA kits (Enzo Life Sciences) in duplicate with randomized pools. Liver and gonad samples were fixed in neutral buffered formalin and are undergoing histological processing by the Louisiana Animal Disease Diagnostic Laboratory. Assessment of histopathology hepatic and gonadal malformations will be performed by CMM and TSC with assistance from D. Siegel (Southeast Missouri State University).

3.4 Alligators

Alligators were captured opportunistically (dependent on weather and shoreline habitat) by hand or snare in each sector. Whole blood was drawn from the spinal vein using a heparinized 23-gauge needle and 3CC syringe within five minutes of capture (Murray et al. 2013). Each animal was sexed, total length and snout to vent length measured, and individually marked via caudal scute removal (Murray et al. 2013). All animals were released at the site of capture. Whole blood was smeared one cell layer thick on a microscope slide, fixed in methanol, and stained using Geimsa Wright stain (VWR). For leukocyte profiles, the first 100 leukocytes were counted, and the ratio of heterophils to leukocytes (HLR) was calculated (Murray et al., 2013). The remaining whole blood was used to quantify blood pH using an Orion Star A211 benchtop pH meter (Thermo Scientific), which was centrifuged, and plasma supernatant was removed for steroid hormone (T and E₂) concentration. Plasma samples were extracted for T using a methanol extraction protocol (Han and Liu. 2019), while E₂ samples were extracted using a 3:2 vol: vol ethyl acetate to hexane protocol (Murray et al. 2017). Samples are currently being analyzed for steroid hormone concentrations using low-detection ELISA kits. Nest survivorship and population demography will be assessed when sample size permits. HLR thresholds for allostatic load (stress) were set at 1:1 H:L, whereby above this ratio indicates a chronic stress response, and below this ratio indicates a lack thereof (Lance et al. 2010).

4. Results

Here, we summarize current results for 23 variables across blue crab, catfish, bullfrog, and alligator samples collected.

4.1 Blue crabs

A total of 116 blue crabs were collected during this phase. However, all variables were not collected for each of the 116 blue crabs caught (see Methods section). Hemolymph density varied between 0.7 and 1.69, with the highest density occurring in the southern and western portions of the lake (Figure 1). Blue crab hemolymph density was, on average, highest in Spring

2024 (Figure 2). Hemolymph pH was relatively stable spatially and temporally, ranging from 7.0 to 7.7.



Figure 1. Spatial distribution of crab hemolymph density collected in Lake Maurepas between 01 November 2023 and 01 November 2024 ($n = 80$, $\min = 0.7$, $\text{mean} = 1.03$, $\text{median} = 1.00$, $\text{max} = 1.69$, $\text{SD} = 0.158$). To improve clarity, transparency was set to 30% and overlapping points were slightly offset using a random dispersal method in ArcGIS Pro 2.4.0—the offset formula, $(\text{Random}() * 20) - 10$, was applied to both latitude and longitude.

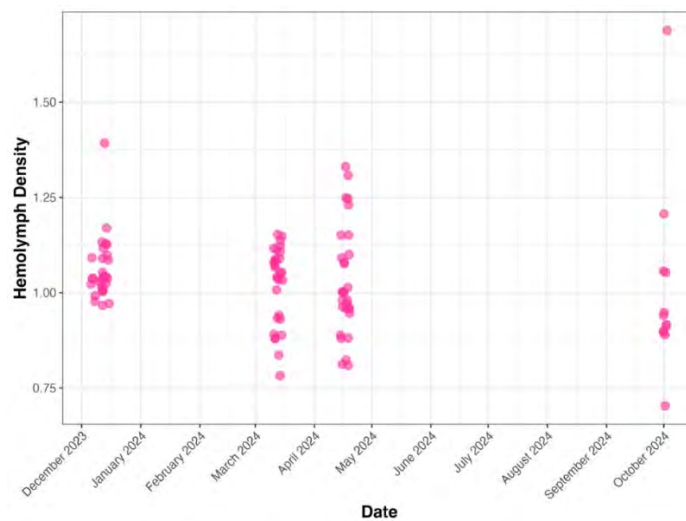


Figure 2. Temporal variation in blue crab hemolymph density in Lake Maurepas between 01 November 2023 and 01 November 2024.

Of the 116 blue crabs collected for physiological assessment, 5 were female, and none possessed roe (Figure 3). As a result, fecundity was 0, but concern regarding sex ratio and sex-biased sampling should take precedence in 2025; as we know, crab pots are a heavily male-biased sampling technique.



Figure 3. Distribution of male and female blue crabs sampled in Lake Maurepas between 01 November 2023 and 01 November 2024. Purple points represent female crabs ($n = 5$), and yellow points represent male crabs ($n = 76$). To improve clarity, transparency was set to 30% and overlapping points were slightly offset using a random dispersal method in ArcGIS Pro 2.4.0—the offset formula, $(Random() * 20) - 10$, was applied to both latitude and longitude.

Hepatopancreas histology revealed very few intact lobular hepatocyte arrangements nor richly uniform connective tissue between hepatocytes. Vacuolations and obliterated lumen were present in all the analyzed samples. Hepatocyte hypertrophy was observed in 25% of specimens. Necrotic fibrosis was observed in a single specimen (Figure 4).

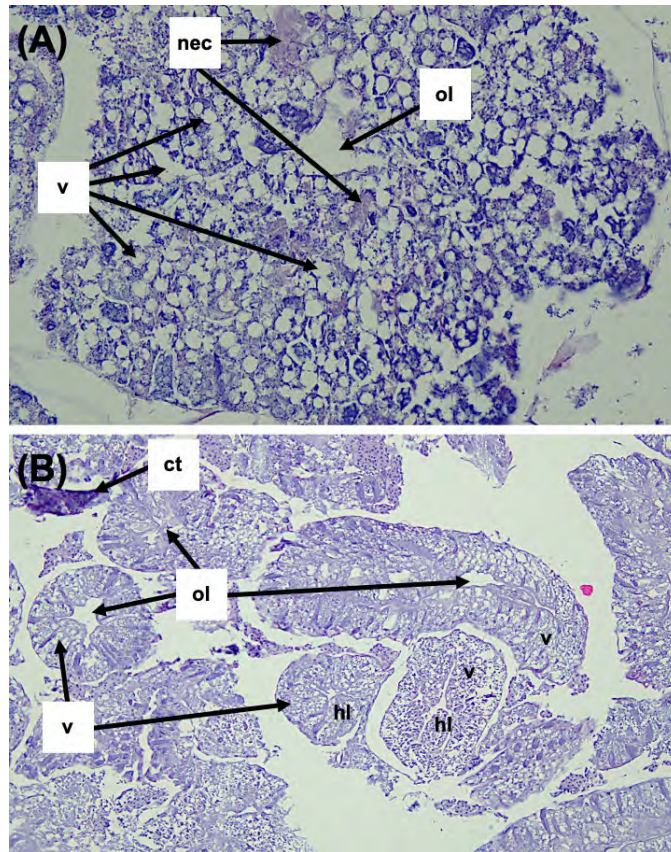


Figure 4. Lake Maurepas, LA, USA, blue crab hepatopancreatic tissue stained using *Nissl* stain. Photo A (x400 magnification) exhibits severe vacuolations (v), necrosis (nec), and large obliterated lumen (ol); photo B (x40 magnification) depicts minor vacuolation (v), loose connective tissue (ct), obliterated lumen (ol), and healthy lumen (hl).

Histological analysis of blue crab gills revealed numerous abnormalities across samples, including basophilic deposition, detached cuticles, lamellar hyperplasia, and isolated necrosis (Figure 5). These pathologies were widespread across specimens, with only one crab (sector 2) exhibiting normal lamellar structure (Figure 5C). The prevalence of pathologies was distributed evenly among samples, with 4 of 13 exhibiting necrosis and 3 of 13 exhibiting basophilic deposition. Five of the samples exhibited cuticle and/or epithelial detachment. Severe swelling of the distal lamellar was also exhibited in association with epithelial lifting (Figure 5B).

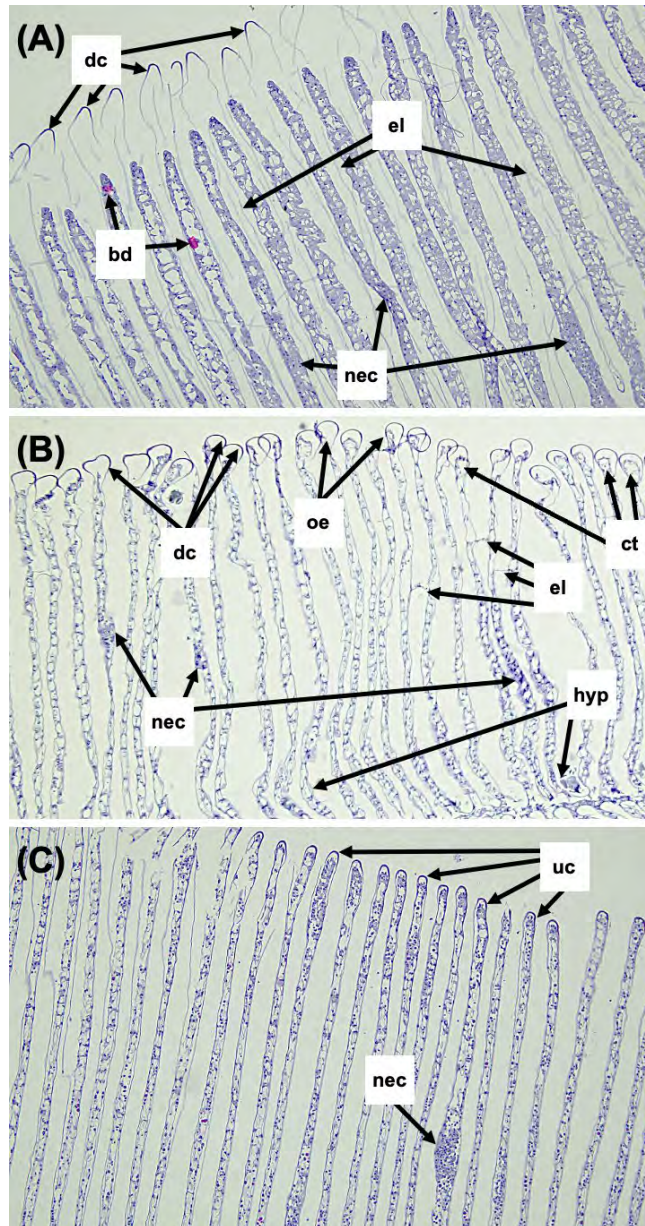


Figure 5. Lake Maurepas, LA, USA, blue crab gill tissue stained using *Nissl* stain. Photo (A) is species ID 409 (female) at x100 magnification, and photo (B) is species ID 410 (male) at x40 magnification, where we observe major degenerative effects, such as oedematous (oe) swelling of the secondary lamella tip, detached cuticles (dc), and clubbed tip (ct), as well as minor to major histopathological lesions including epithelial lifting (el), necrosis (nec), basophilic deposition (bd), and hyperplasia (hyp). Photo (C) is species ID 408 (male) at x40 magnification, where we observe an overall healthy secondary gill lamellar with numerous undetached cuticles (uc) and minor necrosis (nec).

4.2 Catfishes

A total of 125 catfishes were collected throughout the program thus far (from 01 August 2022 to 01 November 2024; Figure 6). Of the 125 catfishes collected, 54 were male, 52 were female, and 19 are unknown, with randomly distributed spatial distributions (Figure 7). In other words, there seems to be no spatial pattern in catfish sex. All catfishes collected from 01 August 2022 to 01 November 2024 are included in this report. Catfish leukocyte profiles (NLR) calculated in Lake Maurepas were greatest in the northernmost portion of the lake (Figure 8) and during the summer of 2023 (Figure 9), representing highest stress.



Figure 6. Location of catfishes sampled in Lake Maurepas from 01 August 2022 to 01 November 2024 (n = 125). To improve clarity, overlapping points were slightly offset using a random dispersal method in ArcGIS Pro 2.4.0. The offset formula, $(Random() * 20) - 10$, was applied to both latitude and longitude. Additionally, point transparency was set to 40% to better visualize overlapping symbols.



Figure 7. Distribution of catfishes sampled that were identified by sex in Lake Maurepas, LA, USA, symbolized by sex since October 2022. Orange points represent catfish identified as female ($n = 52$), and blue points represent catfish identified as male ($n = 54$). To improve clarity, overlapping points were slightly offset using a random dispersal method in ArcGIS Pro 2.4.0. The offset formula, $(Random() * 20) - 10$, was applied to both latitude and longitude. Additionally, point transparency was set to 30% to better visualize overlapping symbols.



Figure 8. Spatial variation in Neutrophil-to-Leukocyte Ratios of catfishes collected in Lake Maurepas since October 2022 ($n = 105$, $\text{min} = 0.04$, $\text{median} = 0.26$, $\text{max} = 5.93$, $\text{SD} = 0.78$). To improve clarity, overlapping points were slightly offset using a random dispersal method in ArcGIS Pro 2.4.0. The offset formula, $(\text{Random}() * 20) - 10$, was applied to both latitude and longitude. Additionally, point transparency was set to 30% to better visualize overlapping symbols.

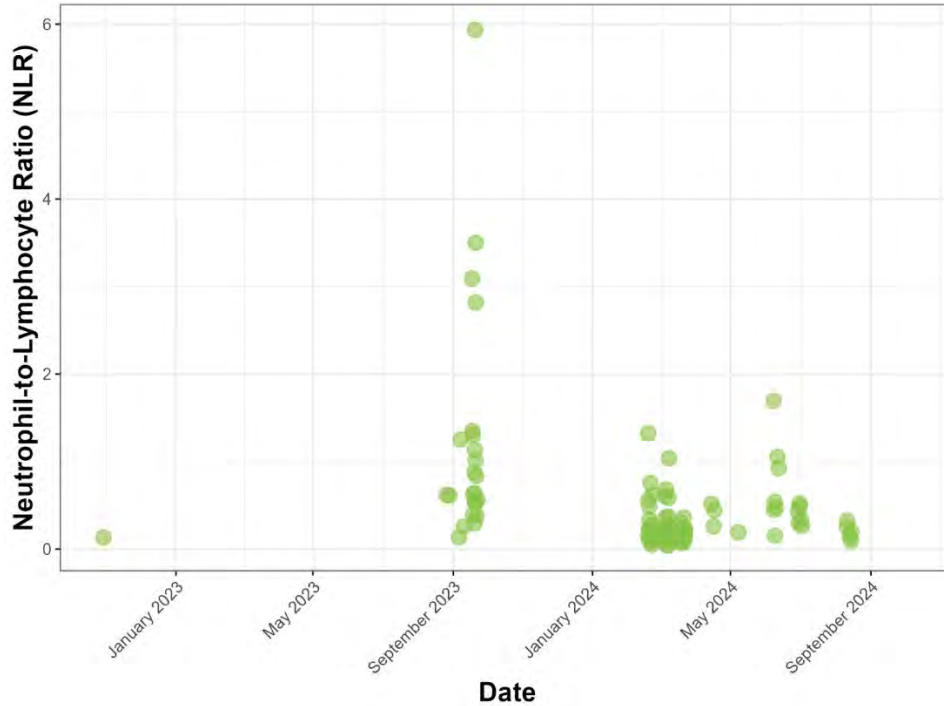


Figure 9. Temporal variation in Neutrophil-to-Leukocyte Ratio (NLR) of catfishes collected in Lake Maurepas since October 2022 (n = 105, min = 0.04, median = 0.26, max = 5.93, SD = 0.78).

Of the 31 catfish blood pH samples, blood pH ranged from 5.4 to 8.2, with a median of 7.3 (Figure 10). In the 106 catfish HSI samples, HSI ranged from 0.0060 to 0.062, and had a median of 0.013. Patterns of higher HSI were located in the eastern portion of the lake (Figure 11), lacking a noticeable temporal pattern (Figure 12). Similar trends were observed in GSI. Male and female catfish were separated when observing GSI because male GSI values are typically much lower than females due to gonad morphology. The minimum and maximum GSI in the 46 female catfish were 0.000096 and 0.22, respectively, and 0.000098 and 0.027 in male catfish, respectively (Figure 13). Highest female GSI was observed along the shoreline of the lake, compared to open water, whereas male GSI was highest in the southeastern portion of the lake (Figure 13). Female GSI seemed overall higher in the spring of 2023, and male GSI had no temporal trend (Figure 14).

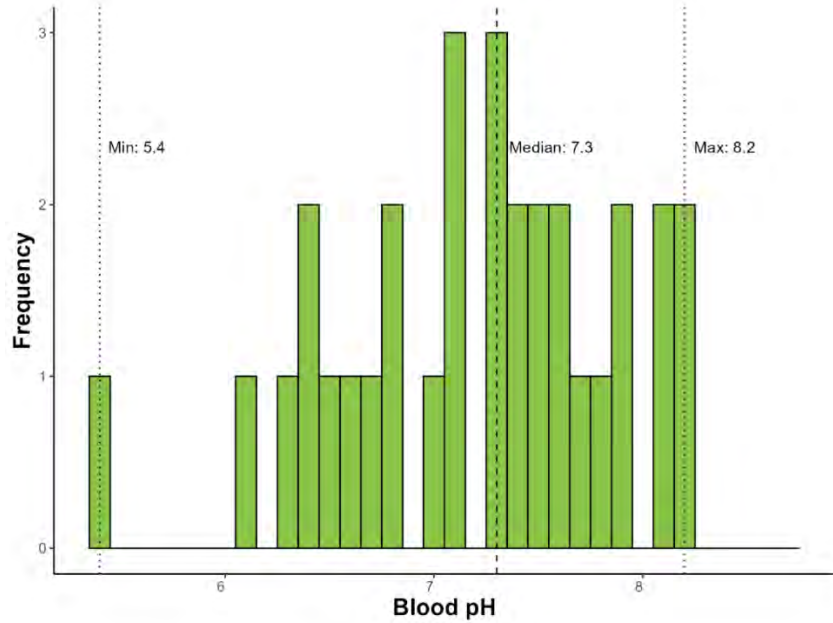


Figure 10. Observed catfish blood pH values in sampled Lake Maurepas, LA, USA, catfish from 01 August 2022 to 01 November 2024 (n = 31, min = .54, median = 7.3, max = 8.2, SD = 0.68).



Figure 11. Spatial distribution of catfish Hepatosomatic Index (HSI) collected in Lake Maurepas, LA, USA, between 01 August 2022 and 01 November 2024 (n = 106, min = 0.0060, median = 0.013, max = 0.062). To improve clarity, overlapping points were slightly offset using a random dispersal method in ArcGIS Pro 2.4.0. The offset formula, $(Random() * 20) - 10$, was applied to both latitude and longitude. Additionally, point transparency was set to 30% to better visualize overlapping symbols.

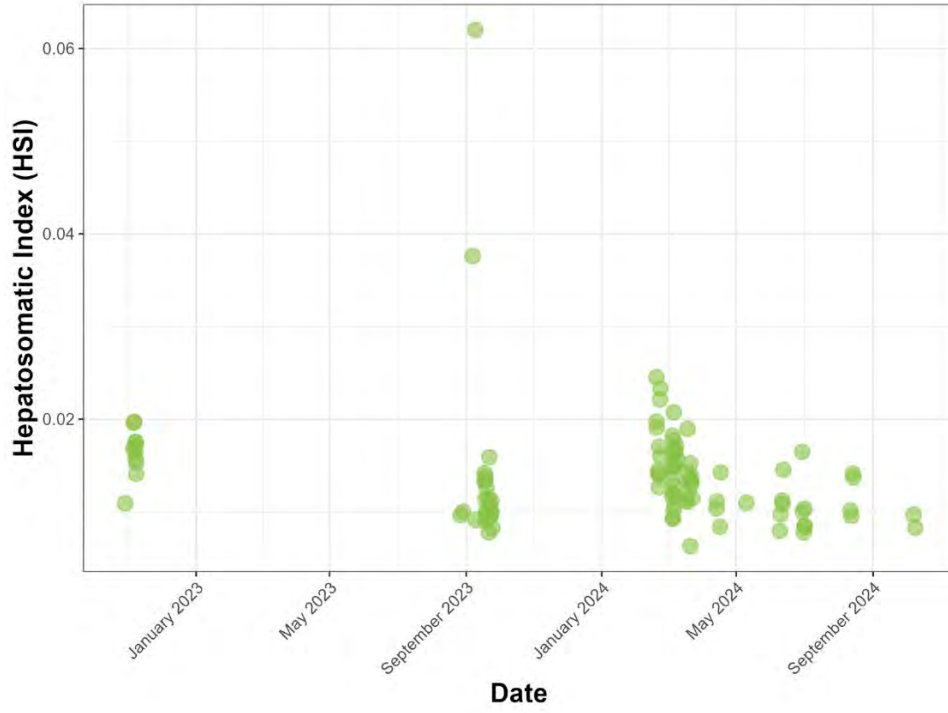


Figure 12. Temporal variation in Hepatosomatic Index (HSI) of catfish collected in Lake Maurepas from 01 August 2022 to 01 November 2024 (n = 106).

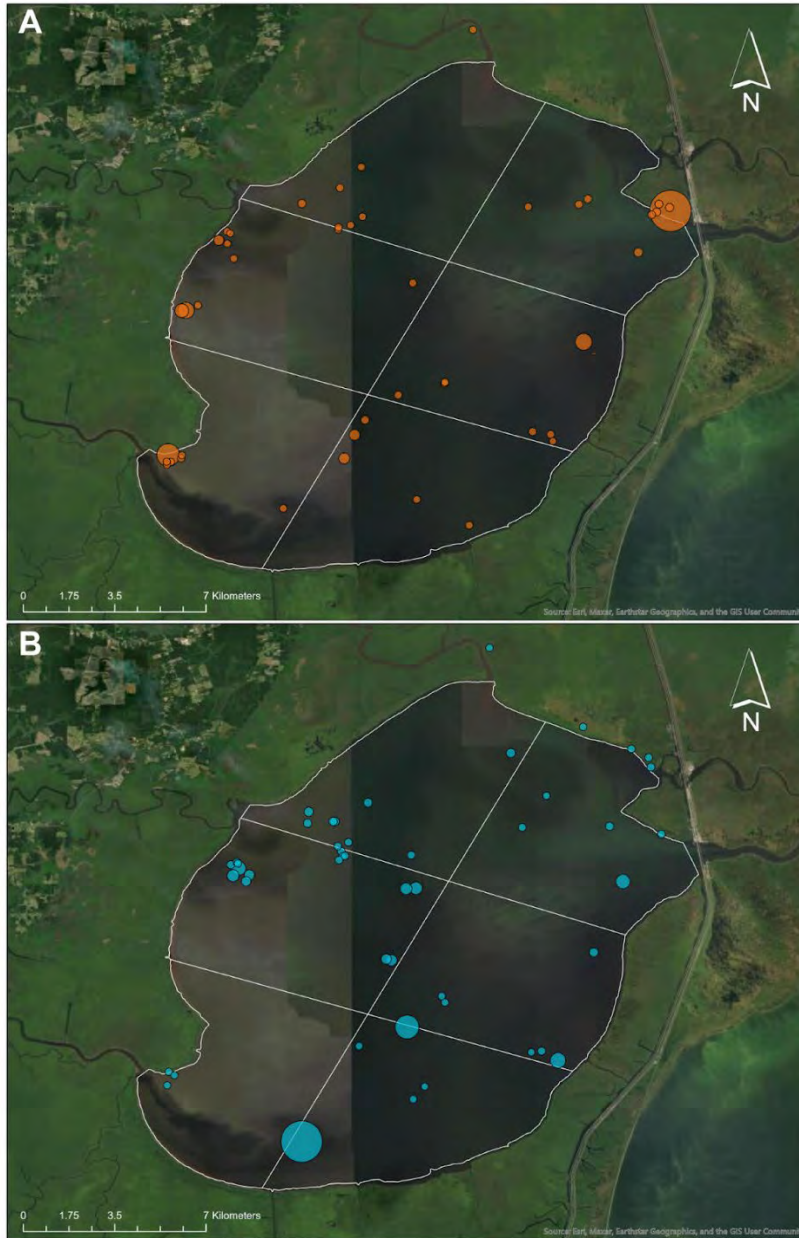


Figure 13. Spatial distribution of Gonadosomatic Index (GSI) of (A) female catfish ($n = 45$, $\min = 0.000096$, $\text{median} = 0.0022$, $\text{max} = 0.22$, $\text{SD} = 0.037$). and (B) male catfish ($n = 48$, $\min = 0.000098$, $\text{median} = 0.00060$, $\text{max} = 0.027$, $\text{SD} = 0.0044$) collected in Lake Maurepas, LA, USA, from 01 August 2022 to 01 November 2024. Proportional point sizes are relative to sex, as male GSI values are typically much lower than females due to gonad morphology. To improve clarity, overlapping symbols were slightly offset using a random dispersal method in ArcGIS Pro, using the formula $(\text{Random}() * 20) - 10$ to offset both latitude and longitude and 30% symbol transparency was used.

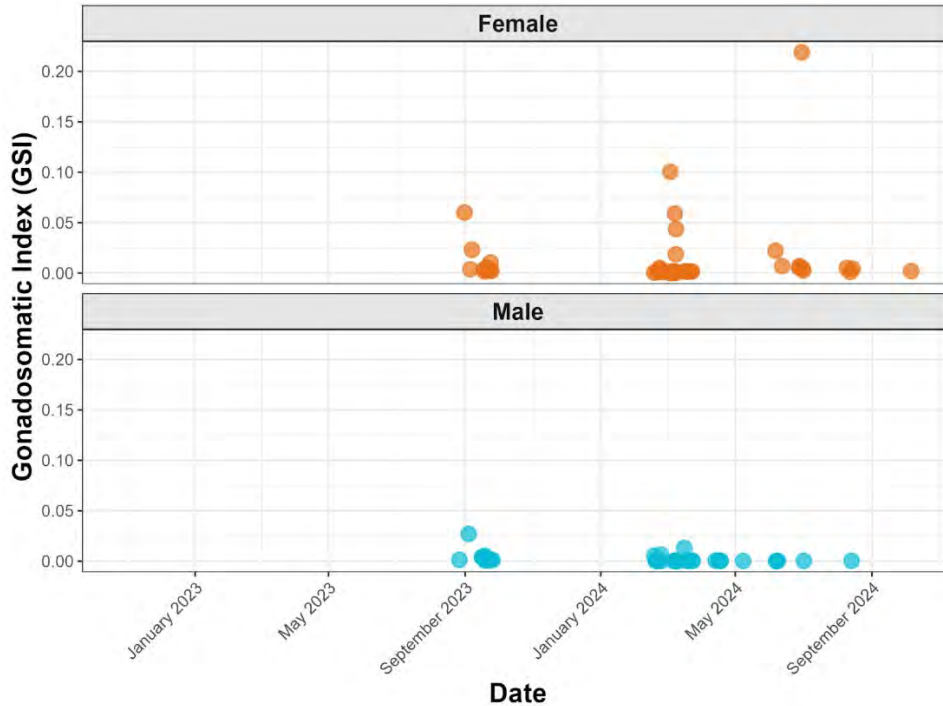


Figure 14. Temporal distribution of Gonadosomatic Index (GSI) of female catfish (top) and male catfish (bottom) collected in Lake Maurepas, LA, USA, from 01 August 2022 to 01 November 2024.

Histological analysis of catfish liver revealed numerous abnormalities across samples, including hepatocyte vacuolation, sporadic fibrosis, and poor hepatocyte organization. These pathologies were widespread across specimens, where over 50% experienced at least minor fibrosis and 75% show some hepatocyte vacuolation (Figure 15). One specimen revealed fibrosis bordering cirrhosis (Figure 16). Another specimen experienced notable fibrosis or collagen buildup, which is indicative of xenobiotic overload (Figure 17). Histological analysis of catfish gonads revealed zero abnormalities across male and female samples. Figure 18 shows large embryos with no abnormalities detected. One specimen revealed an early stage folliculogenesis in testes (Figure 19).

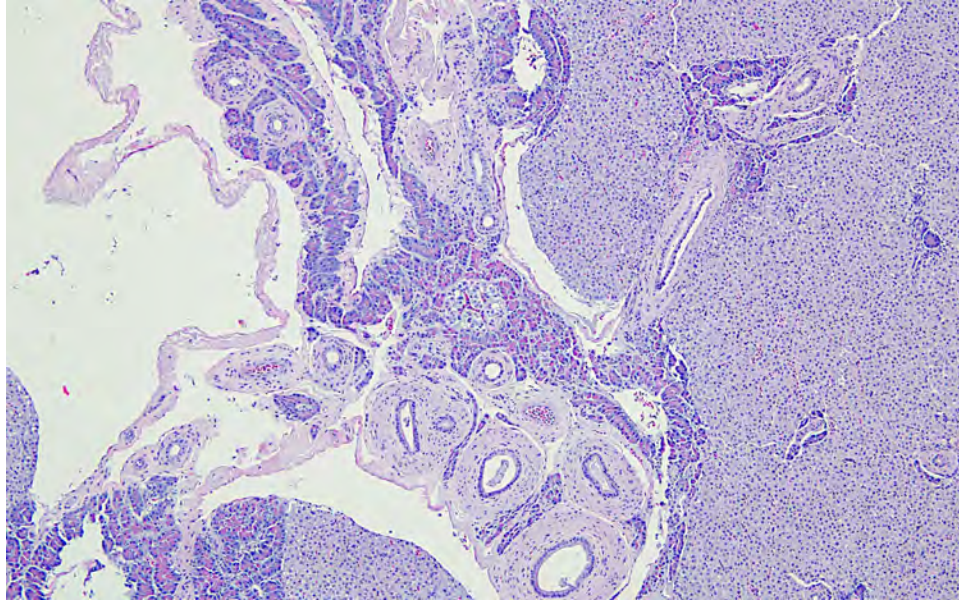


Figure 15. Lake Maurepas, LA, USA, catfish liver tissue stained using *Nissl* stain. Photo (x40 magnification) exhibits severe hepatocyte vacuolation (large circles in hepatocytes) and fibrosis (see Figure 16 for a close-up of fibrosis).

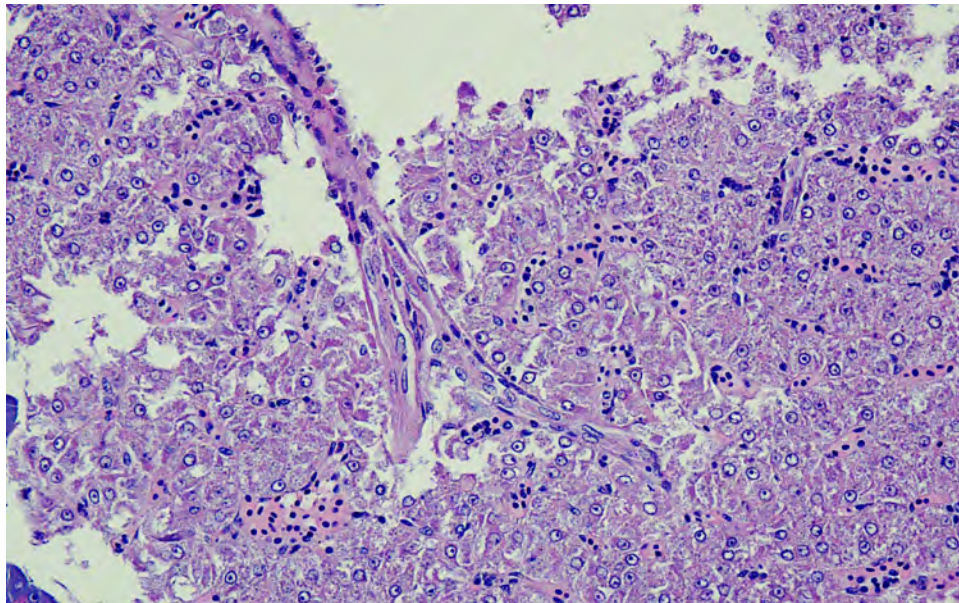


Figure 16. Lake Maurepas, LA, USA, catfish liver tissue ID 76 stained using *Nissl* stain. Photo (x400 magnification) exhibits severe fibrosis bordering cirrhosis.

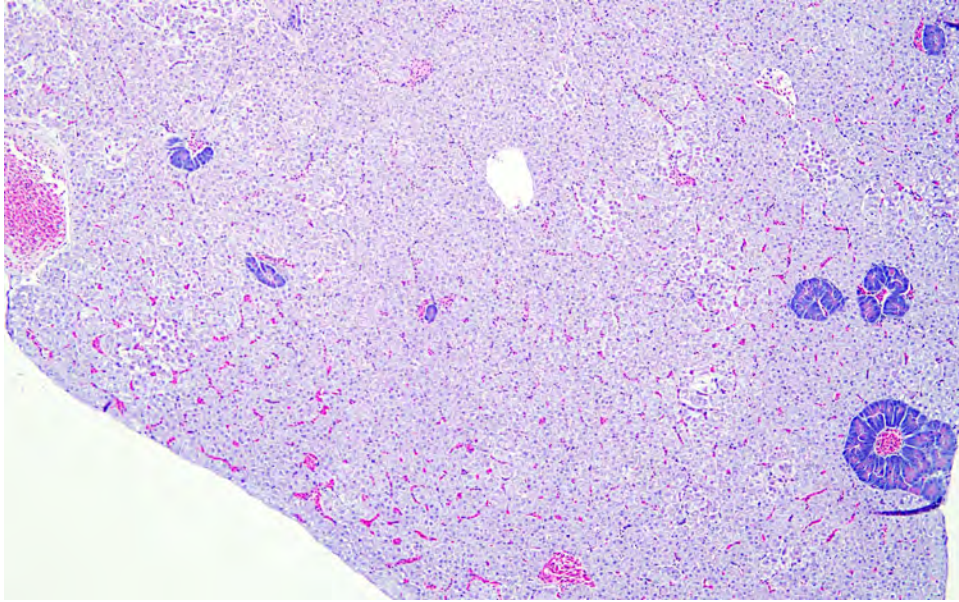


Figure 17. Lake Maurepas, LA, USA, catfish liver tissue ID 68 stained using *Nissl* stain. Photo (x40 magnification) exhibits notable fibrosis or collagen buildup (pink) and severe hepatocyte vacuolation (bottom right).

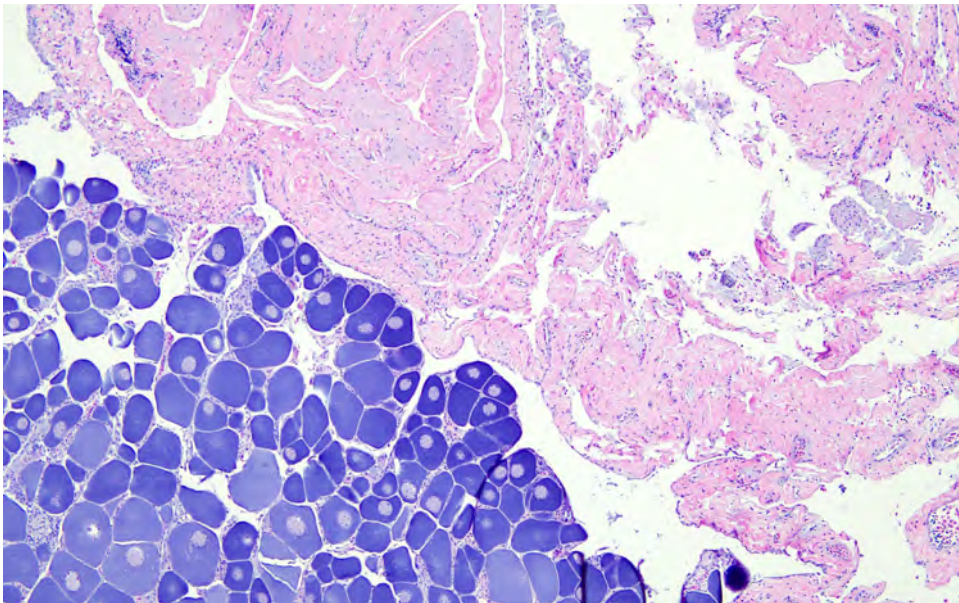


Figure 18. Lake Maurepas, LA, USA, catfish gonad tissue ID 16 stained using *Nissl* stain. Photo (x40 magnification) exhibits large embryos (dark purple) with no abnormalities.

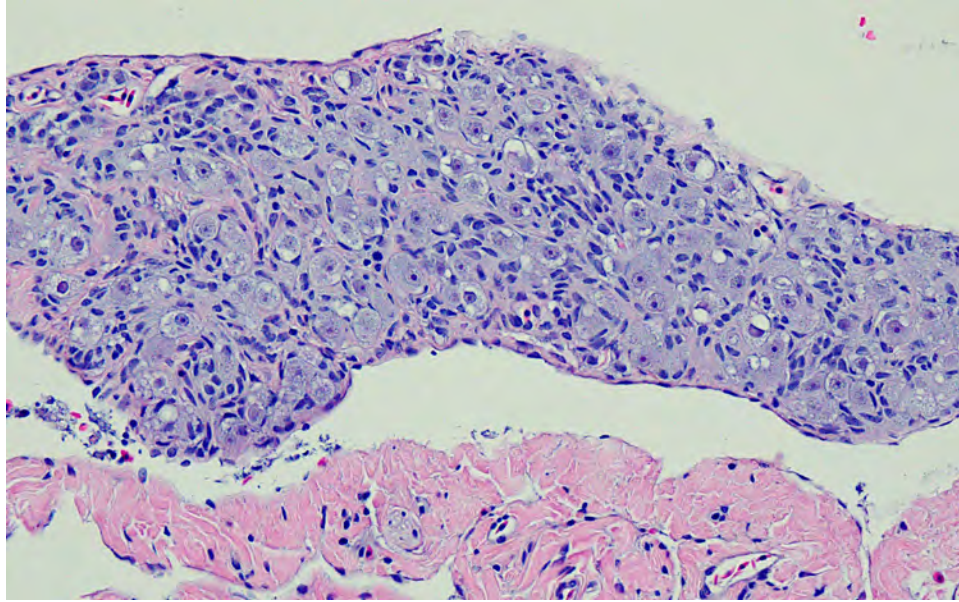


Figure 19. Lake Maurepas, LA, USA, catfish gonad tissue ID 89 stained using *Nissl* stain. Photo (x40 magnification) reveals potentially loose folliculogenesis in what otherwise exhibits testicular structure (dark purple).

Testosterone concentrations ranged from 0.40 ng mL^{-1} to 1.28 ng mL^{-1} in males and from 0.60 ng mL^{-1} to 0.84 ng mL^{-1} in females. Estradiol concentrations ranged from 0.044 ng mL^{-1} to 1.32 ng mL^{-1} in females and from 0.035 ng mL^{-1} to 0.50 ng mL^{-1} in males.

4.3 Bullfrogs

NLR averaged 0.31 (0.14 to 0.94) across all sexes and sizes with the highest NLR located in Galva Canal between the Louisiana Department of Wildlife and Fisheries boat launch and South Pass. HSI ranged from 0.004 to 0.026 across all sexes and sizes. GSI ranged from 0.002 to 0.004 in juveniles and 0.005 to 0.038 in adult females.

4.4 Alligators

Alligators were caught throughout the lake ($n = 92$) with a 1.29:1 male-to-female sex ratio (Figure 20). Total lengths ranged from 28cm to 263cm, and the sampled population exhibited a top-heavy size structure with a high frequency of small adults (Figure 21). Heterophil to lymphocyte ratios (HLR) ranged from 0.19 to 2.28, with the majority of elevated HLR occurring on the east side of Lake Maurepas along the interstate canal and Owl Bayou area (Figure 22). Temporally, the highest HLRs were recorded between March and May 2024 (Figure 23).



Figure 20. Sex distribution of alligators sampled in Lake Maurepas, LA, USA, from 01 August 2023 to 01 November 2024. Magenta points represent alligators identified as female (n = 40), blue represents male (n = 51), and grey represents alligators where sex was not confirmed (n = 1). To improve clarity, overlapping points were slightly offset using a random dispersal method in ArcGIS Pro 2.4.0. The offset formula, $(Random() * 20) - 10$, was applied to both latitude and longitude. Additionally, point transparency was set to 30% to better visualize overlapping symbols.

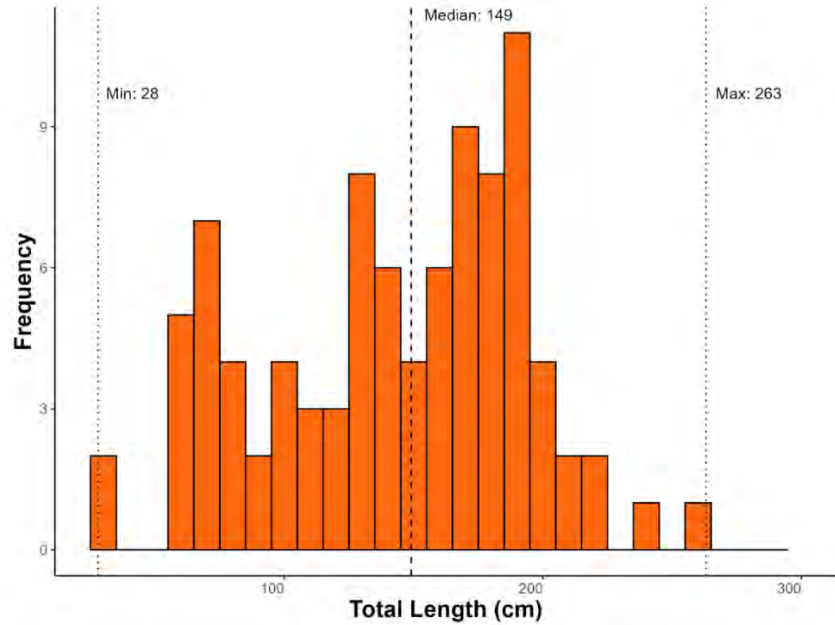


Figure 21. Frequency of alligators sampled in Lake Maurepas, LA, USA, from 01 August 2023 to 01 November 2024 by length in centimeters (n = 92, min = 28cm, median = 149cm, max = 263cm).



Figure 22. Spatial variation in alligator heterophil-to-lymphocyte ratios (HLR) collected in Lake Maurepas, LA, USA, from 01 August 2023 to 01 November 2024 (n = 92, min = 0.19, median = 0.98, max = 2.28). To improve clarity, overlapping points were slightly offset using a random dispersal method in ArcGIS Pro 2.4.0. The offset formula, $(Random() * 20) - 10$, was applied to both latitude and longitude. Additionally, point transparency was set to 30% to better visualize overlapping symbols.

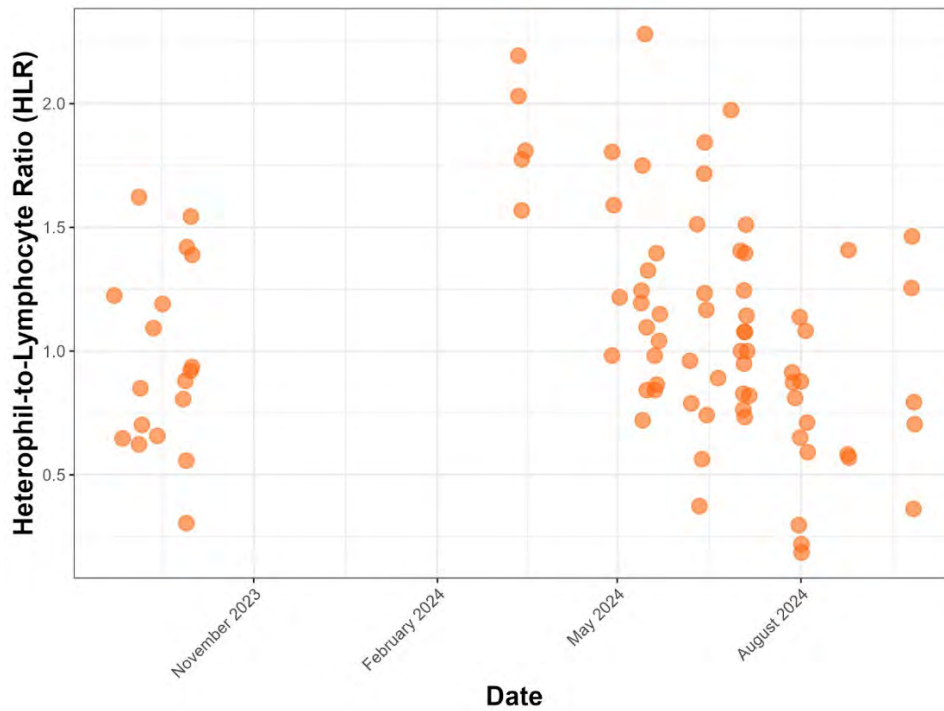


Figure 23. Temporal variation in alligator heterophil-to-lymphocyte ratios (HLR) collected in Lake Maurepas, LA, USA, from 01 August 2023 to 01 November 2024 (n = 92, min = 0.19, median = 0.98, max = 2.28).

Blood pH ranged from 6.7 to 8.4 in the 32 samples collected (Figure 24). Testosterone concentrations ranged from 0.48 ng mL⁻¹ to 1.15 ng mL⁻¹ in males and from 0.51 ng mL⁻¹ to 0.83 ng mL⁻¹ in females. Estradiol concentrations ranged from 0.023 ng mL⁻¹ to 0.14 ng mL⁻¹ in males and from BDL to 0.21 ng mL⁻¹ in females.

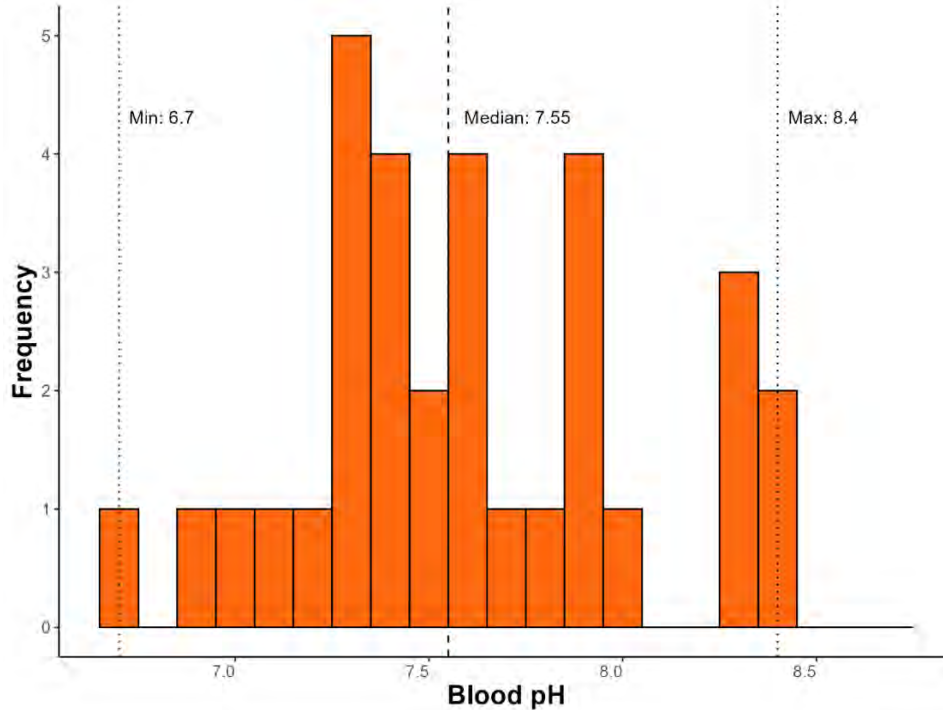


Figure 24. Observed blood pH values in sampled Lake Maurepas, LA, USA, alligators from 01 August 2023 to 01 November 2024 (n = 32, min = 6.7, median = 7.55, max = 8.4).

Nest survival was estimated to be below 10% by the Louisiana Department of Wildlife and Fisheries, which closely relates to our own estimates. Heavy rainfall and Gulf of Mexico tropical storms and hurricanes led to high water levels in the Lake Maurepas basin during early summer, resulting in high nest mortality across southeastern Louisiana. Within the Lake Maurepas basin, only elevated nests along the interstate canal dredge levee remained viable, a low-quality nesting habitat. Mark-recapture demographic sampling continues through phase IV. While 92 animals have been captured and marked, none have been recaptures. Sixteen farm-release alligators, however, have been captured, suggesting industry supplementation may be critical for population sustainability.

5. Discussion

5.1 Blue crabs

Biomarkers collected here indicate physiological impairment as a function of anthropogenic disturbance. Baseline hemolymph density data exhibited variation in nutrient acquisition among specimens (Kwan et al. 2014). Hemolymph pH provided baseline data for acidification monitoring (Meseck et al. 2016) and observed hemolymph pH indicates potential

acidification occurring now relative to oceanic crab experiments modeling climate change projections (Meseck et al. 2016).

Histologically, our specific observation of vacuolated hepatocytes with obliterated lumens in the hepatopancreas of blue crabs could indicate structural damage or stress to the tissue. The damage can result from various factors, including environmental stressors (e.g., pollution, hypoxia, salinity fluctuations), infections, or nutritional deficiencies. Vacuolation often reflects the accumulation of lipids or other substances due to metabolic dysfunction, while obliterated lumens suggest compromised secretion or absorption within the hepatopancreatic tubules (Jerome et al. 2017).

Histopathological analysis of gills indicates toxic heavy metal exposure in Lake Maurepas. Heavy metals cause compounding and successive damage to the gills, muscle and hepatopancreas, in that order, and our data reveal gill damage indicative of heavy metal toxicity (Otitoloju et al. 2009). Copper (Cu) and lead (Pb) exposure have been causally linked to the structural pathology observed in this study, but our findings are not limited to exposure by these two metals. Mercury and cadmium are also prevalent toxins in southeastern LA (Park et al. 2018; Nyachoti et al. 2023) and may be contributing to tissue damage either solely or in part. The hepatopancreas, a key organ for digestion and metabolism in crustaceans, is highly sensitive to environmental changes. The detected alterations can impair a blue crab's normal functions, such as enzyme production and nutrient absorption, potentially affecting the overall health and survival of the organism (McGaw & Reiber 2000; Chung 2020)

5.2 Catfishes

Leukocyte profiles indicate spatial variation in chronic stress among catfish specimens. The highest neutrophil-leukocyte ratios were observed near West Jones Island between Port Manchac and Akers as well as near the mouth of the Amite River, both in the northern region of Lake Maurepas. This area is subject to higher human and boat traffic, so stress in this area may be a function of high fishing pressure, noise or associated effluent (Celi et al. 2016).

Conversely, hepatosomatic index (HSI) exhibited pathologically elevated ratios in the south central region of the lake. HSI is used as a biomarker for liver workload and serves as a crude metric for detoxification effort (Yang and Baumann 2006). Gonadosomatic index (GSI) exhibited variation throughout the lake consistent with healthy reproductive energy allocation in both males and females over the reproductive season. Ecotoxicologically, GSI is indicative of endocrine disrupting exposure that inhibits allocation to gamete production (Louiz et al. 2009). Our results indicate no such impairment at this time.

As a metric, blood pH is indicative of acidification stress, osmoregulatory challenges, and ion exchange impairment (McKenzie et al. 1991). Our observed data exhibit a frequency distribution around neutral pH 7, however, some specimens had a blood pH below 5.5 and over

8. Variation in natural blood pH is understudied *in vivo* and will continue to be monitored across space and time.

Plasma estradiol concentrations in female catfish ranged from 0.044 to 1.32 ng mL⁻¹, a range consistent with normal female HPG axis functionality (Barrero et al. 2007). Male catfish exhibited estradiol concentrations of 0.03 to 0.18 ng mL⁻¹, although this range is not comparable to published literature because contemporary data for North American catfish does not exist. Interestingly, adult male catfish exhibited testosterone concentrations consistent with juvenile catfish that exhibited pre seminiferous functionality (Chatakondi et al. 2013). This finding may indicate the presence of an anti-androgen.

5.3 Bullfrogs

Current legislation allows bullfrog harvest for 10 months of the calendar year, excluding peak reproductive season, with no daily limits (Louisiana Department of Wildlife and Fisheries; <https://www.wlf.louisiana.gov/page/recreational-reptile-and-amphibian-collecting>). This harvest is predominantly recreational but also contributes largely to the local restaurant industry. Bullfrogs experience numerous challenges in Lake Maurepas, such as spring harvest pressure when vegetation has yet to flourish, stochastic winter temperatures, salt-water intrusion and water quality shifts, increased market demand, habitat degradation, export, and advancements in recreational harvest equipment. Southeastern Louisiana, however, is home to the largest bull and pig frog populations in the state and new harvest legislation is currently under consideration as of November 2024 (Louisiana Department of Wildlife and Fisheries; <https://www.wlf.louisiana.gov/news/lwfc-gives-final-approval-to-noi-for-rule-changes-to-reptile-and-amphibian-regulations>).

Data collected here indicate no physiological concerns in chronic stress, liver load and reproductive allocation for frogs in the Lake Maurepas system; however, demographic concerns may be present. Our sampling occurred predominantly in the late summer and fall and catch per unit effort was extremely low. Recreational and market harvest may have depleted the population considerably over the summer months and our collecting will shift to early-to-late spring next year.

5.4 Alligators

The socioeconomic value of alligators in the Lake Maurepas system is responsible for population sustainability. Alligator eggs are harvested annually for ranching by local alligator farms. As such, the harvesters return 5% to Lake Maurepas at a head-started size, per state requirements. High water from early storms in the Gulf of Mexico was responsible for roughly 90% egg mortality in the basin and, as our demographic data reveal, farm returns may make up a significant portion of the population. Monitoring of size class structure will continue in 2025 with particular attention paid to this year's recruitment gap.

HLR varied considerably around the lake. High HLRs indicative of allostatic load were observed along the northern shoreline and along interstate canal, the regions of the system with the highest boat traffic. The HLRs observed here are consistent with other alligator populations experiencing mild stressors (Murray et al. 2013).

Sex steroid concentrations were quantified after courtship and nesting, so concentrations should reflect quiescent periods of activity. Estradiol analysis, however, revealed markedly high female E₂ concentrations (2-3x) relative to published literature from Lake Woodruff, FL (Rooney et al. 2004) and are more comparable to Lake Apopka, FL, a lake that has been severely anthropogenically influenced and continues to serve as a case study for environmental estrogens. Interestingly, males exhibited ~2x higher testosterone concentrations than Lake Woodruff, FL (Rooney et al. 2004) as well. However, this may be an affect of size in our study, as most published literature targeted juvenile animals and our T data indicate a range higher than Rooney et al. (2004) and lower than Hamlin et al. (2011). Further sampling should tease out size as an affect on sex steroid concentrations for further holistic comparison and potential investigation of endocrine disruption.

7. Literature Cited

- Affonso, E. G., Polez, V. L. P., Corrêa, C. F., Mazon, A. D. F., Araujo, M. R. R., Moraes, G., & Rantin, F. T. (2002). Blood parameters and metabolites in the teleost fish *Colossoma macropomum* exposed to sulfide or hypoxia. *Comparative Biochemistry and Physiology Part C: Toxicology & Pharmacology*, 133(3), 375-382.
- AVMA Guidelines for the Euthanasia of Animals: 2020 Edition.
- Barrero, M., Small, B. C., D'Abramo, L. R., Hanson, L. A., & Kelly, A. M. (2007). Comparison of estradiol, testosterone, vitellogenin and cathepsin profiles among young adult channel catfish (*Ictalurus punctatus*) females from four selectively bred strains. *Aquaculture*, 264(1-4), 390-397.
- Celi, M., Filiciotto, F., Maricchiolo, G., Genovese, L., Quinci, E.M., Maccarrone, V., Mazzola, S., Vazzana, M. and Buscaino, G., (2016). Vessel noise pollution as a human threat to fish: assessment of the stress response in gilthead sea bream (*Sparus aurata*, Linnaeus 1758). *Fish Physiology and biochemistry*, 42, pp.631-641.
- Chatakondi, N. G., & Davis, K. B. (2013). Maturity stage and plasma testosterone levels are related to sperm production in blue catfish, *Ictalurus furcatus*. *Aquaculture Research*, 44(2), 161-166.

- Chung, J. S. 2020. Role of hepatopancreas trehalose-6-phosphate synthase in carbohydrate levels of the blue crab *Callinectes sapidus* in feeding and emersion. *Journal of Shellfish Research*. 39(2): 449–459.
- Hamlin, H. J., Lowers, R. H., & Guillette Jr, L. J. (2011). Seasonal androgen cycles in adult male American alligators (*Alligator mississippiensis*) from a barrier island population. *Biology of Reproduction*, 85(6), 1108-1113.
- Han, X., & Liu, D. (2019). Detection and analysis of 17 steroid hormones by ultra-high-performance liquid chromatography-electrospray ionization mass spectrometry (UHPLC-MS) in different sex and maturity stages of Antarctic krill (*Euphausia superba* Dana). *PloS one*, 14(3), e0213398.
- Jerome, F. C., A. Hassan, G. O. Omoniyi-Esan, O. O. Odujoko, & A. V. Chukwuka. 2017. Metal uptake, oxidative stress, and histopathological alterations in gills and hepatopancreas of *Callinectes amnicola* exposed to industrial effluent. *Ecotoxicology and Environmental Safety*. 139: 179–193.
- Kwan, B. K., Chan, A. K., Cheung, S. G., & Shin, P. K. (2014). Hemolymph quality as indicator of health status in juvenile Chinese horseshoe crab *Tachypleus tridentatus* (Xiphosura) under laboratory culture. *Journal of Experimental Marine Biology and Ecology*, 457, 135-142.
- Lance, V. A., Elsey, R. M., Butterstein, G., Trosclair III, P. L., & Merchant, M. (2010). The effects of Hurricane Rita and subsequent drought on alligators in southwest Louisiana. *Journal of Experimental Zoology Part A: Ecological Genetics and Physiology*, 313(2), 106-113.
- Louiz, I., Ben-Attia, M., & Ben-Hassine, O. K. (2009). Gonadosomatic index and gonad histopathology of *Gobius niger* (Gobiidea, Teleost) from Bizerta lagoon (Tunisia): evidence of reproduction disturbance. *Fisheries Research*, 100(3), 266-273.
- McKenzie, D. J., Aota, S., & Randall, D. J. (1991). Ventilatory and cardiovascular responses to blood pH, plasma PCO₂, blood O₂ content, and catecholamines in an air-breathing fish, the bowfin (*Amia calva*). *Physiological Zoology*, 64(2), 432-450.
- McGaw, I. J., & C. L. Reiber. 2000. Integrated physiological responses to feeding in the blue crab *Callinectes Sapidus*. *Journal of Experimental Biology*. 203(2): 359–368.
- Meseck, S. L., Alix, J. H., Swiney, K. M., Long, W. C., Wikfors, G. H., & Foy, R. J. (2016). Ocean acidification affects hemocyte physiology in the Tanner crab (*Chionoecetes bairdi*). *PloS one*, 11(2), e0148477.
- Murray, C. M., Easter, M., Merchant, M., Cooper, A., & Crother, B. I. (2013). Can reproductive allometry assess population marginality in crocodylians? A comparative analysis of Gulf

- Coast American Alligator (*Alligator mississippiensis*) populations. *Copeia*, 2013(2), 268-276.
- Murray, C. M., Merchant, M., Easter, M., Padilla, S., Garrigós, D. B., Marin, M. S., & Guyer, C. (2017). Detection of a synthetic sex steroid in the American crocodile (*Crocodylus acutus*): Evidence for a novel environmental androgen. *Chemosphere*, 180, 125-129.
- Nyachoti, S., Godebo, T. R., Okwori, O. F., Kodsup, P., & TatahMentah, M. K. (2023). Occurrence and Spatial Distribution of Lead, Arsenic, Cadmium, and Uranium in Soils of Southern Louisiana. *Water, Air, & Soil Pollution*, 234(11), 708.
- Otitolaju, A. A., Elegba, O. K., & Osibona, A. O. (2009). Biological responses in edible crab, *Callinectes amnicola* that could serve as markers of heavy metals pollution. *The Environmentalist*, 29, 37-46.
- Rooney, A. A., Crain, D. A., Woodward, A. R., & Guillette Jr, L. J. (2004). Seasonal variation in plasma sex steroid concentrations in juvenile American alligators. *General and Comparative Endocrinology*, 135(1), 25-34.
- Park, J. H., Wang, J. J., Xiao, R., Pensky, S. M., Kongchum, M., DeLaune, R. D., & Seo, D. C. (2018). Mercury adsorption in the Mississippi River deltaic plain freshwater marsh soil of Louisiana Gulf coastal wetlands. *Chemosphere*, 195, 455-462.
- Yang, X., & Baumann, P. C. (2006). Biliary PAH metabolites and the hepatosomatic index of brown bullheads from Lake Erie tributaries. *Ecological Indicators*, 6(3), 567-574.

III. Wetland Monitoring

Gary Shaffer, PhD

Southeastern Louisiana University, Dept. of Biological Sciences

Hammond, LA 70402

shafe@selu.edu

Overview

My team and I set up all ten of our permanent sites (Figure 1), each with two 625 m² permanent stations. We have tagged and measured diameters of 1,077 trees. For our yearly planting of baldcypress (*Taxodium distichum*) and water tupelo (*Nyssa aquatica*) seedlings, we began at the northern tip of West Jones Island (Figure 2). We have grown well over 5,000 seedlings and planted 2,000, each of which was about 3' tall. Unfortunately, the stakes were not strong enough to support the weight of nutria and about 80% of these seedlings were killed. Thus far, measurements of surface elevation, using our surface elevations tables (SETs) and marker horizons, elevation gain has exceeded subsidence by about 19 cm, or over 1 cm per year of net elevation gain.



Figure 1. Locations of sites and stations in the Maurepas swamp.

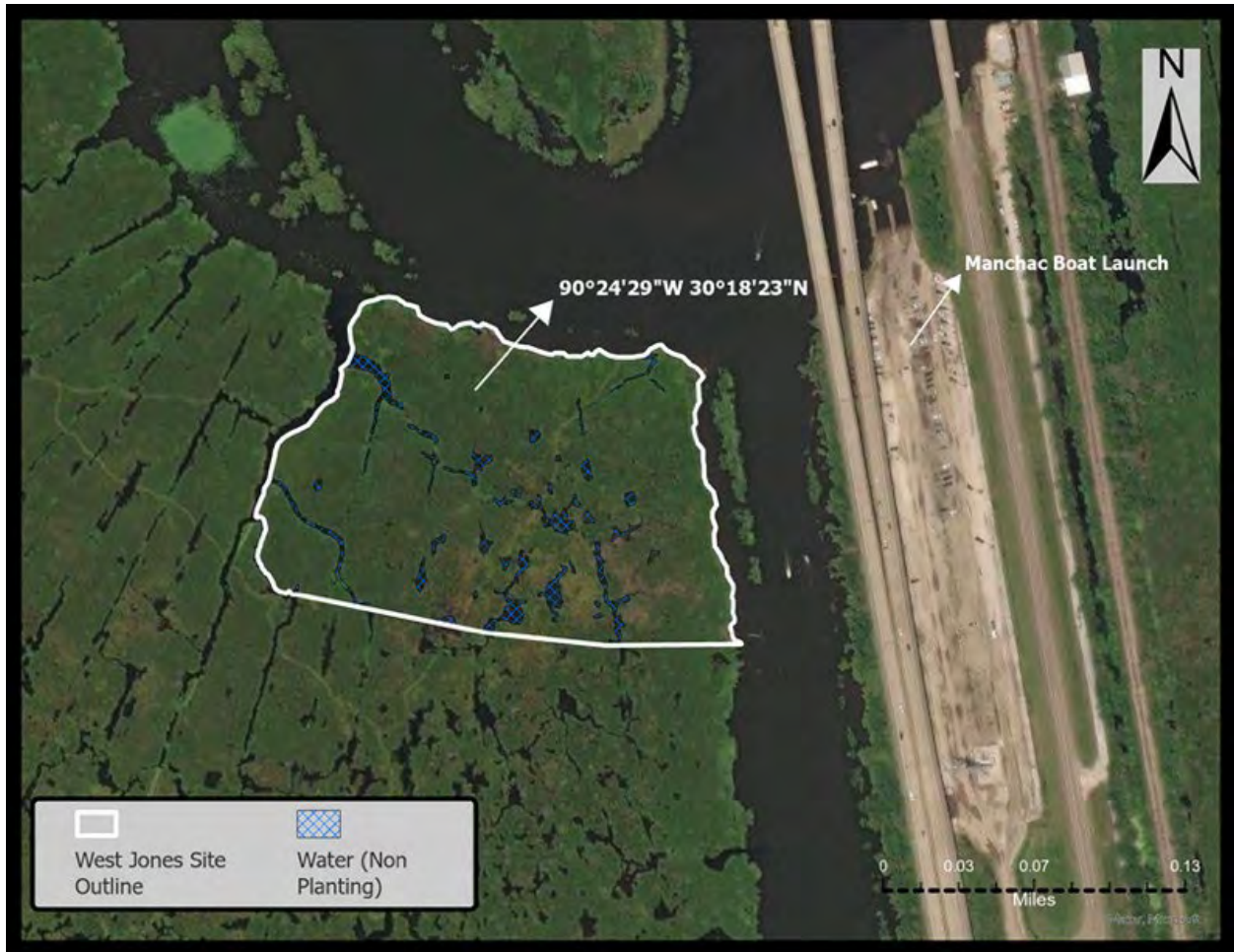


Figure 2. Area encircled in white is the 10.2 acres on West Jones Island that was planted with 2,000 baldcypress and water tupelo seedlings.

Project Objectives

Our first objective was to collect turbidity data for the waters of Lake Maurepas, which we delivered in our previous annual report. Our second objective was to locate fourteen surface elevation tables (SETs, Figure 3) established in the years 2000 and 2006 and measure elevation change to date. We also provided new plastic petri dish marker horizons to all sites where SETs occur to monitor sediment accretion. Our third objective was to establish ten permanent sites with replicate 625 m² stations for monitoring tree productivity. Our fourth objective was to plant and protect 2,000 baldcypress and water tupelo seedlings on West Jones Island. Our fifth objective was to tag and measure the diameter of all trees with greater than a 4 cm diameter in each of the twenty stations. Our final objective was to update our 2011 habitat-state map (Shaffer et al. 2016, Figure 4) to determine the amount of each type of habitat (degraded, relict, sustainable) that now exists.

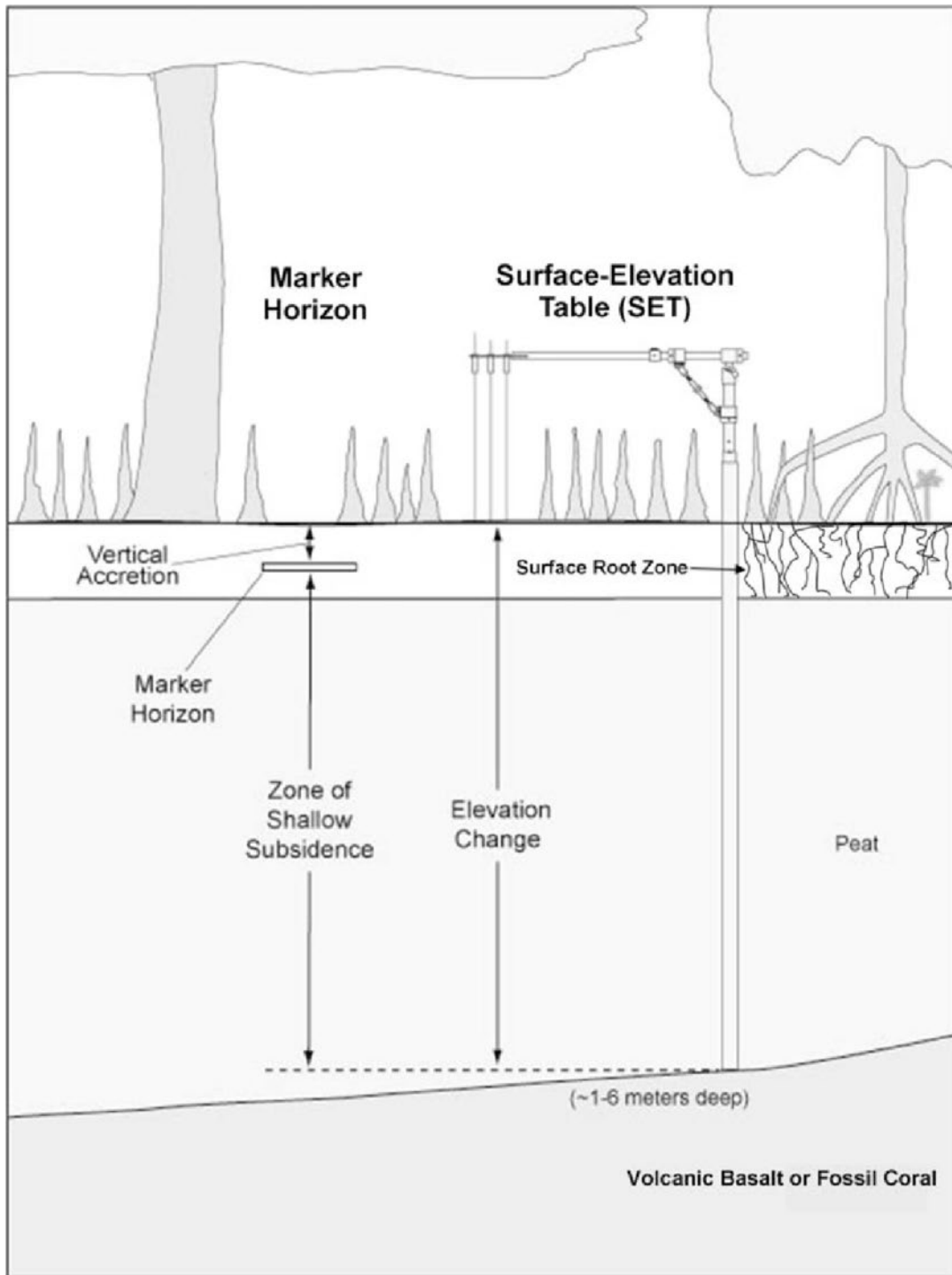


Figure 3. Surface elevation table and marker horizon (redrawn from Krauss et al. 2010).

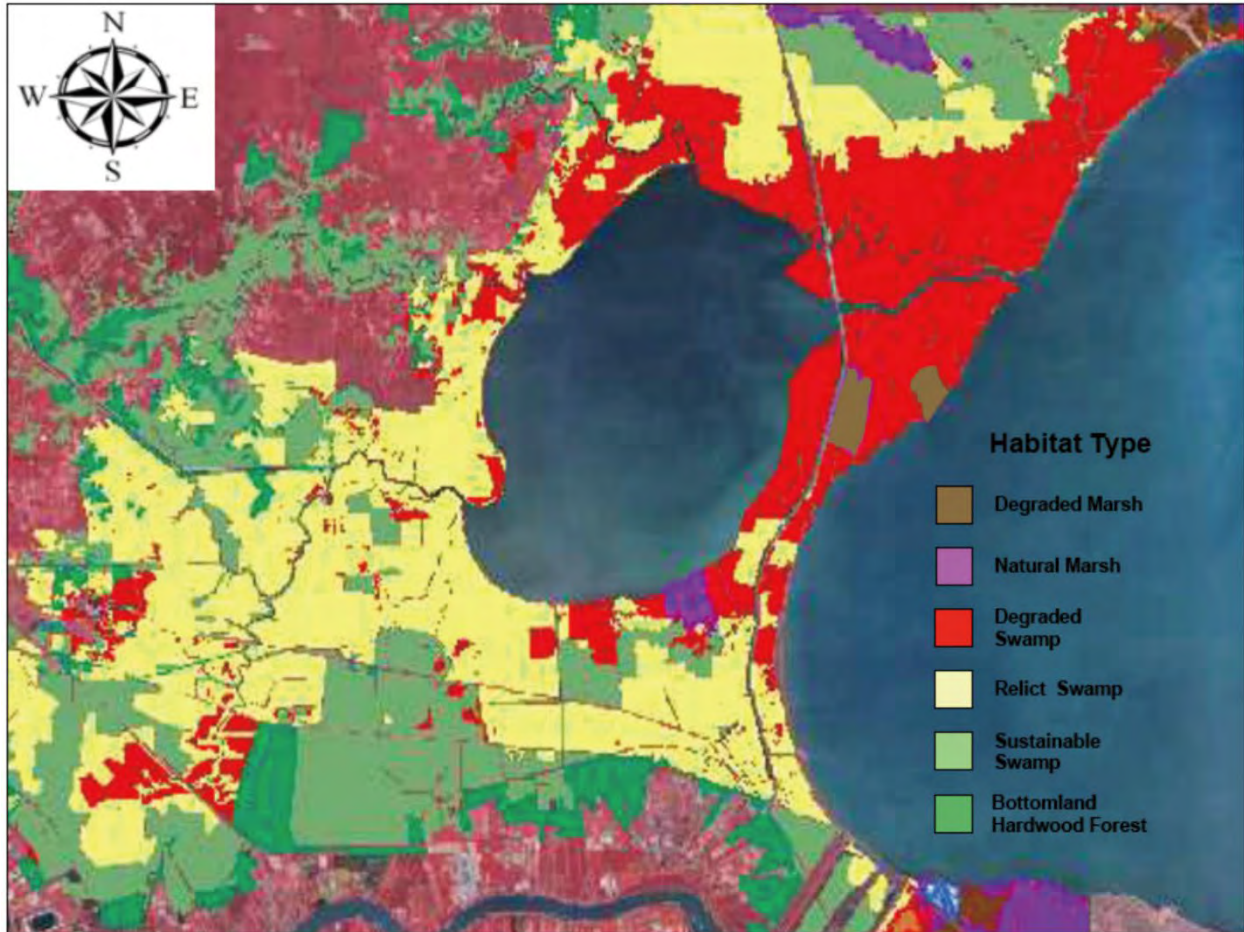


Figure 4. Amount of degraded, relict, and sustainable swamp habitat that existed in 2011 (redrawn from Shaffer et al. 2016).

Methods

Locating the surface elevation table pipes was difficult as the benches marking each site have largely decomposed. Moreover, accretion has been substantial enough that most of the pipes are buried underground. Nevertheless, we have located all SET pipes. For each SET, nine measurements are taken at each of the four cardinal directions. Four marker horizons are placed halfway between each cardinal direction and are flagged for future accretion measurements. There are two types of SETs, namely pipe SETs and rod SETs. Pipe SETs are 4" irrigation pipes that are 5 m long. Rod SETs are stainless steel rods knocked all the way into the Holocene valley wall.

We were unable to install eight permanent stations along Reserve Relief Canal, where the Air Products pipeline will be placed because water hyacinth clogged entire canals. To date, we only established two stations along Reserve. Eighteen other stations were located at West Jones Island, Ruddock Canal, Hope Canal, Tent Bayou, Dutch Bayou, Alligator Island and Lil' Chen Blanc (Figure 1). These stations are a subset from a study implemented in 2000 (Shaffer

et al. 2009, 2016) that contained 26 sites. Each station has 625 m² of aerial coverage and contains four 16 m² plots for measurement of herbaceous and canopy cover. Within each station, diameters were measured for all trees greater than 4 cm in width. In addition, four 0.25 m² litterfall traps were randomly located in each station and leaf litter was collected about every 2 months. Records of natural recruitment are also maintained.

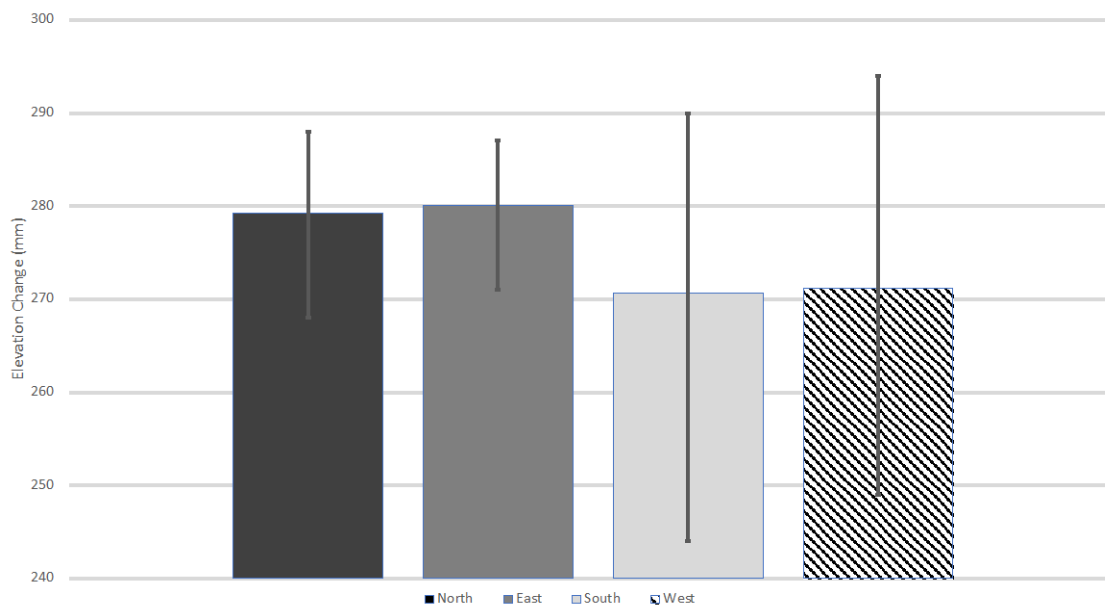
Over the past year we have grown over 5,000 thousand baldcypress and water tupelo seedlings. These seedlings are grown in 1-gallon pots from seeds obtained from a local seed source. Each pot contains 70 g of time-released Osmocote fertilizer.

Results and Discussion

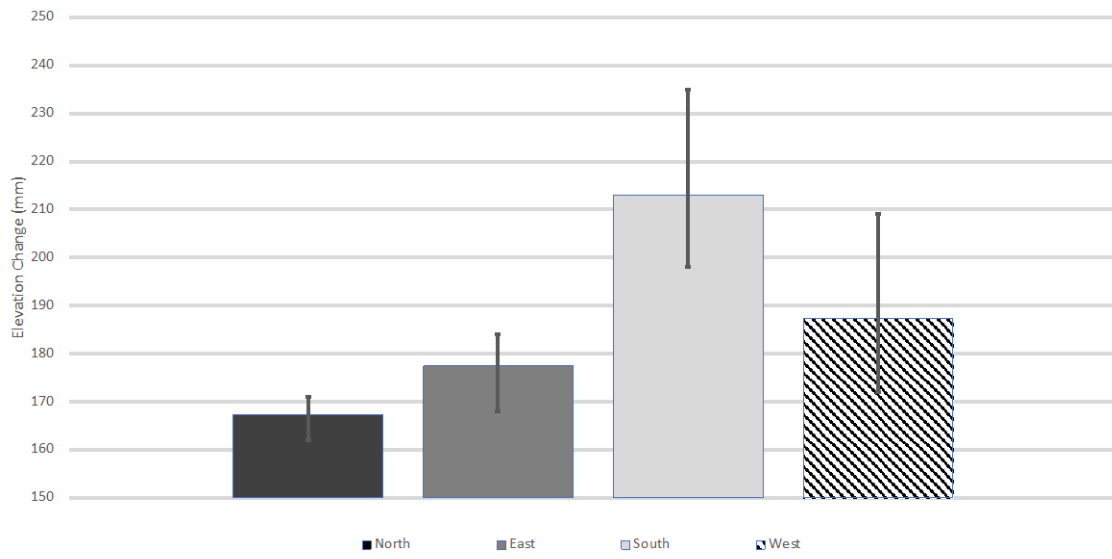
The surface elevation tables for this effort were installed in 2000 and 2006 and until recently, no measurements have been completed for 18 years. All of the original marker horizons (used for measuring accretion) migrated through the very weak swamp soils, so we installed flagged plastic petri-dish covers.

The SET measurements taken thus far demonstrate that accretion exceeds subsidence by a substantial margin (Figure 5). If this pattern holds up for the rest of the SETs, the Maurepas swamp will be one of the few areas in coastal Louisiana to have a net elevation gain. Interestingly, the variation between cardinal directions is as high as the variability between SETs (Figure 5).

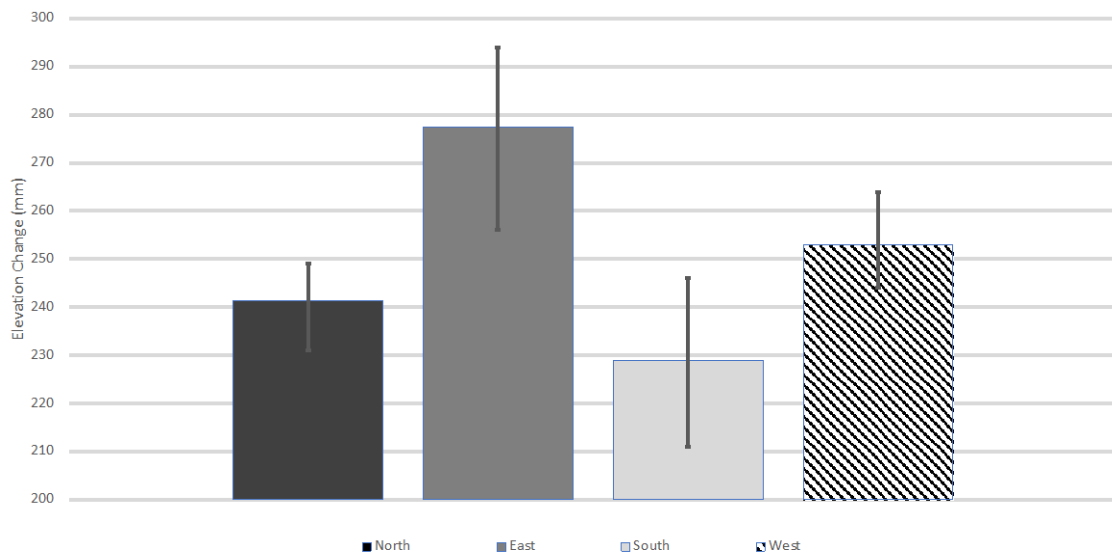
5a



5b



5c



5d

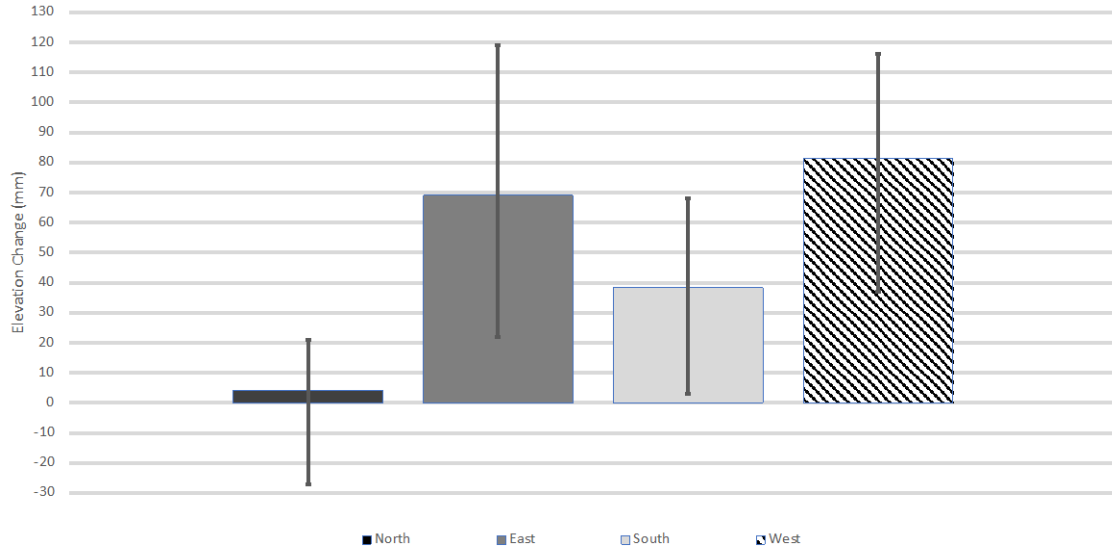


Figure 5. Results from four surface elevation tables demonstrating strong elevation gains for nearly all measurements. 5a-c are pipe SETs, 5d is a rod SET.

Tree Measurements

The Ruddock Canal sites had the lowest number of trees, just below 500 trees per hectare (Figure 6). Alligator Island contained the highest number of trees, with over 3,000 trees per hectare. The average number of trees across sites was just under 1,700 trees per hectare.

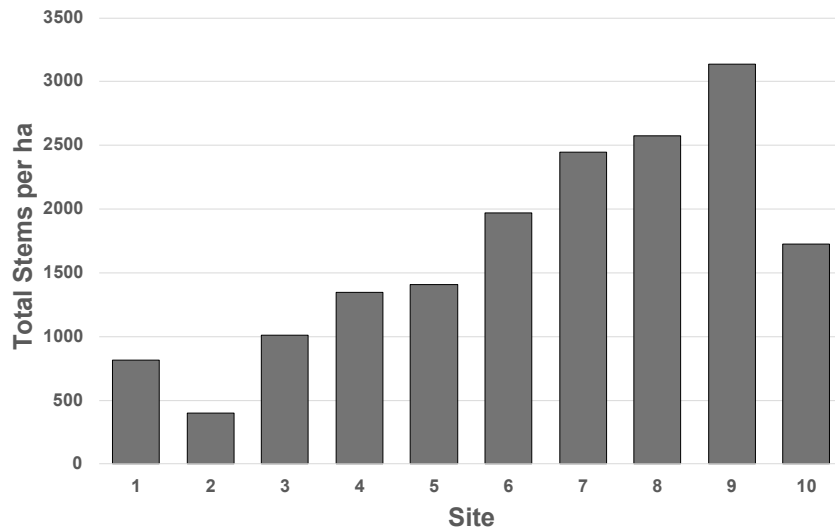


Figure 6. Total number of trees per hectare for all ten sites with all species combined.

Average diameter (cm) of trees (Figure 7) was lowest at West Jones Island, Reserve Relief Canal, Dutch Bayou and Alligator Island, each averaging about a 12-cm diameter. Trees along Hope Canal were the largest, averaging 27 cm in diameter. Across sites the average diameter of trees was just over 17 cm.

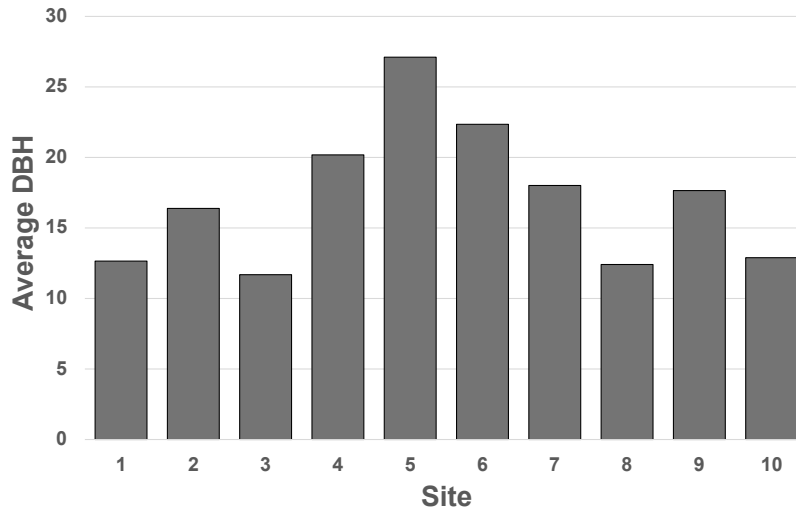


Figure 7. Average diameter (cm) at breast height for all ten sites with all species of trees combined.

Midstory trees (Other), dominated by swamp red maple (*Acer rubrum* var. *drummondii*) and Carolina ash (*Fraxinus caroliniana*), generally were the most abundant, compared to canopy species (Figure 8). West Jones Island, Rudock Canal and Reserve Relief Canal have no water tupelo (*Nyssa aquatica*) due to salt-water intrusion caused by the Mississippi River Gulf Outlet (Shaffer 2009) which was closed in 2009. Of the species present, baldcypress (*Taxodium distichum*) is the most salt tolerant and dominated sites closest to the margin of Lake Maurepas (Figure 8).

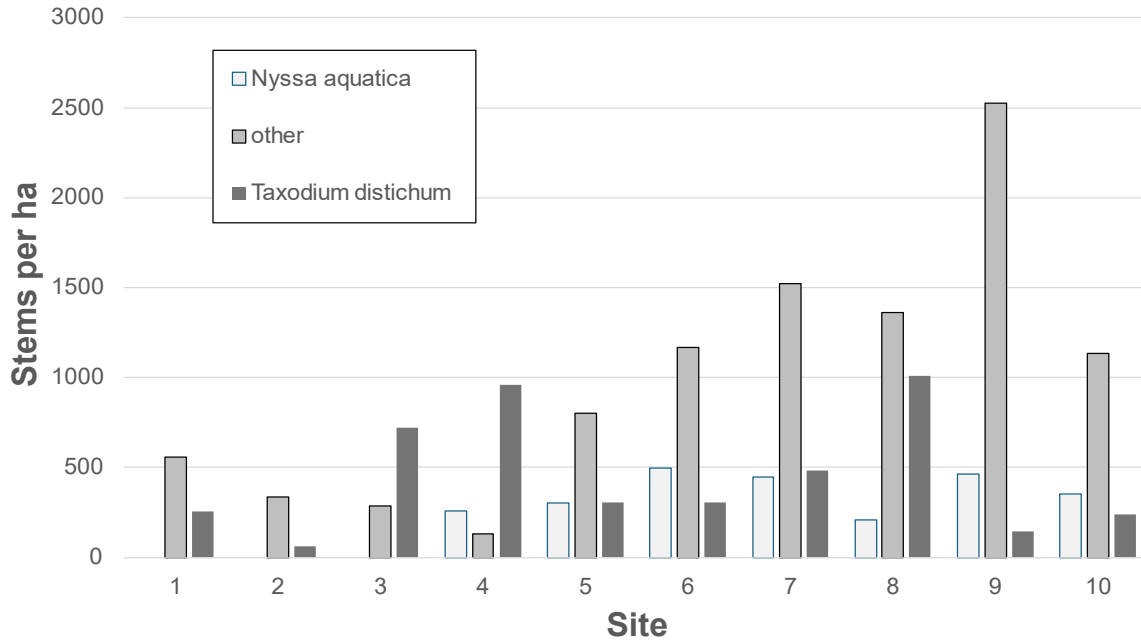


Figure 8. Stems per hectare for *Taxodium distichum* (baldcypress), *Nyssa aquatica* (water tupelo), and midstory species *Acer rubrum* var. *drummondii* (swamp red maple), *Fraxinus caroliniana* (Carolina ash), and *Triadica sebifera* (Chinese tallow).

Baldcypress was the largest tree at four of the ten sites (Figure 10). Water tupelo was the largest tree at three sites. Surprisingly, the midstory species were the one largest trees at one site along Hope Canal (Site 6) as well as the Alligator Island site (Site 10).

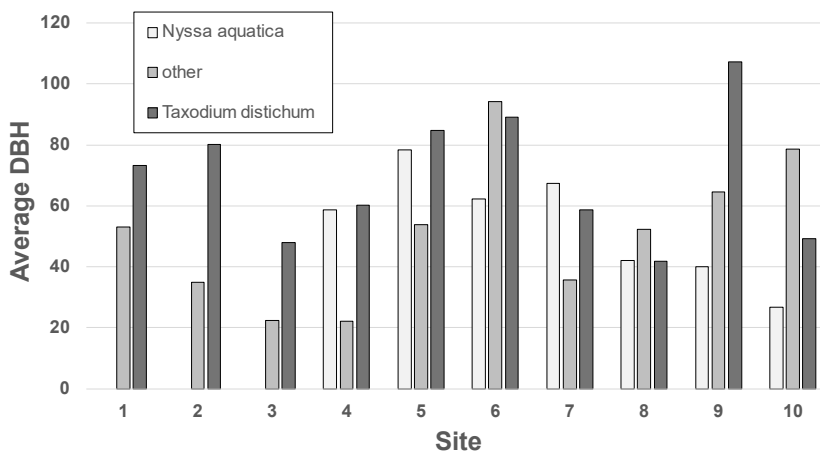


Figure 9. Average diameter at breast height per hectare for *Taxodium distichum* (baldcypress), *Nyssa aquatica* (water tupelo), and midstory species *Acer rubrum* var. *drummondii* (swamp red maple), *Fraxinus caroliniana* (Carolina ash), and *Triadica sebifera* (Chinese tallow).

Herbaceous Measurements

Herbaceous vegetation cover, by species, was also monitored. Each station has four 16 m² vegetation plots, hence there are eight labels for each site (Figure 10). A clearer idea of site separation is found when the eight plots at each site are averaged (Figure 11). Sites closer together have similar species present. A total of 27 herbaceous species were detected, about half of which were commonly found (Figure 12).

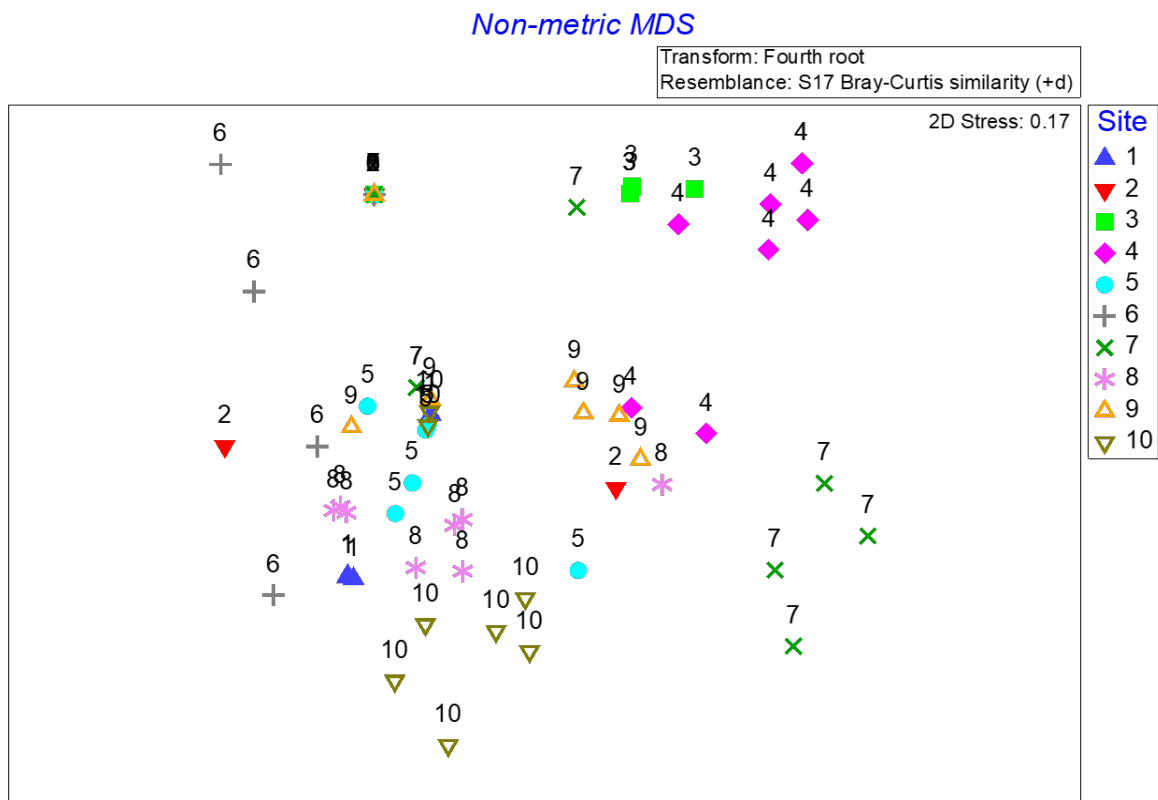


Figure 10. Herbaceous vegetation cover generated by Primer 7 software. The ten sites have a total of eight plots each.

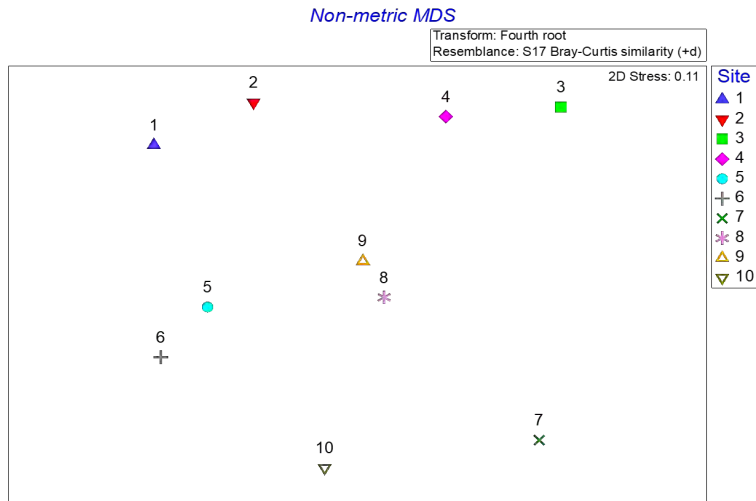


Figure 11. Average vegetative species separation of each site. Low numbered sites are located along the eastern side of the Lake Maurepas margin, whereas interior sites have the highest numbering.

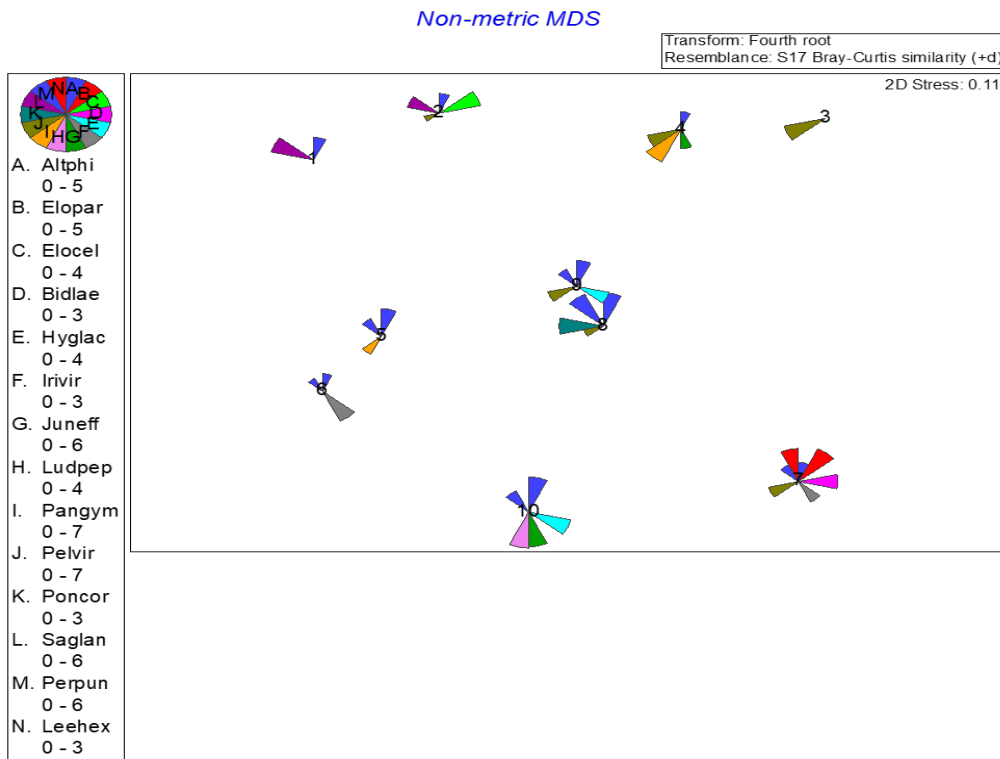


Figure 12. The fourteen most common species. Each color represents the abundance of a particular vegetative species.

Future Direction

Each year we will plant and protect at least 2,000 baldcypress and water tupelo seedlings on West Jones Island and we will begin planting at several other sites, all of which have been chosen. We will also continue to measure subsidence and accretion rates each SET site. Diameter measurements of all 1,077 trees present in our 20 stations will be made once a year. We will soon ground truth the new habitat-state map with use of a drone.

Literature Cited

- Krauss, K., Cahoon, D., Allen, J., Ewel, K., Lynch, J., Cormier, N. 2010. Surface Elevation Change and Susceptibility of Different Mangrove Zones to Sea-Level Rise on Pacific High Islands of Micronesia. *Ecosystems*. 13. 129-143. 10.1007/s10021-009-9307-8.
- Shaffer, G.P., Wood, W.B., Hoepfner, S.S., Perkins, T.E., Zoller, J., and Kandalepas, D. 2009. Degradation of baldcypress-water tupelo swamps to marsh and open water in southeastern Louisiana, U.S.A.: An irreversible trajectory. *Journal of Coastal Research*, v. SI 54, p. 152–165.
- Shaffer, G.P., Day, Jr., J.W., Kandalepas, D., Wood, W.B., Hunter, R.G., Lane, R.R., and Hillmann, E.R. 2016. Decline of the Maurepas Swamp, Pontchartrain Basin, Louisiana, and approaches to restoration. *Water*, v. 8, w8030101.

IV. Chemical Monitoring

Fereshteh Emami, PhD

Southeastern Louisiana University, Dept. of Chemistry and Physics

Hammond, LA 70402

fereshteh.emami@selu.edu

Overview

The Lake Maurepas Chemical Monitoring Project integrates six studies addressing environmental contaminants and their potential health impacts. These projects collectively examine per- and polyfluoroalkyl substances (PFAS) as part of non-targeted analysis (NTA), microplastics (MPs), mercury (Hg), other heavy metals, nutrient pollution, and air quality in and around Lake Maurepas, utilizing advanced analytical methods and statistical modeling:

(1) Per- and polyfluoroalkyl substances (PFAS) are a large class of persistent chemicals that have been used for decades in various industrial and commercial applications. Lake Maurepas, a biodiverse natural ecosystem located near residential, industrial, and recreational areas—and Louisiana in general—has never been assessed for NTA, particularly PFAS contamination. In this study, PFAS were analyzed for water, sediments, and biological samples (i.e., catfish and blue crabs) from Lake Maurepas. Samples were collected from nine sites (for water and sediments) and six zones (for biological samples), respectively, and measured using solid-phase extraction and liquid chromatography. So far, for samples between June and December 2023, out of 44 target PFAS, 24 were detected in Lake Maurepas. Both legacy and emerging PFAS were detected in the lake. Among them, PFOA, PFOS, PFDA, PFBA, and PFHxA have been linked to cancers, elevated cholesterol levels, hepatotoxicity, and more PFAS-associated diseases and toxicities.

(2) Microplastics (MPs) are tiny plastic particles less than 5 millimeters in size, originating from the degradation of larger plastic items. Due to their small size, MPs are easily ingested by aquatic organisms, entering the food chain and posing potential risks to animal and human health. In recent decades, considerable concern has emerged about the presence and impacts of MPs in aquatic environments worldwide. Despite being a widely studied global issue, no previous research has been conducted on MPs in Lake Maurepas and its surrounding region. This study focuses on the occurrence of MPs in the water, sediment, and aquatic organisms of Lake Maurepas, as well as the distribution of MPs in different tissues of crabs and catfish. This research has been started since October 2024 and sampling will be conducted monthly. So far, the analysis of water samples collected in October revealed that the ND1, ND2, and ND3 sites—situated near the mouths of the Tickfaw, Amite, and Blind Rivers, respectively—had the highest concentrations of MPs, averaging 363, 440, and 316 particles per liter. Although other sampling sites had comparatively lower concentrations, all exceeded 100 particles per liter. Color-based

analysis revealed that blue and white MPs were the most abundant across all sampling locations. Fibers were the predominant shape type of MPs, followed by fragments. MPs in the 100–500 μm size range dominated, while particles smaller than 100 μm were the second most prevalent.

(3) Mercury (Hg) is a highly toxic and bioaccumulative metal that poses significant risks to aquatic ecosystems and human health, especially through the consumption of contaminated seafood. The lake's organic-rich, low-oxygen environment supports microbial methylation of inorganic Hg into methylmercury (CH_3Hg^+), a more toxic and bioavailable form that biomagnifies through the food web. This study has assessed Hg levels in water, sediment, aquatic plants, and organisms across Lake Maurepas from June 2023 to July 2024, revealing distinct spatial and temporal patterns. Water samples showed elevated Hg concentrations at sites influenced by river discharge. These values exceeded the safety threshold of 0.002 mg/L for drinking water, indicating potential risks to aquatic organisms. Sediment analyses revealed consistently high Hg levels near anthropogenic sources frequently surpassed the safety threshold of 0.18 $\mu\text{g/g}$, such as ND1 (Tickfaw mouth) and ND2 (Amite mouth), with seasonal increases likely driven by rainfall and sedimentation during the rainy season. Aquatic plants exhibited site-specific variability in Hg accumulation, with higher levels observed in areas with elevated sediment Hg. Among plant species, blue-green algae showed the highest Hg concentrations, followed by *Salvinia minima*, water hyacinth, and Gulf swampweed. However, these values do not exceed the limit of 0.5 $\mu\text{g/g}$ safety limit for food crops. Aquatic organisms, including catfish and blue crabs, displayed significant spatial and temporal changes in Hg levels. Catfish muscle tissues generally had higher Hg concentrations than skin, consistent with known bioaccumulation patterns. In some cases, fish tissue Hg levels exceeded the regulatory threshold of 0.15 $\mu\text{g/g}$. No significant species-specific differences in Hg accumulation were observed between Channel Catfish and Blue Catfish. These findings underscore the complex interplay of natural and anthropogenic factors driving Hg dynamics in Lake Maurepas. The study highlights the importance of long-term monitoring to manage contamination risks, protect aquatic ecosystems, and ensure public health safety in the face of industrial and environmental pressures. Continuous measurements are undergoing.

(4) This completed part of the study that has been recently published in *Environments* 11(12) (2024) 268 focuses on water and sediment quality at nine sites across three depths between June and November 2023. The findings indicated that $\text{NH}_3\text{-N}$ levels remained within safety limits (0.11 ± 0.10 mg/L). However, levels of Total Nitrogen (TN, 0.83 ± 0.65 mg/L), Total Phosphorus (TP, 0.32 ± 0.13 mg/L), Chemical Oxygen Demand (COD, 25.94 ± 11.37 mg/L), Arsenic (As, 0.26 ± 0.17 mg/L), and Lead (Pb, 0.23 ± 0.002 mg/L) exceeded acceptable thresholds. Spatial-temporal analysis revealed significant variations across sites, depths, and sampling dates. Major potential sources of contamination included discharges from the

Tickfaw, Amite, and Blind Rivers, as well as catastrophic "super fog" multi-car pileup on October 23, 2023, on Pass Manchac. Seismic and drilling activities by Air Products and Chemicals Inc. appeared to have minimal observable impact. Additionally, four AI algorithms were assessed using physical parameter inputs to forecast chemical pollutant levels for December, when adverse weather conditions prevented sampling. Among these, the LSTM model performed best, achieving R^2 values of 0.852 for COD, 0.869 for TN, 0.842 for As, and 0.921 for TP and Pb. The predictions indicated decreasing pollutant levels in December, which aligned with salinity and specific conductance data. These levels reverted to values observed in September and October, likely due to the settling of contaminants from the Pass Manchac accident and continued pollutant inputs from earlier months. This study highlights the need for ongoing monitoring and mitigation strategies to protect Lake Maurepas from cumulative and episodic pollution sources.

(5) Continuing project (4), this study presents the first comprehensive assessment of toxic chemicals and heavy metals (HMs) sources in Lake Maurepas. The research continued quantifying more HMs at three depths across nine sampling sites. Findings revealed elevated concentrations of cadmium (Cd) (≥ 0.2 mg/L), and nickel (Ni) (≥ 0.05 mg/L) at the confluence of the Tickfaw, Amite, and Blind rivers. Additionally, manganese (Mn) (≥ 0.12 mg/L) surpassed threshold levels near the Interstate 55 highway bridge, railway, and Port Manchac. Statistical analysis identified significant spatiotemporal differences among 375 analyzed samples, with notable variations of 92.44% for TN, 76.23% for TP, and 45.08% for COD and ammonia nitrogen ($\text{NH}_3\text{-N}$). While manganese (38.52%) and cadmium (31.95%) showed higher spatial-temporal differences, other elements such as lead (Pb), barium (Ba), copper (Cu), strontium (Sr), and nickel (Ni) displayed differences below 30%. Next, the sources of these pollutants were investigated using Bayesian multivariate receptor model (BSMRM) to discover contributing sources at the monitored sites and predict contributions at an unmonitored site, South Test Well (STW), where dredging operations commenced in mid-August 2023 by Air Products and Chemicals Inc. The results indicate six independent sources. Using the other most relevant environmental studies, we identified and named them as Transportation-Recreational-Accidental Release (TRAR), Death and Decay of Biological Species (DDBS), River Input-1 (RI-1), River Input-2 (RI-2), River Input-3 (RI-3), and Geological Release (GR). Further measurements and analysis are ongoing to achieve a more accurate understanding of the number of sources and their contributions to the lake's pollutant levels.

(6) Air pollution is a critical global concern that poses significant threats to human health, ecosystems, and the stability of the earth's climate. The region surrounding Lake Maurepas in Louisiana is particularly vulnerable due to its proximity to numerous industrial petrochemical facilities. It makes the Lake Maurepas ecosystem a high-risk area for air pollution. This study focuses on the systematic monitoring of air pollution levels and the identification of pollution

sources within the Lake Maurepas airshed. Data was being collected in real-time using a single station strategically located near the lake during the period from January 26, 2024, to September 23, 2024. Several common atmospheric pollutant species, including CO₂, CO, NO₂, SO₂, H₂S, TVOC, PM₁, PM_{2.5}, PM₄, and PM₁₀, were measured in this study. The original dataset was recorded at 15-minute intervals. Preliminary analysis has identified eight potential source candidates based on the geographic characteristics of the area. The identified sources include industrial emissions, vehicular traffic emissions, combustion sources, secondary organic aerosol formation, biogenic emissions, constructions and dust resuspension. Additionally, a mixed source is considered to account for unknown variability in the source apportionment. Preliminary trend analyses indicated that concentrations of CO₂ and PM_{2.5} exceeded standard safe limits declared by EPA. Furthermore, all PM values showed a similar upward trend during the recorded period. Positive matrix factorization (PMF) will be employed as the primary analytical tool to identify and quantify the contribution of various pollution sources. However, further work will be carried out to validate PMF findings and quantify the contributions of individual sources.

Project Objectives

Project 1: Identification of per- and polyfluoroalkyl substances (PFAS) in environmental samples from Lake Maurepas, USA, and their potential health implications

- To identify and quantify PFAS in environmental samples, including water, sediment, blue crab, and catfish, from Lake Maurepas.
- To compare the identified PFAS and concentrations in Lake Maurepas with reported values in the scientific literature, particularly those from the Great Lakes.
- To compile and evaluate literature-based data on diseases and toxicities associated with the detected PFAS.

Project 2: Detection and characterization of microplastics in water, sediment and biological samples from Lake Maurepas

- To investigate the presence and distribution of microplastics (MPs) in Lake Maurepas' water, sediment, and aquatic creatures (catfish and crab).
- To identify the degree of MPs pollution in Lake Maurepas and how it is distributed across several ecosystem components.
- To identify physical (color, shape, and size) and chemical characterization of the detected MPs.

Project 3: Mercury in Lake Maurepas and risk assessment of fish and crab consumption

- To collect water, sediment, and plant samples from nine sites and aquatic samples (catfish, and blue crab) from six zones, analyzing for Hg, and comparing results with permissible safety limits.

- To identify temporal and spatial variations in Hg concentrations in water and sediment using Inverse Distance Weighting (IDW) over a full hydrological year encompassing wet and dry seasons.
- To explore the relationship between catfish length-weight and accumulated Hg levels.
- To identify the impact of industrial and anthropogenic activities on Hg levels.

Project 4: Spatial-temporal contaminant spreading analysis in Lake Maurepas in terms of the quality of water and sedimentary mud samples (Gunawardhana et al., 2024)

- To collect water and sedimentary mud samples from nine different sites in the lake on a weekly basis.
- To characterize water quality by determining the physical and chemical properties of the water, including temperature, pH, specific conductance, salinity, and potential contaminant and nutrient concentrations, and assessing the presence of heavy metals (HMs).
- To identify the spatial-temporal variation of these compounds using Inverse Distance Weighting (IDW).
- To forecast water quality for the upcoming weeks using AI.

Project 5: Quantitative Analysis of Contaminants in Lake Maurepas and Source Identification Using BSMRM

- To quantify the levels of more HMs and chemical contamination in Lake Maurepas, with a focus on understanding their vertical distributions and spatial and temporal variability across both drilling and non-drilling sampling sites.
- To identify and analyze the sources of these contaminants using the BSMRM algorithm for nine monitored sites.
- To predict the source profiles' contributions for one unmonitored site, the South Test Well (STW).
- To provide insights into the dynamics of chemical pollution sources in the lake.

Project 6: Air pollution monitoring and source apportionment in Lake Maurepas airshed

- To monitor air pollutant concentrations across the Lake Maurepas airshed.
- To identify major sources contributing to air pollution using PMF.
- To assess seasonal and spatial variations in pollution levels.
- To explore potential correlations between air and water pollutants.

Materials & Methods

Study site

Lake Maurepas (~260 ha), located in southeastern Louisiana, USA (N 30.336260, W 90.481102), is a brackish, round-shaped, shallow lake with an average depth of approximately 3

meters. It is a tidal estuarine system fed by three rivers: the Blind River, the Amite River, and the Tickfaw River (**Figure 1**). The lake is surrounded by swampy areas dominated by bald cypress (*Taxodium distichum*) and tupelo (*Nyssa sylvatica*) trees. Its water levels are influenced by rainfall, wind, and tidal movements from Lake Pontchartrain, which is connected to Lake Maurepas via cypress swamps and fresh-to-intermediate marshland. The lake's wetland fringe and open waters are occasionally populated by floating aquatic plants, including invasive species like water hyacinth (*Eichhornia crassipes*), Gulf swampweed (*Hygrophila lacustris*), water spangles (*Salvinia minima*), and blue-green algae (*Cyanobacteria*). The region experiences a humid subtropical climate, characterized by wet summers and short, mild winters. Lake Maurepas supports a local fishing economy, providing a variety of seafood such as fish, shellfish, and crabs. The most commonly caught commercial fish include channel catfish (*Ictalurus punctatus*), blue catfish (*Ictalurus furcatus*), largemouth bass (*Micropterus salmoides*), sunfish (*Mola mola*), and crappie (*Pomoxis nigromaculatus*). Blue crab (*Callinectes sapidus*) is the predominant species of crab harvested from the lake. In addition to fishing, the lake serves as a hub for recreational activities, including boating and swimming, enjoyed by the local population.

To represent the lake and capture diverse characteristics and potential sources of variability, such as river discharge and anthropogenic activities, seven non-drilling (ND) sites and two of the APC's test well construction sites were chosen for water, sediment, and plant sampling. These sampling sites were named ND1, ND2, ND3, ND4, ND5, ND6, and ND7. The STW and NTW sites are the two test well locations established by Air Products. Sampling at these sites was intended to investigate whether test well construction activities disturb deposited pollutants and release them into the water column. As the South Test Well (STW) construction has been completed, sampling is feasible at the exact STW site. However, due to ongoing construction at the North Test Well (NTW), sampling directly at this site is restricted for safety reasons. Therefore, NTW and ND6 were introduced as additional locations to monitor potential disturbances to the lake caused by NTW construction activities. The ND1, ND2, and ND3 sites are situated near the mouth of the Tickfaw, Amite, and Blind Rivers, respectively. The ND7 site is located near the Manchac swamp bridge and was designated to track pollutant exchange with Lake Pontchartrain via Pass Manchac. **Figure 1** shows the study area, including the water, sediment, and biological sampling locations. Water and sediments were sampled from nine sites. To account for random and continuous mobility of crabs and fish, the lake was divided into six zones for their sampling. The sampling sites and zones were designated to cover the entire lake, ensuring the collection of representative environmental samples that capture the lake's diverse characteristics and potential sources of variability. These locations were chosen based on factors such as pollutant inputs from river discharges and proximity to anthropogenic and industrial activities. A global positioning system (GPS - Garmin eTrex 10) was used to identify and mark each sampling site.

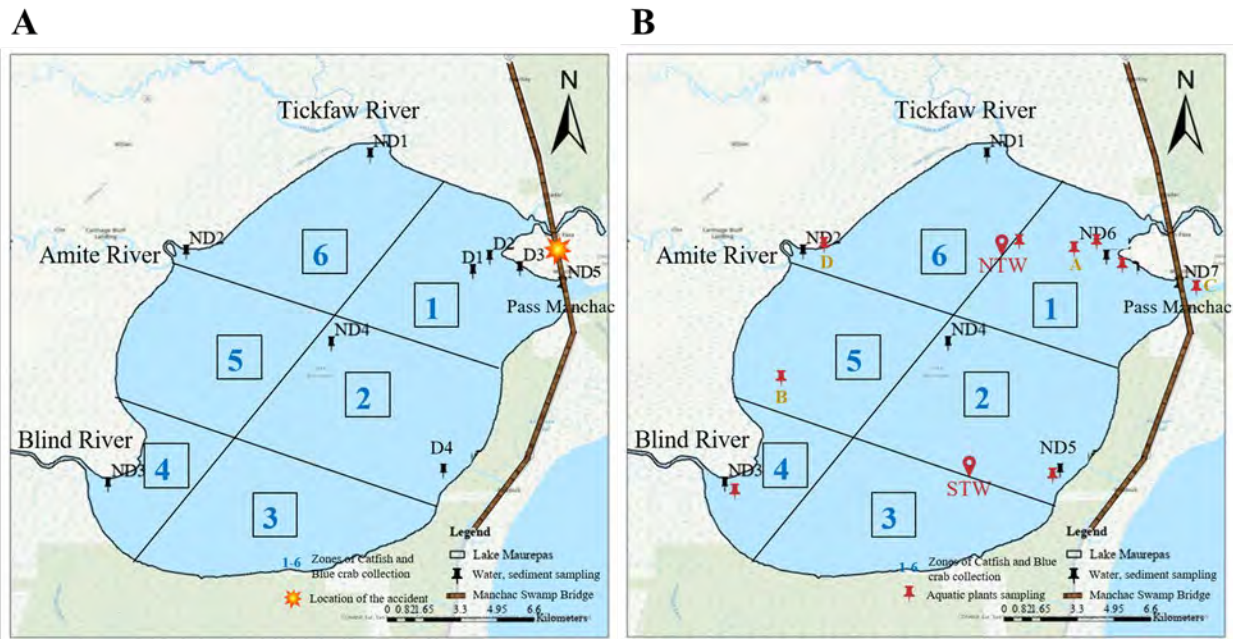


Figure 1. Sampling sites for **(A)** 2023, and **(B)** 2024 in Lake Maurepas, southeastern Louisiana, USA. The black pins indicate the 9 sampling sites where water and sediment samples were collected. STW and NTW represent the south and north test wells, respectively and they were included as water and sediment sampling locations in 2024. The red pins indicate the aquatic plants collection sites. The zones considered for Catfish and Blue crab collection are shown as 1-6. The Tickfaw, Amite, and Blind Rivers discharge freshwater into Lake Maurepas. Black lines mark the boundaries of model compartments, while the yellow icon indicates the site of the catastrophic 'super fog' multi-car pileup on October 23, 2023

Sample Collection

On a weekly basis pending the weather conditions, water, sediment, and aquatic plant samples were collected (**Figure 2**). Water samples were gathered from three different depths: the surface, middle depth (~1.5 m), and lake bed depth (~3 m) using a water sampler (depth sampler, Vernier, Beaverton, OR, USA) in 250 ml polypropylene bottles. Sedimentary mud samples were collected from the lake bed at each site using a grab sampling dredger (Wildco Ekman dredge, Cole Parmer, Vernon Hills, IL, USA). Before use, the tools for sampling were properly rinsed and cleaned. Four types of aquatic plants were collected from the lake: Water Hyacinth (*Eichhornia crassipes*), Gulf Swampweed (*Hygrophila lacustris*), Water Spangles (*Salvinia minima*), and Blue-Green Algae (*Cyanobacteria*). The collection locations for these plants were determined based on their natural presence, as shown in **Figure 1**. The Biological samples were collected by the aquatic monitoring team from six zones. All samples were labeled with the sampling date, depth, and time. All samples were then transported to the

laboratory in an ice chest (Coleman, 94.6 L) with dry ice and stored at -20°C until analysis. For MPs analysis, sampling is conducted monthly starting from October 2024. Water and sedimentary mud samples were stored in clean, labeled 300 mL Glass bottles to prevent contamination. From each depth 100 ml representative samples were combined to make a 300 ml composite sample to represent each sampling site. Metadata, including the sampling date and time, were meticulously recorded for each collection.

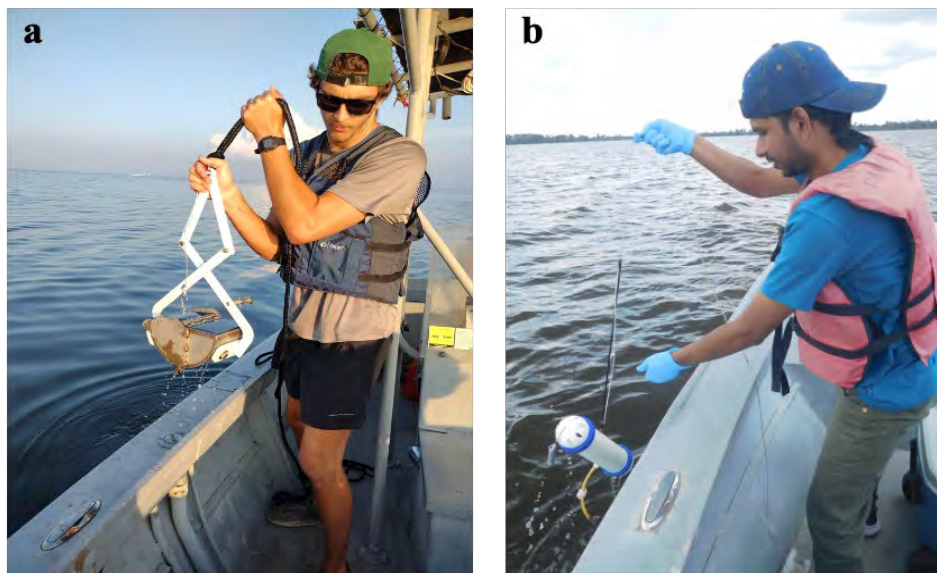


Figure 2. (a) Collecting sediment and (b) water samples from lake.



Figure 3. Environmental samples collected from Lake Maurepas for PFAS analysis: (a) catfish, (b) blue crab, (c) water, and (d) sediment.

Sample Processing, Analysis, and Measurements

Project 1: Identification of per- and polyfluoroalkyl substances (PFAS) in environmental samples from Lake Maurepas, USA, and their potential health implications

Sample preparation. To prepare a well-homogenized water sample for PFAS analysis, 1 mL of water collected on each sampling date, from 9 sites and three distinct depths was combined, resulting in approximately 400 mL of a well-homogenized water sample. Similarly, to prepare a well-homogenized sediment sample, sediments collected over the sampling period from 9 sites were combined, resulting in a 200 g sample. Frozen fish samples were first removed from the freezer and allowed to reach room temperature. Once warmed, the skin and outer surfaces of each fish were cleaned to remove scales and residual water. Using a fillet knife (BUBBA™), each fish was then cut into two pieces, (diagonally along the skeleton from head to tail) and the bones were removed, as this study is only focusing on the edible parts of the fish. The skin and muscle tissues were separated and cut into small pieces. These pieces were then mixed and ground using a laboratory mortar and pestle to obtain a well-homogenized fish sample. This process was repeated separately for each fish collected during the study period. Finally, for the analysis of PFAS, one representative and well-homogenized combined fish sample was prepared. To achieve this, a portion from each homogenized fish sample (representing each fish) was combined to create a single homogenized fish sample of 50g (a mixture of skin and tissues). Each of these steps ensured that the sample accurately represented the fish collected during the entire sampling period. Following the same procedure, blue crab samples were preprocessed. In each crab, the gill tissues, muscle tissues, and hepatopancreas were separated and homogenized in the same manner to obtain a representative sample. Once homogenized, both the catfish and blue crab samples were ready for PFAS analysis (**Figure 3**).

Experimentation. The PFAS measurement of environmental samples was conducted at the Center for Air Resources Engineering and Science, Clarkson University, Potsdam, New York. The methodology for measuring PFAS in environmental samples was followed as described in previous studies by Parvizian et al. (2024); Fakouri Baygi et al. (2016) and (2019) ; Fernando et al. (2018); Ren et al. (2022) and Point et al. (2019). Fourty four PFAS, which are frequently detected in environmental samples such as lake water, sediments, and biological samples, were targeted in this analysis. The extraction method for linear perfluoroalkyl substances (PFAS) was adapted from the approach outlined by Point et al. (2019). Approximately 0.5 g of homogenized sample was measured and transferred into a 15 mL polypropylene centrifuge tube. A mass-labeled PFAS solution containing 4 ng of specific PFAS standards (PFAS-MAX, M2PFTeDA, and M2PFHxDA) and 3 mL of 0.2% formic acid in acetonitrile was added. The mixture was homogenized using an ultrasonic probe and centrifuged at 4,000 × g for 10 minutes. The supernatant was collected, and the remaining tissue was re-extracted with another 3 mL of

0.2% formic acid in acetonitrile, following the same procedure. The combined extracts were then processed further. To purify the combined extract, solid-phase extraction (SPE) was employed using Oasis WAX cartridges (3 cc, 60 mg, 30 µm particle size). Prior to sample loading, the cartridges were conditioned sequentially with 3 mL of methanol containing 1% ammonium hydroxide, 3 mL of methanol, and 3 mL of LC-MS-grade deionized water. After adding 2.62 mL of water to the cartridge, 0.5 mL of sample was loaded at a controlled flow rate (1-2 mL/min). The loading process was repeated three times. The cartridges were washed with 1 mL of 2% aqueous formic acid, followed by two 1-mL rinses with deionized water. The cartridges were dried under vacuum (20 in Hg) until the sorbent bed appeared uniformly lighter, indicating complete drying. Elution was carried out with 3 mL of methanol containing 1% ammonium hydroxide. The eluate was collected in a polypropylene tube, evaporated to a volume of 0.5 mL under nitrogen at 55°C, and transferred to autosampler vials (0.7 mL). A 25 µL spike of an injection standard solution (40 ng/mL M7PFUdA and M5PFHxA) was added to each vial for analysis. The quantification of linear PFAS compounds was performed using a Thermo Vanquish liquid chromatography coupled to a Thermo Altis triple quadrupole mass spectrometer. Sample injection volumes were 10 µL. Separation of PFAS isomers was achieved on an Acquity UPLC HSS T3 column (2.1 × 100 mm, 1.8 µm) with a mobile phase starting composition of 75:25 methanol/water containing 0.2% formic acid at a flow rate of 0.4 mL/min. Instrumental settings, including solvent gradient, quantification transitions, collision energy, and retention times, adhered to the specifications reported by Point et al. (2019). Data acquisition was managed using Xcalibur (version 4.2.28.14), and data processing utilized TraceFinder™ (4.1 – EFS, Thermo Scientific™) (Ren et al., 2022).

Quality control. The method detection limits (MDLs) for targeted PFAS in previous analyses ranged from 0.01 to 0.11 ng/g. Extraction blanks were analyzed alongside sample matrices in each batch to control for contamination. A series of recovery standards were employed in the PFAS analyses. The mean recoveries of these PFAS standards were typically 80 to 120%. A method blank was coextracted with each batch of samples (10 samples per batch) for PFAS analysis. PFAS were not detected in the method blanks, and the mean recoveries of PFAS standards in method blanks were greater than 72%.

Project 2: Detection and characterization of microplastics in water, sediment and biological samples from Lake Maurepas

Sample preparation. Three replicates of 100 mL of water samples were measured with a measuring cylinder. All samples were digested with 30% hydrogen peroxide (H₂O₂) to dissolve organic matters for 24 hours at 60° C temperature. After complete digestion, the water sample was filtered using a 1.2 µm Whatman glass microfiber filter through air-free vacuum filtration. So far we have completed analysis of 27 water samples. The filter paper was then dried at 50° C

using an oven, and stored into a glass petri dish for microscopic examinations (Alam et al., 2023), **Figure 4**. The sediment sample was first completely dehydrated in the oven at 60 °C for 1–2 days. After drying, three replicate samples of 1 g were taken in a glass beaker. Then 30% hydrogen peroxide was added to break down the organic debris at 60 °C, 300 rpm for 48 h. The digestion step should continue until no foaming was observed while adding H₂O₂ (Simon-Sánchez et al., 2024). To separate MP particles from debris, density separation was performed with saturated ZnCl₂ solution (1.7 g cm⁻³) (Teampanpong et al., 2024), and stirred for 5 minutes, then the sample was kept at room temperature for 48 hours to settle debris. After settling the sediment sample, surface water was vacuum filtered using a 1.2 µm Whatman glass microfiber filter through air-free vacuum filtration. 27 sediment samples have been processed so far, and MPs counting for those samples are underway, **Figure 5**. Prior to dissection of biological samples, frozen samples were placed in a pre-cleaned aluminium dissecting tray without wax (Fisher Scientific) and kept to thaw for 3 to 4 h at room temperature inside the fume hood. After that aquatic species (Blue Crabs, Catfish) were dissected with a knife, and different tissues were segregated and grounded using mortar. Soft tissues were placed individually in pre-cleaned glass bottles. The height and weight of the aquatic species samples were carefully measured. A chemical digestion with 10 % KOH (10:1, v/w ratio) was performed for 48 h or until complete digestion at 60 °C and 180 rpm (Leistenschneider et al., 2024; Piyawardhana et al., 2022; Lefebvre et al., 2024). A secondary digestion was performed with 30 % H₂O₂ removing any remaining organic materials in the sample. So far, we have completed the digestion and filtration of 27 biological samples, **Figure 6**.

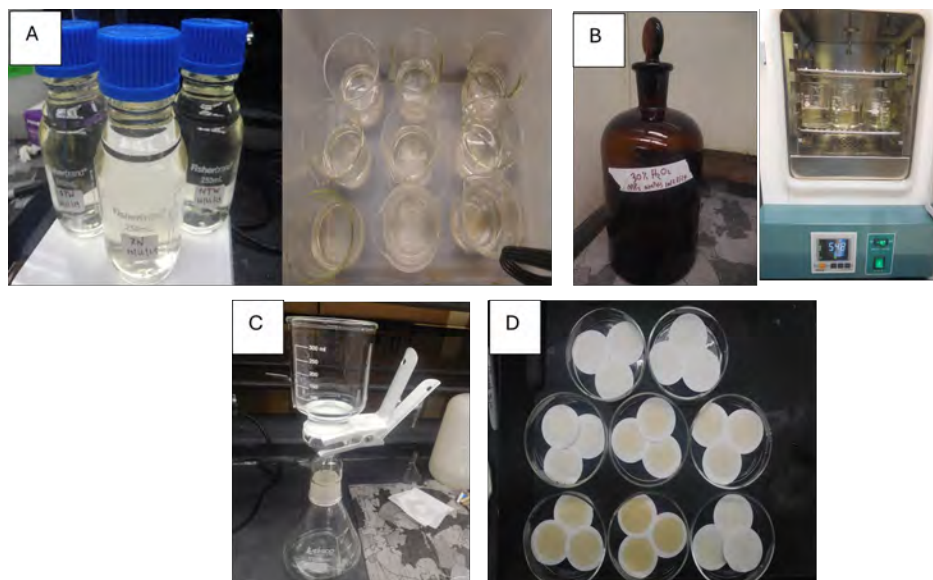


Figure 4. Water sample processing for MPs analysis; **(a)** Water sample from the lake in glass bottle, **(b)** Digestion to remove organic components, **(c)** Vacuum filtration, **(d)** filter paper for MPs identification.

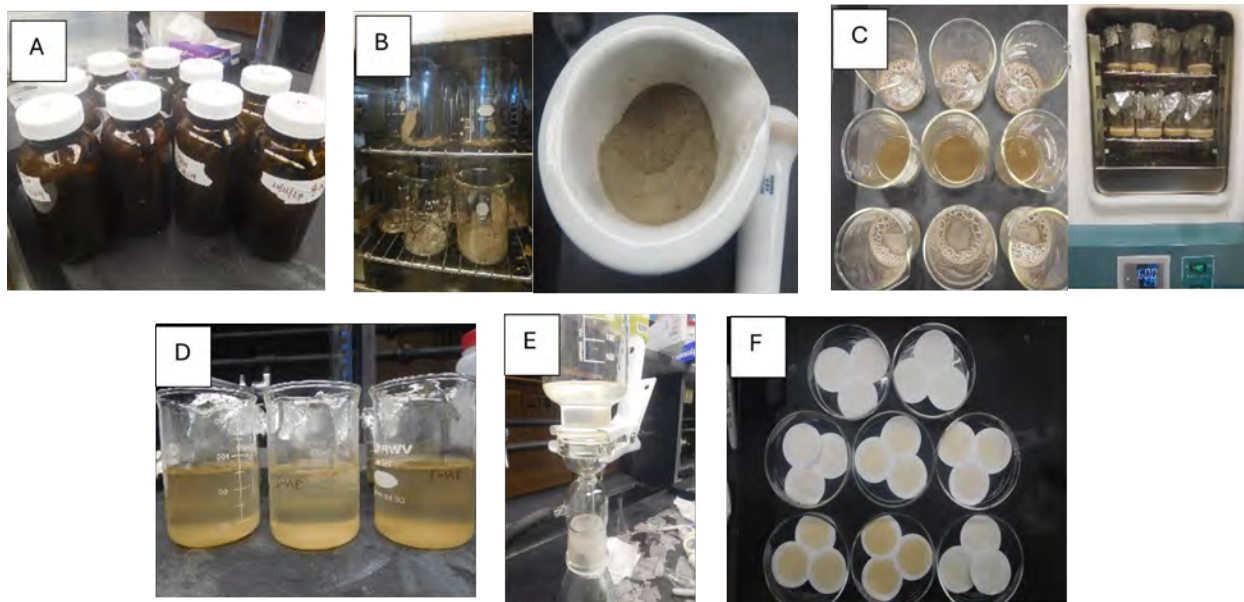


Figure 5. Sediment sample processing for MPs analysis; **(a)** Sediment sample from the lake in glass bottle, **(b)** Drying and grinding, **(c)** Digestion of the sample to eliminate organic components, **(d)** Density separation, **(e)** Vacuum filtration, **(f)** filter paper for MPs identification.

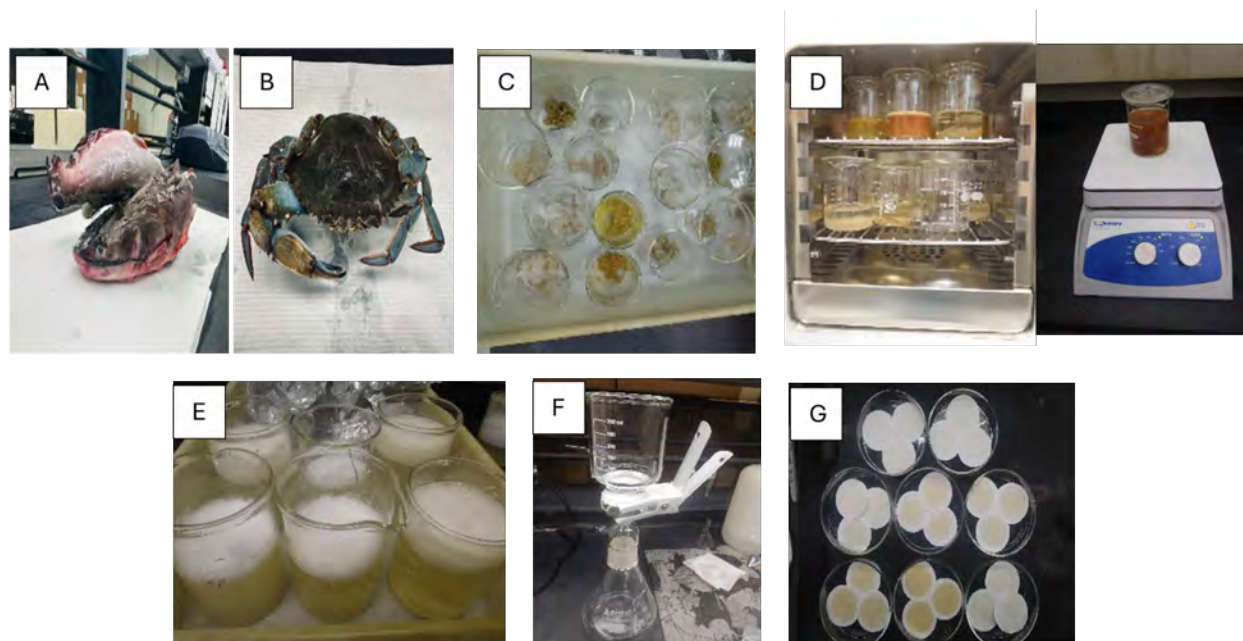


Figure 6. Biological sample processing for MPs analysis; **(a)** and **(b)** Catfish and Blue crab samples from the lake, **(c)** Dissection and segregation into different tissues, **(d)** Digestion with KOH to separate organic compounds, **(e)** Secondary digestion with H₂O₂, **(f)** Vacuum filtration, **(g)** filter paper for MPs identification.

Experimentation. A stereo microscope was used to examine the filter paper for MPs particle detection. Visual identification of MPs was conducted using Olympus SZ-61TR Stereomicroscope with 6.7x - 45x magnification range, and built-in InFocus software was used to maintain and capture images of MPs with a 4k camera attached to the microscope. Alongside the quantification of MPs, particles were classified into fiber, fragment, foam, film and pellet based on their shape. They were also separated into different color categories such as blue, white, red, transparent, green, yellow, brown, and black. Moreover, MPs were categorized into four groups based on their size such as $< 100 \mu\text{m}$, $100\text{-}500 \mu\text{m}$, $500\text{-}1000 \mu\text{m}$ and $1000\text{-}5000 \mu\text{m}$, **Figure 7**. During the microscopic observation, different types of MPs particles are randomly depicted for their chemical characterization by ATR-FTIR. Nicolet iS 10 FTIR was used to collect sample spectra in absorbance mode. All spectra were recorded with 32 scans in the region of $4000\text{--}400 \text{ cm}^{-1}$, with 4 cm^{-1} sampling resolution. The spectra obtained from the FTIR need to be compared against the spectral database of synthetic polymers to match polymer type, **Figure 8**. This step is ongoing.



Figure 7. Stereo microscope with attached camera for MPs quantification.



Figure 8. Fourier Transform Infrared Spectroscopy (FT-IR) for chemical characterization of MPs.

Quality control. Glass sampling bottles and apparatus were used to avoid contamination. To prevent contamination during work, 100% cotton made lab coats are worn while experimenting. In each measurement, two to three replications were carried out to get an impartial result. Moreover, the blank samples were also studied to find any contamination. Additionally, all the sample preprocessing and analysis was performed inside the fume hood to reduce airborne contamination. Milli-Q water was used for chemical preparation and rinsing glassware before use.

Project 3: Mercury in Lake Maurepas and risk assessment of fish and crab consumption

Sample preparation. Similar to water and sedimentary mud samples, the aquatic plant samples were transported to the laboratory in an ice chest. Upon arrival, the plants' weights were recorded, and the longest root, stem, and leaf lengths were measured. Each plant part (roots, stems, and leaves) was then separately homogenized. Initial homogenization was performed using a multifunction food chopper (VEVOR, 7 L), followed by further homogenization using a laboratory mortar and pestle. The homogenized samples were individually placed in labeled, sealed bags and stored in a laboratory freezer at -20°C until analysis. Frozen fish samples were thawed and cleaned to remove external contaminants such as scales or residual water. The weight of each fish was recorded using a laboratory scale (VWR-203B), and length measurements were taken using a ruler. Muscle tissues and skin were carefully separated using a fillet knife (BUBBA™), cut into smaller pieces, and thoroughly homogenized using a laboratory mortar and pestle. This homogenization ensured even distribution of Hg within the sample, providing a representative tissue sample for analysis. Blue crabs were thawed and cleaned using paper towels (Bounty). The weight of each crab was measured using a laboratory scale (VWR-203B), and length measurements were recorded using a ruler. Specific tissues, including

gill tissue, muscle tissue, and hepatopancreas (as illustrated in **Figure 9**), were carefully separated and homogenized thoroughly with a laboratory mortar and pestle to ensure even Hg distribution. After homogenization, both catfish and Blue Crab samples were placed in sterile, leakproof, transparent sampling bags (Nasco Whirl-Pak) and stored at -20°C in the laboratory freezer until analysis. This pre-processing step ensured the samples were adequately prepared for direct Hg analysis, facilitating accurate measurement of total Hg content using the analytical instrument.

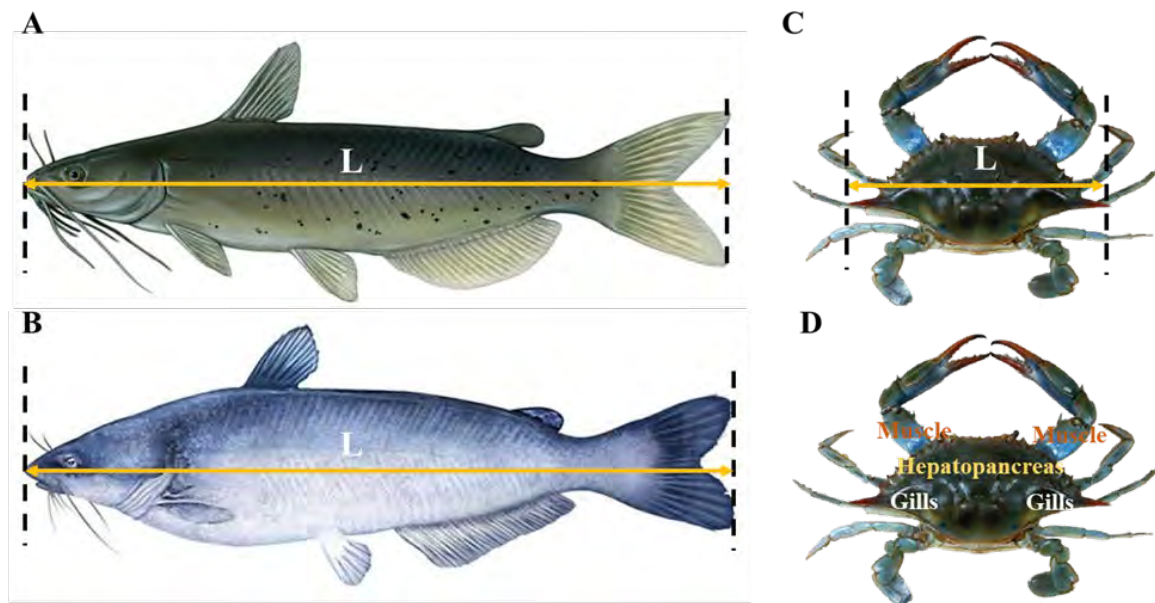


Figure 9. Length measurements for **(A)** Channel Catfish, **(B)** Blue Catfish, **(C)** Blue Crab, **(D)** Different parts of the body of the Blue Crab which were analyzed for Hg.

Experimentation. The Direct Mercury Analyzer (Milestone DMA-80 evo) was used to measure Hg concentrations in three replicates of all sample types. An accurately weighed portion (approximately 0.1–0.2 g) of water, sedimentary mud, aquatic plant, homogenized catfish, and homogenized Blue Crab samples was measured using a high-precision analytical balance (Sartorius BCE64-1S). The sample was then placed in a quartz cuvette and loaded into the analyzer's autosampler for analysis. The precise weight of each sample was recorded in the datalogger, as the DMA relies on this value to calculate Hg concentrations in each sample. The instrument output provided results in the unit of $\mu\text{g}/\text{kg}$. The calibration curve used in the instrument covered a measurement range of low ppt level (parts per trillion) to the high ppm level, with a detection limit of 0.0003 ng of Hg.

Project 4: Spatial-temporal contaminant spreading analysis in Lake Maurepas in terms of the quality of water and sedimentary mud samples (Gunawardhana et al., 2024)

Measurements. Water temperature (T), salinity, and specific conductivity (SC) were collected from the USGS monitoring station. pH was measured in situ during field sampling using a pH meter (YSI Environmental, Yellow Springs, OH, USA), which was calibrated with appropriate solutions prior to each fieldwork session. Total nitrogen (TN), ammonia nitrogen (NH₃-N), and total phosphorus (TP) were measured using the persulfate digestion method, the salicylate TNT method, and the USEPA PhosVer® 3 with acid persulfate digestion method, respectively. Chemical oxygen demand (COD) was measured using the reactor digestion method with a sample digester (HACH DRB 200), a UV-visible spectrometer (HACH DR 3900), and manufacturer-provided analysis kits. Mercury (Hg) was analyzed using a Direct Mercury Analyzer (Milestone DMA-80 evo, Shelton, CT, USA), while other heavy metals were measured using a Microwave Plasma Atomic Emission Spectrometer (Agilent MP-AES 4210, Santa Clara, CA, USA). Water samples were filtered through syringe filters with a pore size of 0.45 µm (VWR International, LLC, Radnor, PA, USA) before chemical analysis. All measurements were performed in triplicate.

COD. COD is a measure of the total quantity of oxygen required to chemically oxidize both organic and inorganic matter in water. Organic pollutants are the primary contributors to COD. The results in mg/L COD are defined as the milligrams of O₂ consumed per liter of sample under the conditions of this procedure. In this method, the sample is heated for two hours with sulfuric acid and a strong oxidizing agent, potassium dichromate. During this process, oxidizable organic compounds react and reduce the dichromate ion (Cr₂O₇²⁻) to green chromic ion (Cr³⁺). The following kinetic reaction happens with all organic compounds present in the sample selectively. $C_nH_aO_bN_c + dCr_2O_7^{2-} + (8d + c) H^+ \rightarrow nCO_2 + ((a+8d-3c)/2) H_2O + cNH_4 + + 2dCr^{3+}$ The COD reagent also contains silver and mercury ions, where silver acts as a catalyst and mercury is used to complex chloride interferences. The color intensity is measured based on the amount of Cr³⁺ produced after the oxidation reaction. The UV-visible spectrometer measurement is taken within the wavelength range of 600 to 620 nm. Following the stoichiometry ratio, the corresponding amount of COD is directly read from the UV-visible spectrophotometer screen and is determined.

TN. The alkaline persulfate digestion converts all forms of nitrogen to nitrate (NO₃⁻). Following the digestion, sodium metabisulfite is added to eliminate halogen oxide interferences. The nitrate then reacts with chromotropic acid under strongly acidic conditions to form a yellow complex. The measurement wavelength is 410 nm for UV-visible spectrophotometer.

NH₃-N. Ammonia compounds react with chlorine to form monochloramine (NH₂Cl), which then reacts with salicylate to produce 5-aminosalicylate. This 5-aminosalicylate is subsequently oxidized in the presence of a sodium nitroprusside catalyst, forming a blue-colored indophenol complex (OC₆H₄NC₆H₄OH). The blue color is masked by the yellow color from the excess reagent, resulting in a green-colored solution. The measurement wavelength is 655 nm for UV-visible spectrophotometer.

TP. Phosphates in organic and condensed inorganic forms (meta-, pyro-, or other polyphosphates) must be converted to reactive orthophosphate before analysis. Pretreating the sample with acid and heat facilitates the hydrolysis of condensed inorganic forms. Organic phosphates are converted to orthophosphates by heating with acid and persulfate. Orthophosphate then reacts with molybdate in an acidic medium to form a mixed phosphate/molybdate complex. Ascorbic acid reduces this complex, producing an intense molybdenum blue color. The measurement wavelength is 880 nm for UV-visible spectrophotometer.

Spatiotemporal analysis. In our study, we used Inverse Distance Weighting (IDW) method incorporated in Geographic Information Systems (GIS) interpolation modeling as a valuable method for predicting attributes at sites where no direct measurements are available. The equation below represents the mathematical expression for the inverse distance weighting (IDW) interpolation technique.

$$Z(S_0) = \sum_{i=1}^n W_i Z(S_i)$$

where $Z(S_0)$ is the concentration value in unsampled site S_0 , $Z(S_i)$ is the concentration value at the sampling site S_i , n is the number of sampling sites, and W_i represents the weight of the S_i which is defined according to the following equation;

$$W_i = \frac{\frac{1}{d_i^k}}{\left(\sum_{i=1}^n \frac{1}{d_i^k}\right)} \quad i=1,2,\dots,n$$

where d_i is the horizontal distance between the interpolation points and the points observed, and k is the distance exponent. In this equation, the weights are inversely proportional to the distance (between the data point and the prediction location). All interpolation calculations were performed with ArcGIS Pro 3.3 software (Esri, Redlands, CA, USA) and for the mapping purposes, Lake Maurepas shape files were extracted from the United States Geological Survey (USGS) website.

Water quality forecasting. We examined four forecasting models—basic curve fitting, exponential smoothing, forest-based approach, and Long Short-Term Memory networks (LSTM)—to predict the concentrations of COD, TN, TP, As, and Pb in nine different sampling sites for December 2023. December was selected for analysis due to missed sampling caused by

adverse weather conditions. The highest rainfall occurred on December 2, 2023 with a sudden reduction in salinity and specific conductance in the lake water. Additionally, STW construction work was ongoing during this month. This analysis aimed to assess how these conditions could potentially impact the lake's water quality. The curve fitting forecast method predicts values across each site of a space-time cube, which represents data in a three-dimensional format where one axis denotes time and the other two represent spatial dimensions such as latitude and longitude. It employs curve fitting techniques such as linear, parabolic, exponential, and S-shaped/Gompertz functions. In contrast, the exponential smoothing forecast method uses the Holt-Winters method to predict future values at each site within the space-time cube. This involves decomposing the time series at each site into seasonal patterns and trends. The forest-based forecast method predicts future values for each site in a space-time cube using a modified version of the random forest algorithm, a supervised machine learning technique. This method trains a forest regression model on time windows at each site within the cube. On the other hand, the LSTM model was employed to predict water quality parameters using past data and associated environmental factors. The approach involved training the LSTM network on time series data to capture temporal dependencies between water quality parameters and environmental factors. Three scenarios were evaluated to determine the optimal input configuration. Scenario 1 considered only the environmental factors that showed a significant correlation with the specific water quality parameter. Scenario 2 excluded environmental factors that were highly correlated with each other and focused on the remaining factors. Scenario 3 considered all available environmental factors as input features without filtering based on correlation. The environmental factors considered for this analysis included pH, temperature, dew point, humidity, pressure, precipitation, wind speed, wind direction, salinity, and specific conductance. While pH values were measured during sampling, precipitation and wind data were collected from Kenner, LA Weather History at Louis Armstrong New Orleans International Airport Station. The remaining data were collected from the United States Geological Survey Pass Manchac, Lake Maurepas, LA monitoring station. Finally, the Root Mean Square Error (RMSE) is calculated and compared to evaluate the most suitable model for each site. The following equation gives the forecast RMSE formula:

$$\text{Forecast RMSE} = \sqrt{\frac{\sum_{t=1}^T (ct - rt)^2}{T}}$$

where T is the number of time steps, ct is the value of the forest model, and rt is the raw/measured value of the time series at time t. The measured and forecasted values of the pollutants were statistically compared using one-way analysis of variance (One-way ANOVA) with a 95% confidence interval (CI) library in RStudio software (V: 2023.12.1).

Project 5: Quantitative Analysis of Contaminants in Lake Maurepas and Source Identification Using BSMRM

Sample processing and measurements. Prior to analysis, each sample was filtered through a 0.45 µm pore size syringe filter (VWR International, LLC). The analyses were carried out at room temperature, with triplicate measurements performed for each sample. The reported results include average values along with standard deviations from the repeated measurements. Physical parameters such as temperature and pH were measured directly at the site using a pre-calibrated pH meter (YSI Environmental, USA). Biochemical parameters, including COD and nutrient concentrations (TP, TN, NH₃-N), were analyzed using colorimetric techniques with HACH testing kits and reagent supplies. Sample digestion was conducted using a HACH DRB 200 reactor, with subsequent measurements taken using a HACH DR3900 spectrophotometer. For elemental analysis, including Hg, As, Zn, Cd, Sr, Ba, Cu, Ni, Pb, and Mn, a microwave plasma atomic emission spectrometer (MP-AES, Agilent-4210, USA) with an autosampler was utilized. All sample collection and analytical procedures adhered to the standard protocols for water and wastewater treatment specified by the American Public Health Association (APHA, 2012). The detailed procedures and methodology have been documented in previous work by Gunawardha et al. (2024), Project 4.

Statistical analysis. All collected data were analyzed using RStudio Desktop (Version 2024.04.2) to ensure robust statistical interpretation. Initially, we assessed the normality of the dataset by conducting a Kolmogorov-Smirnov (KS) test (Steinskog et al., 2007). A p-value greater than 0.05 indicated that the null hypothesis was not rejected, suggesting the data likely conforms to a normal distribution. Following the normality assessment, ANOVA was employed to evaluate the statistical significance of contaminant levels across three vertical depths at nine sampling sites over fifteen sampling dates. This statistical method helped identify variations in contaminant concentrations and their potential interactions with depth and location.

Receptor modeling. Furthermore, the study implemented the Bayesian Spatial Multivariate Receptor Model (BSMRM), an advanced extension of traditional multivariate receptor models. This approach integrates spatial features to account for varying influences across multiple sampling sites, thus enhancing the model's ability to reflect complex interactions between contamination sources and environmental factors (Park et al., 2021). This comprehensive statistical framework allowed for a thorough investigation of the contaminant dynamics in the studied environment, contributing to a better understanding of the factors affecting water quality. This extended model is referred to as the spatially extended Bayesian multivariate receptor model (BSMRM) (Park et al., 2021). For N number of receptors sites, the model explained in matrix term is as follow:

$$X_t = KG_tP + E_t \quad (1)$$

where, X_t is an $N \times J$ matrix, that consists of the concentration of J pollutants observed at N locations. G_t represents q underlying processes located at L spatial locations selected from a coarse grid that covers a spatial domain, K . E_t is a J dimensional error vector for each observation.

Project 6: Air pollution monitoring and source apportionment in Lake Maurepas airshed

Data collection. The overall abstract of the methodology used in this study is shown in **Figure 10**. Real-time data collection was accomplished using a single monitoring station located near Lake Maurepas (30°17'38.9"N, 90°20'05.9"W). The station was equipped with advanced sensors capable of measuring multiple air pollutants in real time. These sensors provided high-frequency data with measurements recorded every 15 minutes from January 26, 2024 to September 23, 2024. The location of the monitoring station is shown in **Figure 11**. The collected data was automatically uploaded to a secure cloud database which was accessible via a user-friendly web dashboard. This setup allowed for efficient data storage, retrieval, and visualization. The pollutants measured, their respective detection ranges, limits of detection (LOD), and accuracies are detailed in **Table 1**. Using the 15-minute interval data, daily, weekly, and monthly averages were calculated using a basic averaging method (Venkatram, 2002) to analyze temporal trends and patterns. Missing data was addressed using the K-nearest neighbor (KNN) algorithm, with $K=10$ (Junninen et al., 2004).

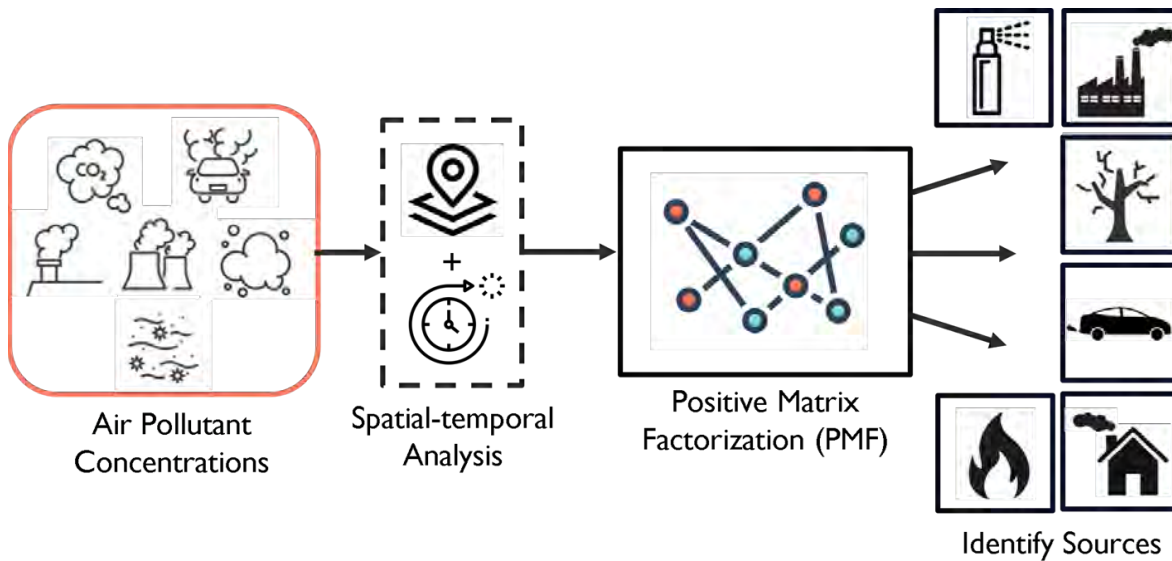


Figure 10. Abstract illustration of the methodology.

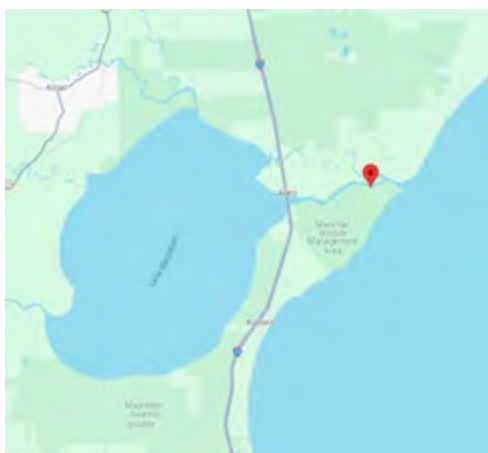


Figure 11. Location of the air pollution monitoring station (30°17'38.9"N, 90°20'05.9"W)

Table 1. Pollutants measured, their respective detection ranges, limits of detection (LOD), and accuracies.

Measurement	Unit	Range	Limit of Detection (LOD)	Accuracy
CO	ppb	0-8000	<30	20
CO ₂	ppb	0-5x10 ⁶	<1000	50
TVOC	ppb	0-2500	<10	50
H ₂ S	ppb	0-10000	<1	1
NO ₂	ppb	0-4900	<1	4
SO ₂	Ppb	0-1100	<2	20
PM1	µg/m ³	0-100000	0	5
PM2.5	µg/m ³	0-150000	0	5
PM4	µg/m ³	0-225000	0	5
PM10	µg/m ³	0-250000	0	5
Pressure	Mbar	500-1500	1	5
Humidity	% RH	0-100	1	5
Temperature	°C	(-20)-(+100)	0.1	2

Preliminary data analysis. A preliminary data analysis was conducted to examine the descriptive statistics of the collected dataset (Costabile et al., 2006). Key parameters, including data count, mean, standard deviation, minimum and maximum values, as well as the primary quartiles (Q1, Q2, and Q3), were calculated. This analysis provided a foundational understanding of the dataset's distribution and variability, offering critical insights into the overall trends and characteristics of the recorded measurements. Next, the time series variations of seasonal patterns were visualized and compared against the safe threshold limits established by the environmental protection agency (EPA). These thresholds, outlined in **Table 2**, serve as benchmarks for assessing air quality. However, it is important to note that neither the EPA nor any other governing body has defined safe limits for certain pollutants, such as PM1 and PM4. This lack of standardized thresholds for these fine particulate matter fractions highlights a critical gap in regulatory frameworks and underscores the need for further research to evaluate their potential health and environmental impacts.

Table 2. Safe threshold limits established by the US EPA

Species	Safe limit
CO	9000 ppb
CO ₂	5,000,000 ppb
TVOC	610 ppb
H ₂ S	10000 ppb
NO ₂	100 ppb
SO ₂	75 ppb
PM1	Not defined
PM2.5	9 µg/m ³
PM4	Not defined
PM10	15 µg/m ³

Positive Matrix Factorization (PMF). PMF (Paatero & Tapper, 1994) is a mathematical technique used to decompose a matrix X into two lower-dimensional matrices, W and H , while ensuring that all elements in these matrices are non-negative. The main goal is to approximate the original matrix X by the product of W and H , i.e.,

$$X \approx W \cdot H$$

where:

$X \in R^{m \times n}$ is the original concentration matrix;

$W \in R^{m \times r}$ is the source contribution matrix;

$H \in R^{r \times n}$ is the source profile matrix;
 r is the rank of the factorization, which is typically much smaller than both m and n .

The factorization aims to discover a low-rank approximation of X , where each element of W and H is non-negative. This makes PMF suitable for problems where negative values are not meaningful, especially in source identification of air pollutants (Reff et al., 2007). The primary objective of PMF is to minimize the reconstruction error between the original matrix X and its approximation $W \cdot H$. This is done by solving the following optimization problem:

$$\sum_{(i,j) \in \Omega} \frac{(x_{i,j} - W_i H_j)^2}{\sigma_{i,j}} + \lambda (\|W\|_F^2 + \|H\|_F^2)$$

where:

- Ω represents the set of observed entries in X ;
- $X_{i,j}$ is the observed value at position (i, j) in the matrix X ;
- W_i is the i^{th} row of W and H_j is the j^{th} column of H ;
- $\|W\|_F^2$ and $\|H\|_F^2$ are the Frobenius norms of the matrices W and H respectively, which serve as regularization terms;
- λ is the regularization parameter that controls the trade-off between the reconstruction error and the magnitude of the model parameters;
- $\sigma_{i,j}$ is the uncertainty of the data point at the location (i, j) in the matrix X (Paatero et al., 2014).

The first term in the objective function minimizes the squared error between the predicted and actual values of the observed entries. The second term is a regularization that prevents overfitting by penalizing large values in W and H (Paatero et al., 2014). The experiments related to PMF analysis will be conducted using the EPA PMF V5 software, applied to 1-hour averaged size-resolved number concentrations and total number concentrations obtained from the recorded dataset (Squizzato et al., 2019). All missing concentrations were replaced by the median value for the given species and their uncertainties were set at four times the value (Squizzato et al., 2019). The particle number concentration uncertainties will be estimated using (Ogulei et al., 2006):

$$\sigma_{i,j} = \alpha (N_{i,j} + \underline{N_j})$$

where $\alpha = 0.01$; N is the observed number concentration; and $\underline{N_j}$ is the arithmetic mean of the reported values N .

Results

Project 1: Identification of per- and polyfluoroalkyl substances (PFAS) in environmental samples from Lake Maurepas, USA, and their potential health implications

Table 3. Analyzed PFAS in environmental samples.

Compound	Full name
11Cl-PF3OudS	11-chloroeicosafluoro-3-oxaundecane-1-sulfonic acid
3:3 FTCA (FPrPA)	Fluorotelomer carboxylic acid
4:2 FTS	4:2 Fluorotelomer sulfonic acid
5:3 FTCA (FPePA)	5:3 Fluorotelomer carboxylic acid
6:2 FTS	6:2 fluorotelomer sulfonate
7:3 FTCA (FHpPA)	3-Perfluoroheptyl propanoic acid
8:2 FTS	8:2 Fluorotelomer sulfonic acid
9Cl-PF3ONS	9-Chlorohexadecafluoro-3-Oxanone-1-Sulfonic Acid
EtFOSA	N-ethyl perfluorooctane sulfonamide
EtFOSAA	N-ethyl perfluorooctane sulfonamido acetic acid
EtFOSE	N-ethyl perfluorooctanesulfonamidoethanol
FOSA-1	Perfluorooctanesulfonamide
Gen X (HFPO-DA)	Hexafluoropropylene oxide dimer acid
MeFOSA	N-Methyl perfluorooctane sulfonamide
MeFOSAA	N-methylperfluorooctane sulfonamidoacetic acid
MeFOSE	N-Methyl perfluorooctane sulfonamidoethanol
NaDONA	Sodium dodecafluoro-3H-4,8-dioxanonanoate
NFDHA (3,6-OPFHpA)	Perfluoro-3,6-dioxaheptanoic acid
PFBA	Perfluorobutanoic acid
PFBS	Perfluorobutane sulfonate
PFDA	Perfluorodecanoic Acid
PFDoA	Perfluorododecanoic acid
PFDoS	Perfluorododecanesulfonic acid
PFDS	Perfluorodecanesulfonic Acid
PFEESA	Perfluoro(2-ethoxyethane) sulfonic acid
PFHpA	PFHpA - Perfluoroheptanoic acid
PFHpS	Perfluoroheptane sulfonic acid
PFHxA	Perfluorohexanoic Acid
PFHxS	Perfluorohexanesulfonic acid
PFMBA (PF50HxA)	Perfluoro(4-methoxybutanoic) acid
PFMPA (PF40PeA)	Perfluoro-3-methoxypropanoic acid
PFNA	Perfluorononanoic acid
PFNS	Perfluorononanesulfonic acid
PFOA	Perfluorooctanoic acid
PFOS	Perfluorooctanesulfonic acid
PFPeA	Perfluoropentanoic acid

PFPeS	Perfluoropentane sulfonic acid
PFTeDA	Perfluorotetradecanoic acid
PFTrDA	Perfluorotridecanoic acid
PfUDA	Perfluoroundecanoic acid
11Cl-PF3OudS	11-chloroeicosafluoro-3-oxaundecane-1-sulfonic acid
3:3 FTCA (FPrPA)	Fluorotelomer carboxylic acid

Table 4. The detected PFAS in environmental samples.

PFAS	Sample type			
	Water (ng/L)	Sediment (ng/g)	Catfish (ng/g) (n=19)	Blue Crab (ng/g) (n=10)
PFDA	O*	O	O	O
PFDoA	O	O	O	O
PFNA	O	O	ND	O
PFOA	O	NA	O	O
PFOA Linear	NA	O	NA	NA
PFOA Branched	NA	ND	NA	NA
PFOS Linear	O	O	O	O
PFOS Branched	O	O	ND	ND
PFuDA	O	O	O	O
5:3 FTCA (FPePA)	ND	ND	O	ND
6:2 FTS	ND	O	O	O
7:3 FTCA (FHpPA)	ND	ND	O	O
FOSA-1	O	O	O	O
MeFOSAA	ND	ND	ND	ND
NaDONA	O	ND	ND	ND
PFBA	O	O	ND	ND
PFBS	O	O	ND	ND
PFHpA	O	ND	ND	ND
PFHxA	O	O	ND	ND
PFPeA	O	O	ND	ND
PFTeDA	ND	ND	O	O
PFTrDA	ND	ND	O	O
11Cl-PF3OudS	ND	ND	ND	ND
3:3 FTCA (FPrPA)	ND	ND	ND	ND
4:2 FTS	ND	ND	ND	ND
8:2 FTS	ND	ND	ND	ND
9Cl-PF3ONS	ND	ND	ND	ND
EtFOSA	ND	ND	ND	ND
EtFOSAA	ND	ND	ND	ND

EtFOSE	ND	ND	ND	ND
Gen X (HFPO-DA)	ND	ND	ND	ND
MeFOSA	ND	ND	ND	ND
MeFOSE	ND	ND	ND	ND
NFDHA (3,6-OPFHpA)	ND	ND	ND	ND
PFDoS	ND	ND	ND	ND
PFDS	ND	ND	O	O
PFEESA	ND	ND	ND	ND
PFHxS Branched	ND	O	ND	ND
PFHxS Linear	ND	O	ND	ND
PFMBA (PF50HxA)	ND	ND	ND	ND
PFMPA (PF40PeA)	ND	O	ND	ND
PFHpS	ND	ND	ND	ND
PFNS	ND	ND	ND	ND
PFPeS	ND	ND	ND	ND

* "O" indicates the detection of the PFAS in an environmental sample, while ND represents "non-detection" and NA means "not analyzed." The symbol "n" denotes the number of fish and crabs collected, and each concentration value represents the concentration of a well-homogenized sample prepared from 19 catfish and 10 crabs.

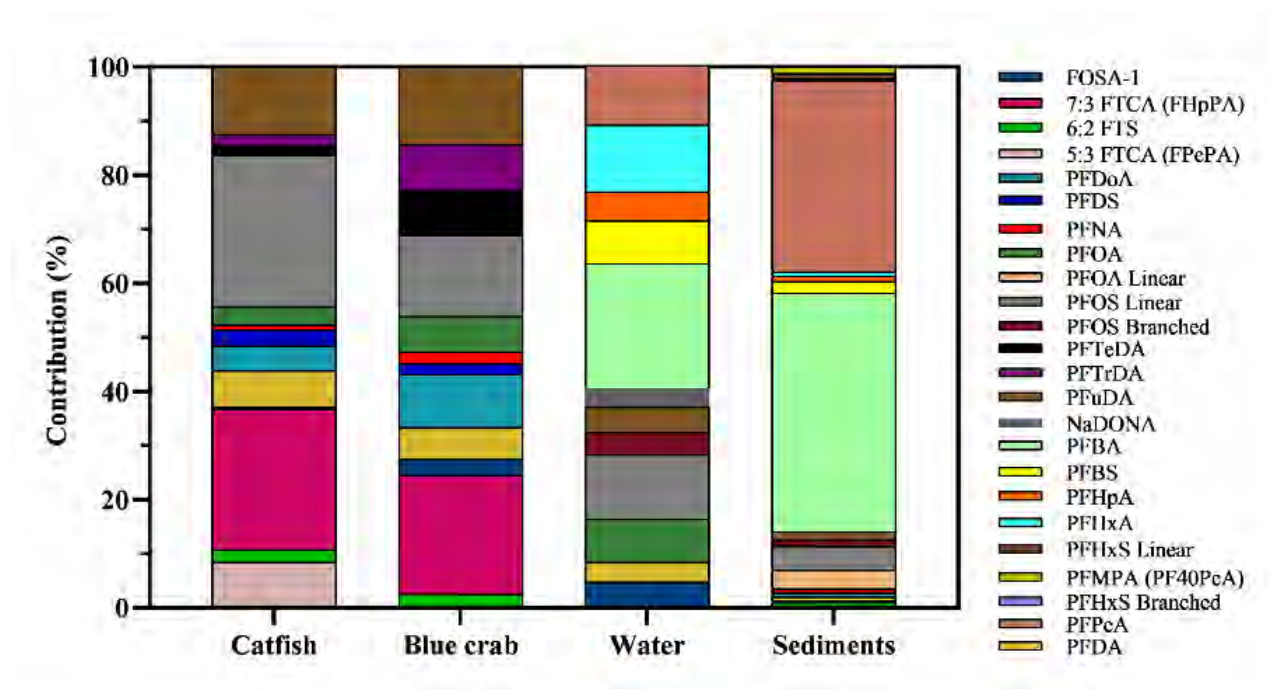


Figure 12. Profile of the contribution % of detected PFAS in environmental samples.

Table 5. Diseases and toxicities associated with PFAS detected in biological samples from Lake Maurepas: Insights from toxicological studies and animal model experiments.

PFAS	Potential Diseases/Toxicities	References
5:3 FTCA (FPePA)	Effect on hormones	(Eaton, 2024)
6:2 FTS	Impact on spleen weight Effect on immune functions Skin irritation Kidney and liver toxicity	(Eaton, 2024)
7:3 FTCA (FHpPA)	Effect on hormones Immunotoxicity	(Eaton, 2024)
FOSA-1	Increased risk of cardiovascular disease Higher prevalence of lower respiratory tract infections (in children up to age 10) Reproduction related abnormalities (i.e., increased time to get pregnant) Risk of breast cancer in women	(Bonefeld-Jørgensen et al., 2014; Buck Louis et al., 2013; Huang et al., 2018)
PFDA	Increased cholesterol levels Lower antibody responses Impact on gene expressions Risk of pneumonia Impact on thyroid functions	(ATSDR, 2024; Ait Bamai et al., 2020; De Toni et al., 2022)
PFDoA	Cognitive deficit Disturb Ca ²⁺ homeostasis in the brain	(Kawabata et al., 2017a)
PFDS	Negative effects on biological functions in neurons Impact on gene expressions	(Running et al., 2024a)
PFNA	Reduction in antibody response to vaccines Thymic and splenic alterations Negative effects on liver (i.e., effects on liver weight, including hepatocellular vacuolation and lipid accumulation, abnormal liver functions) Reduced spleen weight Increased cytokine levels Negatively effects on reproductive health Negative effects on the gastrointestinal tract Impacts on thyroid functions Increase the risk of cardiovascular diseases	(ATSDR, 2021; Boafo et al., 2023; De Toni et al., 2022a; Fang et al., 2008, 2009, 2010)

PFOA	<p>Elevated cholesterol levels</p> <p>Reproduction and birth associated abnormalities (i.e., small reductions in birth weight of human, diminished antibody responses to certain vaccines, and increased risks of pregnancy-induced hypertension and preeclampsia)</p> <p>Risk of cancers: kidney, testicular, prostate gland, ovaries, liver, pancreas, bladder, colon, colorectal, and breasts</p> <p>Negative effects on liver (i.e., effects on liver weight, alteration in liver enzymes)</p> <p>Disturb Ca²⁺ homeostasis in the brain</p> <p>Negative effects on biological functions in neurons</p> <p>Respiratory tract related diseases</p> <p>Risk of Diabetes</p> <p>Negative impact on thyroid cells</p> <p>Risk of cardiovascular disease in postmenopausal women</p>	(ATSDR, 2024; Ait Bamai et al., 2020; De Toni et al., 2022; Eve et al., 2024; Kawabata et al., 2017; Raleigh et al., 2014; Reiko Kishi, 2019; Running et al., 2024; Steenland et al., 2009; Vieira et al., 2013)
PFOS	<p>Associated with rising cholesterol levels</p> <p>Reproduction-associated abnormalities (i.e., reduced birth weight, and compromised vaccine responses)</p> <p>Negative effects on the liver (i.e., effects on liver weight, Liver enzyme changes)</p> <p>Disturb Ca²⁺ homeostasis in the brain</p> <p>Negative effects on biological functions in neurons</p> <p>Impact on gene expressions</p> <p>Risk of Diabetes: Bladder, colon, prostate gland, colorectal</p> <p>Negative effects on thyroid cells</p> <p>Risk of cardiovascular disease in postmenopausal women</p>	(ATSDR, 2024; De Toni et al., 2022; Eve et al., 2024; Kawabata et al., 2017; Raleigh et al., 2014; Running et al., 2024; Steenland et al., 2009)
PFTeDA	<p>Alterations of gene expression</p> <p>Hormonal imbalance in serum</p> <p>Reproduction associated toxicity</p>	(Zhang et al., 2021)
PFTTrDA	<p>Immunosuppressive effect on allergic diseases</p> <p>development related issues</p> <p>Endocrine disruption</p> <p>Decrease in the production of testosterone in males</p> <p>Effects the gene expression</p>	(Goudarzi et al., 2016; Khazaei et al., 2020; Patel et al., 2022)

Project 2.: Detection and characterization of microplastics in water, sediment and biological samples from Lake Maurepas

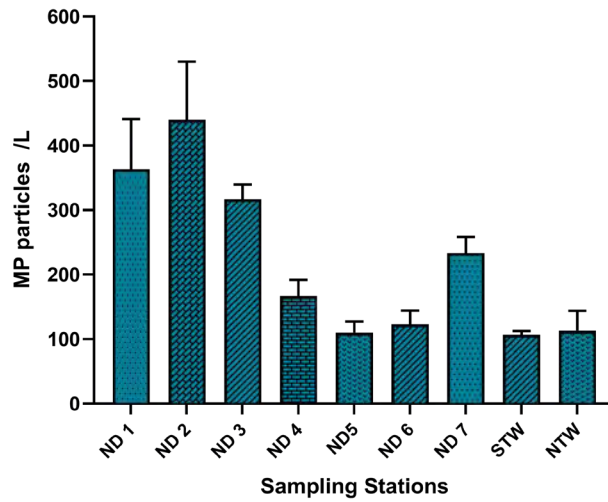


Figure 13. MPs concentration at different sampling stations in the Lake Maurepas.

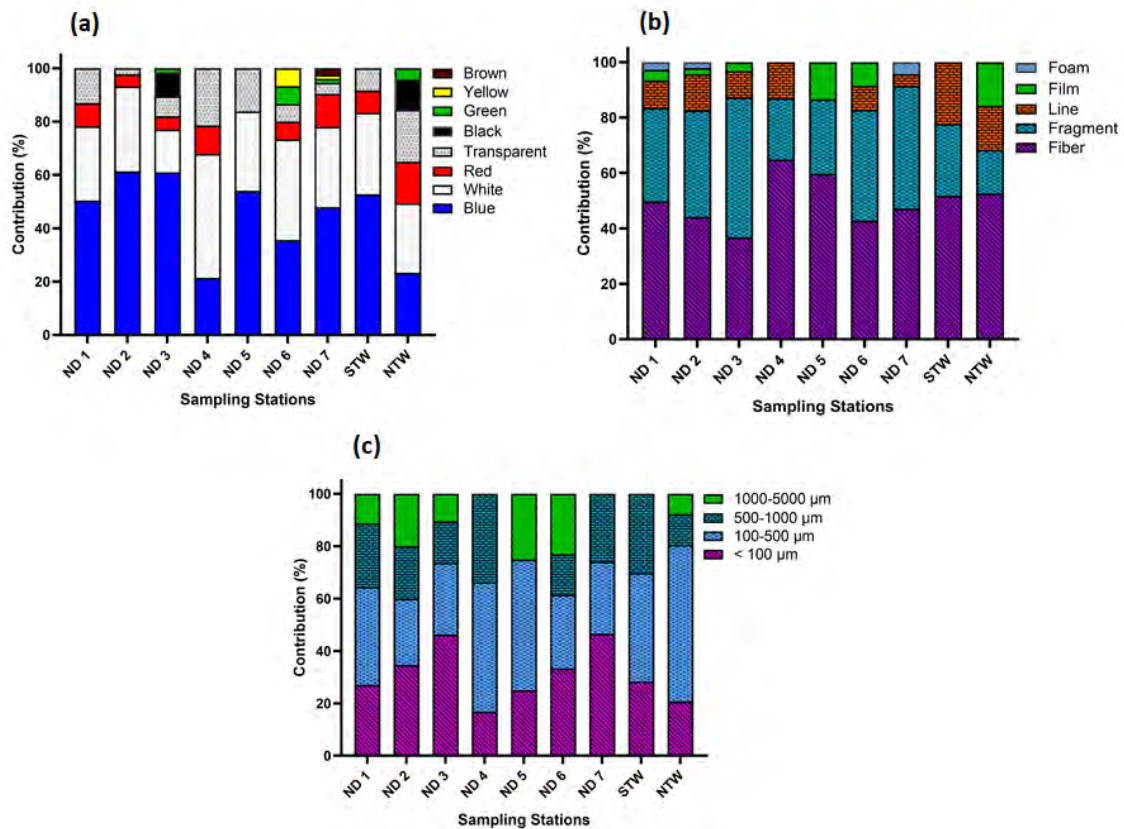


Figure 14. Different (a) colors, (b) shapes, and (c) sizes of MPs detected from the water sample, respectively.

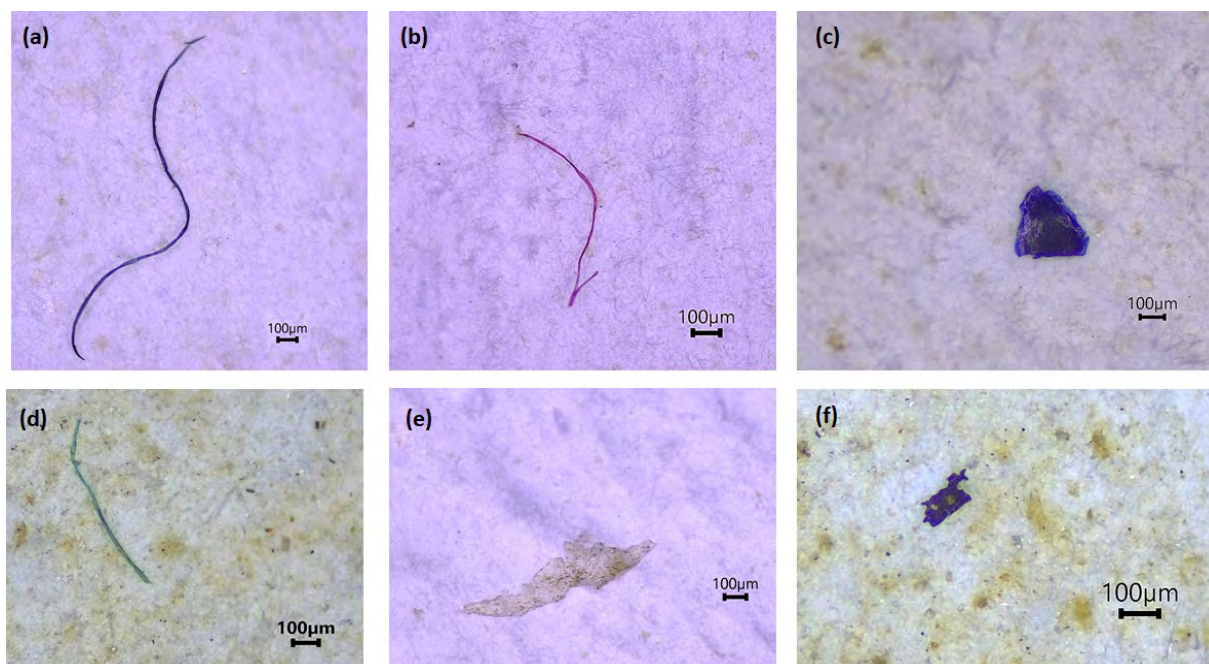


Figure 15. MPs images under microscope from water samples from the lake; **(a)** Blue fiber, **(b)** Red fiber, **(c)** Blue fragments, **(d)** Green fiber, **(e)** Transparent film, **(f)** Blue fragments.

Project 3: Mercury in Lake Maurepas and risk assessment of fish and crab consumption.

Spatio-temporal variation of Hg in lake water and sedimentary mud. Figure 16 illustrates the geospatial variation of Hg concentrations in water samples collected from Lake Maurepas between June and November 2023, across nine different sites at three depths (surface, middle, and bottom). The data reveal distinct spatial and vertical distribution patterns, with notable variations in Hg levels across sites and depths. For example, site ND2 exhibits relatively higher Hg concentrations at the surface and middle depths compared to other locations. Conversely, site ND4 shows a pronounced increase in Hg concentration at the bottom layer, likely indicating localized sources such as deposited sediment. Moderate Hg concentrations were also observed at sites D2 and D3 across all depths. The Hg patterns indicate polluted river inputs, as moderate to high concentrations were recorded consistently at ND1, ND2, and ND3, which are influenced by river discharge. Across multiple sites, depth-based variations are evident, with bottom layers often showing higher Hg concentrations, as seen at ND2 and ND3. This trend suggests that Hg may settle and accumulate in deeper regions due to sedimentation or limited mixing at greater depths. These findings reflect the influence of anthropogenic sources and variations in lake hydrodynamics, which may enhance Hg deposition in specific areas. Elevated bottom-layer Hg concentrations pose potential risks to benthic organisms and could contribute to bioaccumulation within the food web. While elevated in some locations, the measured Hg concentrations in water are below regulatory limits for safe use. Additionally, surface and middle-layer Hg concentrations at certain sites could result from atmospheric deposition or watershed runoff from the lake's tributaries, which transport Hg into the system.

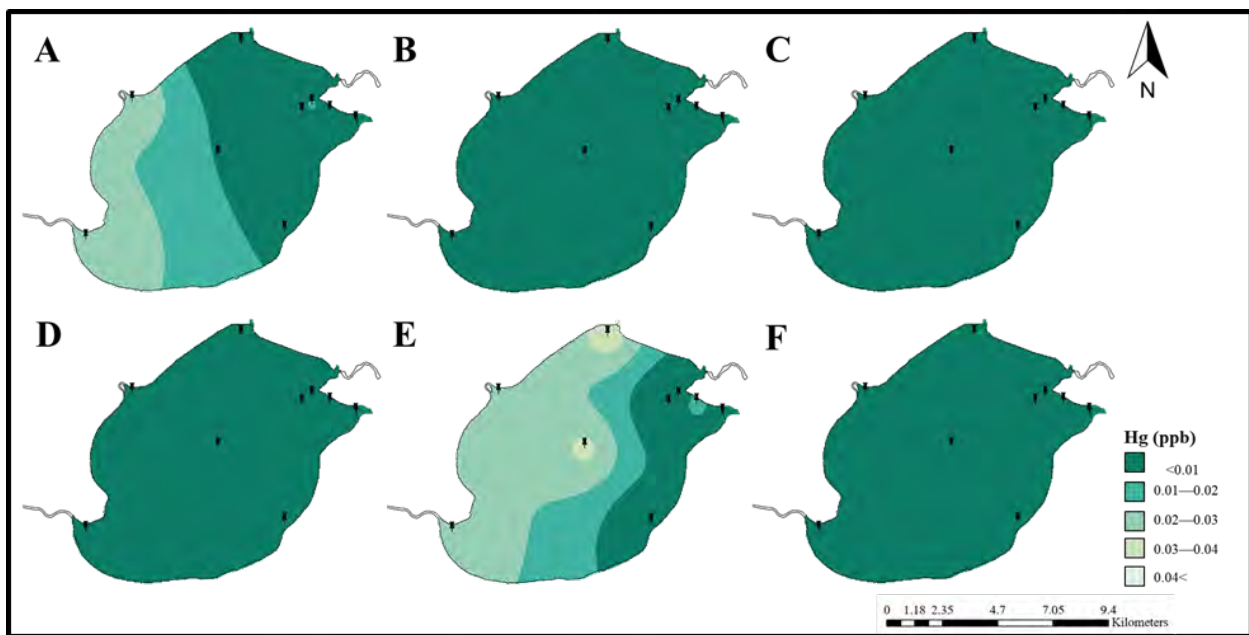
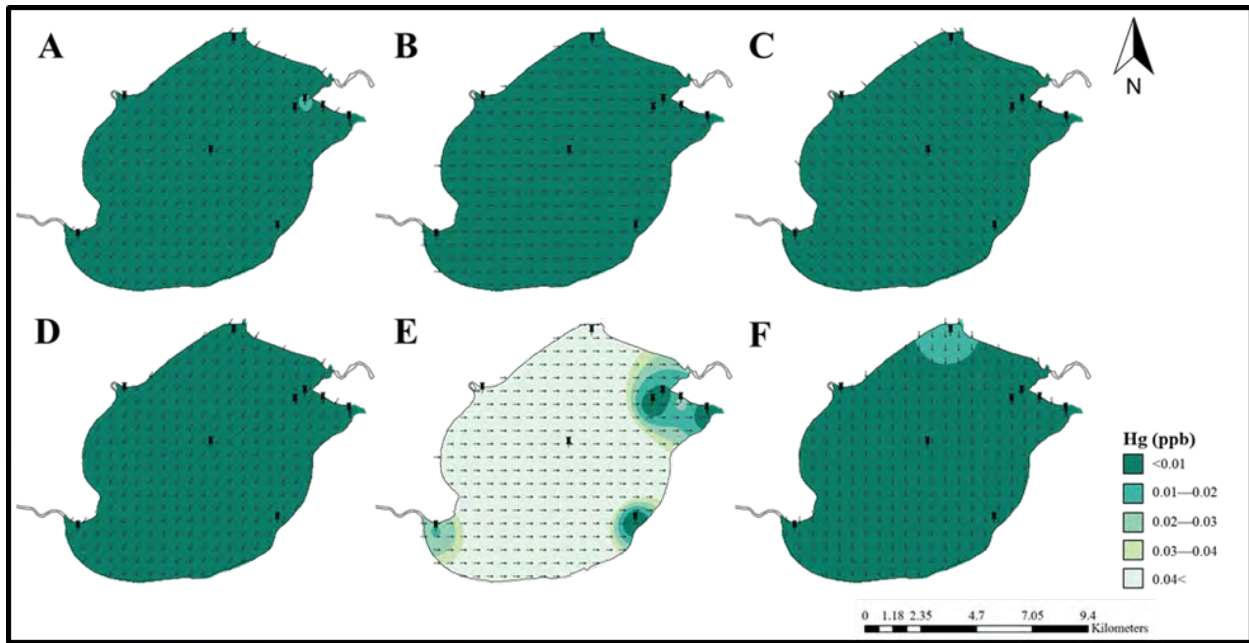


Figure 16. Maps generated for geospatial variation of Hg (surface, middle, bottom layers of water) from June-November 2023 using IDW function in ArcGIS: **(A)** June, **(B)** July, **(C)** August, **(D)** September, **(E)** October, **(F)** November. The black pins indicate the sampling sites and the arrows indicate the wind direction ~9.00 am in the specific sampling dates (6/22/2023, 7/20/2023, 8/18/2023, 9/22/2023, 10/20/2023, 11/17/2023). 9.00 am was selected considering the sampling time.

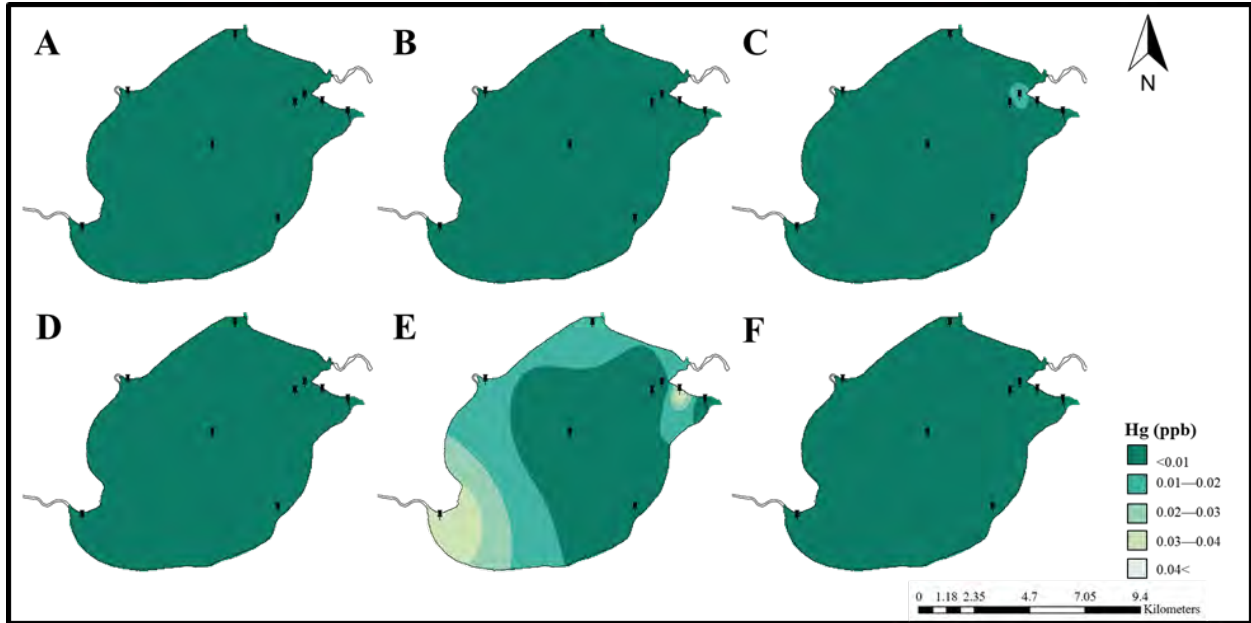


Figure 17. The mean Hg concentrations in sediment samples from nine sites, collected between June 2023 and July 2024. Each subplot represents a specific site, with data divided into two periods: June–November 2023 and January–July 2024. Sites closer to anthropogenic sources, such as ND1 and ND2, generally exhibit higher Hg concentrations, suggesting persistent input from nearby industrial or urban runoff via river discharge. Across both sampling periods, there is a seasonal trend, with slightly higher Hg concentrations recorded in the second period. This increase could be attributed to variations in hydrological conditions, enhanced sedimentation during rainy seasons, or seasonal fluctuations in pollutant inputs.

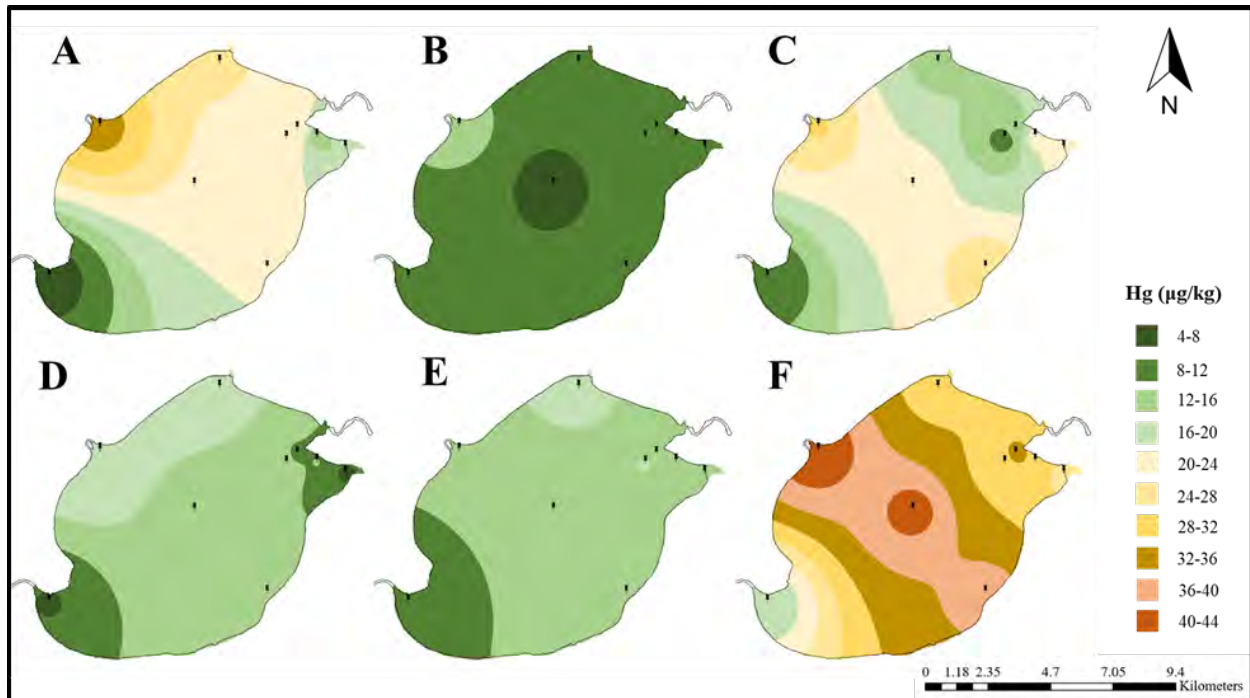


Figure 17. Maps generated for geospatial variation of Hg in sedimentary mud samples from June-November 2023 using IDW function in ArcGIS: **(A)** June, **(B)** July, **(C)** August, **(D)** September, **(E)** October, **(F)** November. The black pins indicate the sampling sites.

Hg in aquatic plants. Figure 18 shows the Hg concentration, measured on a wet weight basis, in aquatic plant samples collected from Lake Maurepas, highlighting variability in Hg content among different plants at various sampling locations. It reveals significant differences in Hg levels across sites, with plants from ND6, ND5, and D1 exhibiting relatively higher Hg concentrations compared to those from locations such as Galva Canal and ND3. This spatial variation likely reflects the influence of localized Hg sources or environmental factors such as sediment Hg levels or water flow patterns that affect Hg bioavailability. Sites with elevated Hg levels in plants may be closer to contamination sources or areas with higher sediment Hg accumulation, which could enhance Hg uptake by plants. Among the plant species investigated, the accumulated Hg concentration followed the order: blue-green algae > *Salvinia minima* > water hyacinth > Gulf swampweed. This variation in Hg accumulation may be attributed to species-specific differences in uptake mechanisms, growth rates, or habitat preferences, further emphasizing the complex interactions between environmental factors and biological characteristics in determining Hg bioaccumulation in aquatic plants.

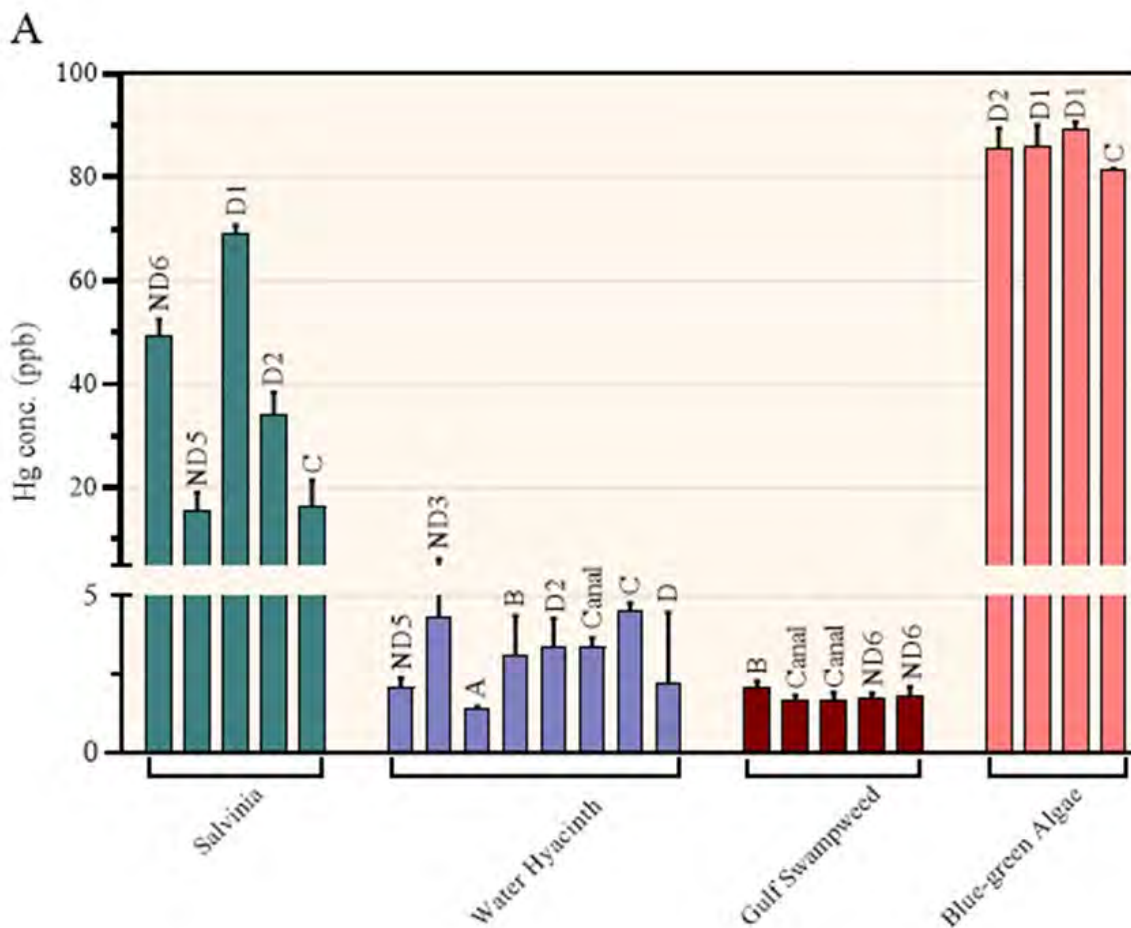


Figure 18. Hg concentration in aquatic plants (wet weight) collected from Lake Maurepas on 7/3/2024. One bar represents one plant, the places where they are collected are mentioned. The values plotted are the average of triplicate measurements while the error bar gives the standard deviation from the average.

Hg in Blue crabs and Catfish. Results of Hg concentrations in catfish and blue crabs across different zones in Lake Maurepas highlights both spatial and temporal fluctuations. Hg accumulation in catfish collected in 2023 and 2024 shows significant variation among different zones (see **Figures 19 and 20**). The highest Hg levels were observed in zone 3 in September, followed by zone 2 in December, with muscle tissues generally exhibiting higher Hg concentrations than skin tissues, consistent with known patterns of Hg bioaccumulation. In 2024, Hg concentrations appeared more evenly distributed across zones, with a notable decline compared to 2023, suggesting changes in Hg contamination or reduced bioavailability. Further analysis of Hg concentrations in the muscle and skin tissues of Channel Catfish and Blue Catfish collected from July 2023 to April 2024 reveal substantial fluctuations across different zones,

with elevated Hg levels in zones 3 and 2 in 2023, and more consistent levels in 2024. No significant species-specific differences in Hg uptake were observed between Channel Catfish and Blue Catfish, indicating that Hg accumulation in catfish may be largely independent of species under similar environmental conditions. These findings emphasize that Hg bioaccumulation in Lake Maurepas varies spatially, temporally, and by tissue type, likely influenced by environmental factors such as sediment disturbance, water flow patterns, and anthropogenic activities.

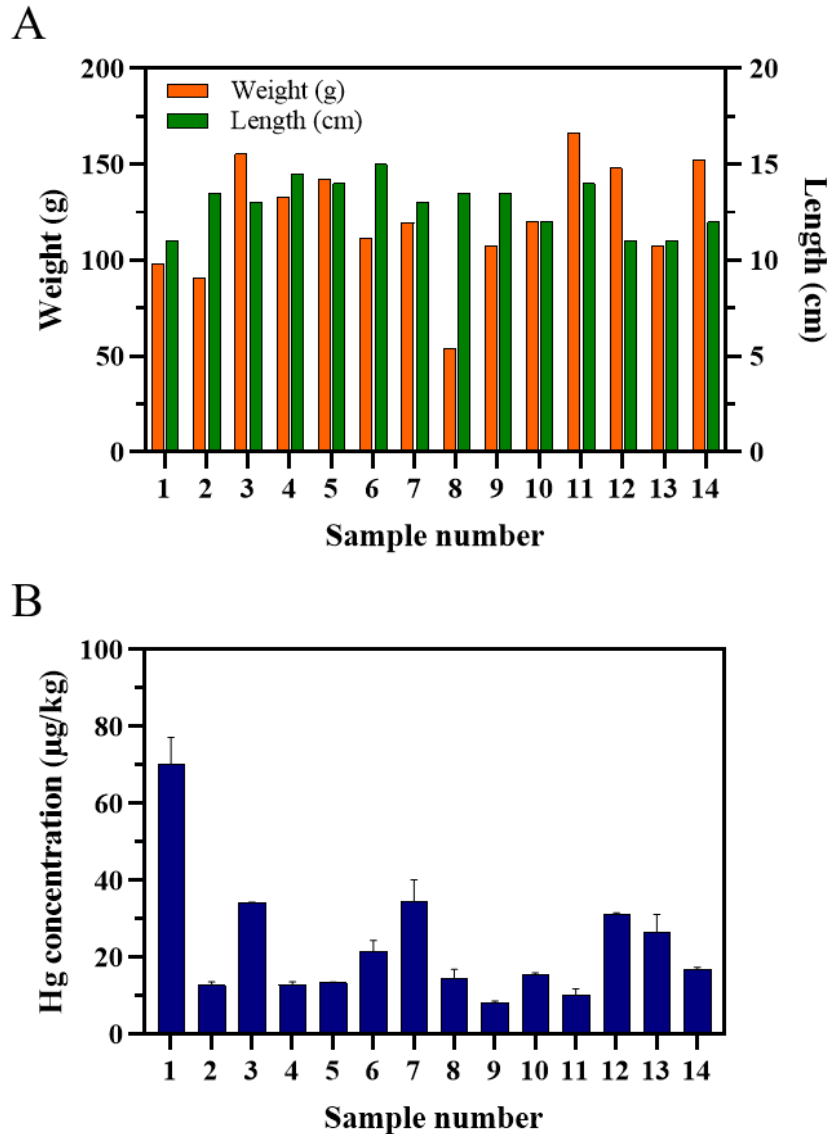


Figure 19. Hg concentration in Blue crabs (wet weight, male) collected from Lake Maurepas in 2023, **(A)** weight and length measurements, **(B)** Hg concentration in the homogenized crab samples. The values plotted are the average of triplicate measurements while the error bar gives the standard deviation from the average.

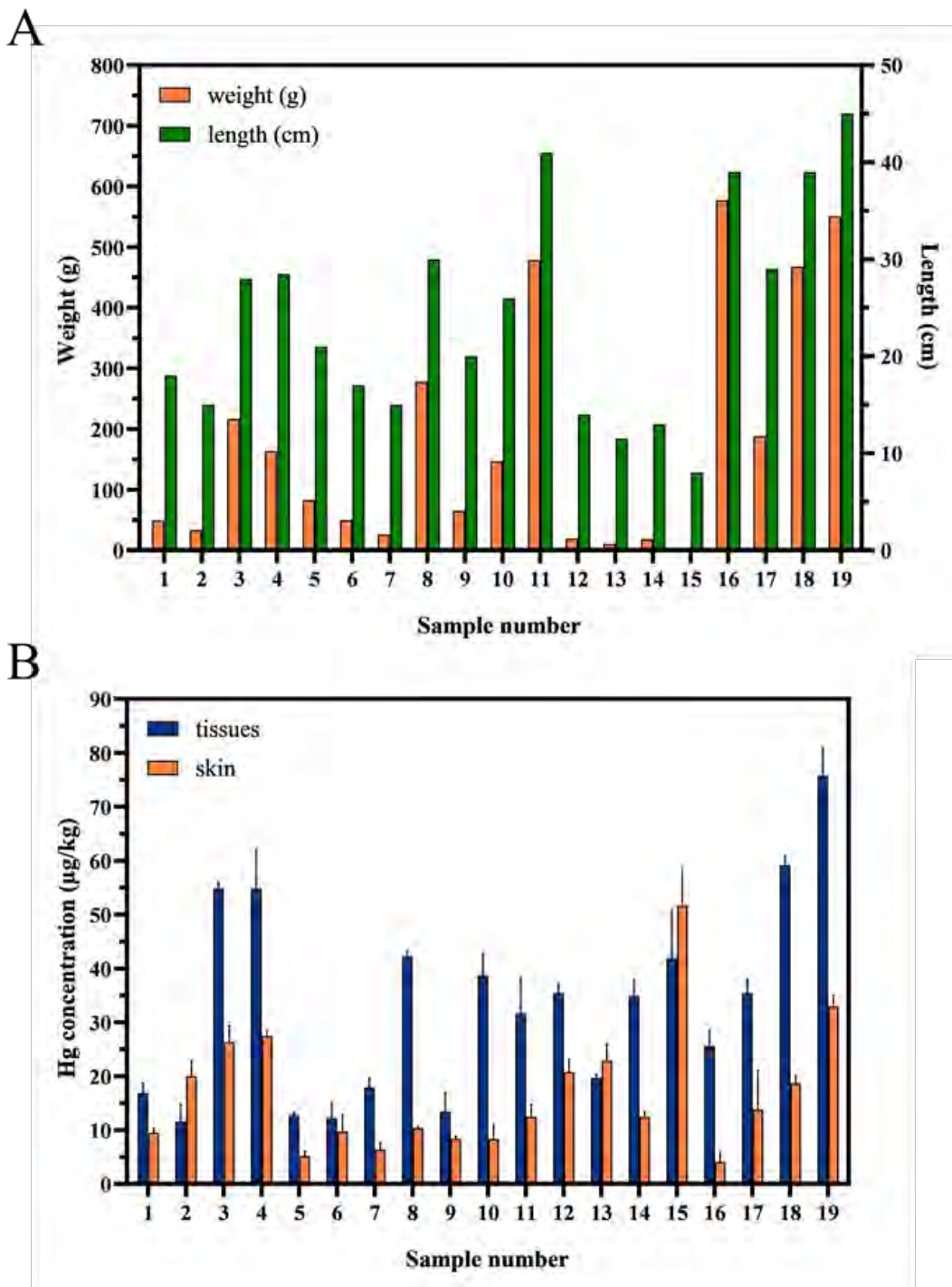


Figure 20. Hg concentration in Catfish (wet weight) collected from Lake Maurepas in 2023, **(A)** weight and length measurements, **(B)** Hg concentration in muscle tissues and skin tissues. The values plotted are the average of triplicate measurements while the error bar gives the standard deviation from the average.

Project 4: Spatial-temporal contaminant spreading analysis in Lake Maurepas in terms of the quality of water and sedimentary mud samples (Gunawardhana et al., 2024)

Physical Properties of Lake Water in 2023. Measuring physical properties of lake water, such as temperature, pH, specific conductivity (SC), and salinity, is important as these indicators reflect the overall water quality. Changes in these parameters can signal pollution, nutrient runoff, or other environmental disturbances that may impact the health of the lake ecosystem.

Monitoring these properties helps identify potential sources of contamination and guides management efforts to maintain or improve water quality. **Figure 21** shows the trends of these properties in Lake Maurepas surface water from January to December 2023, except for pH. pH data was not available from the USGS monitoring station; therefore, in-situ measurements of pH are included in **Figure 21** only during the sampling period. The weekly trends of these water quality parameters are presented **Figure 22**. The acceptable limits for these properties are presented in **Table 6**.

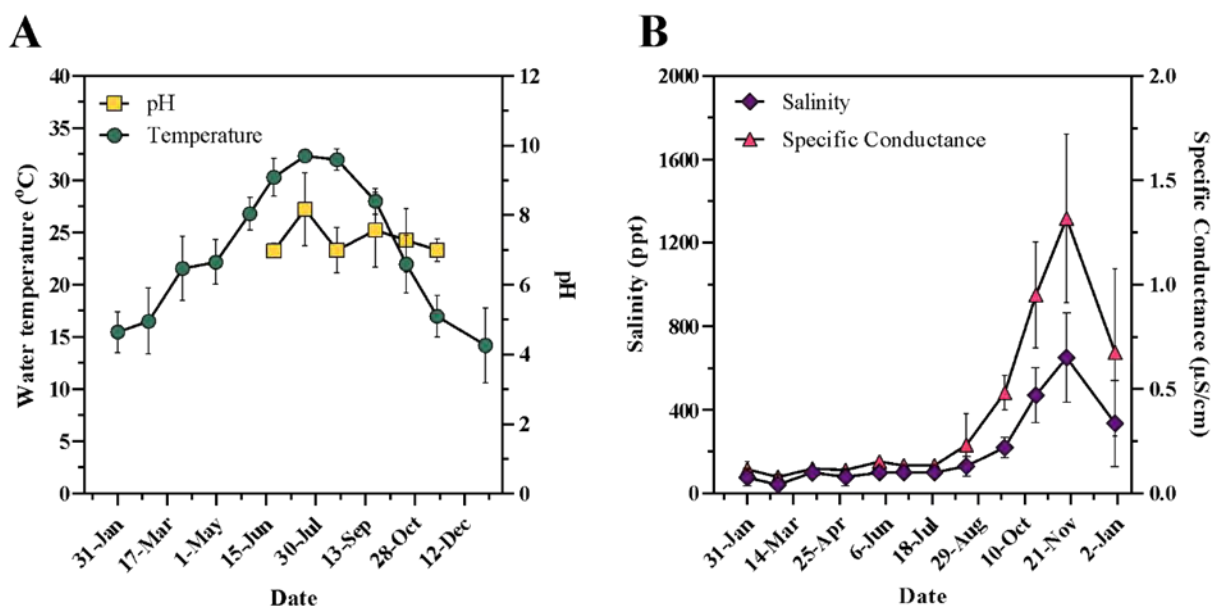


Figure 21. Monthly trends of physical properties of water: **(A)** water temperature and pH, **(B)** Salinity and specific conductance (measured at 25 °C). The symbols indicate the monthly average values while the error bars indicate the standard deviation from the mean (n = 30 or 31) (Except pH, other data was extracted from the United States Geological Survey Pass Manchac, Lake Maurepas, LA monitoring station—073802302, 30.28356667, -90.3978389).

Considering the temperature variation, an increasing trend was observed between January and July, followed by a decreasing trend from August to December. The maximum water temperature was recorded on August 7th (34.44 °C), while the minimum was on December 14th (7.17 °C). The pH of the lake water fluctuated between 6.41 and 8.80, with an

average value of 7.42 ± 0.19 during the study period. Compared to other months, July showed a slight increase in average monthly pH (8.18 ± 1.05), with higher values observed during this month. This pattern aligns with observations in similar lakes, where pH values often increase during warmer months due to enhanced biological activity.

There were only a few rainfall events during July, with intensities of 7.9 mm, 9.4 mm, 10.7 mm, 26.2 mm, and 26.4 mm on the 6th, 12th, 17th, 23rd, and 24th, respectively. Despite subsurface seismic survey-related cleanup work carried out by APC in July—which included collecting and removing all seismic survey equipment such as cables, nodes, and other hardware to ensure no remnants or debris were left in the lake—no significant impact on pH values was observed. The pH values for the closest sampling sites, ND4 and D4, remained within the ranges of 6.9–7.4 and 7.4–7.7, respectively. The pH ranges observed near the inputs of the Tickfaw and Amite rivers were 6.6–8.8 and 7.0–9.7, respectively, representing the highest ranges in the lake. The pH increase in July could be attributed to discharge inputs from these rivers. Biological processes such as photosynthesis, respiration, and the decomposition of organic matter can also influence pH levels in lake water. During the summer months of June to August, higher temperatures exceeding 30 °C can have complex effects on photosynthesis, including changes in oxygen availability, thermal stratification, metabolic rates, and the composition of algal assemblages.

Table 6. Maximum permissible limits of water quality parameters for inland surface water.

Water quality parameter	Maximum permissible limit
pH	6.5-8.5 †
Temperature	40 °C
SC	250 µS/cm
Salinity	200-600 ppt
COD	5 mg/L †
	10 mg/L †
TN	25 mg/L
	0.1 mg/L
Phosphate	0.3 mg/L
	1 mg/L
NH ₃ -N	1 mg/L
	3 mg/L
As	0.01 mg/L †
Pb	0.01 mg/L †
	0.015 mg/L
Hg	0.05 mg/L
	0.002 mg/L †
	0.006 mg/L (inorganic)
Zn	5 mg/L
Cd	0.003 mg/L †
Ba	2 mg/L
Cu	2 mg/L
Cr	0.05 mg/L †
Ni	0.07 mg/L †
Hg in sediments	0.18 µg/g

† These values are reported for drinking water

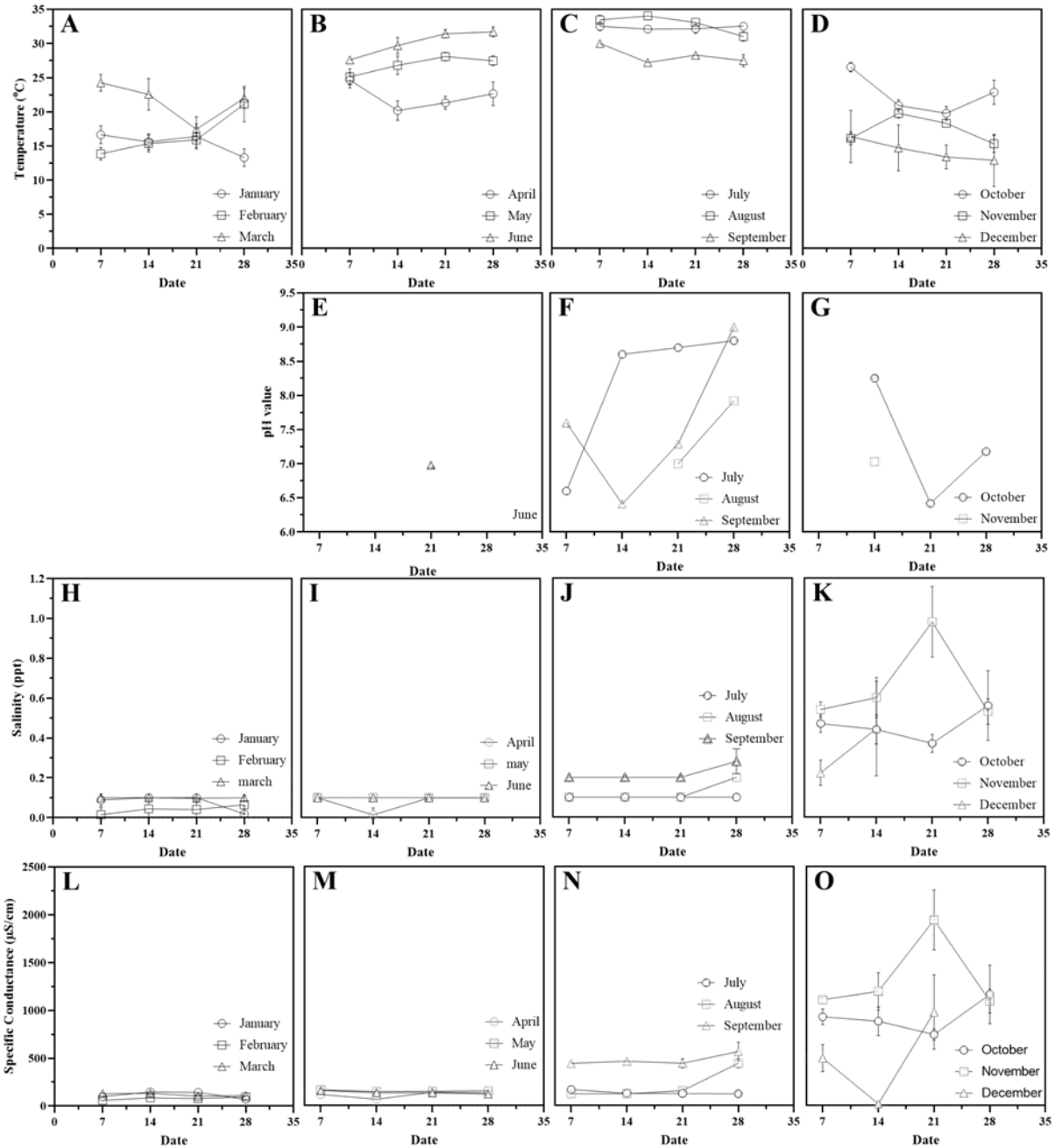


Figure 22. Weekly trends of physical properties of water quality parameters: (A-D; water temperature, E-G; pH, H-K; salinity and L-O; specific conductance). The symbols indicate the weekly average values while the error bars indicate the standard deviation from the mean (n=7).

During photosynthesis, aquatic plants absorb carbon dioxide from the water, which can increase pH levels by reducing the concentration of carbonic acid. Although the observed pH values fall within the range defined for drinking water (6.5–8.5), large variations in pH can cause

stress to aquatic organisms, as many species are adapted to stable pH conditions. Such stress can adversely affect their growth, behavior, reproduction, and survival.

Both salinity and specific conductivity (SC) showed an increasing trend up to November, followed by a sudden decrease in December. Salinity ranged from 0.1 to 0.7 ppt, while SC varied between 110.63 and 2325.83 $\mu\text{S}/\text{cm}$. Similar patterns have been observed in other estuarine lakes, where seasonal variations and saltwater intrusion cause fluctuations in salinity levels, particularly during high tides or coastal storms. Lake Maurepas, located in a tidal estuarine system, is prone to saltwater intrusion. This occurs when saline seawater infiltrates freshwater aquifers or nearby surface water bodies like Lake Pontchartrain due to sea level rise or changes in coastal hydrology, resulting in elevated salinity and SC levels in adjacent freshwater systems. Additionally, both natural and human activities influence salinity and SC in Lake Maurepas. Agricultural runoff can introduce salts and nutrients from fertilizers, while urbanization contributes through road salts, sewage, and industrial discharges. Urban stormwater runoff often carries pollutants into lakes, raising salinity and SC. A significant increase in these parameters was observed in September, nearly doubling compared to August, and peaked in November, coinciding with a major accident near Pass Manchac. The catastrophic "super fog" multi-car pileup on October 23, 2023, involving over 160 vehicles, caused extensive property and environmental damage. Leaking fluids, debris, and wreckage from this incident likely contributed to both air and water pollution. Another potential contributor could be disturbances to the lakebed caused by industrial activities, such as drilling related to subsurface test well (STW) operations. These disturbances can resuspended sediments, release nutrients, expose underlying geology, and alter water circulation, affecting water chemistry. However, the impact of drilling appears to be minimal, as the STW site is approximately 11.9 km away from the areas with elevated salinity and SC, and wind directions were unfavorable for the spread of pollutants from the site.

Chemical Properties of Lake Water from June-November 2023. Figure 23 illustrates the temporal changes in the chemical properties of Lake Maurepas surface water from June to November 2023. During the sampling period, the COD concentration showed an upward trend, increasing from 11.3 ± 8.04 mg/L in June to 39.6 ± 19.8 mg/L in November, exceeding the safety threshold of 25 mg/L. Regarding nutrient concentrations, TN ranged from 0.70 to 0.99 mg/L, surpassing the safety limit, while $\text{NH}_3\text{-N}$ ranged from 0.06 to 0.14 mg/L, remaining below the safety limit. Both parameters displayed relative stability. The $\text{NH}_3\text{-N}$ concentration varied between trace levels to ~ 0.7 mg/L during the sampling period. Few environmental agencies have set standards for $\text{NH}_3\text{-N}$ in lakes to protect aquatic life. These standards often range from 0.02-2.0 mg/L, depending on the sensitivity of the ecosystem and the designated use of the waterbody. Hence, it can be observed that the $\text{NH}_3\text{-N}$ level in Lake Maurepas is below the standard limit defined for surface waters. However, it is higher in September than the other

months considered. The maximum $\text{NH}_3\text{-N}$ was found in the surface layer of ND2 (0.68 ± 0.02 mg/L), and the lowest amount was found to be zero in the middle depth of ND5. Similar to the COD, $\text{NH}_3\text{-N}$ concentration is higher near Amite River.

In contrast, TP concentration showed a slight increase from June to September, followed by a significant decrease to 0.09 mg/L in October. The observed exceedances in COD and TN levels can be attributed to various factors, including polluted stormwater runoff, contamination from the three rivers connected to the lake, and ongoing drilling activities. Pollutants that elevate COD concentrations in lake water often originate from multiple sources. These include domestic and municipal wastewater containing organic substances like food particles, human waste, and household cleaning products; agricultural runoff carrying organic materials from fertilizers, pesticides, and animal waste; and industrial effluents releasing organic chemicals from manufacturing processes. Stormwater runoff further contributes pollutants such as oils, grease, and organic debris from urban areas into the lake. Inorganic substances, such as ammonia and nitrites found in wastewater and agricultural runoff, can also increase COD levels. Once in the lake, biological processes such as microbial decomposition and nutrient cycling further alter nutrient concentrations. For example, microbial activity in sediments or the water column can convert organic nitrogen compounds into ammonia. Reduced metals, such as iron (Fe^{2+}) and manganese (Mn^{2+}), may also influence COD levels by undergoing oxidation, which consumes oxygen. However, elemental analysis detected trace levels of metals such as Fe, Hg, Zn, Cd, Ba, Cu, Mn, and Ni, ruling out significant contributions from these metals to the COD levels observed. Pollutants stimulating microbial activity can indirectly raise COD levels. Elevated nutrient levels, for instance, can lead to algal blooms, resulting in large biomasses that, upon decomposition, significantly increase COD levels. Reports of cyanobacteria and blue-green algae presence in Lake Maurepas suggest that algal blooms could be a contributing factor. These blooms can also limit oxygen diffusion from the atmosphere into the water, potentially causing hypoxic events. Such events can have severe impacts on aquatic life, particularly for less-mobile species like crabs, which cannot relocate to areas with more oxygenated water. This emphasizes the interconnectedness of freshwater ecosystems and the critical importance of managing nutrient inputs to preserve lake water quality.

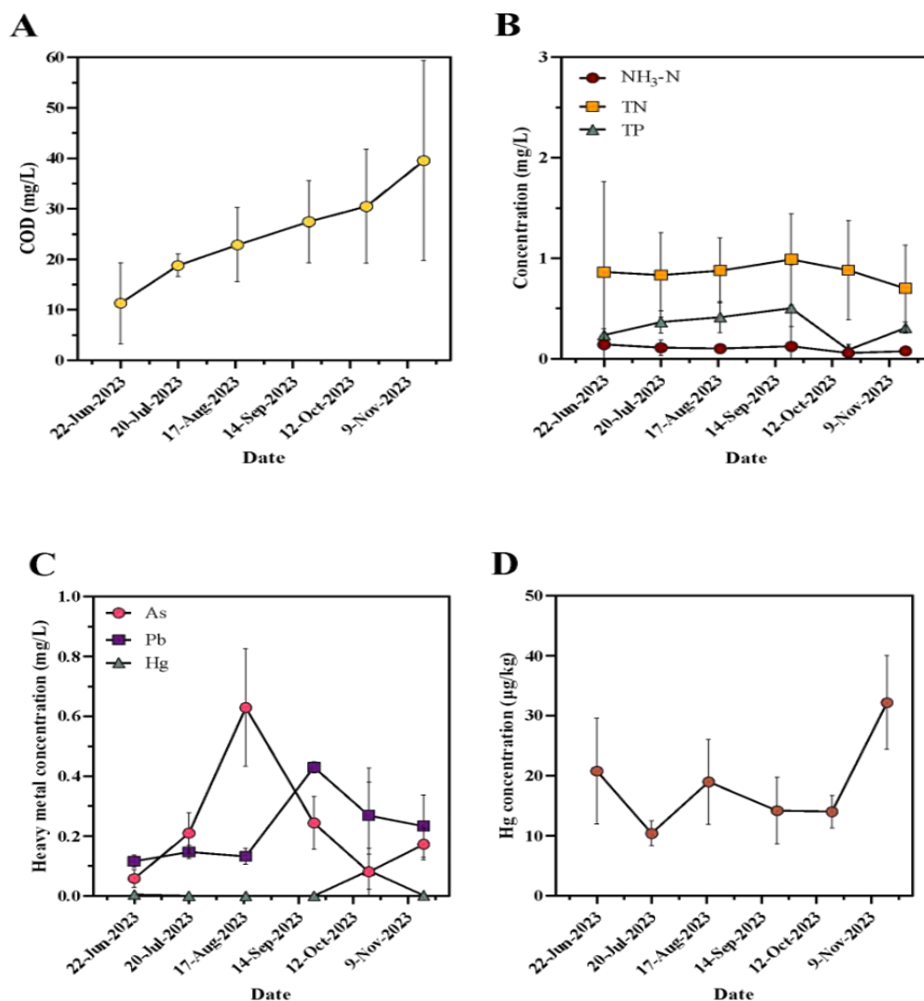


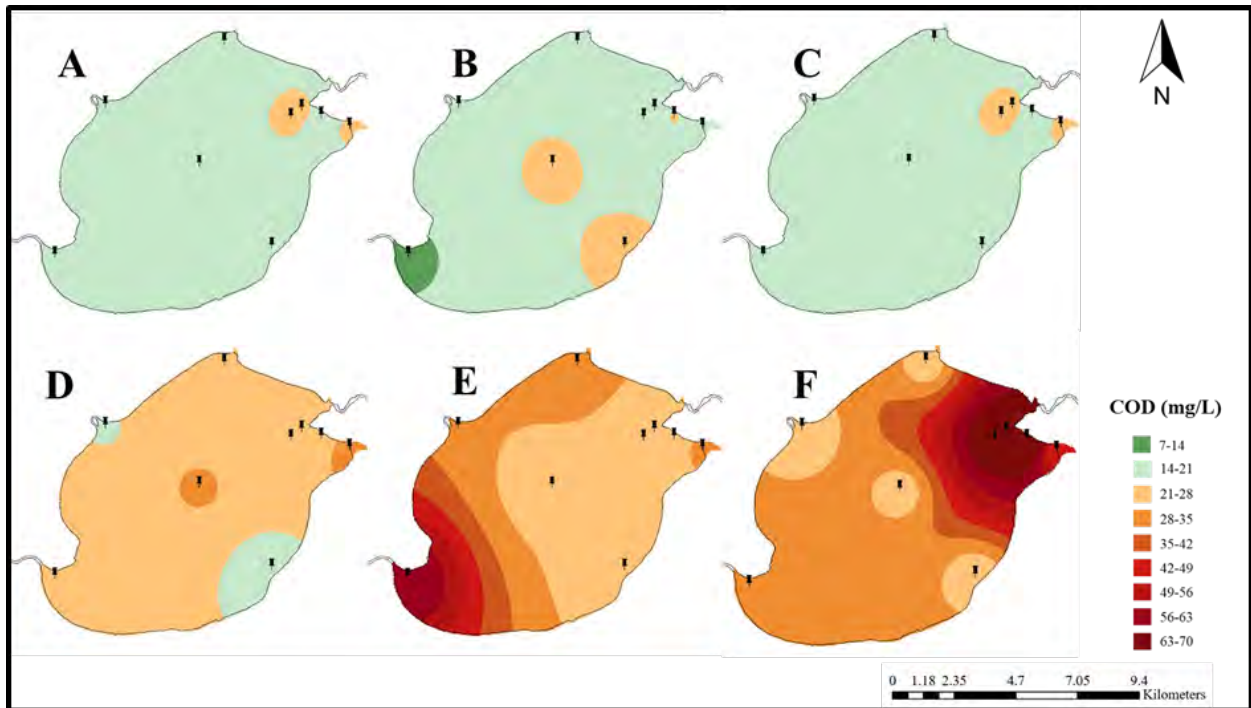
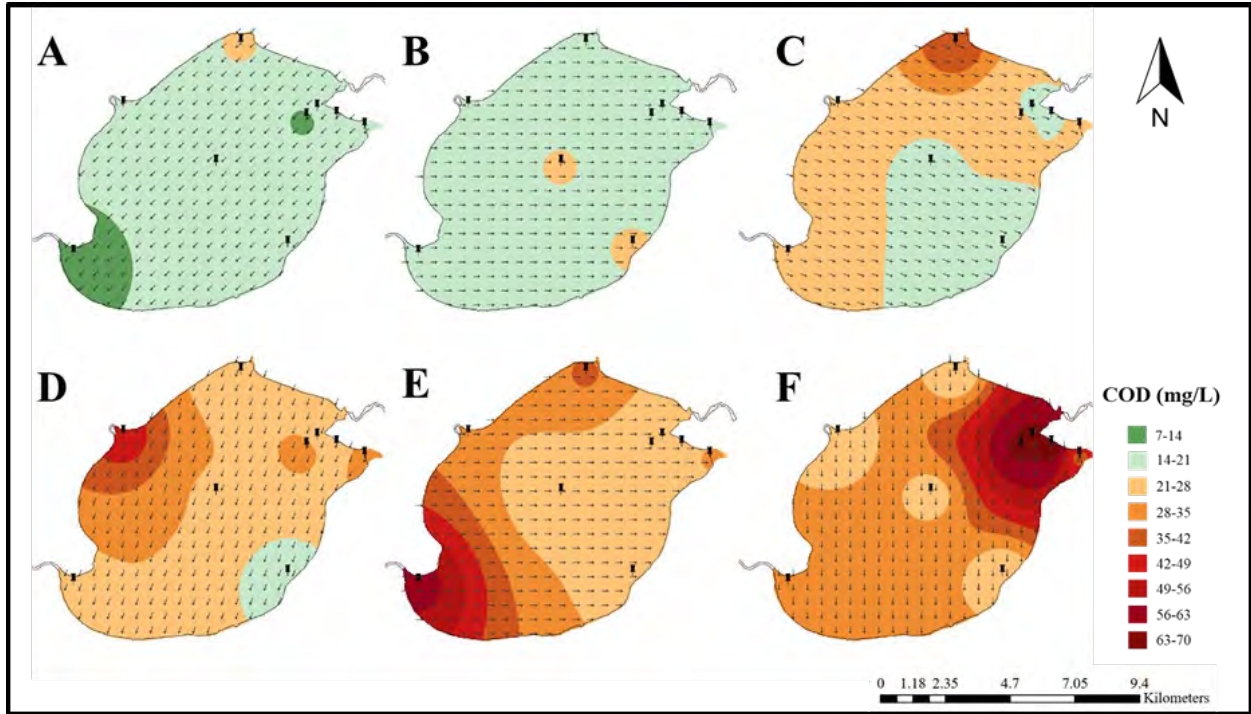
Figure 23. Time series variation of contaminant concentrations during the sampling period: **(A)** COD in water, **(B)** TN, NH₃-N, and TP in water, **(C)** As, Pb, and Hg in water, **(D)** Hg in sedimentary mud. The symbols represent the monthly average values where the error bars represent the standard deviation from the mean (n = 27).

Figure 23 (C) shows the concentration variations of the three heavy metals in the order of As > Pb > Hg. The significantly higher concentrations of As and Pb, compared to the established thresholds, raise concerns about the current health and safety of the lake for aquatic life, fishing, and recreational activities. Both As and Pb are toxic to aquatic organisms even at low concentrations, affecting their growth, reproduction, behavior, and mortality. Due to the non-biodegradable and bioaccumulative nature of these heavy metals, they can accumulate and biomagnify in fish and other aquatic animals, eventually entering the human body through the food chain. The highest concentrations of As, Pb, and Hg were observed in August (0.63 ± 0.19 mg/L), September (0.43 ± 0.02 mg/L), and October (0.08 ± 0.03 mg/L),

respectively. This monthly data helps assess whether there is any correlation between the spikes in heavy metal concentrations and the construction activities of the STW. Although Hg was found at very trace levels in the water, it showed higher concentrations in sediment samples, as illustrated in **Figure 23 (D)**. The lowest value was observed in July, prior to the start of STW construction ($10.35 \pm 2.09 \mu\text{g}/\text{kg}$), while the highest concentration was recorded in November, after construction began ($32.18 \pm 7.82 \mu\text{g}/\text{kg}$). However, these values remain below the USEPA's permissible limit for Hg in sediments, which is $180 \mu\text{g}/\text{kg}$. These heavy metals can enter the lake water and sediments through various natural and anthropogenic pathways. Natural sources, such as the geological weathering of rocks and soils containing heavy metals, release these elements into water bodies. This process is accelerated by factors such as acidic pH, higher temperatures, and the presence of organic acids.

As shown in **Figure 21**, temperatures were higher during the summer months of June to September. Overall, water impairment in the lake can be attributed to various sources, including industrial point sources, runoff from pasturelands, urban areas, petroleum products, and recreational activities. There are between 1 and 25 industries within a five-mile radius of the lake, with the highest concentration located near the Amite River around Baton Rouge. Industries along the Blind River include restaurants, bars, parks offering boat rides, and chemical manufacturing plants; along the Amite River, electrical equipment repair shops, spice manufacturing facilities, and pharmacies are located; and along the Tickfaw River, industries include farms, bars, restaurants, vacation spots, golf courses, and smoke and spice companies. These industries could potentially contribute to heavy metal pollution through processes such as machinery maintenance, the use of contaminated ingredients, and the application of fertilizers and pesticides in golf courses. Agricultural runoff, carrying heavy metals from pesticides and fertilizers during rain events, could also transport these contaminants into the lake. Additionally, 17.84% of the land in the Lake Pontchartrain basin is agricultural, while 7.77% is urban, with the remainder consisting of wetland forests, scrubs, or marshy areas. Urban runoff can also contain heavy metals from road runoff, atmospheric deposition from vehicle emissions, and waste from urban areas, all of which can enter the lake through stormwater drainage systems. Furthermore, industrial processes and vehicular emissions can release heavy metals into the atmosphere, which may then settle on the lake's surface or be washed into it through precipitation. It is important to note that the values in **Figure 21** represent averages for the entire lake on specific sampling dates, and they can vary significantly depending on the sampling site.

Geostatistical Modeling of Chemical Properties. We studied the spatial-temporal distribution of COD, TN, TP, As, and Pb using the IDW algorithm in ArcGIS software (version 3.3) on data collected from nine sampling sites. **Figures 24, 26-30**, illustrates these distributions for the lake's surface water, the middle depth ($\sim 1.5 \text{ m}$), and the lake bed ($\sim 3 \text{ m}$).



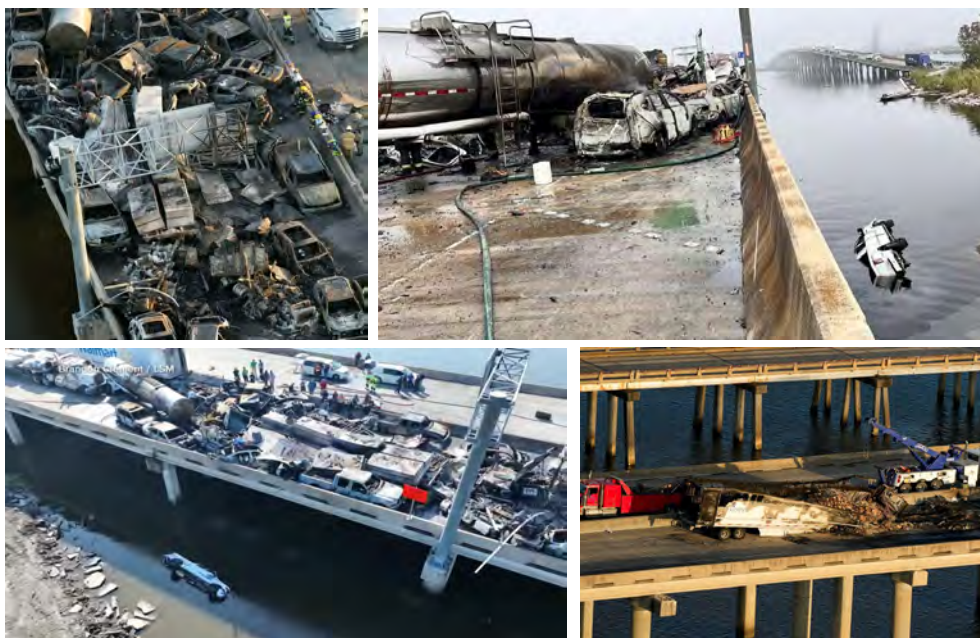
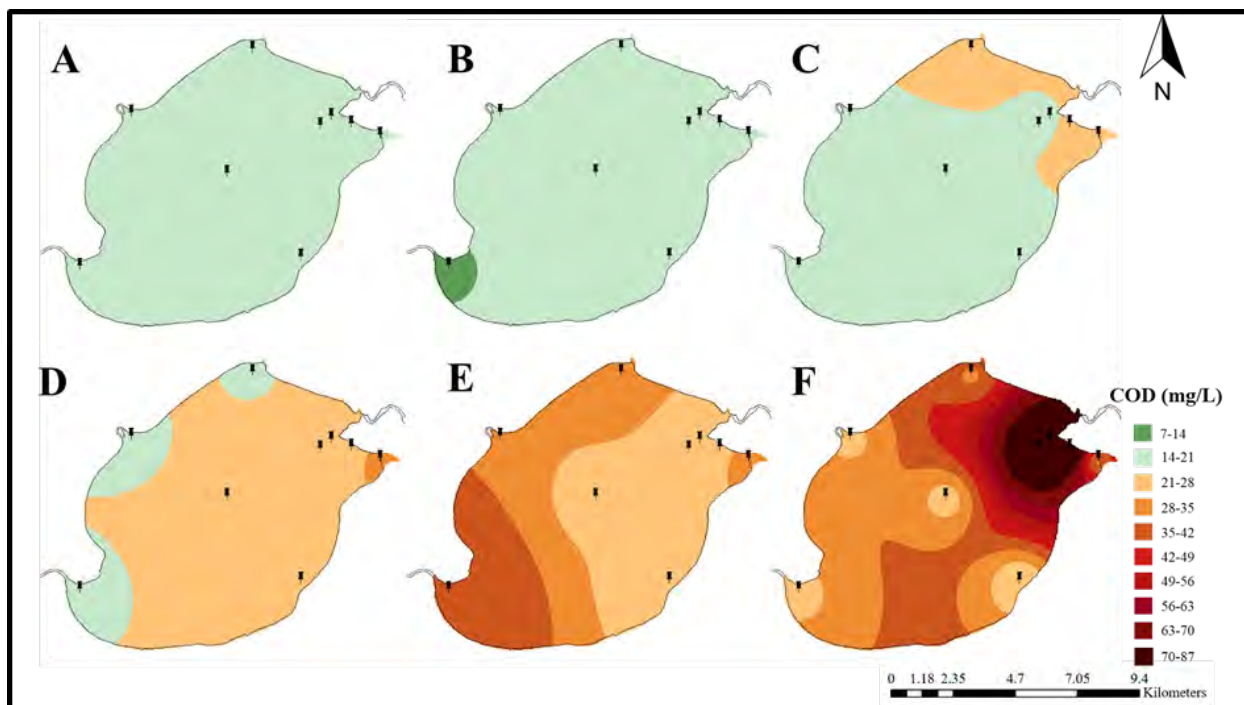


Figure 24. Maps generated for geospatial variation of COD (surface, middle and bottom layers in order) from June–November 2023 using IDW function in ArcGIS. The subgraphs indicate: **(A)** June, **(B)** July, **(C)** August, **(D)** September, **(E)** October, **(F)** November. The black pins indicate the sampling sites and the arrows indicate the wind direction ~9.00 am in the specific sampling dates (22 June 2023, 20 July 2023, 18 August 2023, 22 September 2023, 20 October 2023, 17 November 2023). 9.00 am was selected considering the sampling time. The very bottom figure shows ‘super fog’ multi-car pileup on Louisiana highway near Pass Manchac on 23rd October 2023.

COD levels ranged from 7–42 mg/L in the summer and 14–70 mg/L in the winter, both exceeding the standard limit for COD (25 mg/L, Table S2). The highest value was recorded at the bottom layer of site D1 (86.67 ± 4.24 mg/L), while the lowest was at the surface layer of D1 (11.67 ± 0.97 mg/L). During the winter, surface COD concentrations were generally higher compared to the summer. This increase could be attributed to a higher pollution load on the aquatic system, leading to greater oxygen consumption. Similar seasonal increases in COD due to higher pollution loads have been observed in other freshwater ecosystems. The higher concentrations of COD near the Tickfaw River in August (**Figure 24(1-C)**), near the Amite River in September (**Figure 24(1-D)**), and near the Blind River in October (**Figure 24(1-E)**) suggest elevated pollutant loads from these streams. The relatively higher COD concentrations from September to November, compared to other months, may be linked to leaf fall and vegetation decay, which peaks in November, particularly in Southern Louisiana. Notably, COD and As concentrations were alarmingly high near sites D1, D2, and D3 in November. This spike is likely related to the catastrophic ‘super fog’ multi-car pileup on Louisiana Highway near Pass Manchac on October 23, 2023. With rainfall at the end of October and in November (**Figure 24(F,G)**), these pollutants could have been washed into the lake. They were likely transported via wind-induced waves (towards the south), as the lake area experienced high wind speeds: 3.73 ± 1.47 m/s in October and 3.21 ± 1.16 m/s in November. Wind speeds above 3 to 4 m/s are generally sufficient to generate noticeable waves on a lake. The wind data is presented graphically in **Figure 25**.

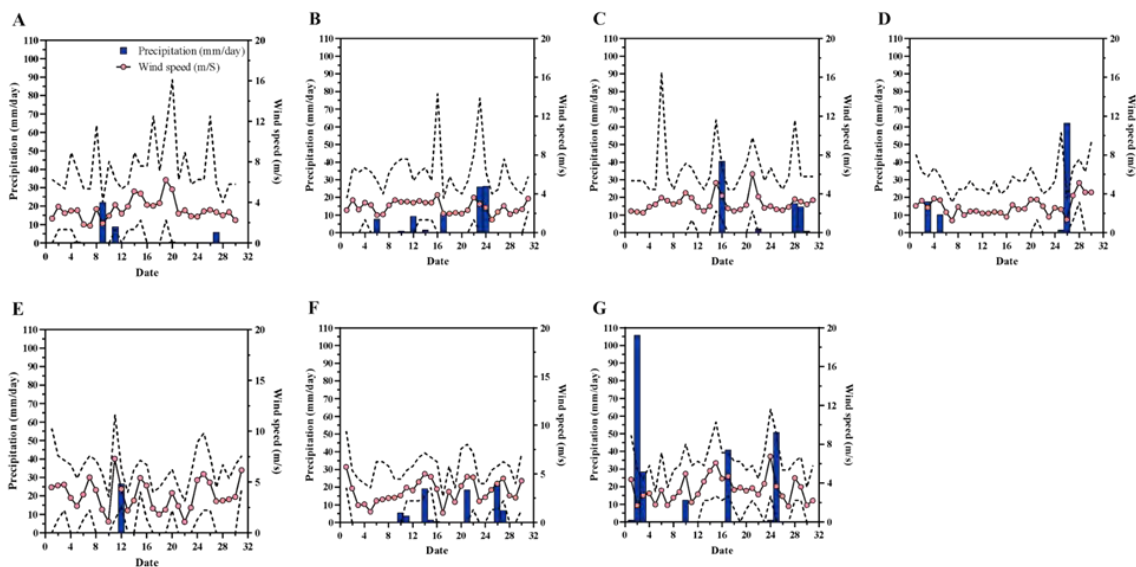
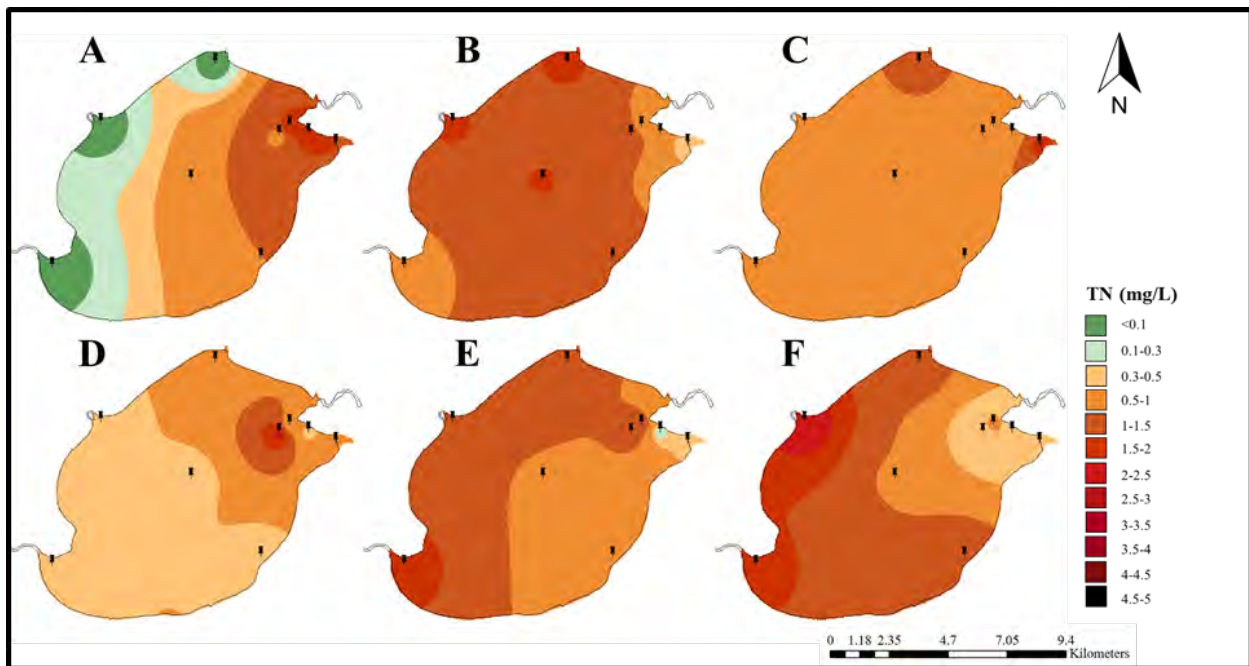
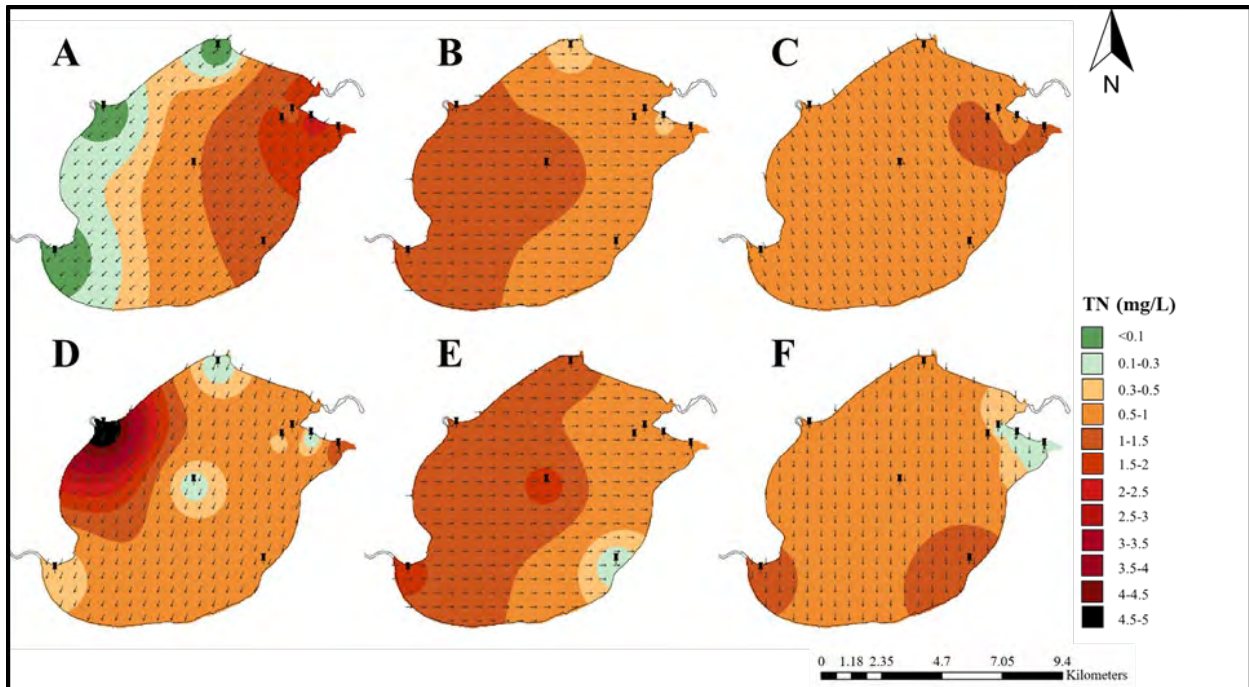


Figure 25. Precipitation (mm/day) (bar graph) and wind speed (m/S) (point graph) data from June–December 2023: **(A)** June, **(B)** July, **(C)** August, **(D)** September, **(E)** October, **(F)** November, **(G)** December. The dotted lines represent the lowest and highest wind speeds observed in the specific dates while the points represent the average wind speed. Bar graphs represent the precipitation data. The data was extracted from the nearest weather station to Lake Maurepas (Kenner, LA Weather History from Louis Armstrong New Orleans International Airport Station (29.99, -90.24)).



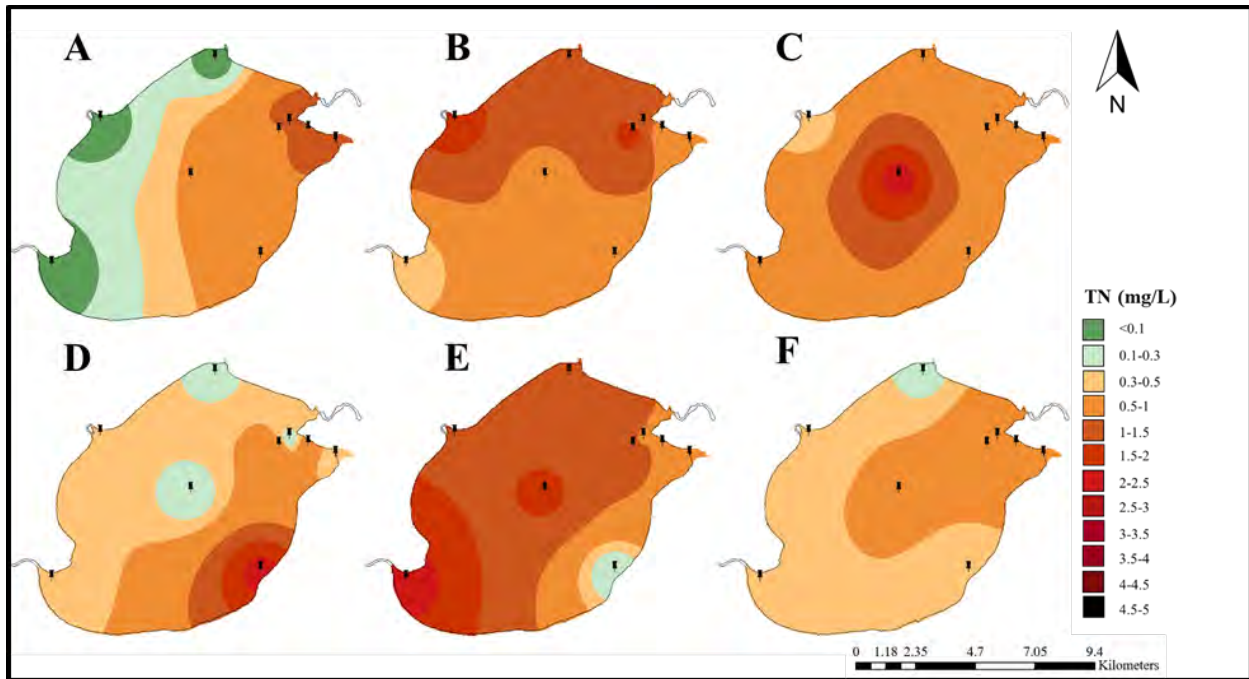
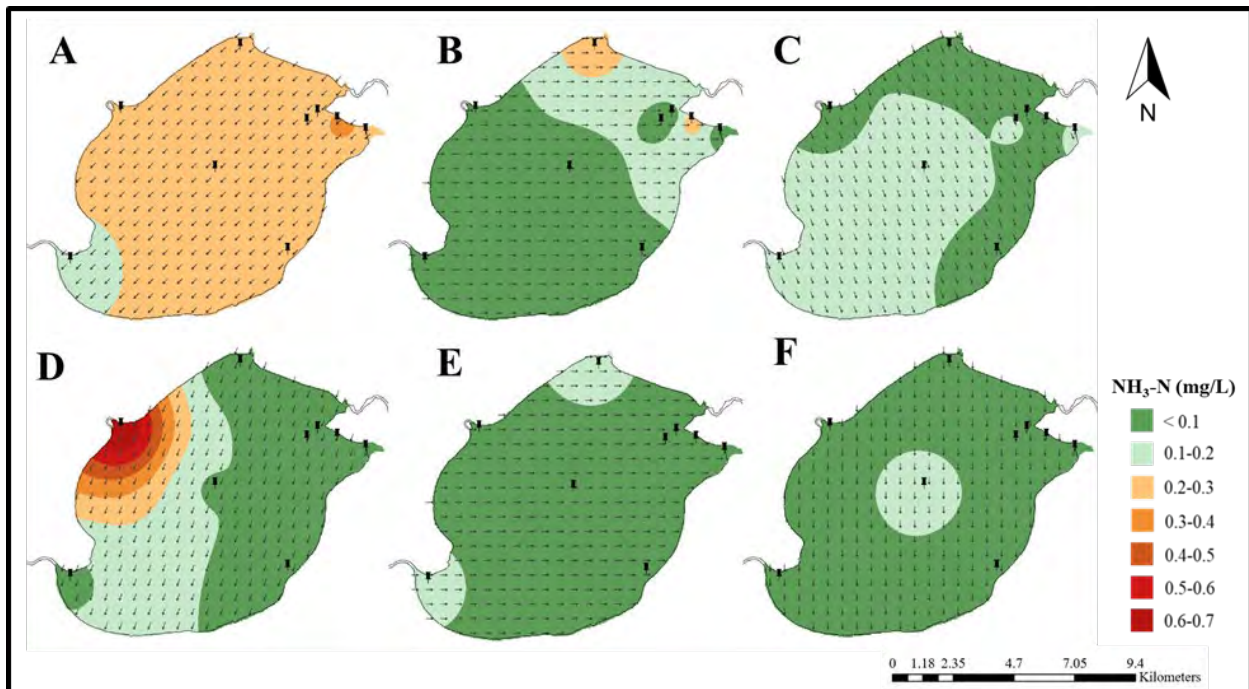


Figure 26. Maps generated for geospatial variation of TN (surface, middle and bottom layers in order) from June–November 2023 using IDW function in ArcGIS. The subgraphs indicate: **(A)** June, **(B)** July, **(C)** August, **(D)** September, **(E)** October, **(F)** November. The black pins indicate the sampling sites and the arrows indicate the wind direction \sim 9.00 am in the specific sampling dates (22 June 2023, 20 July 2023, 18 August 2023, 22 September 2023, 20 October 2023, 17 November 2023). 9.00 am was selected considering the sampling time.



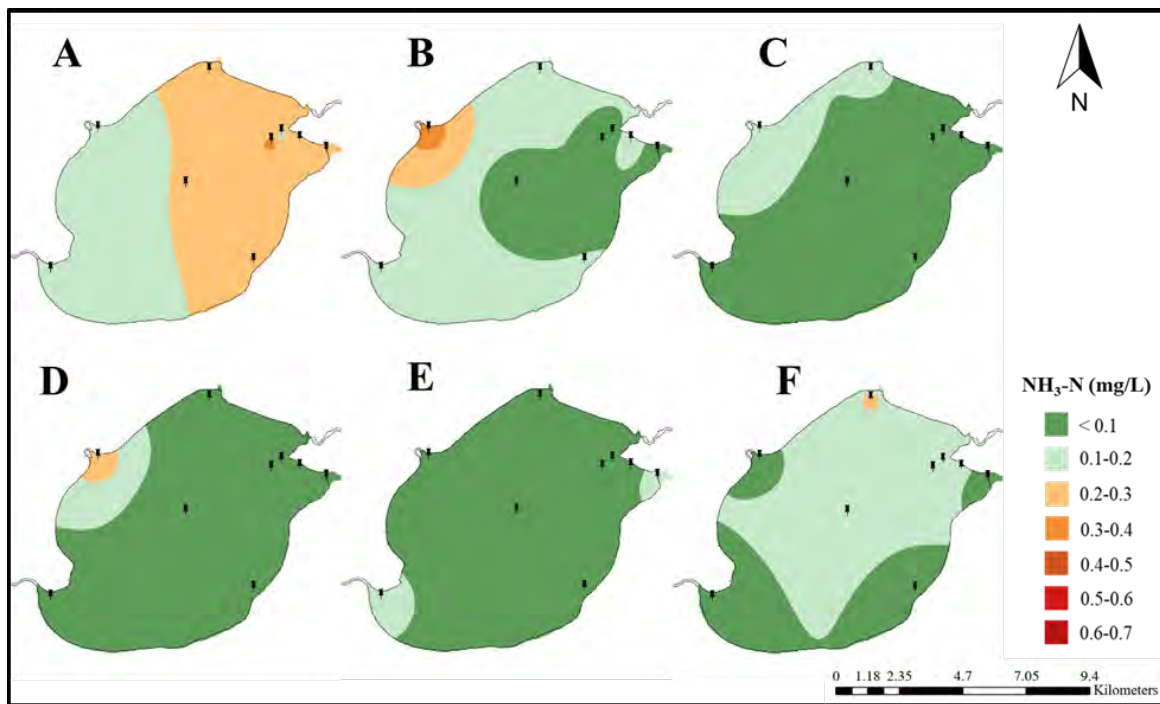
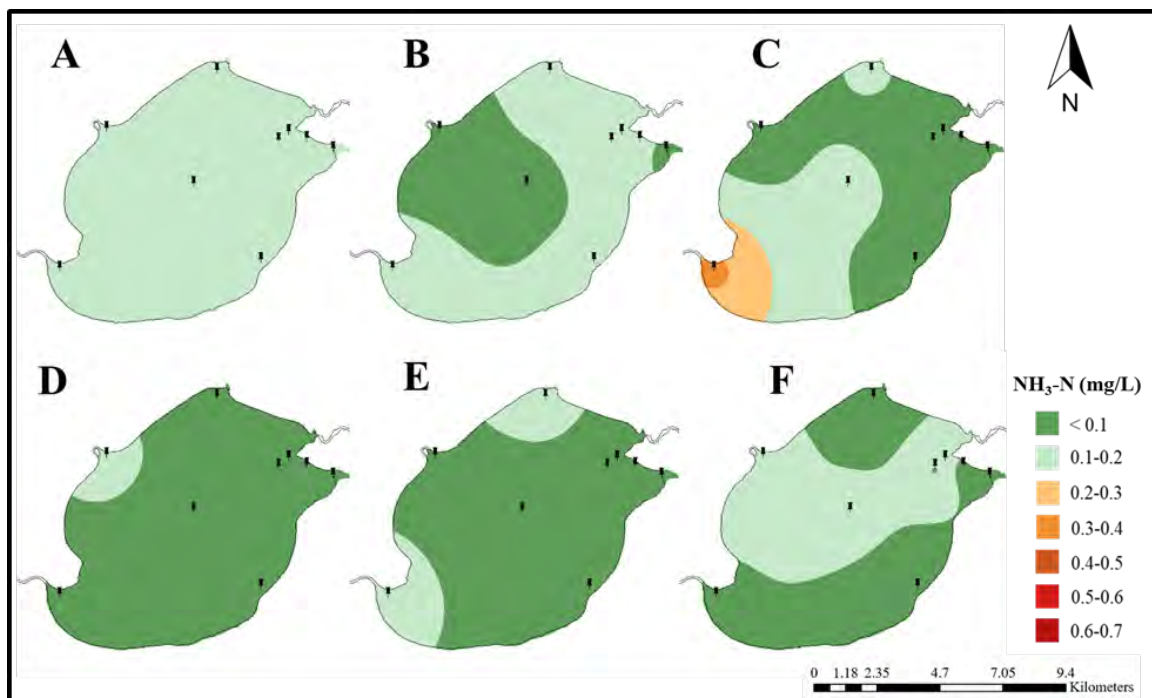
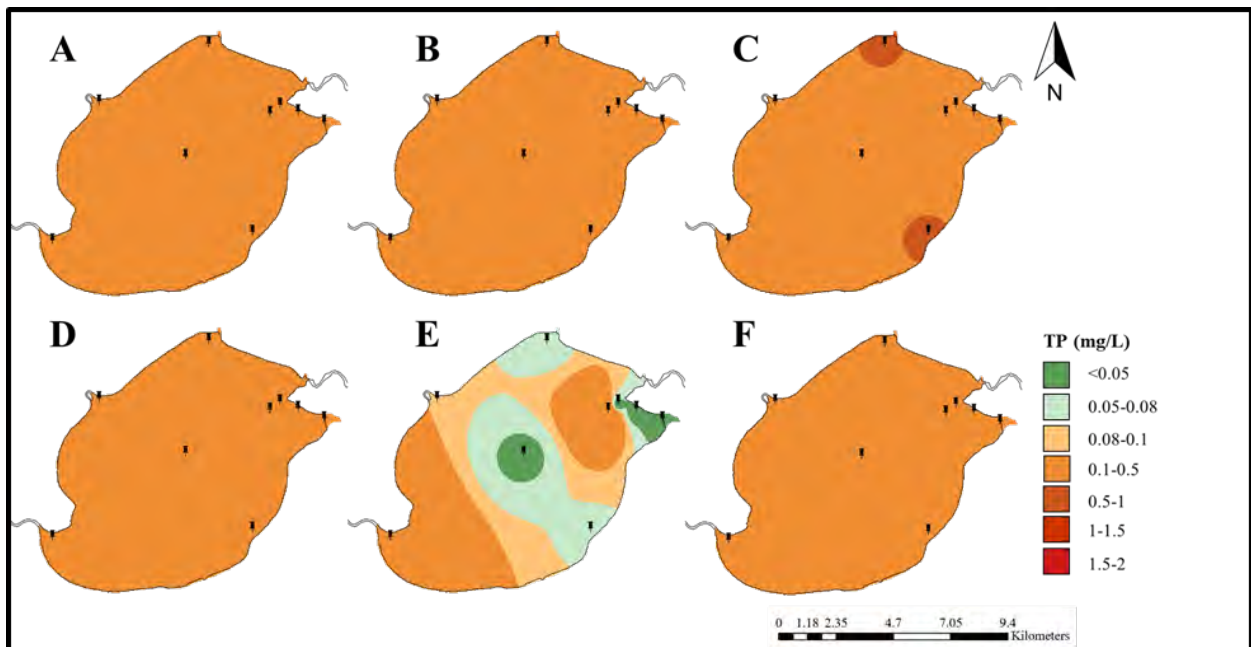
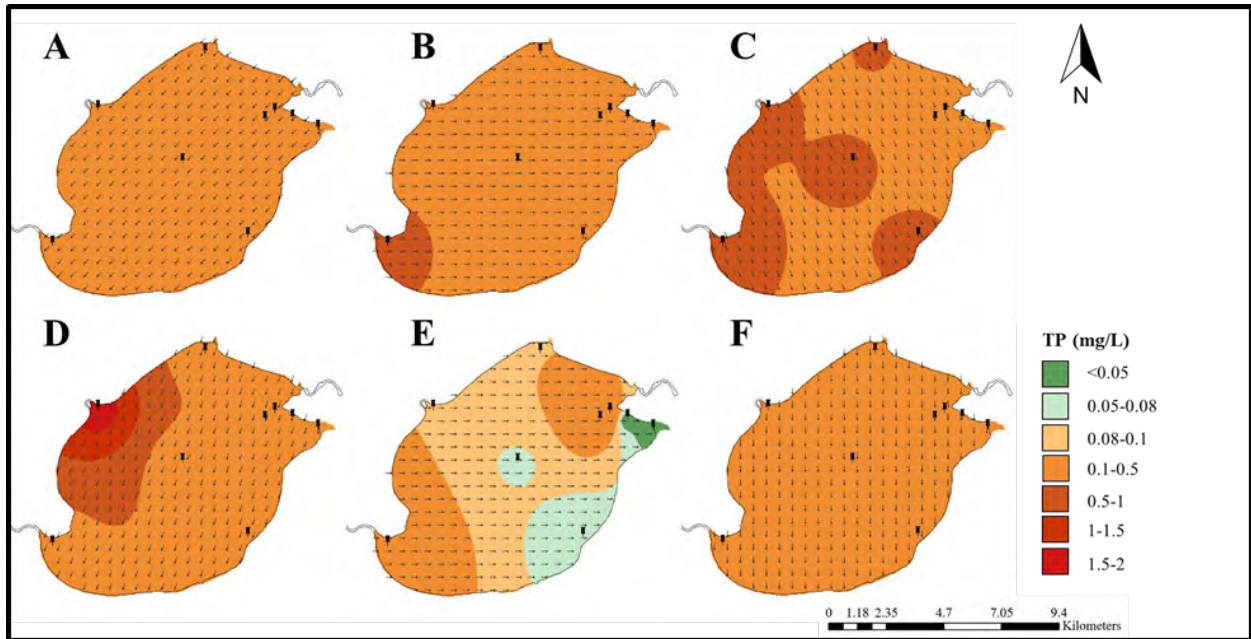


Figure 27. Maps generated for geospatial variation of $\text{NH}_3\text{-N}$ (surface, middle and bottom layers in order) from June–November 2023 using IDW function in ArcGIS. The subgraphs indicate: **(A)** June, **(B)** July, **(C)** August, **(D)** September, **(E)** October, **(F)** November. The black pins indicate the sampling sites and the arrows indicate the wind direction ~ 9.00 am in the specific sampling dates (22 June 2023, 20 July 2023, 18 August 2023, 22 September 2023, 20 October 2023, 17 November 2023). 9.00 am was selected considering the sampling time.



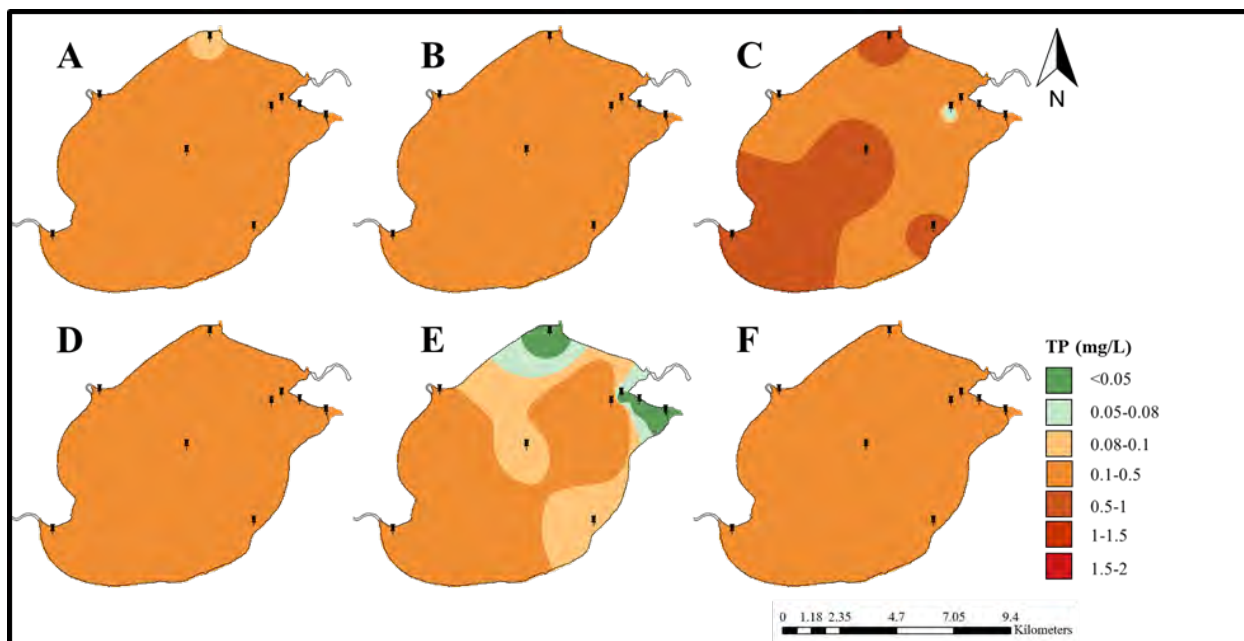
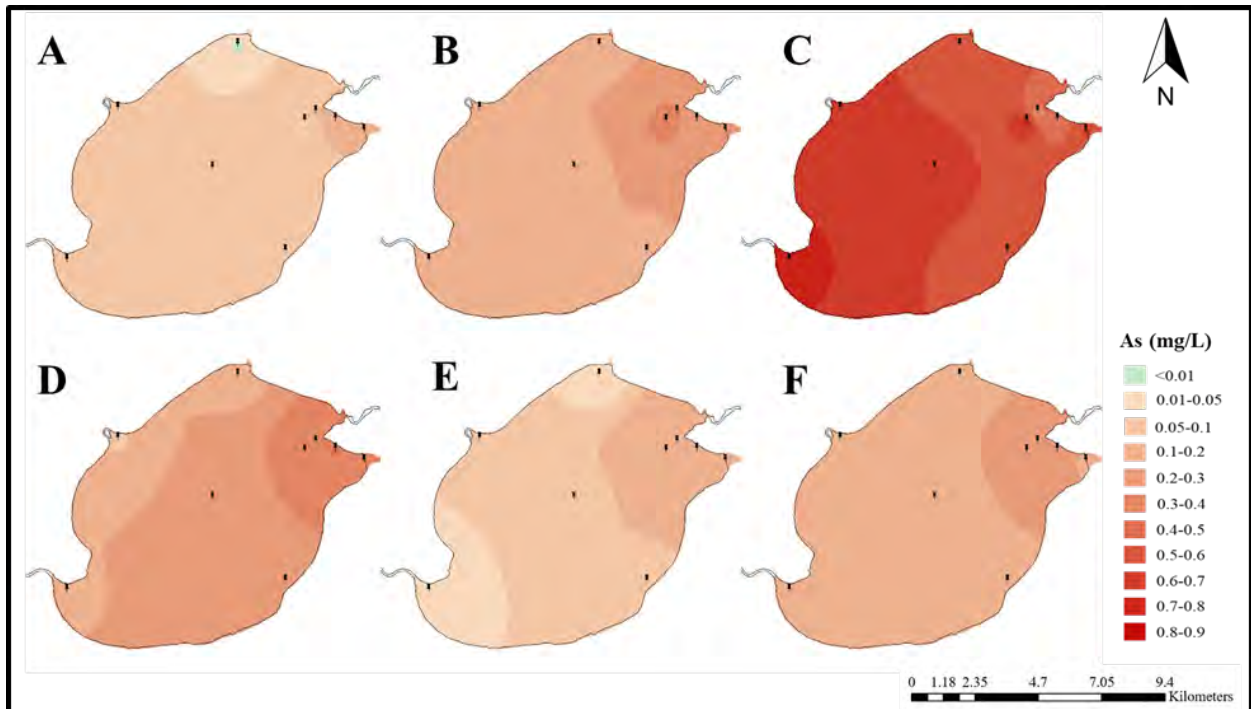
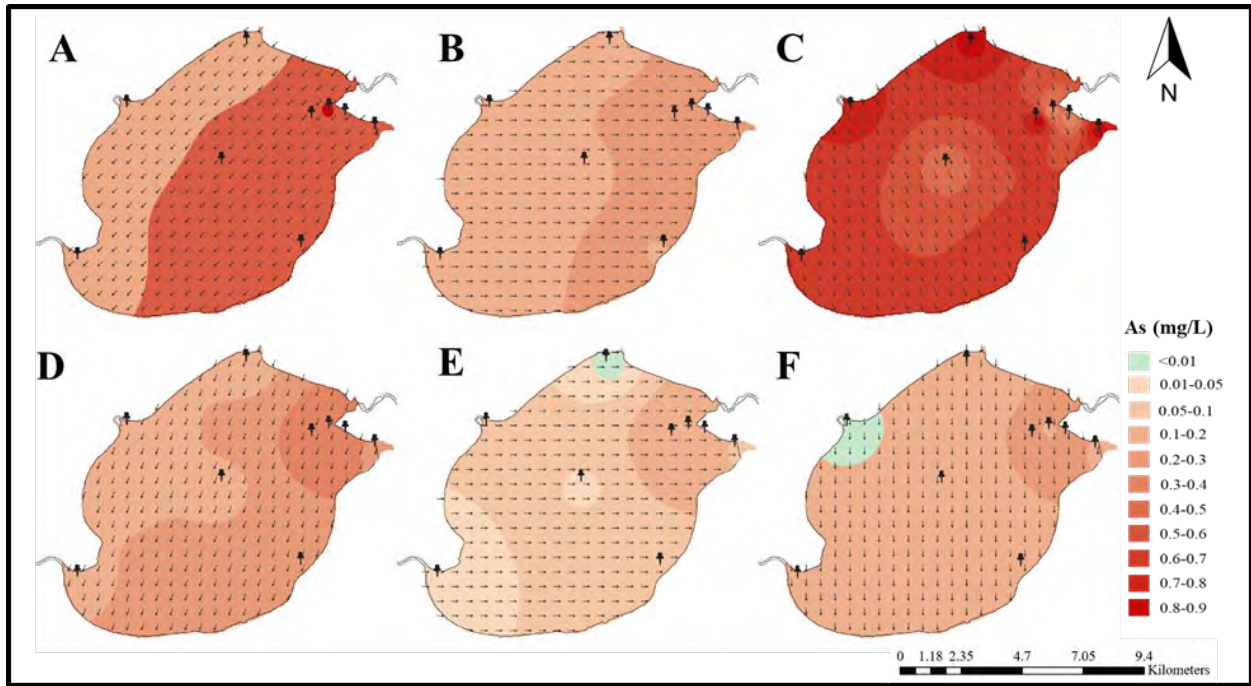


Figure 28. Maps generated for geospatial variation of TP (surface, middle and bottom layers in order) from June–November 2023 using IDW function in ArcGIS. The subgraphs indicate: **(A)** June, **(B)** July, **(C)** August, **(D)** September, **(E)** October, **(F)** November. The black pins indicate the sampling sites and the arrows indicate the wind direction ~9.00 am in the specific sampling dates (22 June 2023, 20 July 2023, 18 August 2023, 22 September 2023, 20 October 2023, 17 November 2023). 9.00 am was selected considering the sampling time.

The TN concentration varied from trace levels to approximately 5 mg/L during the sampling period. While few environmental agencies have set standards for TN in lakes to protect aquatic life, these standards typically range from 0.02 mg/L to 2.00 mg/L, depending on the ecosystem's sensitivity and the designated use of the waterbody. TN levels were relatively higher in June and August at sites D1–D3, in July at sites ND2 and ND3, in September at ND2 near the Amite River (with the highest recorded value of 4.97 ± 0.19 mg/L), in October at sites ND1–ND4, and in November at sites ND3 and D4. As shown in Figures 7, wind speed and direction likely caused the high discharge from the Amite River to move eastward, eventually settling in the bottom layers near the STW. The opposing force generated by drilling activities during these months may have prevented further migration toward the D4 site. A similar pattern was observed for $\text{NH}_3\text{-N}$ (**Figure 27**) and TP (**Figure 28**). $\text{NH}_3\text{-N}$ concentrations were generally higher in June and September, especially near the Amite River, which closely aligned with TN concentration variations. TP concentrations ranged from 0.09 to 2 mg/L during the sampling period, with higher concentrations observed in August and September compared to the other months. The highest TP concentration was found in the surface layer of ND2 ($1.71 \pm$

0.05 mg/L), while the lowest was in the middle layer of D3 and the bottom layer of D2 (0.01 mg/L).



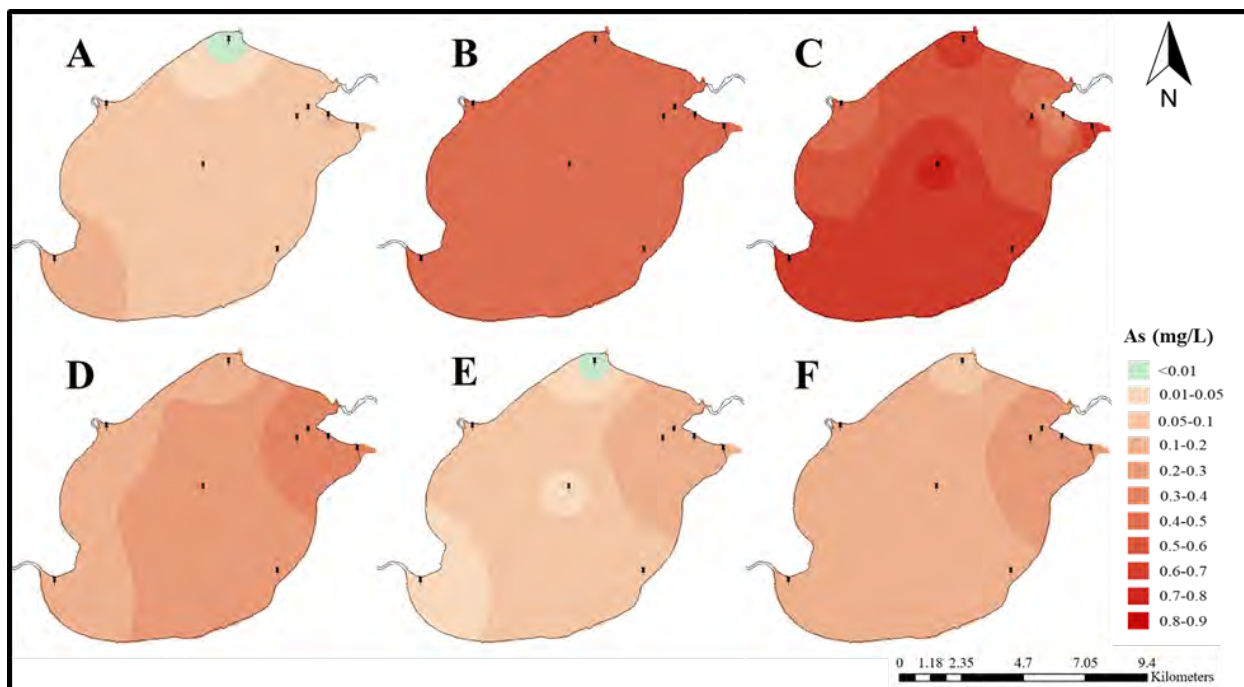
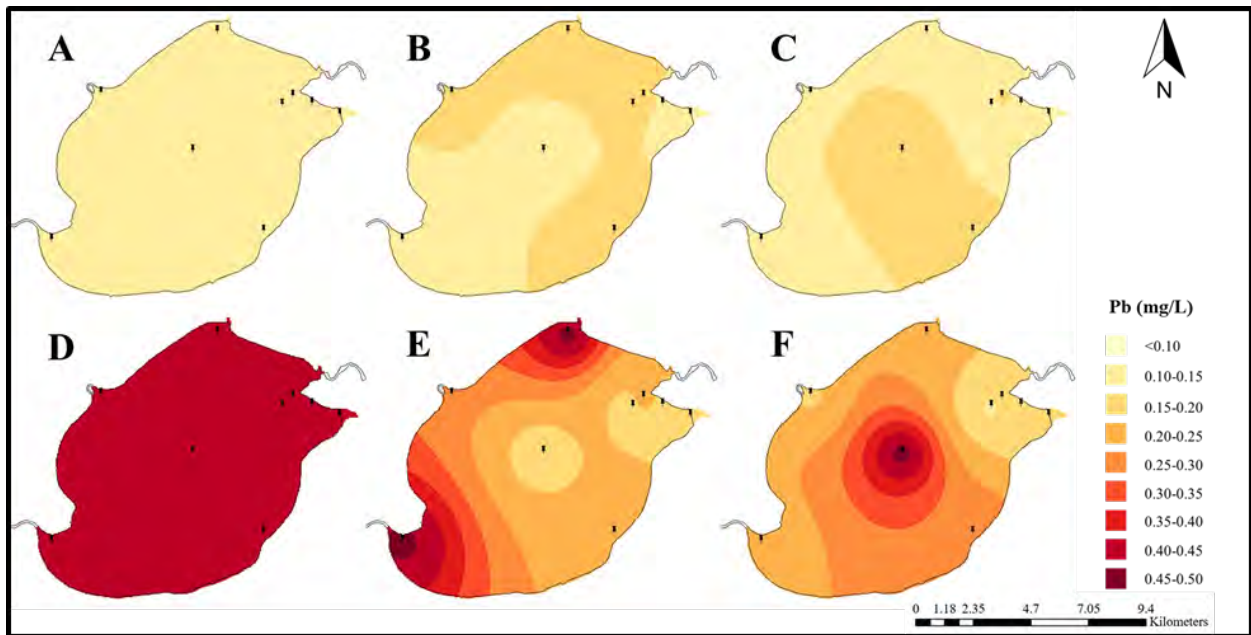
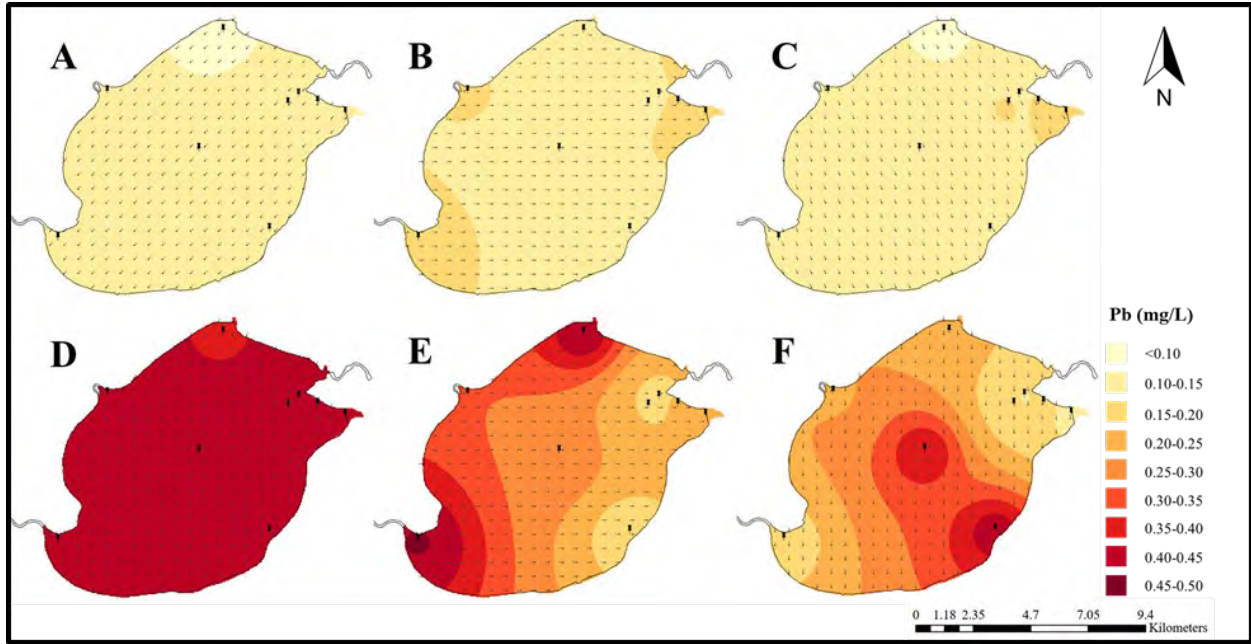


Figure 29. Maps generated for geospatial variation of As (surface, middle and bottom layers in order) from June–November 2023 using IDW function in ArcGIS. The subgraphs indicate: **(A)** June, **(B)** July, **(C)** August, **(D)** September, **(E)** October, **(F)** November. The black pins indicate the sampling sites and the arrows indicate the wind direction ~9.00 am in the specific sampling dates (22 June 2023, 20 July 2023, 18 August 2023, 22 September 2023, 20 October 2023, 17 November 2023). 9.00 am was selected considering the sampling time.



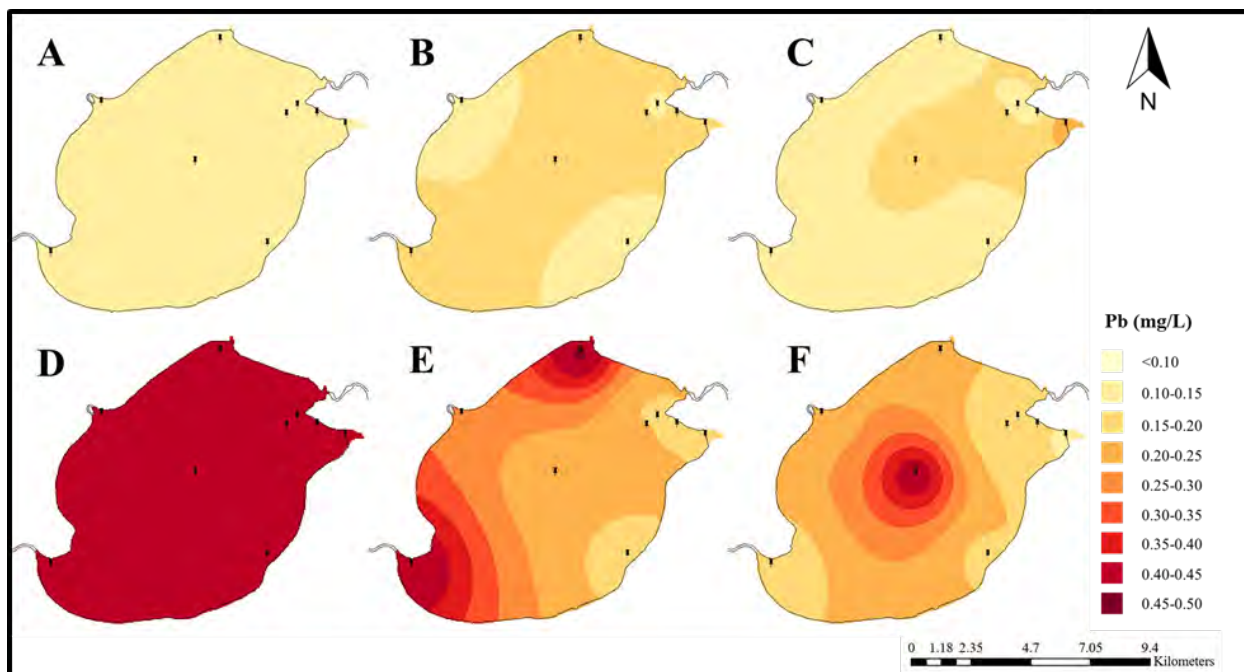


Figure 30. Maps generated for geospatial variation of Pb (surface, middle and bottom layers in order) from June–November 2023 using IDW function in ArcGIS. The subgraphs indicate: **(A)** June, **(B)** July, **(C)** August, **(D)** September, **(E)** October, **(F)** November. The black pins indicate the sampling sites and the arrows indicate the wind direction ~9.00 am in the specific sampling dates (22 June 2023, 20 July 2023, 18 August 2023, 22 September 2023, 20 October 2023, 17 November 2023). 9.00 am was selected considering the sampling time.

Both As and Pb concentrations exceeded safety limits throughout Lake Maurepas during the sampling period at all three depths (see **Table 6** and **Figures 29-30**). Spatial-temporal analysis showed an increase in As concentrations from June to August, with the highest contamination observed in August. Pb concentrations were notably higher from September to November compared to other months. The influence of river discharges was most apparent in August for As (**Figure 29**). Similarly, elevated Pb concentrations near river discharges, as shown in **Figure 30**, highlighted the rivers' contribution to lake water pollution. The subsurface seismic survey previously conducted and the ongoing drilling activities by APC in the lake may have also influenced contaminant concentrations in both water and sediment. However, **Figure 30** shows low concentrations of contaminants near the D4 sampling site, the closest site to the STW, indicating minimal impact from APC's drilling and seismic activities on the observed contaminant levels. The exception was higher Pb concentrations around the D4 site in November 2023 (**Figure 30**).

Geospatial Analysis of Mercury (Hg) Distribution in Sedimentary Mud of Lake Maurepas.

Mercury was not detected in significant amounts in the water samples, but higher

concentrations were found in sediment samples, though they remained below the threshold. **Figure 31** shows the distribution of Hg concentrations in sedimentary muds across the lake during the sampling period. The highest levels were recorded at ND2 ($25.61 \pm 6.04 \mu\text{g}/\text{kg}$) in November (**Figure 31F**), while the lowest were found at ND3 ($7.53 \pm 1.09 \mu\text{g}/\text{kg}$) in September (**Figure 31D**). Hg concentrations were relatively higher in June, August, and November compared to other months, with peak concentrations observed in November near the Amite River input and at ND4 in the middle of the lake. Increased rainfall and wind inflow can generate surface, subsurface, or density currents, which transport sediment within the lake. This phenomenon likely explains the higher sediment Hg concentrations observed at ND2, ND4, and D4 in November (**Figure 31F**). Specifically, on November 14th, 21st, and 26th, the lake received substantial rainfall amounts of 19.3 mm, 18.5 mm, and 22.1 mm, respectively, as shown in Figure 6F.

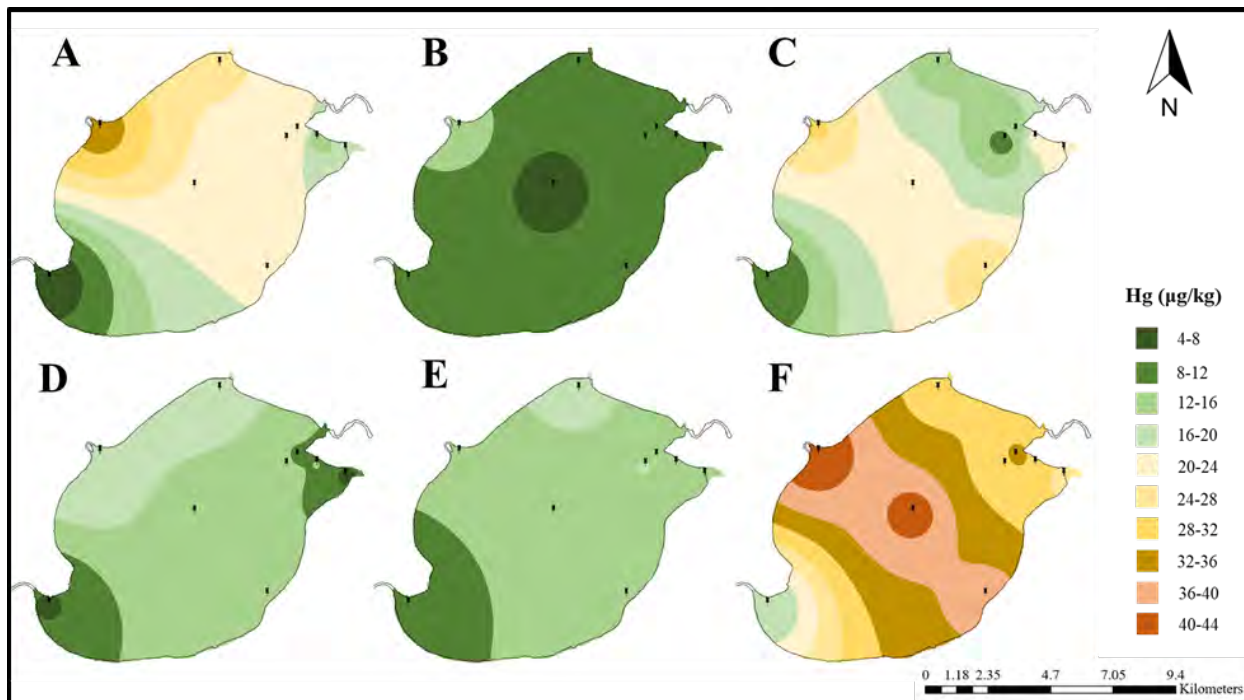
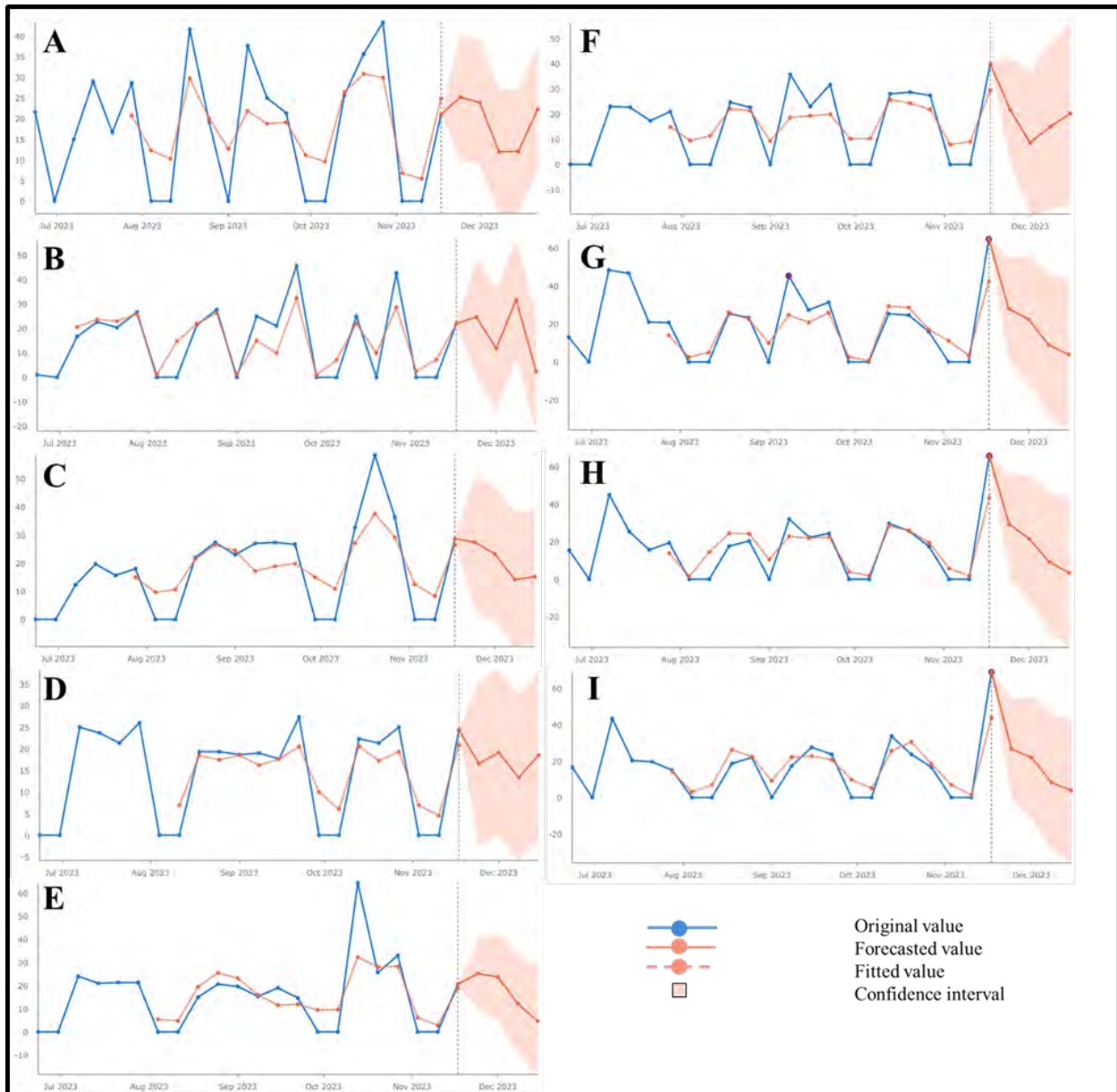


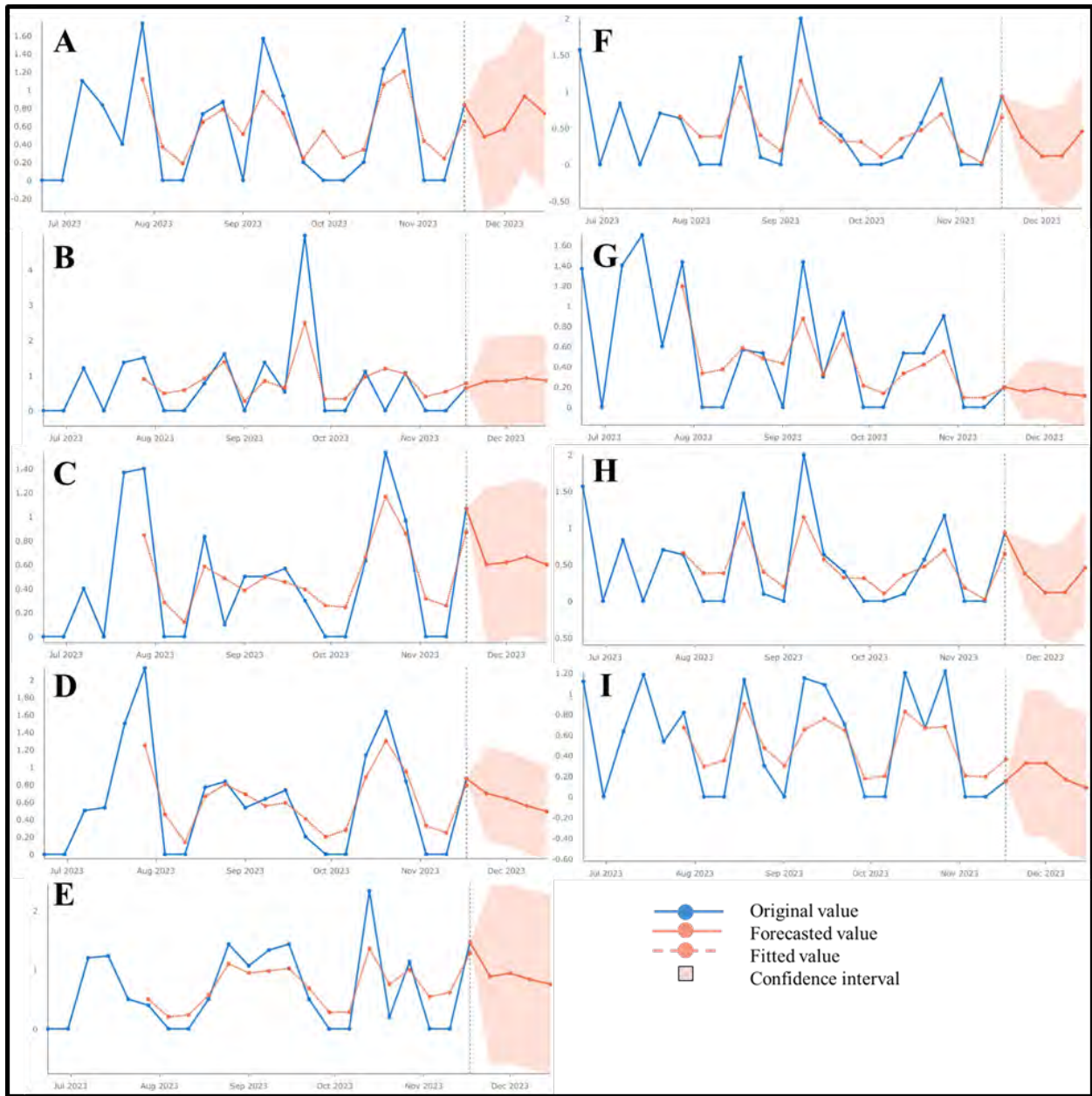
Figure 31. Maps generated for geospatial variation of Hg in sedimentary mud samples from June-November 2023 using IDW function in ArcGIS: (A) June, (B) July, (C) August, (D) September, (E) October, (F) November. The black pins indicate the sampling sites.

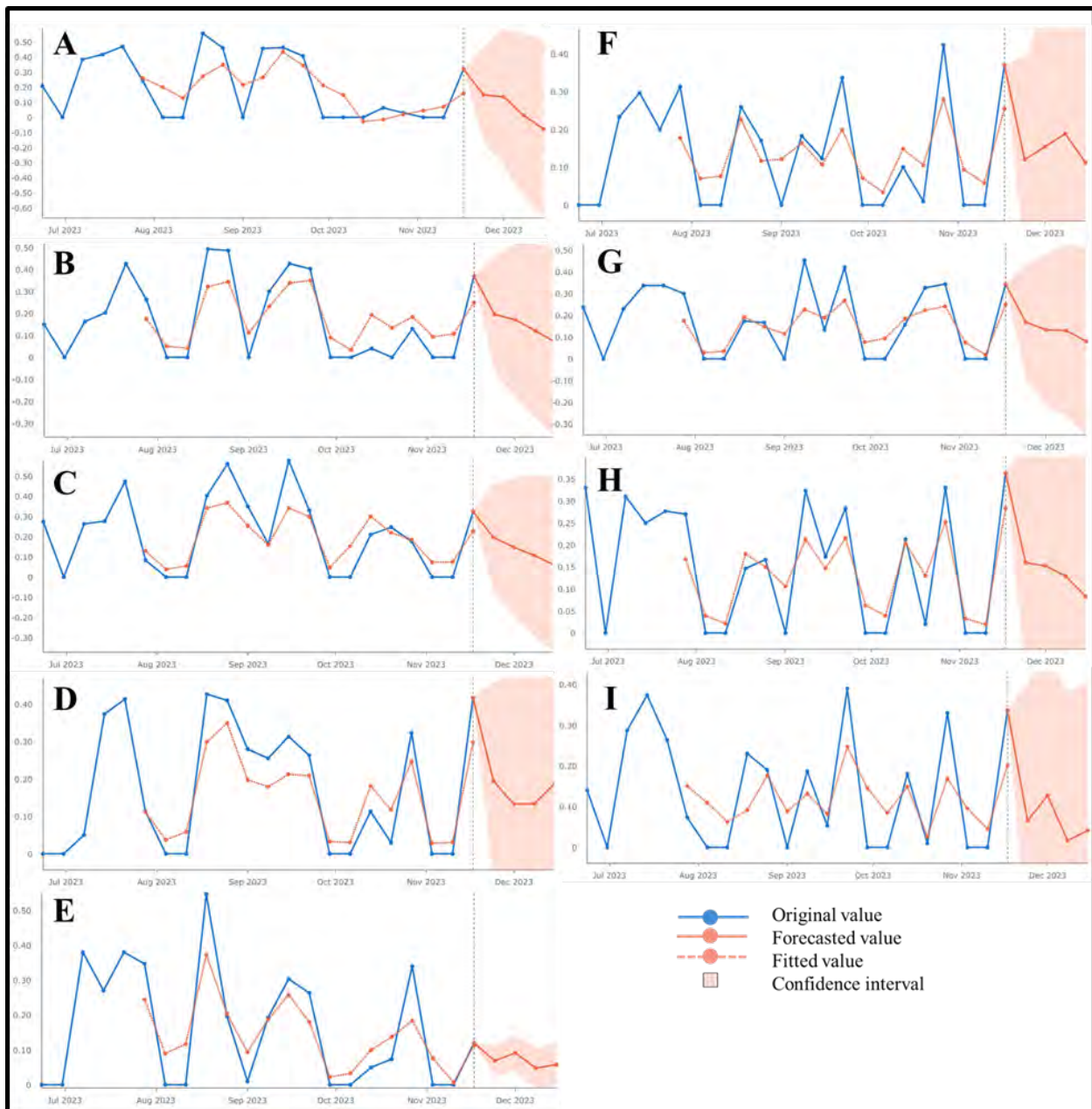
Predictive Modeling of Water Quality. Data collected from the USGS monitoring station (**Figure 21**) showed steep increases in salinity and specific conductance (SC) until November, followed by a decrease of 49.2% for salinity and 48.8% for SC in December. These reductions brought the values back to the levels observed between September and October. Since the start of our study in June, we have collected samples from the lake at least once a month. Unfortunately,

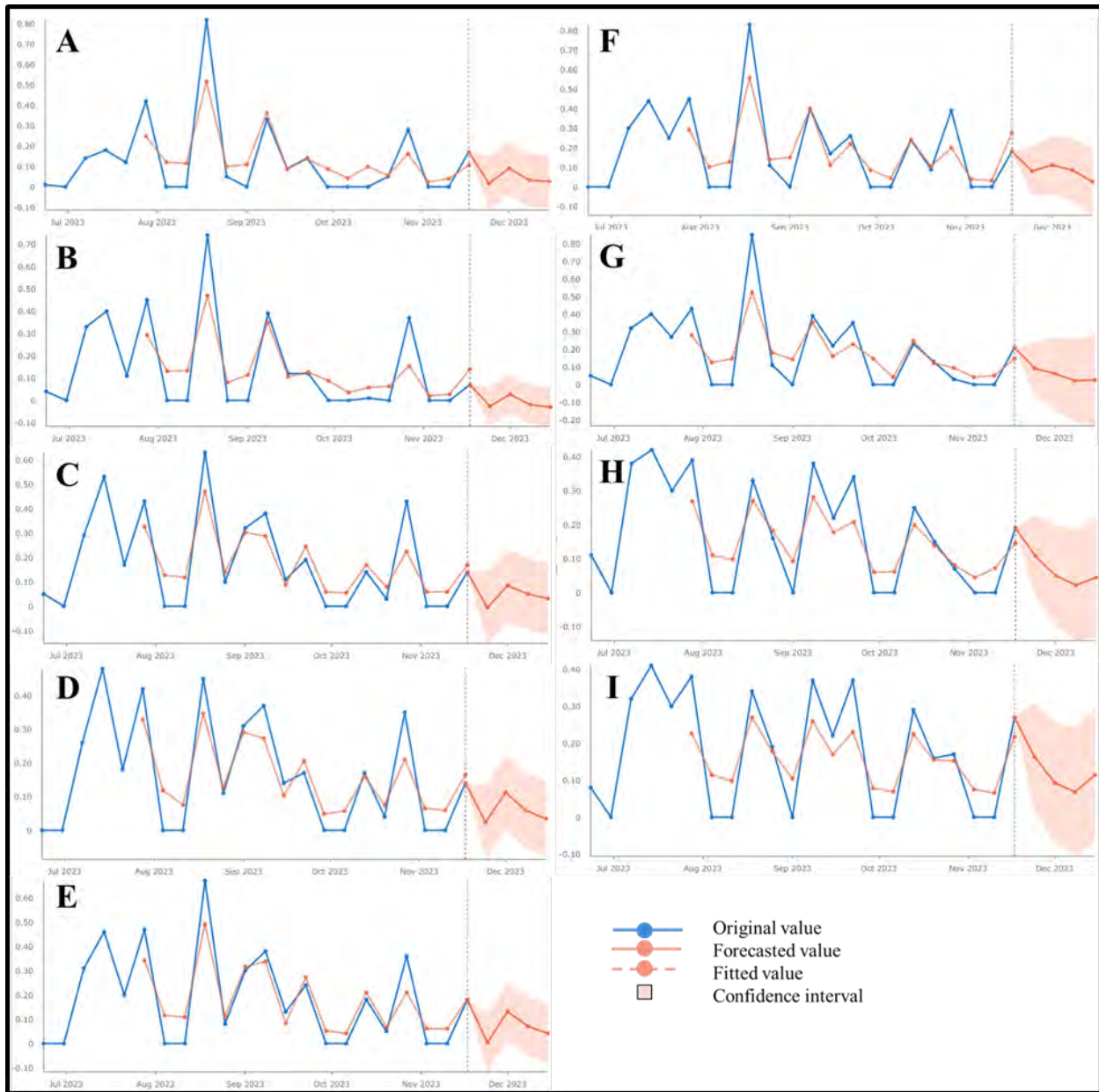
sampling in December 2023 was not possible due to a combination of high precipitation and wind speed (Figure 6). To predict the spatial-temporal changes of COD, TN, TP, As, and Pb pollutants for this month, we examined several forecasting methods, including curve fitting, exponential smoothing, forest-based, and LSTM models. These pollutants showed correlations with salinity and SC. The key question was whether the spatial-temporal patterns of these pollutants aligned with the decreasing trends in salinity and SC observed in December.

Among the evaluated water quality forecasting methods, the forest-based machine learning model and LSTM 2 model demonstrated robust performance. All the prediction results are presented in **Figures 32-35**. Predictions were based solely on water quality data collected from June to November 2023 in the forest-based model, due to limitations in ArcGIS. It was trained using 100 trees with a maximum depth of 10. The average R^2 values for the nine sampling sites are 0.746 for COD, 0.759 for TN, 0.819 for As, 0.731 for TP, and 0.838 for Pb. All parameters showed decreasing trends in December across almost all sampling sites. While both forest-based and LSTM models exhibited satisfactory predictive capabilities, LSTM offers the advantage of potentially greater robustness due to its ability to incorporate a broader range of physical parameters as inputs. This inclusion of diverse variables may enhance the model's ability to make more reliable predictions while reducing the risk of overfitting. The predicted concentration trends for December did not significantly differ from the measured values for September and October in most cases ($p > 0.05$). Exceptions included COD in ND3 and D4, TN in ND4 and D4, TP in ND1, and Pb in ND1 and ND5. These anomalies may be attributed to the connections of ND1, ND3, and ND5 to the Tickfaw and Blind Rivers and Manchac, which are independent sources of COD, TP, TN, and Pb, as well as the proximity of D4 to the STW. The observed similarity between salinity and SC behaviors in December and the predicted trends of these pollutants, particularly for COD in D1-D3, may be explained by the removal or settlement of contaminants from the Pass Manchac vehicle accident. This aligns with the persistence of pollutant sources previously identified in September and October.









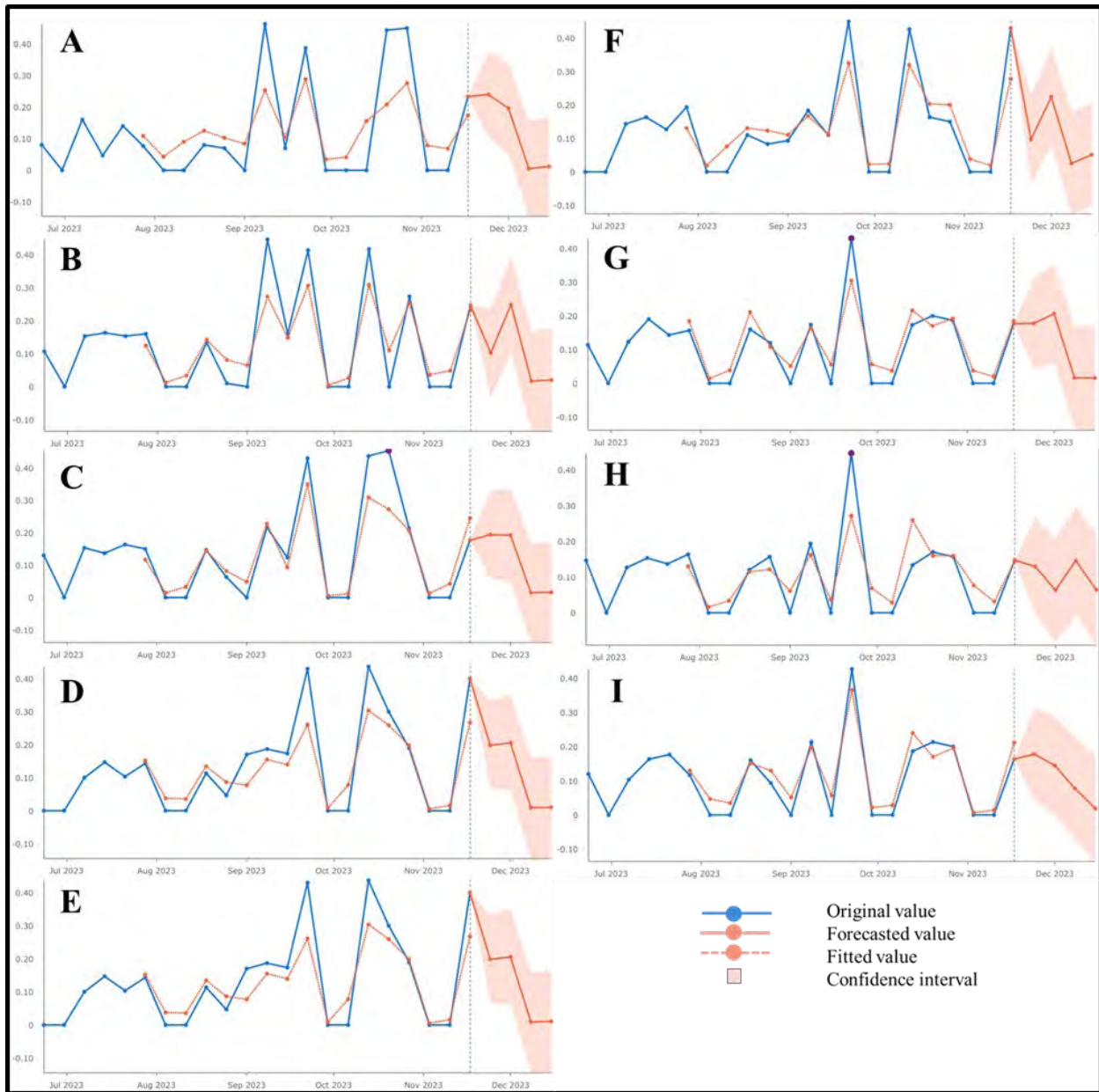
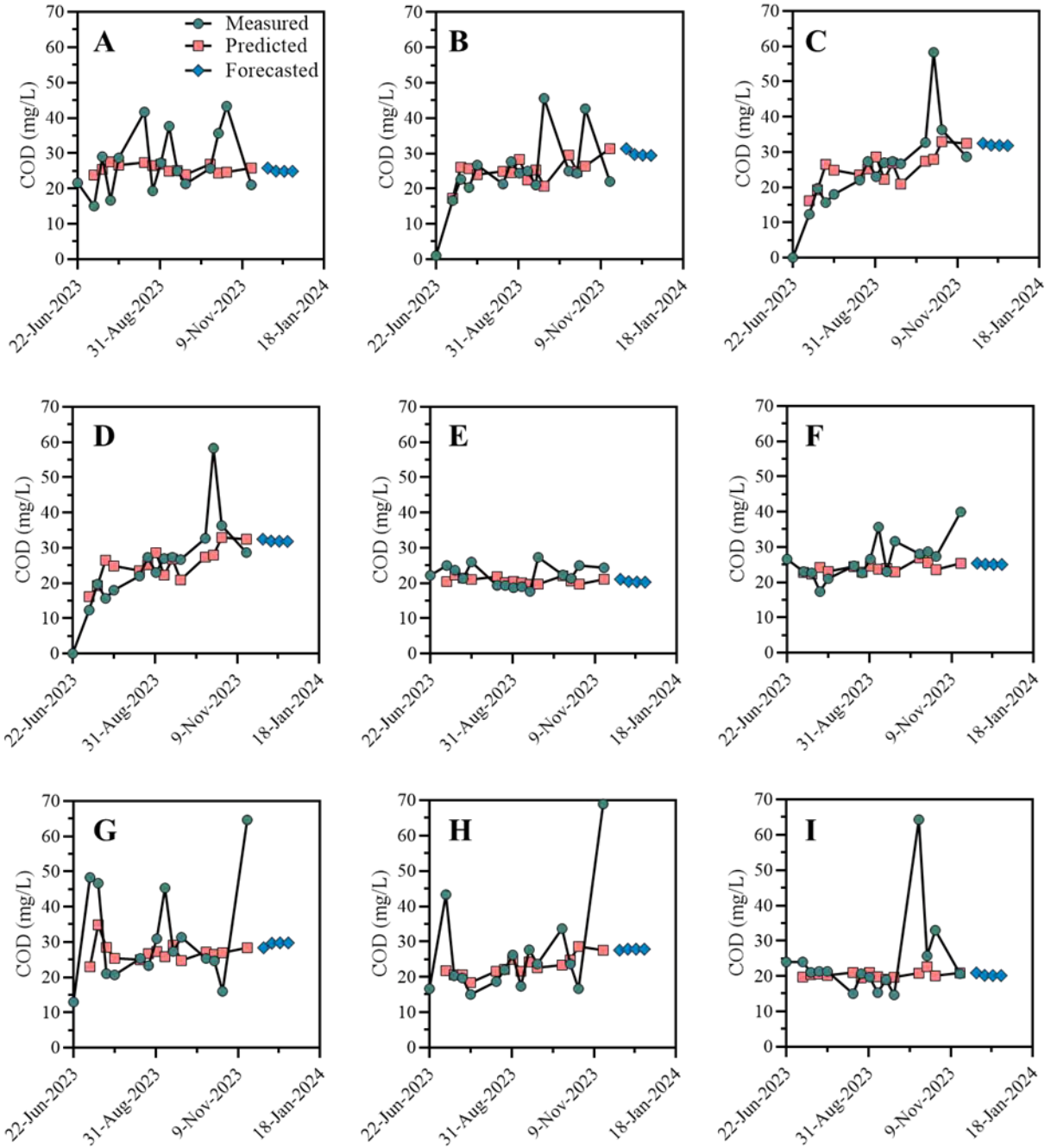
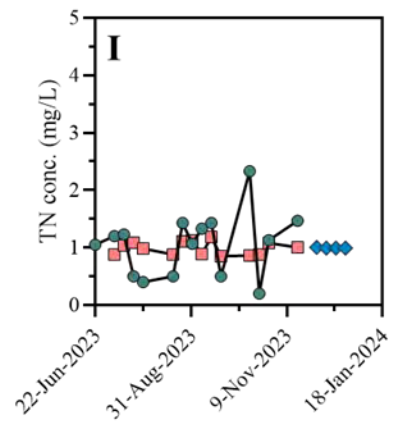
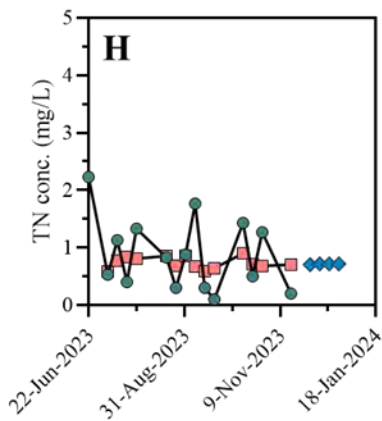
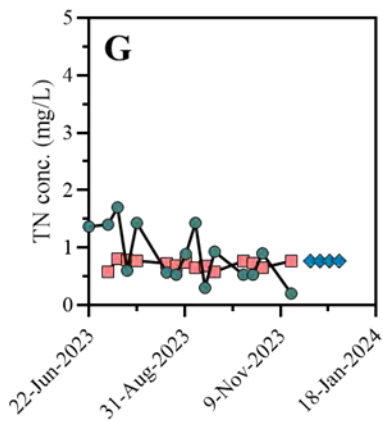
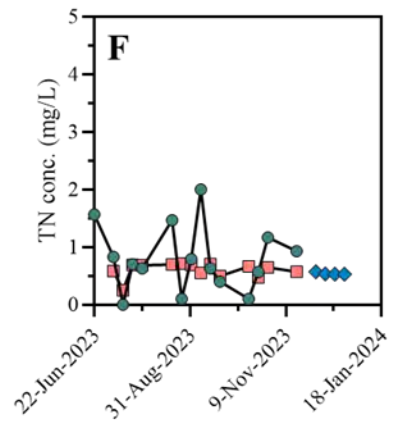
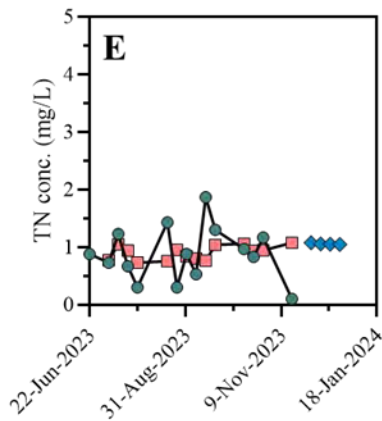
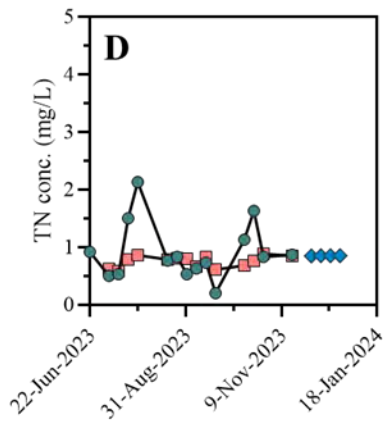
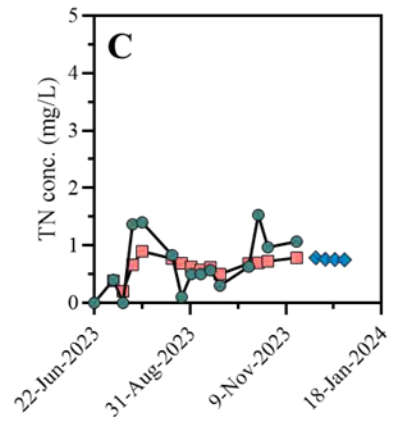
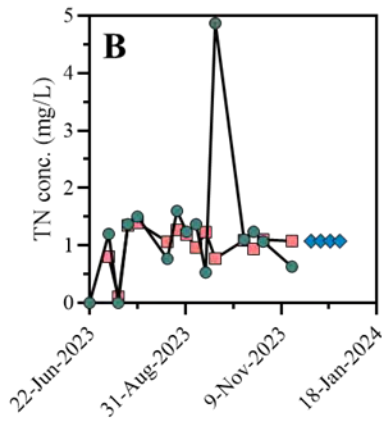
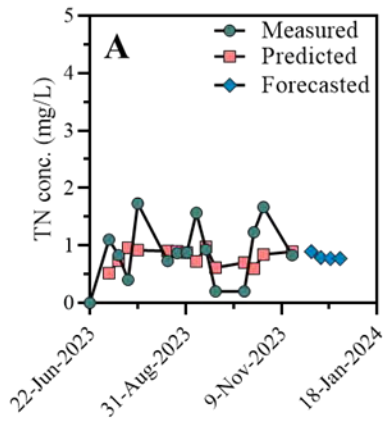


Figure 32. Forecasted values of COD, TN, TP, As and Pb for December 2023 based on the data from June–November 2023 using Forest-based forecasting method: **(A)** ND1, **(B)** ND2, **(C)** ND3, **(D)** ND4, **(E)** D4, **(F)** ND5, **(G)** D1, **(H)** D2 and **(I)** D3. The shaded area gives the 95% confidence interval of the forecasted value.

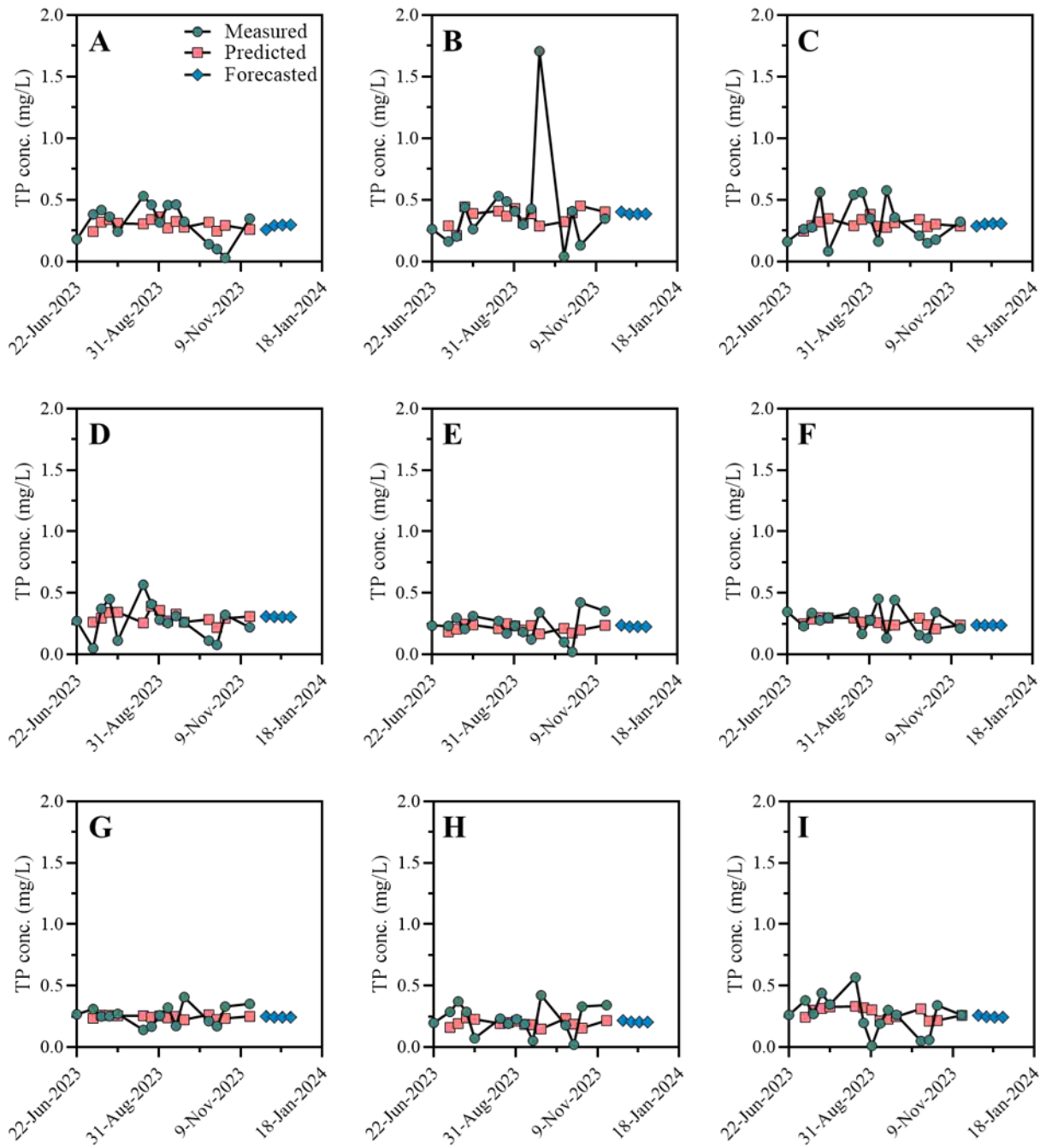
(1)



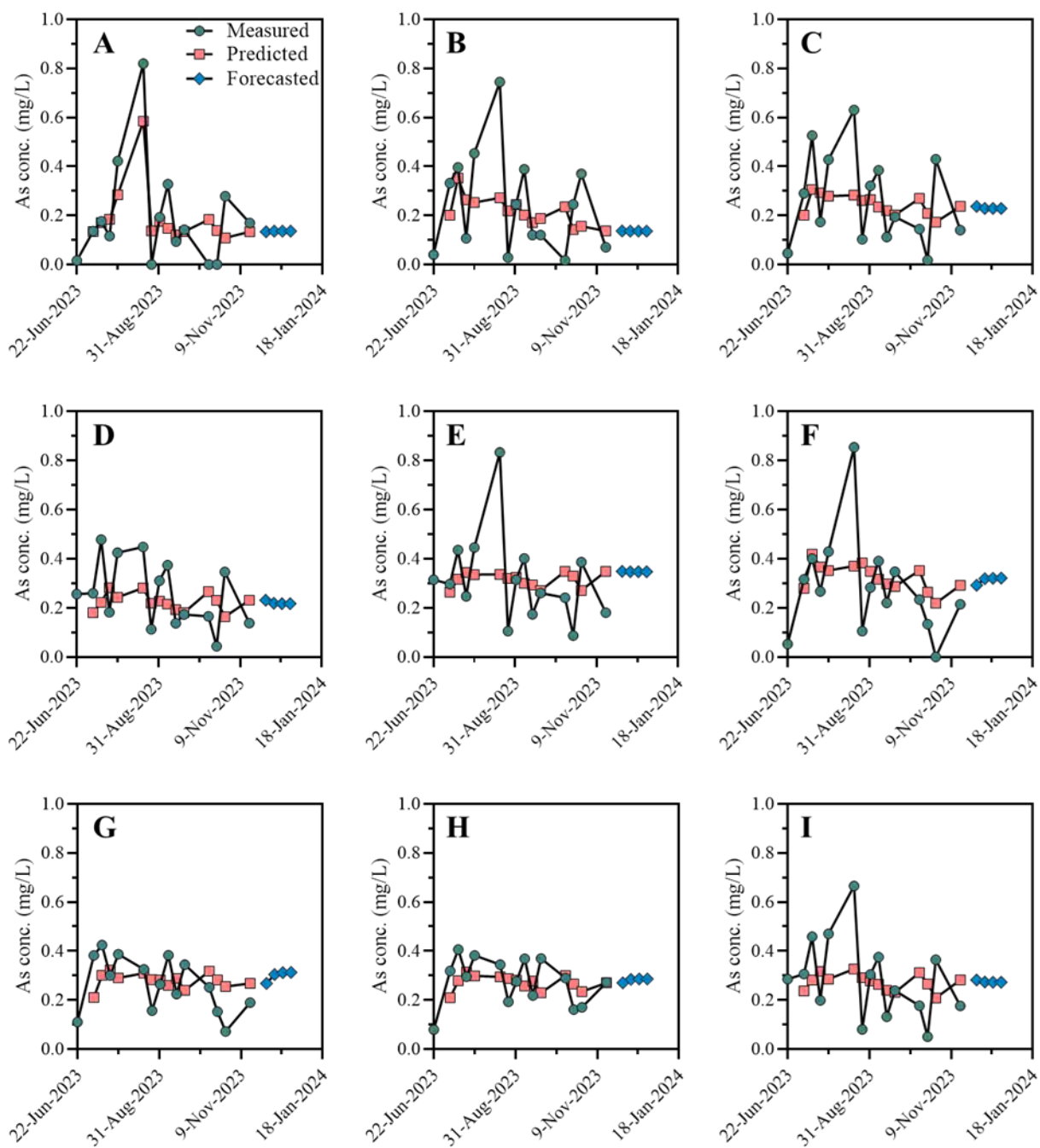
(2)



(3)



(4)



(5)

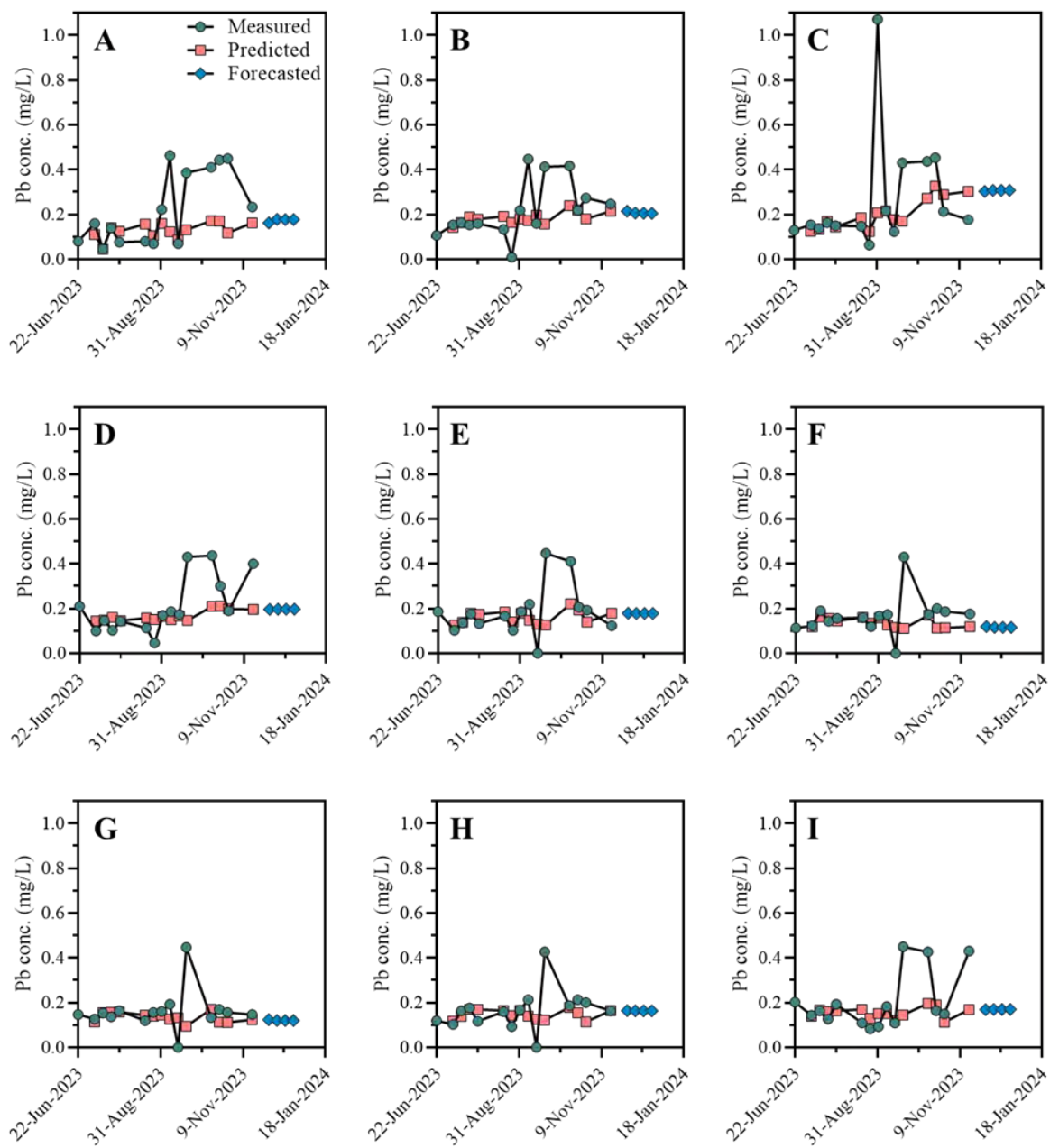
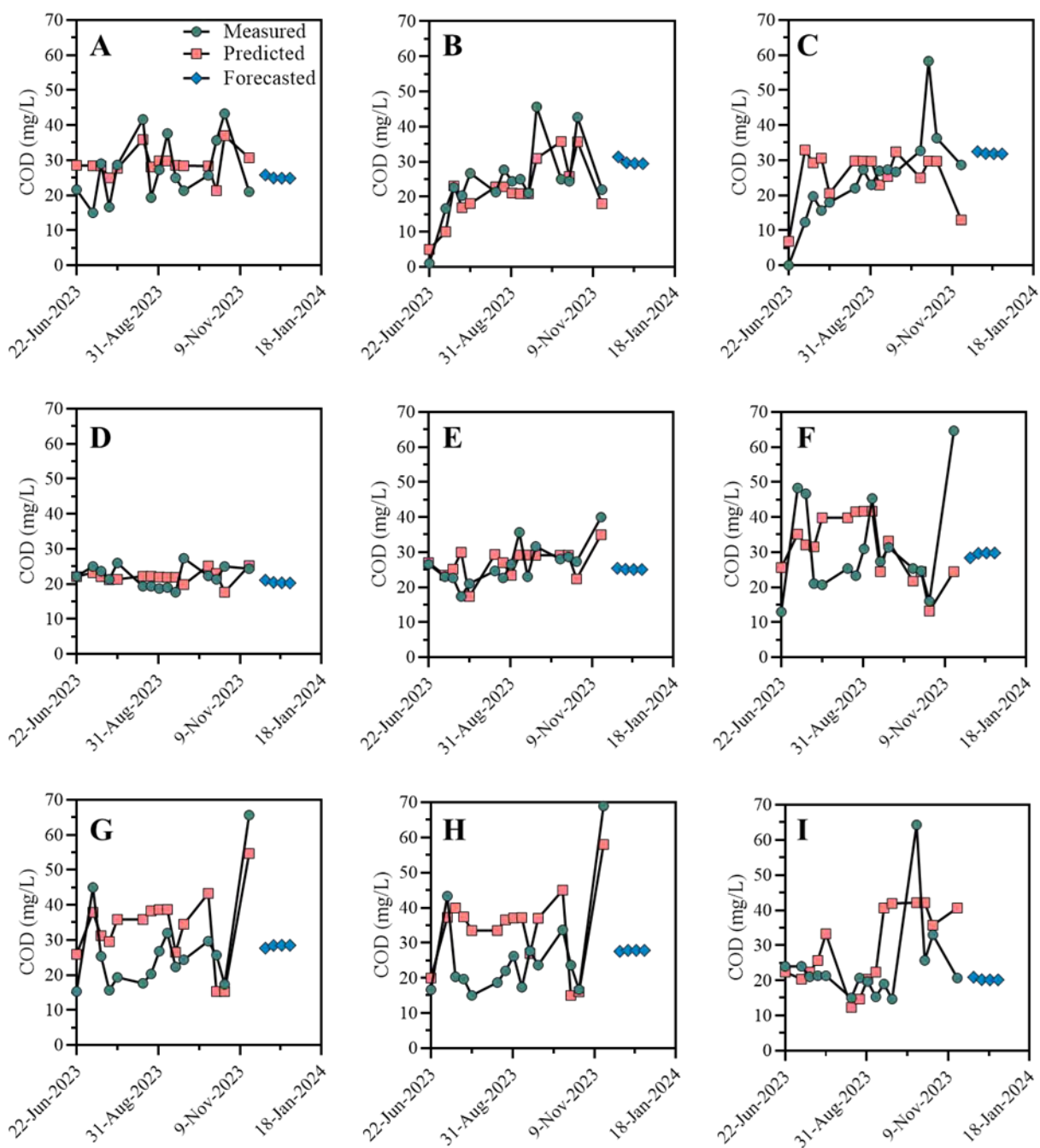
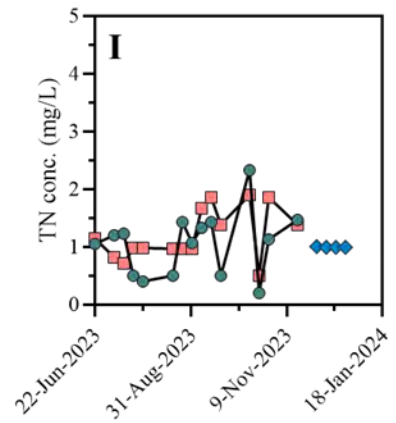
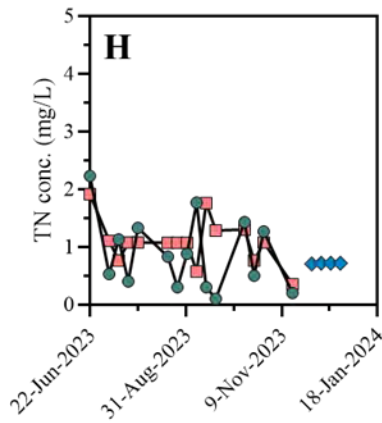
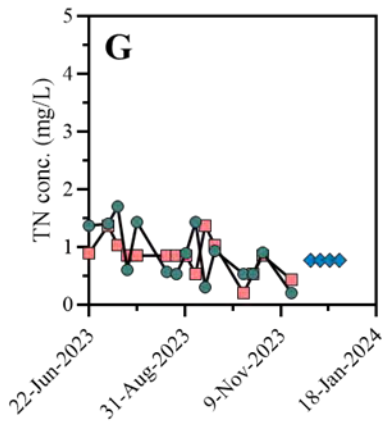
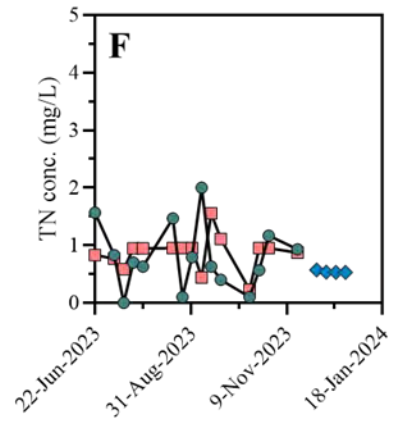
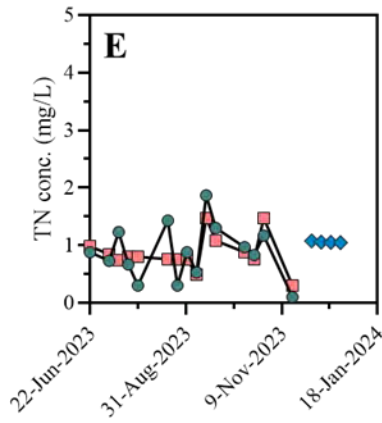
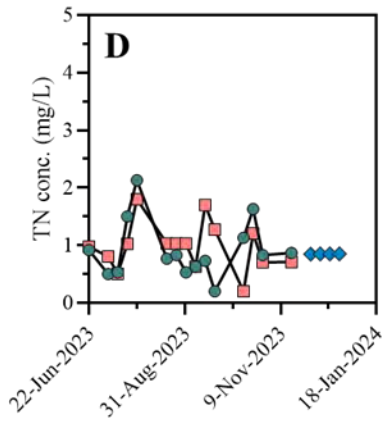
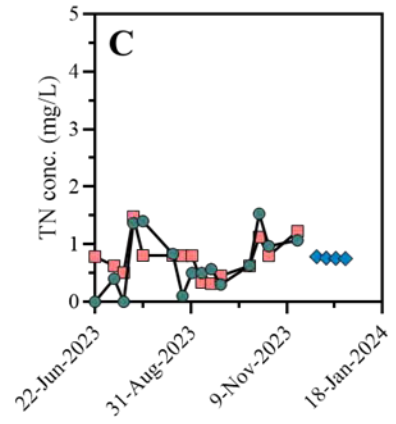
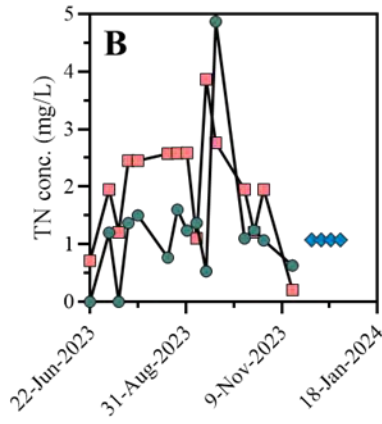
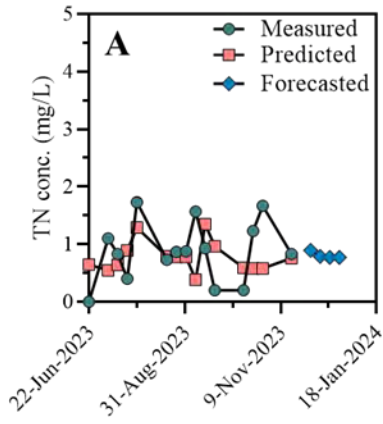


Figure 33. Measured, predicted and forecasted values for 9 sampling sites using the model, LSTM1: (1) COD, (2) TN, (3) TP, (4) As and (5) Pb. Subfigures A–I represent the sampling sites of ND1, ND2, ND3, ND4, ND5, D1, D2, D3 and D4, respectively. Green circles show the measured values, orange boxes represent the predicted values using model LSTM1, while the blue diamond shape symbols represent the predicted values using model LSTM1 as stated in the subfigure (A) of each (1)–(5).

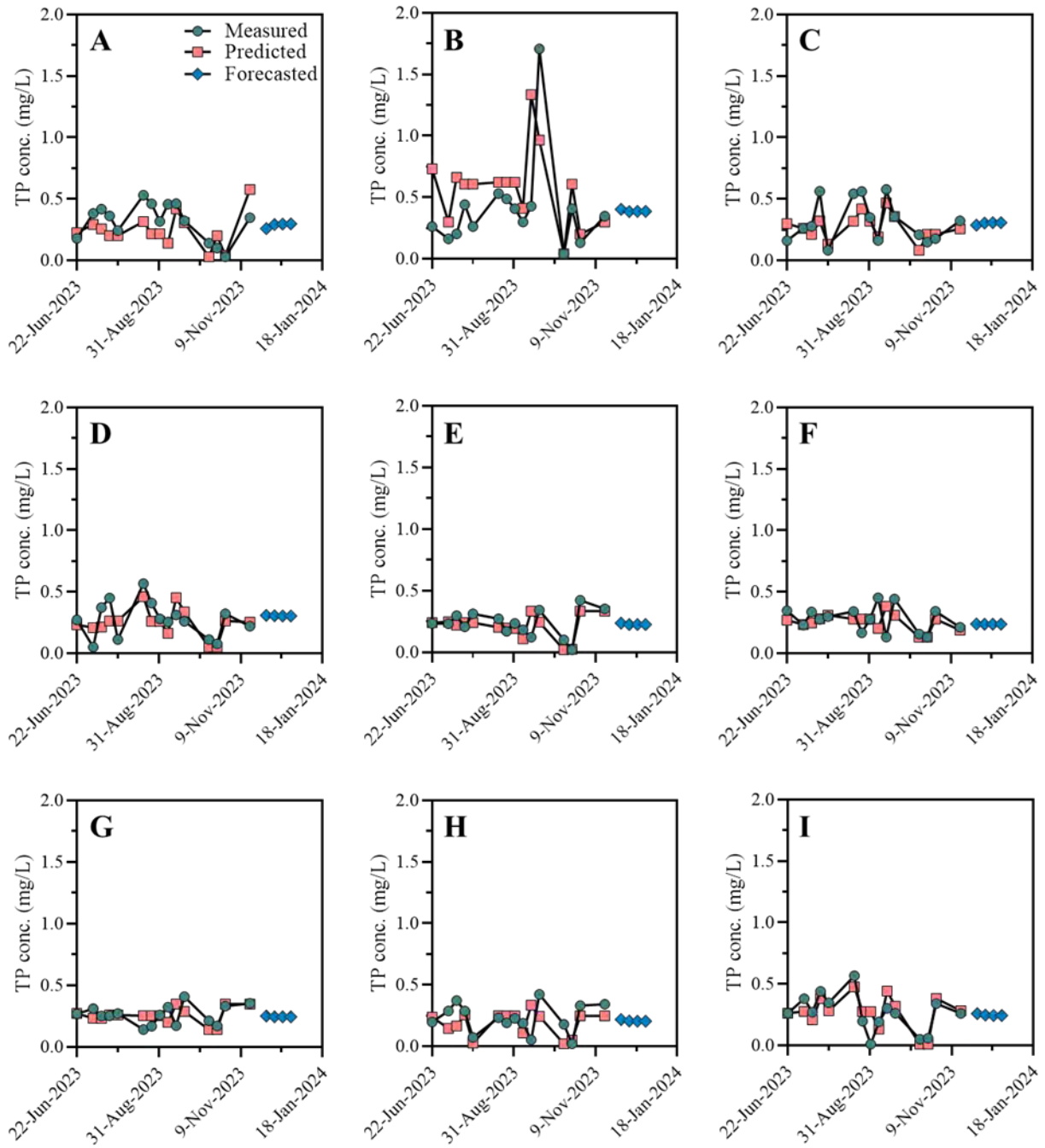
(1)



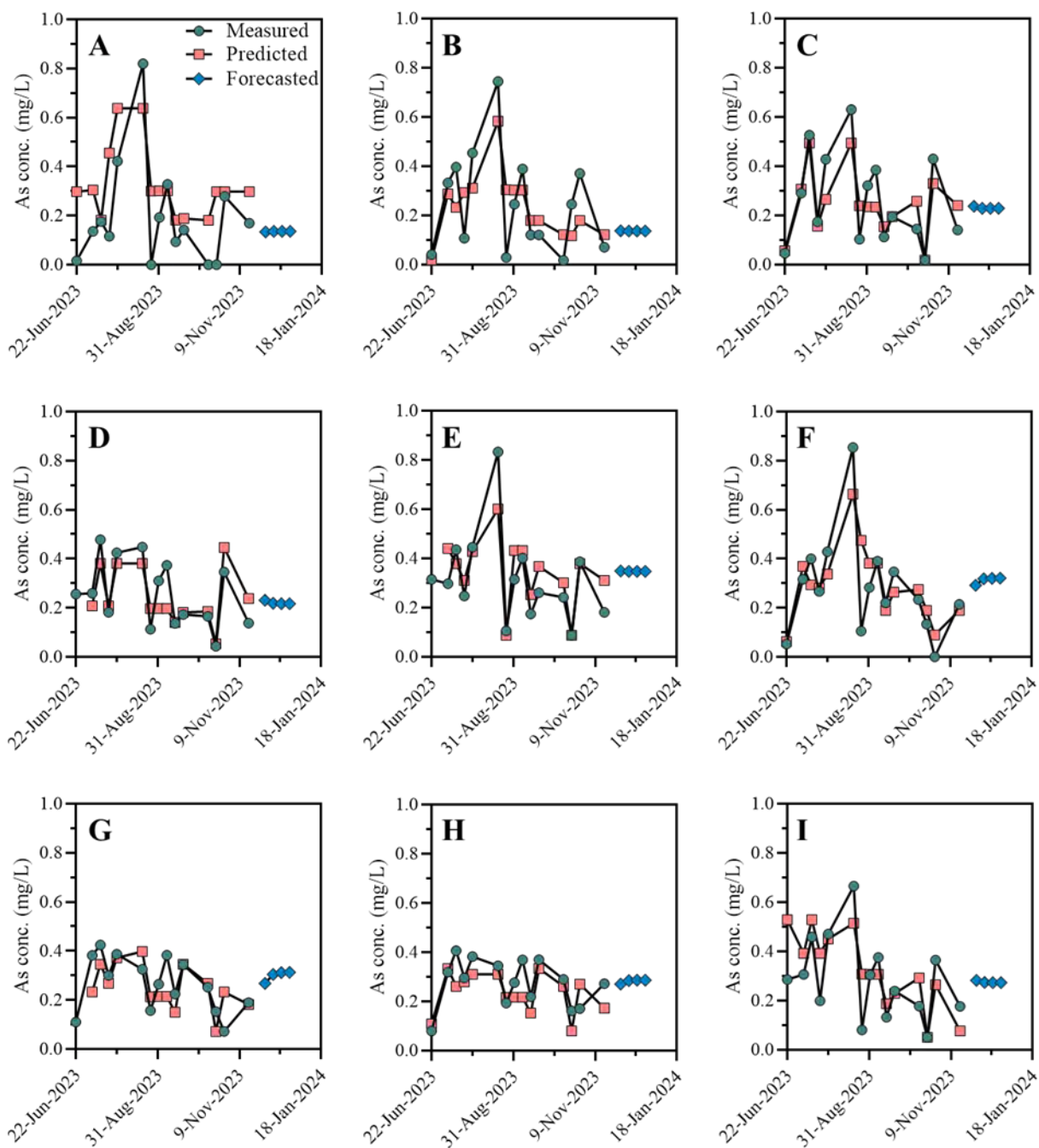
(2)



(3)



(4)



(5)

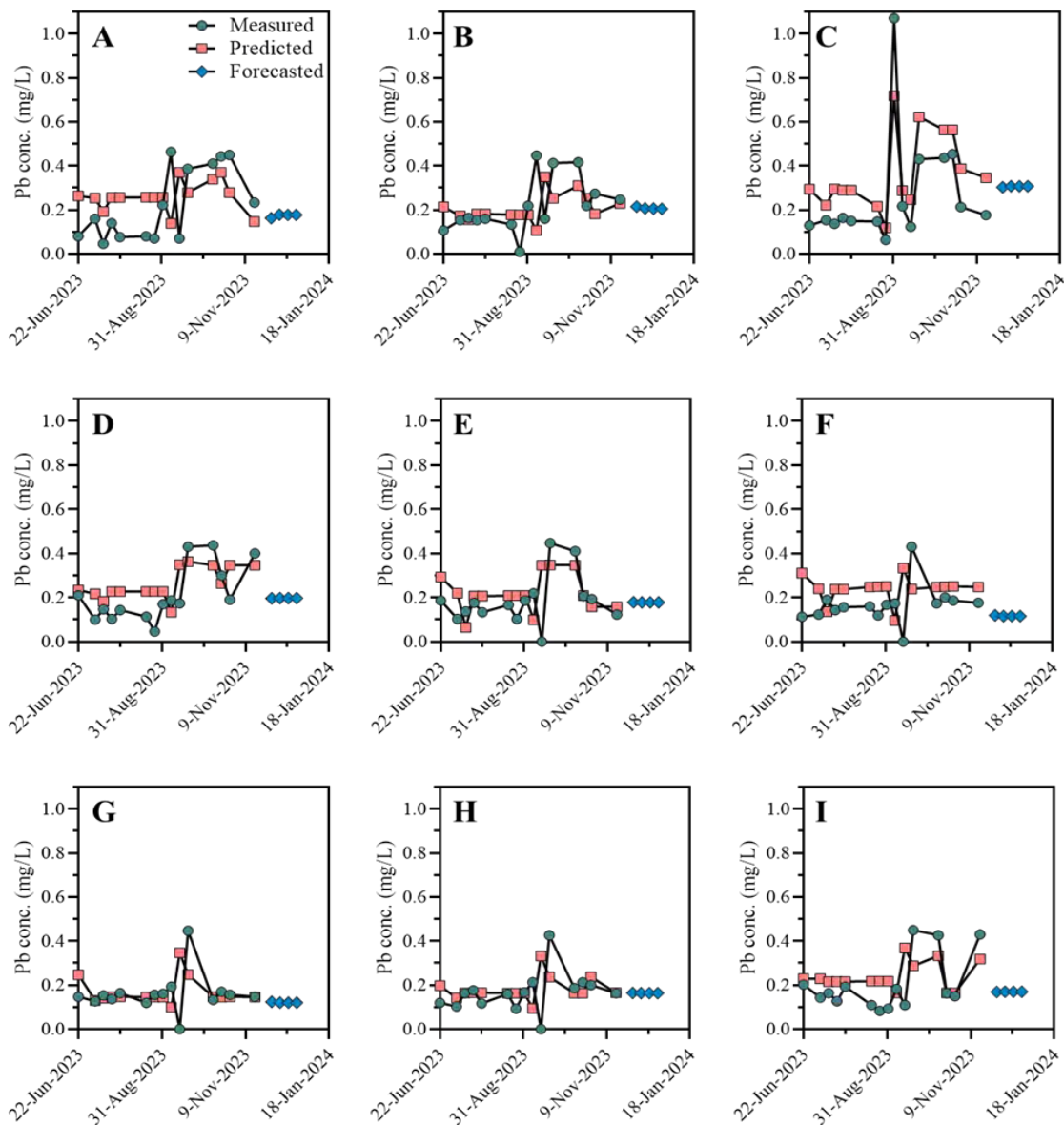
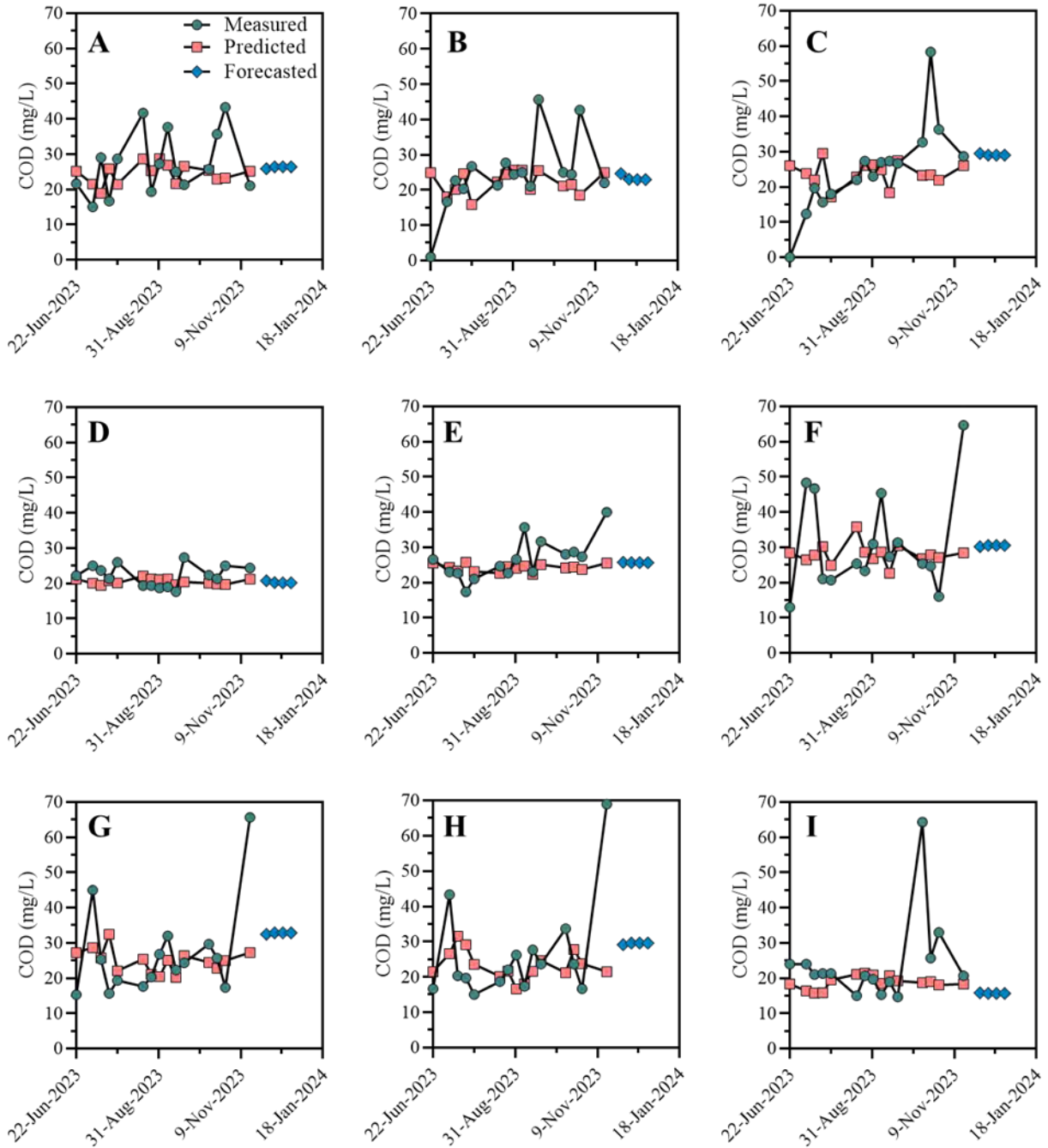
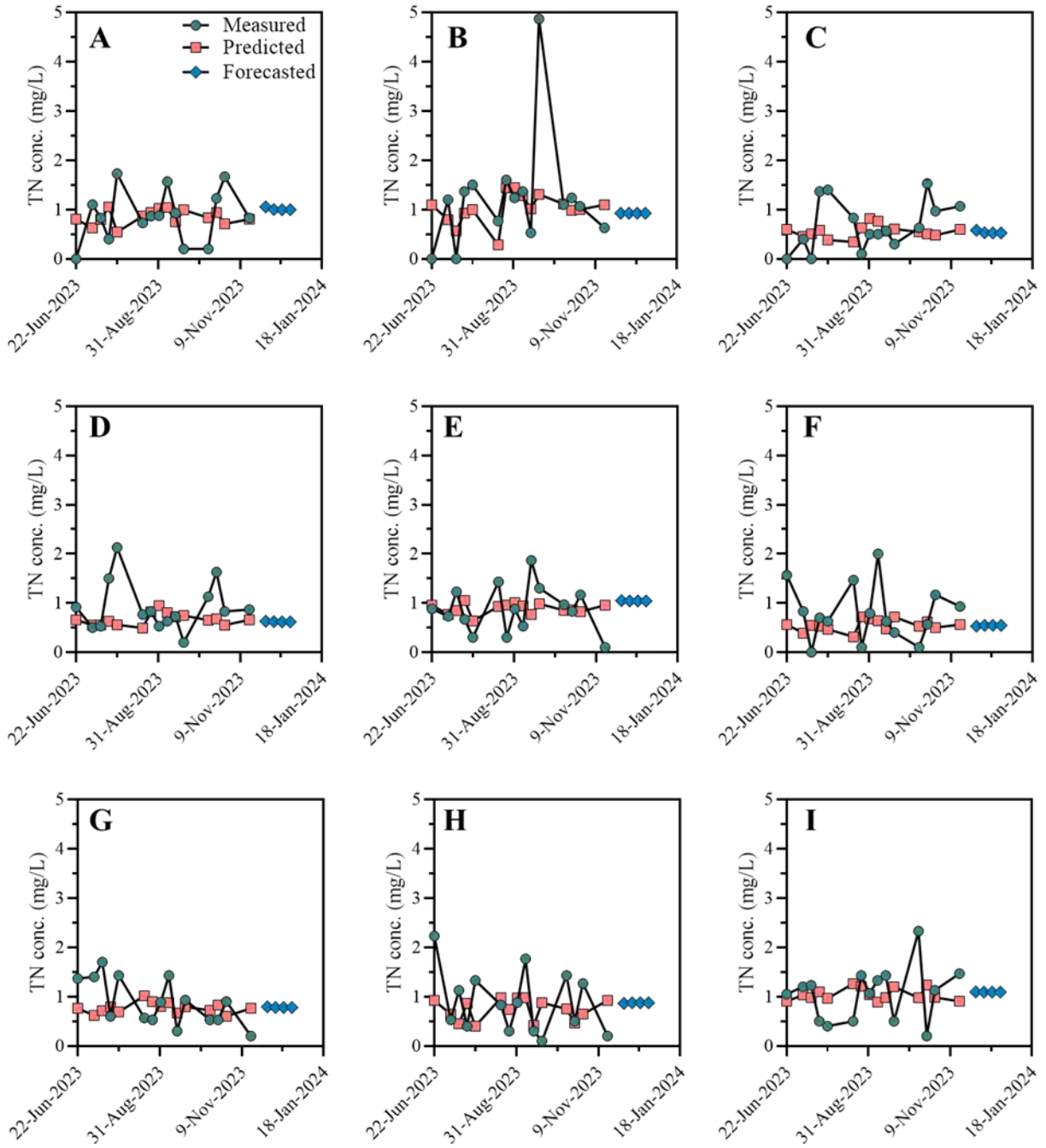


Figure 34. Measured, predicted, and forecasted values for 9 sampling sites using the model, LSTM2: (1) COD, (2) TN, (3) TP, (4) As and (5) Pb. Subfigures A–I represent the sampling sites of ND1, ND2, ND3, ND4, ND5, D1, D2, D3 and D4, respectively. Green circles show the measured values, orange boxes represent the predicted values using model LSTM2, while the blue diamond shape symbols represent the predicted values using model LSTM2 as stated in the subfigure (A) of each (1)–(5).

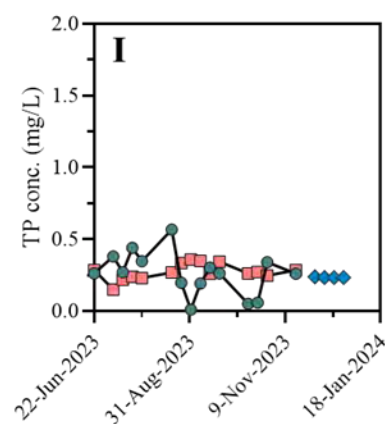
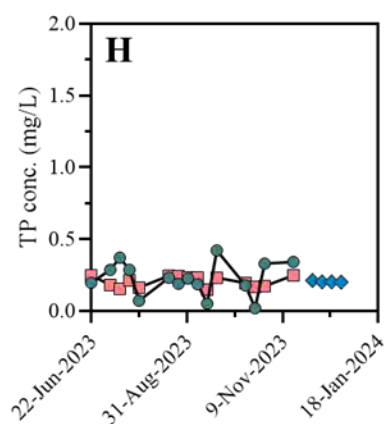
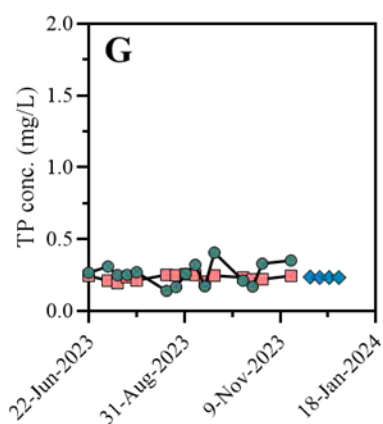
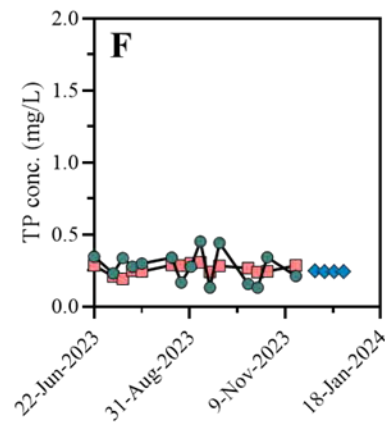
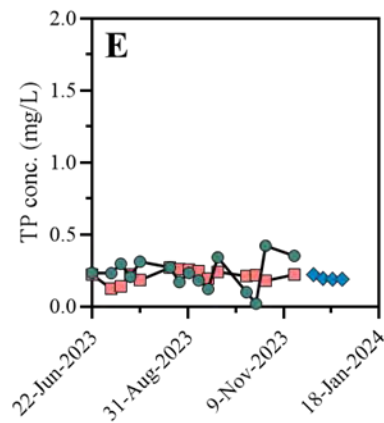
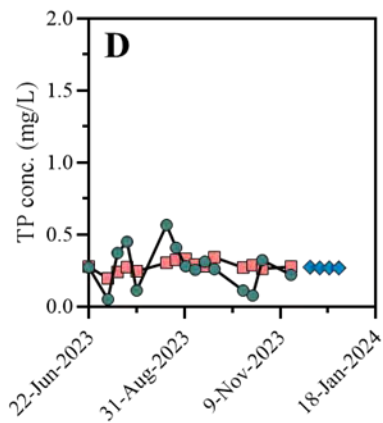
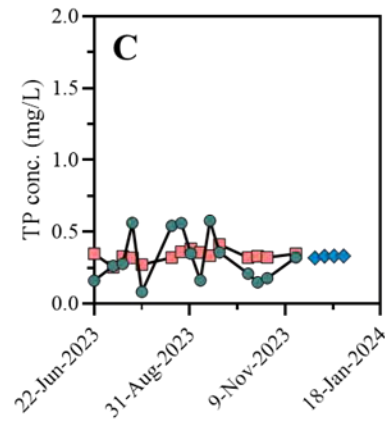
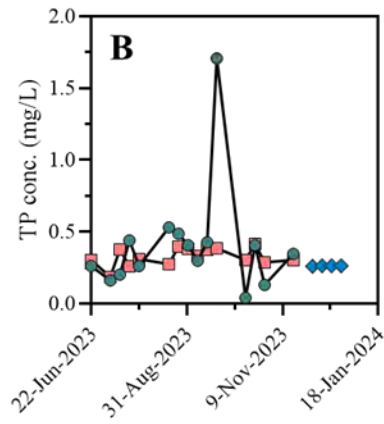
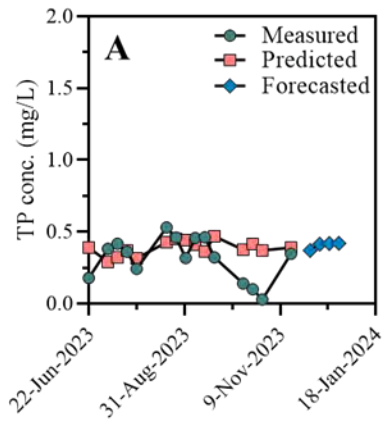
(1)



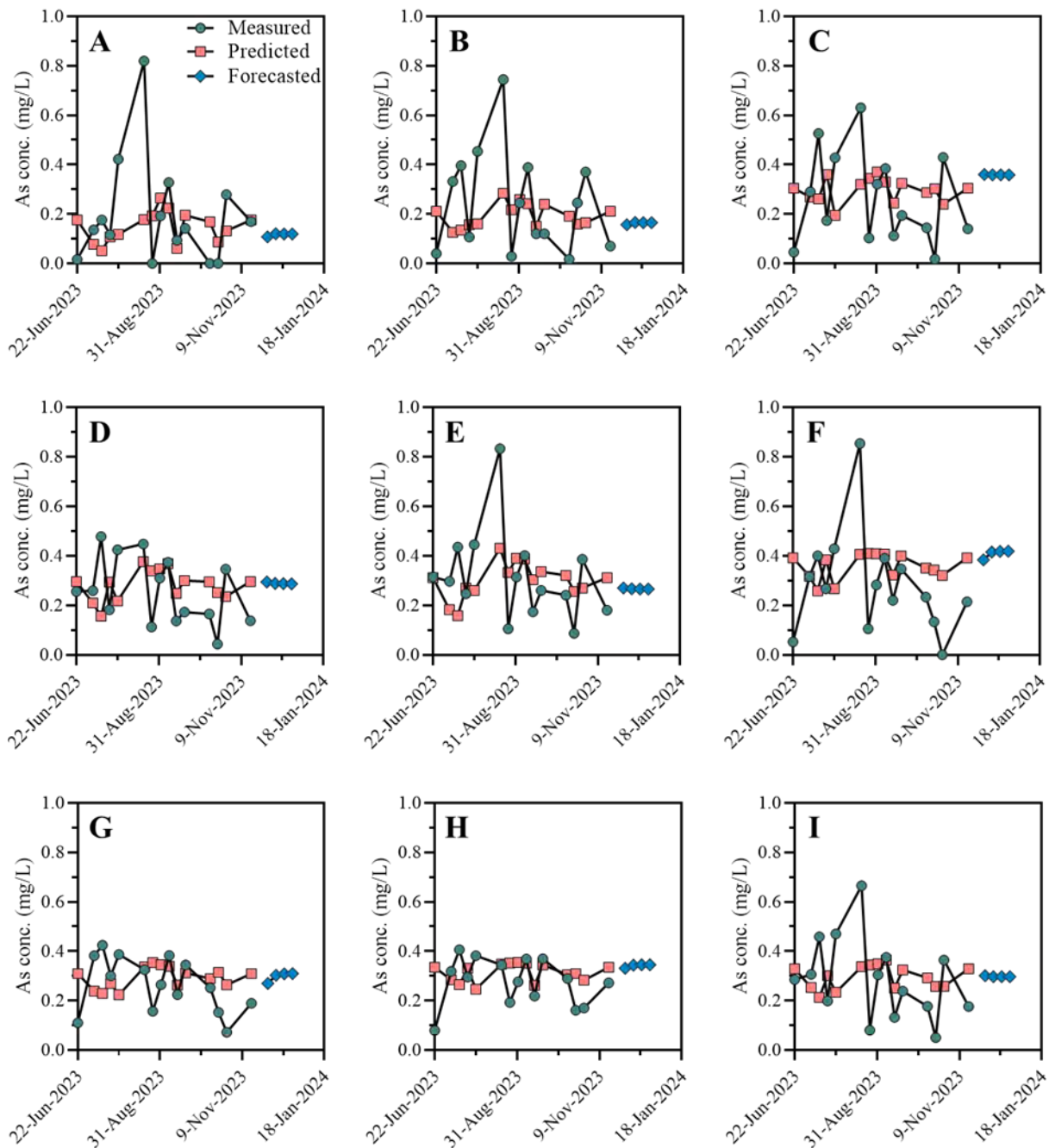
(2)



(3)



(4)



(5)

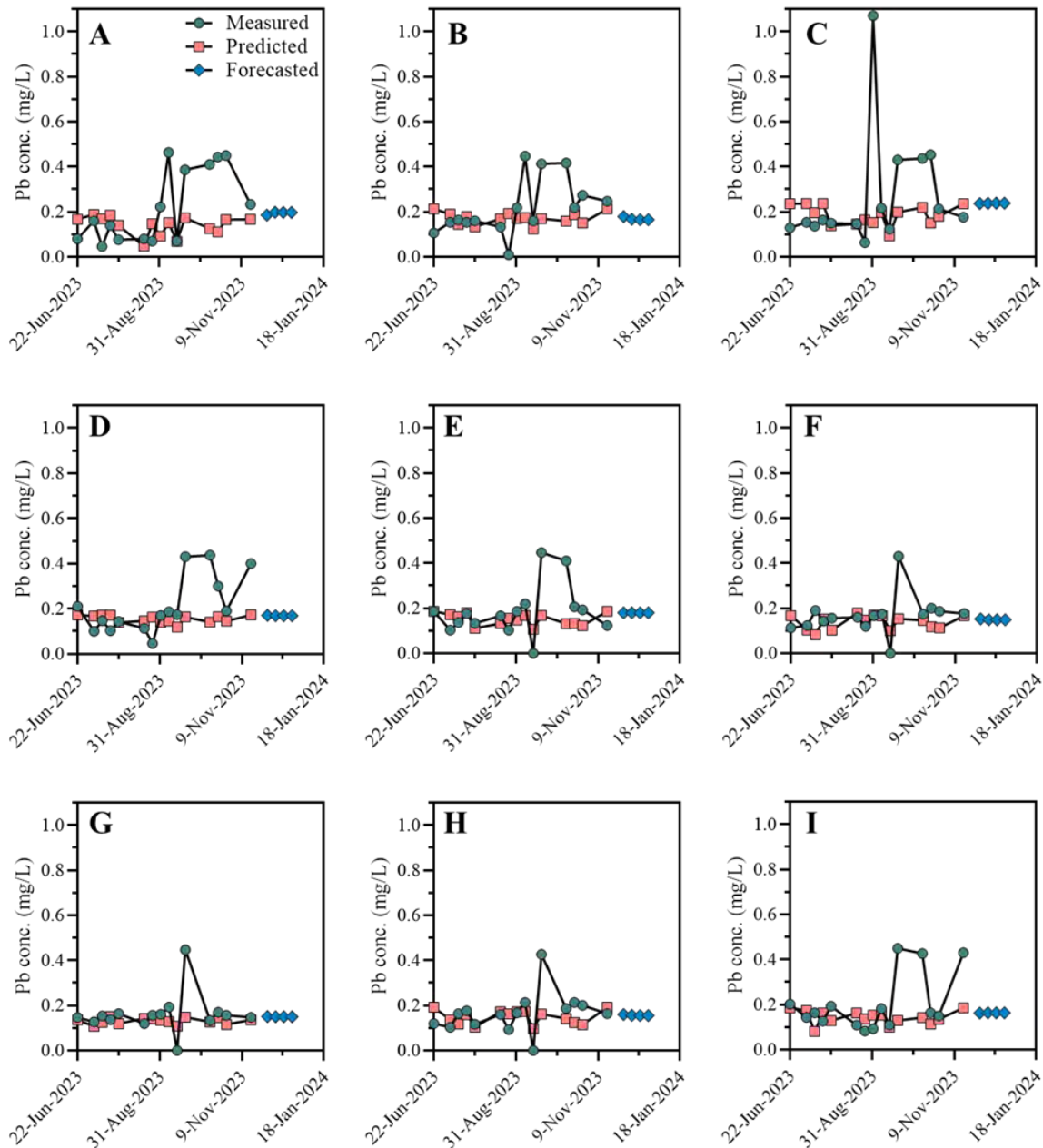


Figure 35. Measured, predicted and forecasted values for 9 sampling sites using the model, LSTM3: (1) COD, (2) TN, (3) TP, (4) As and (5) Pb. Subfigures A–I represent the sampling sites of ND1, ND2, ND3, ND4, ND5, D1, D2, D3 and D4, respectively. Green circles show the measured values, orange boxes represent the predicted values using model LSTM3, while the blue diamond shape symbols represent the predicted values using model LSTM3 as stated in the subfigure (A) of each (1)–(5).

Table 7. Evaluating the differences between September–October measurements and forecasted levels in December for water quality parameters using ANOVA.

Parameter	Model	F and p-Values	ND1	ND2	ND3	ND4	ND5	D1	D2	D3	D4	
COD	Forest-based	F value	0.2005	2.8752	61.8143	0.4363	0.2932	1.4208	0.3859	0.4923	16.7613	
		Pr(>F)	0.6775	0.1886	0.0043	0.5450	0.6169	0.2992	0.5681	0.5213	0.0264	
	LSTM 1	F value	0.6393	0.4677	0.3155	3.9862	2.6958	0.3473	0.3920	1.5783	0.9475	
		Pr(>F)	0.4301	0.4991	0.5783	0.0547	0.1107	0.5599	0.5358	0.2184	0.3379	
	LSTM 2	F value	0.5434	0.5831	0.0489	0.0127	0.0646	2.3692	2.8606	1.5204	0.0099	
		Pr(>F)	0.4671	0.4515	0.8266	0.9110	0.8013	0.1349	0.1019	0.2278	0.9213	
	LSTM 3	F value	1.2683	0.6405	0.0001	5.6714	0.5113	0.0047	0.2345	4.3179	2.3387	
		Pr(>F)	0.2685	0.4294	0.9932	0.0234	0.4798	0.9456	0.6315	0.0458	0.1360	
	TN	Forest-based	F value	0.1011	0.1282	0.5759	8.4744	0.1895	0.0047	5.8859	0.7097	23.3348
			Pr(>F)	0.7714	0.7440	0.5031	0.1005	0.6928	0.9514	0.0937	0.4614	0.0403
LSTM 1		F value	0.3706	0.5218	0.0191	1.4282	0.2613	2.1600	0.9700	0.2058	2.2248	
		Pr(>F)	0.5471	0.4755	0.8909	0.2411	0.6128	0.1517	0.3323	0.6532	0.1459	
LSTM 2		F value	0.4764	3.6569	0.3429	0.1239	0.21661	0.0228	1.1150	0.7148	0.0163	
		Pr(>F)	0.4958	0.0661	0.5628	0.7275	0.6452	0.7103	0.3000	0.4050	0.8994	
LSTM 3		F value	0.0023	0.7467	1.0664	4.7402	3.3711	1.0762	0.5759	0.0007	0.1553	
		Pr(>F)	0.9622	0.3939	0.3095	0.0369	0.0757	0.3073	0.4535	0.9793	0.6962	
TP		Forest-based	F value	0.0000	0.2569	0.4794	0.4472	0.2624	0.2287	0.7738	0.8618	0.4584
			Pr(>F)	0.9977	0.6471	0.5385	0.5515	0.6438	0.6652	0.1473	0.4217	0.5682
	LSTM 1	F value	0.3075	0.1713	0.0699	0.7581	0.4134	0.4632	1.0043	0.0255	0.5442	
		Pr(>F)	0.5832	0.6818	0.7933	0.3906	0.5249	0.5012	0.3240	0.8741	0.4663	
	LSTM 2	F value	2.0172	1.7078	0.8051	0.2195	0.4961	0.0300	0.9498	0.0108	0.3430	
		Pr(>F)	0.1666	0.2019	0.3772	0.6430	0.4870	0.8637	0.3381	0.9178	0.5628	
	LSTM 3	F value	4.2512	1.1093	0.1575	0.0372	0.5497	1.9807	0.5299	0.0085	0.3723	
		Pr(>F)	0.0474	0.3001	0.6941	0.8483	0.4638	0.1689	0.4719	0.9271	0.8188	
	As	Forest-based	F value	0.7582	0.2916	0.8074	0.0829	0.1939	0.1632	2.7679	2.5531	0.5196
			Pr(>F)	0.4479	0.6433	0.4637	0.8005	0.6824	0.7254	0.1715	0.1853	0.5459
LSTM 1		F value	0.7546	0.8382	0.2249	1.0399	0.0270	0.4962	0.0134	0.0961	0.6305	
		Pr(>F)	0.3917	0.3669	0.6386	0.3157	0.8705	0.4864	0.9085	0.7587	0.4332	
LSTM 2		F value	3.8779	0.0253	0.0946	0.0922	0.0401	0.1346	1.7021	0.3992	0.2219	
		Pr(>F)	0.0589	0.8747	0.7607	0.7637	0.8428	0.7165	0.2026	0.5326	0.6413	
LSTM 3		F value	1.0432	1.4559	1.1519	0.6461	3.2017	1.1805	3.4113	0.0747	0.2046	
		Pr(>F)	0.3147	0.2364	0.2912	0.4274	0.0830	0.2854	0.0740	0.7863	0.6541	
Pb		Forest-based	F value	0.0000	0.0112	0.2753	0.5888	0.0013	0.3611	3.7738	0.7878	1.3885
			Pr(>F)	0.9992	0.9254	0.6361	0.2966	0.9733	0.6089	0.1473	0.4401	0.3236
	LSTM 1	F value	4.4307	0.8902	0.5130	1.3805	0.5709	1.7543	0.5004	2.1109	2.8127	
		Pr(>F)	0.0435	0.3527	0.4792	0.2489	0.4556	0.1950	0.4846	0.1563	0.1036	
	LSTM 2	F value	0.7331	0.0758	1.3789	1.9274	6.8861	0.0842	0.2787	0.9618	0.8095	
		Pr(>F)	0.3991	0.7851	0.2502	0.1759	0.0139	0.7738	0.6017	0.3351	0.3759	
	LSTM 3	F value	3.2917	2.6514	1.5849	3.3234	1.6302	1.4932	0.6018	3.3923	1.1976	
		Pr(>F)	0.0790	0.1133	0.2172	0.0777	0.2109	0.2306	0.4436	0.0748	0.2819	

Project 5: Quantitative Analysis of Contaminants in Lake Maurepas and Source Identification Using BSMRM

Chemical oxygen demand and other nutrients distribution in Lake Maurepas. The study on Lake Maurepas from June to November 2023 examined the variations in pH, temperature, COD, and nutrient levels, including TP, TN, and NH₃-N across various sampling sites for over 45% of samples concerning TN, TP, NH₃-N, and COD. Significant temporal variations in temperature and pH were observed ($p < 0.05$), although no significant differences were noted across locations. The pH levels were mostly alkaline, fluctuating between 6.6 and 9.7, with an average pH range of 7.22 to 7.6, which was higher compared to some Louisiana streams but remained within the WHO guidelines (6.5-8.5). Temperature showed a gradual decrease over the sampling months, peaking in August at $31 \pm 1.48^{\circ}\text{C}$ and dropping to 18.7°C in November.

The observed pH values ranged from slightly acidic to alkaline, with average values (7.22 to 7.6) higher than those reported in other Louisiana streams (Hill et al., 2005). This alkaline nature can be attributed to the presence of alkaline minerals and ions in the water, consistent with findings from Chandrasekhar et al. (2023), and remains within WHO recommended limits (WHO, 2017). In terms of temperature, the lake demonstrated notable fluctuations, with surface temperatures peaking in August, which may influence biological activity and contaminant dynamics. Furthermore, significant increases in COD concentrations were recorded as sampling progressed, particularly reaching a peak of 85 mg/L in November (**Figure 36**). This accumulation can be attributed to organic content from various sources, including surface runoff and degradation of biological material. The increasing levels of COD at the surface layer contrast with the findings of Stahl (1979), which suggested decreases in dissolved oxygen levels at greater depths. This discrepancy may be explained by the dynamic nature of Lake Maurepas, which allows for vertical mixing due to inflows from multiple rivers.

Nutrient levels showed notable findings as well, with TP exhibiting significant vertical differences for approximately 76.22% of samples, showing higher concentrations at the surface except at two sites, indicating potential external inputs from agriculture and industrial sources (**Figure 37**). Furthermore, TN measurements indicated relevance with 92.43% significance across depths, revealing higher surface concentrations in some sites while remaining within the recommended limits for aquatic ecosystems (**Figure 38**). In terms of NH₃-N, concentrations were less variable than other parameters, with the highest recorded at the surface in June, and values consistently remained below the recommended limits.

The study also reported statistically significant differences in TP concentrations across depths for 76.22% of samples, with elevated levels in surface water linked to anthropogenic influences such as livestock farming and industrial runoff (Zhang et al., 2023). These findings diverge from research by Xue et al. (2023), which noted higher TP levels at the bottom due to anoxic

conditions. Such inconsistencies underline the need for further investigation into the sediment-water interactions and nutrient dynamics in the lake.

Moreover, the high concentrations of TN and NH₃-N, particularly in the surface and middle layers, are indicative of nutrient enrichment driven by river inputs and precipitation runoff, as noted by Dong et al. (2020). The influence of recent rainfall on nutrient transport emphasizes the role of hydrological events in shaping water quality in Lake Maurepas. These results collectively underscore the complex interactions among environmental conditions, human activities, and water quality parameters in a dynamic aquatic system. Continued monitoring and analysis are essential to inform management strategies aimed at mitigating contamination and preserving ecosystem health.

Distribution of heavy metals (HMs) in the lake. The heavy metals (HMs) and other elements in Lake Maurepas indicated significant depth-related differences (**Table 8**). However, variation was lower for several metals such as Pb, Cu, Sr, Ba, and Ni, with significant differences observed in only 22.13% to 10.65% of samples. Initial sampling showed similar Mn profiles across sites, except for D1 and D3. However, profiles diverged in subsequent sampling events, particularly in July and August. Chemical parameters were generally higher in the middle and bottom layers compared to the surface, supporting findings from previous studies. The average concentrations for Pb, Cu, Sr, Ba, and Ni ranged from 0.03 to 0.12 mg/L, with Pb levels exceeding the acute and chronic thresholds for freshwater ecosystems from September to November. Increases in Ni concentrations were noted alongside anthropogenic disturbances and natural factors such as rainfall and runoff.

River input appeared to influence Ba and Sr levels, with maximum detected values occurring at river confluences. Copper concentrations were consistently higher than US EPA recommended levels, while other HMs like Mn, As, Cd, and Zn showed significant depth variations in over 30% of samples. Concentrations of these metals were particularly elevated in the middle and bottom layers. Mn concentrations varied significantly, reaching 1.27 mg/L by September, while As and Cd were notably higher in the summer months at D1 to D4. Although Zn levels remained within regulatory guidelines, K concentrations were lower and showed minimal statistical significance. The proximity of four sampling sites to the I-55 highway and railway lines raised concerns regarding the introduction of HMs from chemical transport, vehicular emissions, and atmospheric deposition. These sites might serve as both sinks and sources of HMs and organic contaminants, with summer temperatures potentially causing sediment release of HMs. Consequently, the increased concentrations of HMs from June to August could be attributed to such releases near the I-55 bridge locations.

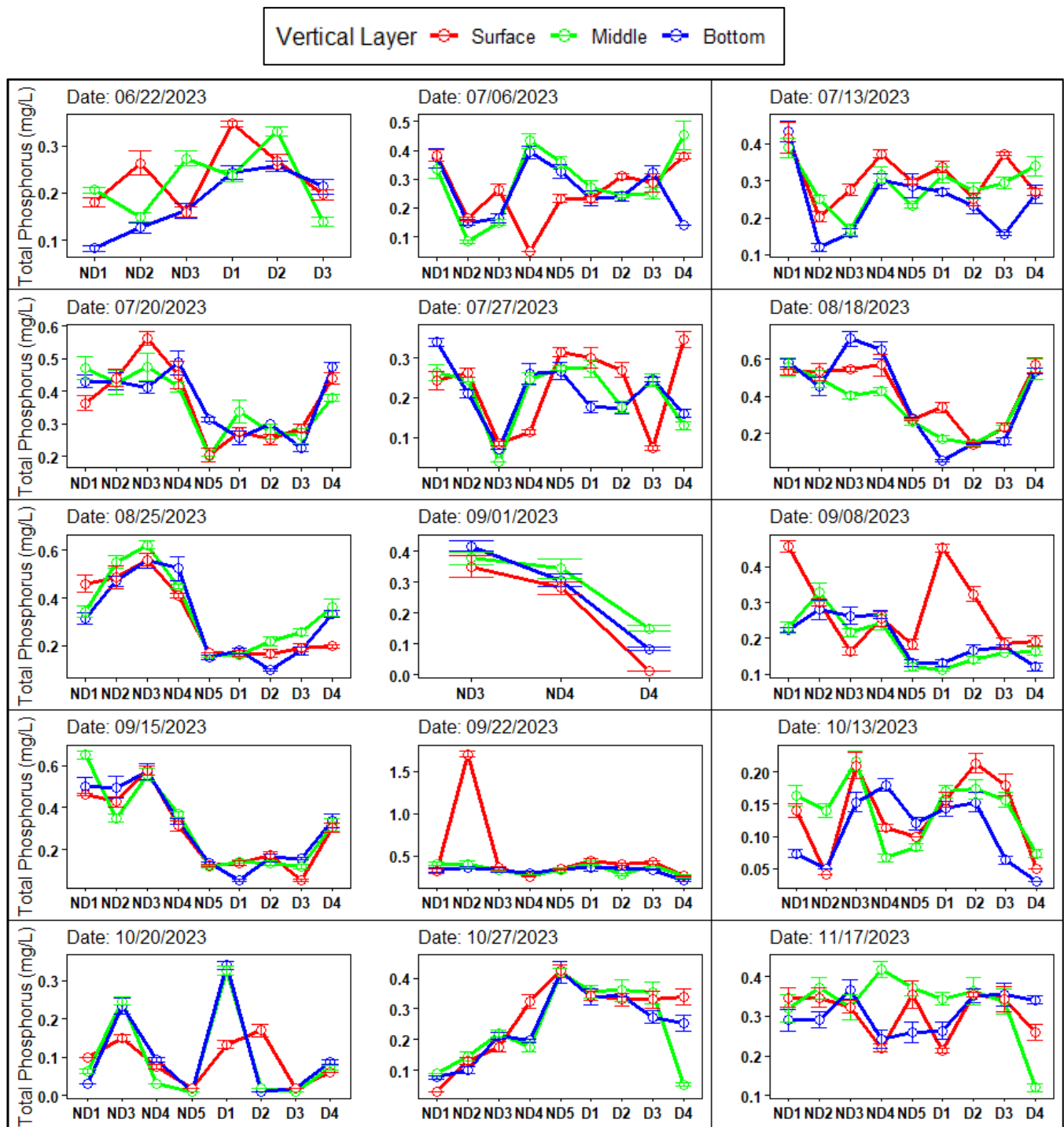


Figure 36. Chemical oxygen demand (COD) at all sampling points. The line plot displays COD measurements in three vertical layers: surface, middle, and bottom. Data comprise samples collected from June to November 2023 at different sampling sites (ND = Non-drilled, D = Drilled). Each data point represents the average of triplicate measurements with standard error indicated.

Vertical Layer ○ Surface ○ Middle ○ Bottom

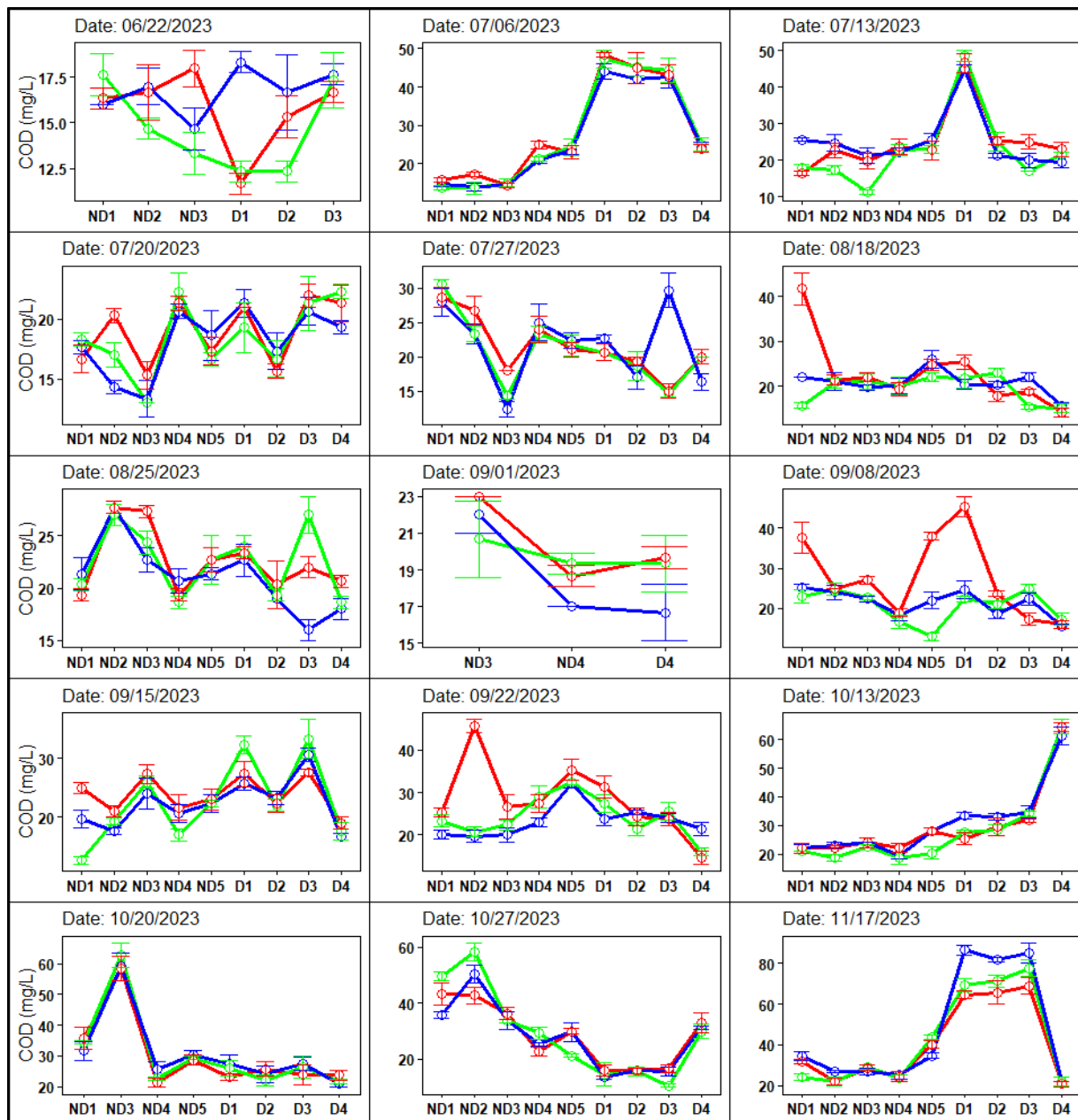


Figure 37. Total phosphorus (TP) in Lake Maurepas and their distribution. The line plot shows TP measurements in three vertical layers: surface, middle, and bottom. Data comprise samples collected from June to November 2023 at different sampling sites (ND = Non-drilled, D = Drilled). Each data point represents the average of triplicate measurements of TP with standard error indicated.

Vertical Layer ○ Surface ○ Middle ○ Bottom

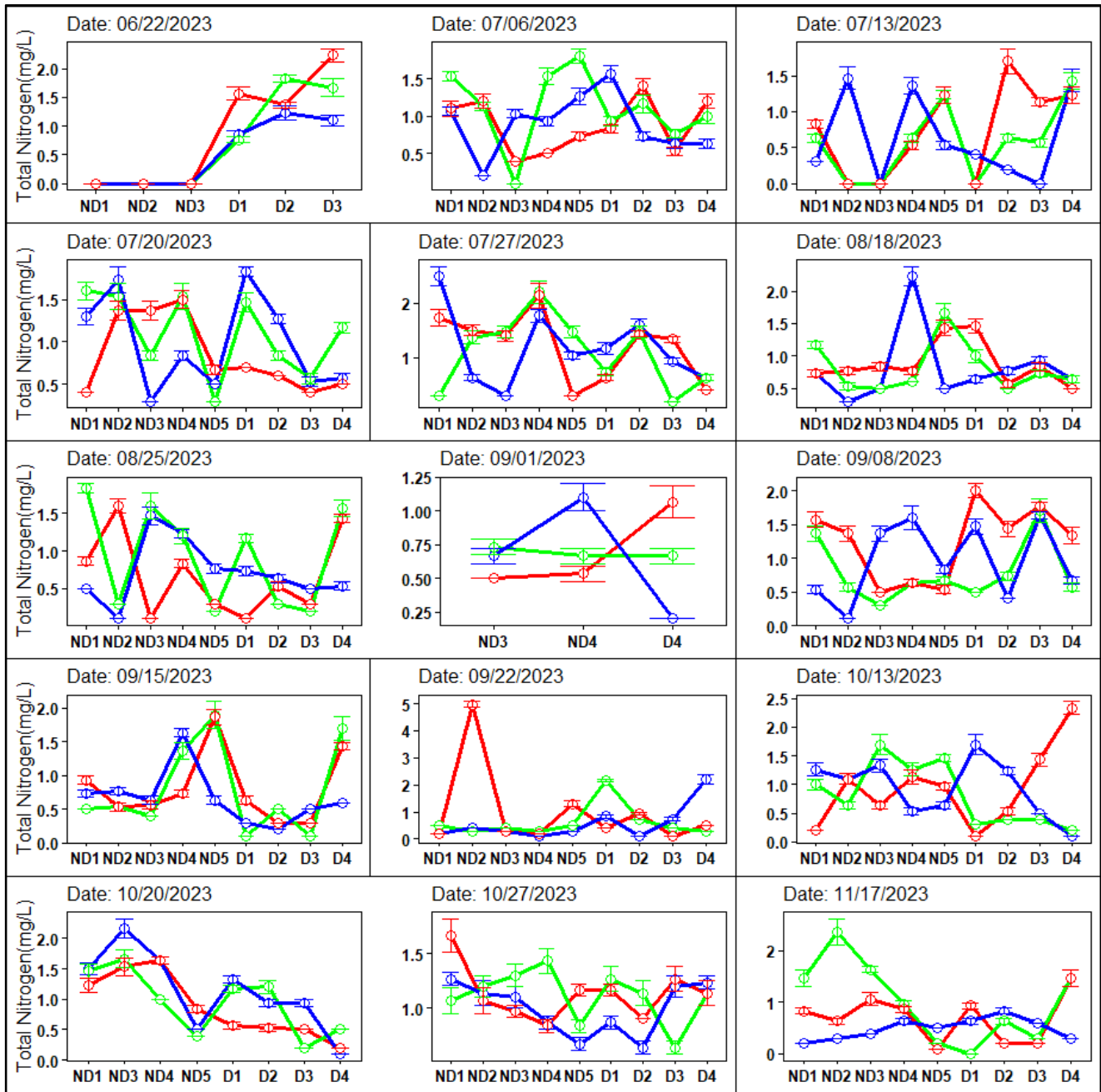


Figure 38. Total Nitrogen (TN) in Lake Maurepas and their distribution. The line plot shows TN measurements in three vertical layers: surface, middle, and bottom. Data comprise samples collected from June to November 2023 at different sampling sites (ND = Non-drilled, D = Drilled). Each data point represents the average of triplicate measurements of TP with standard error indicated.

Table 8. Elemental concentration averages in different sampling sites in Lake Maurepas during June-November, 2023.

SS	VLS	Mn	As	Cd	Zn	Pb	Cu	Sr	Ba	Ni
ND1	S	0.09 ± 0.03	0.18±0. 23	0.24 ± 0.27	0.09 ± 0.05	0.11 ± 0.04	0.05 ± 0.01	0.07 ± 0.02	0.09 ± 0.02	0.11 ± 0.07
	M	0.09 ± 0.03	0.17 ± 0.2	0.21 ± 0.26	0.07 ± 0.06	0.11 ± 0.03	0.05 ± 0.01	0.07 ± 0.02	0.09 ± 0.02	0.09 ± 0.07
	B	0.09 ± 0.01	0.2 ± 0.21	0.25 ± 0.29	0.1 ± 0.06	0.11 ± 0.03	0.05 ± 0.01	0.08 ± 0.02	0.09 ± 0.01	0.09 ± 0.07
ND2	S	0.09 ± 0.01	0.24 ± 0.22	0.27 ± 0.3	0.1 ± 0.06	0.11 ± 0.03	0.05 ± 0.01	0.08 ± 0.02	0.09 ± 0.03	0.07 ± 0.06
	M	0.09 ± 0.01	0.24 ± 0.2	0.27 ± 0.3	0.08 ± 0.07	0.1 ± 0.02	0.05 ± 0	0.07 ± 0.02	0.09 ± 0.02	0.06 ± 0.06
	B	0.09 ± 0	0.24 ± 0.15	0.23 ± 0.24	0.07 ± 0.06	0.1 ± 0.03	0.05 ± 0	0.08 ± 0.02	0.09 ± 0.02	0.06 ± 0.06
ND3	S	0.09 ± 0.02	0.26 ± 0.19	0.21 ± 0.22	0.09 ± 0.07	0.12 ± 0.06	0.05 ± 0	0.07 ± 0.01	0.09 ± 0.02	0.07 ± 0.07
	M	0.12 ± 0.14	0.26 ± 0.2	0.22 ± 0.24	0.06 ± 0.05	0.11 ± 0.04	0.05 ± 0	0.07 ± 0.02	0.09 ± 0.01	0.07 ± 0.06
	B	0.09 ± 0.02	0.25 ± 0.18	0.21 ± 0.24	0.06 ± 0.05	0.11 ± 0.03	0.05 ± 0	0.07 ± 0.01	0.08 ± 0.01	0.07 ± 0.07
ND4	S	0.11 ± 0.08	0.26 ± 0.14	0.15 ± 0.17	0.1 ± 0.06	0.11 ± 0.03	0.05 ± 0	0.07 ± 0.01	0.08 ± 0	0.08 ± 0.06
	M	0.1 ± 0.02	0.29 ± 0.18	0.25 ± 0.27	0.11 ± 0.06	0.11 ± 0.03	0.05 ± 0	0.07 ± 0.01	0.08 ± 0	0.07 ± 0.07
	B	0.09 ± 0.01	0.29 ± 0.19	0.17 ± 0.22	0.1 ± 0.05	0.11 ± 0.03	0.05 ± 0	0.07 ± 0.01	0.08 ± 0	0.07 ± 0.07
ND5	S	0.21 ± 0.31	0.29 ± 0.17	0.23 ± 0.26	0.08 ± 0.05	0.1 ± 0.03	0.05 ± 0	0.07 ± 0.02	0.08 ± 0.01	0.07 ± 0.06
	M	0.11 ± 0.06	0.29 ± 0.14	0.22 ± 0.25	0.08 ± 0.05	0.11 ± 0.03	0.05 ± 0	0.07 ± 0.02	0.08 ± 0.01	0.07 ± 0.06
	B	0.16 ± 0.19	0.3 ± 0.16	0.22 ± 0.23	0.06 ± 0.05	0.1 ± 0.02	0.05 ± 0	0.07 ± 0.01	0.08 ± 0	0.06 ± 0.06
D1	S	0.16 ± 0.13	0.28 ± 0.21	0.17 ± 0.22	0.1 ± 0.06	0.1 ± 0.03	0.05 ± 0	0.07 ± 0.01	0.09 ± 0.02	0.05 ± 0.04
	M	0.19 ± 0.21	0.28 ± 0.18	0.13 ± 0.19	0.1 ± 0.05	0.1 ± 0.03	0.05 ± 0	0.07 ± 0.01	0.08 ± 0	0.03 ± 0.08
	B	0.15 ± 0.12	0.29 ± 0.15	0.15 ± 0.18	0.08 ± 0.05	0.1 ± 0.03	0.05 ± 0	0.07 ± 0.01	0.08 ± 0	0.03 ± 0.08
D2	S	0.14 ± 0.09	0.26 ± 0.11	0.15 ± 0.19	0.06 ± 0.04	0.09 ± 0.03	0.05 ± 0	0.08 ± 0.04	0.08 ± 0.01	0.03 ± 0.09
	M	0.13 ± 0.08	0.28 ± 0.11	0.15 ± 0.18	0.06 ± 0.04	0.09 ± 0.03	0.05 ± 0	0.07 ± 0.02	0.08 ± 0	0.03 ± 0.08

Source identification using BSMRM. In study, source identification of contaminants in Lake Maurepas was conducted using a Bayesian Statistical Model for the Runoff Matrix (BSMRM). The analysis, which is the first of its kind for the lake, utilized seven models based on the prespecified zero values for certain heavy metals (HMs) and contaminants assumed to be absent from various sources (Park et al., 2021).. Model 5, chosen for its highest marginal likelihood, apportioned the data into six primary sources of contamination: Transportation-Recreational-Accidental Release (TRAR), Death and Decay of Biological Species (DDBS), and three river inputs (RI-1, RI-2, and RI-3), along with Geological Release (GR) (Figure 39). Each source contributed significantly to various contaminants, with river inputs notably delivering high levels TP, TN, and heavy metals such as Cu and As. The dominance of anthropogenic contributions from the rivers underscores the impact of human activity in the surrounding watersheds, consistent with findings from Keddy et al. (2007a), which highlight the accumulation of anthropogenic chemicals transported via river discharges. At the sampling site connected to the Tickfaw River (ND1), for instance, RI-3 was responsible for a considerable proportion of Ba and Cu, while GR accounted for a significant percentage of Cd and Ni. This pattern reflects the geochemical weathering of local geological formations and human interventions that transport metals into the lake system (Chen et al., 2004). Notably, the detection of high Hg levels associated with the DDBS reveals potential bioaccumulation risks, particularly in aquatic organisms, which can have cascading effects on the food web.

The analysis also indicates that dissolved oxygen dynamics and organic matter decomposition from DDBS notably contribute to COD levels, which affect overall water quality. Human-induced factors, such as industrial activity, traffic emissions, and agricultural runoff, further exacerbate these conditions, emphasizing the interconnectedness of nutrient input and contamination dynamics observed in similar studies (Su et al., 2024; Baldwin et al., 2016). Moreover, the significant contributions of nitrogen and phosphorus from various sources indicate increased nutrient enrichment in the lake, which could lead to potential eutrophication. The rising trends in contaminant concentrations, particularly in river inputs, underline the importance of continual monitoring and management to mitigate the ecological and health risks posed by nutrient runoff and heavy metal pollution. The findings confirm previous research by Bhattarai (2000), which reported multiple contaminations in the Pontchartrain basin, highlighting the need for comprehensive strategies to address both point and nonpoint source pollution in aquatic ecosystems.

The analysis indicated significant contributions of contaminants from river inputs at the confluence of the Tickfaw, Amite, and Blind Rivers. For instance, at site ND1, RI-3 accounted for the majority of barium (64.58%) and copper (91.35%) contamination, whereas GR was responsible for significant levels of cadmium (82.9%) and nickel (69.94%). Across other sites,

such as ND2 and ND5, river inputs also played a major role in transporting total TP, zinc, and arsenic (**Figure 40**).

Notably, GR was identified as a critical source of HMs, with high percentages of cadmium and nickel recorded near the I-55 highway and railway lines. The study suggested that anthropogenic activities, including transportation and industrial discharges, have heightened contamination levels. Additionally, the influence of natural factors like sediment release during warmer months significantly contributed to contaminant levels in the lake water, especially for HMs. Regarding the contaminant profile from unmonitored source (STW), GR again emerged as a major contributor. TRAR was linked to elevated levels of COD, nitrogen, and phosphorus, primarily affecting sites D1, D2, D3, and D4.

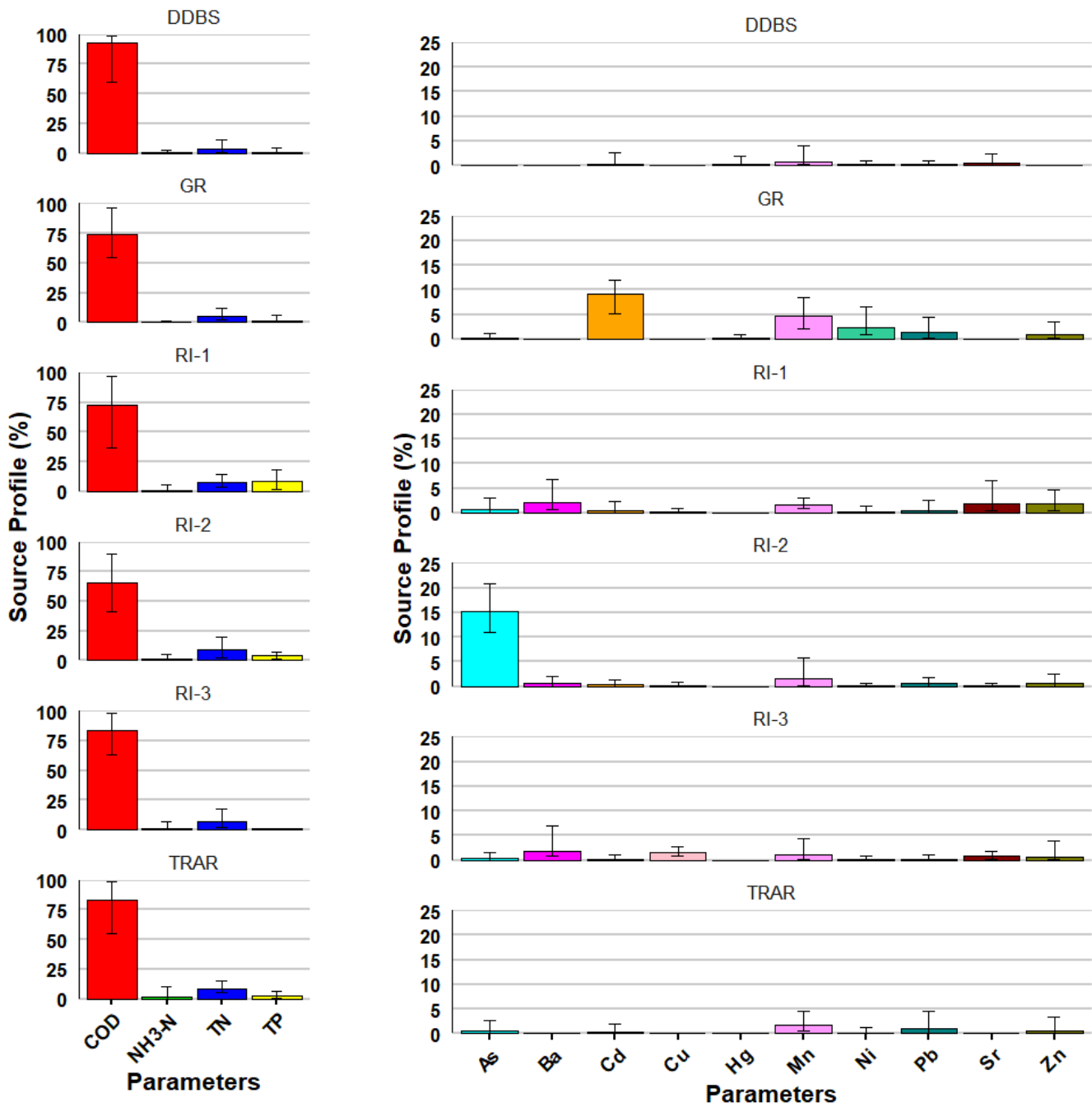
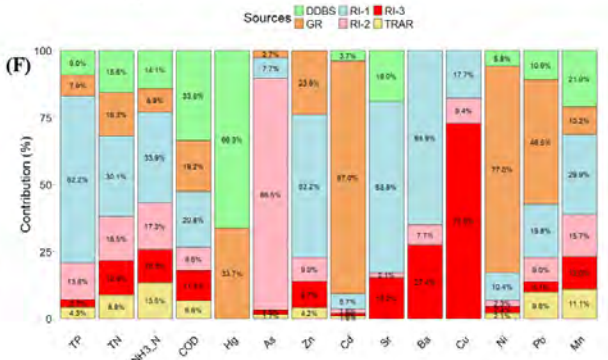
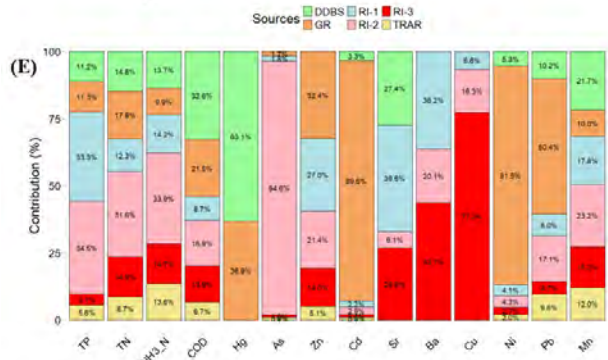
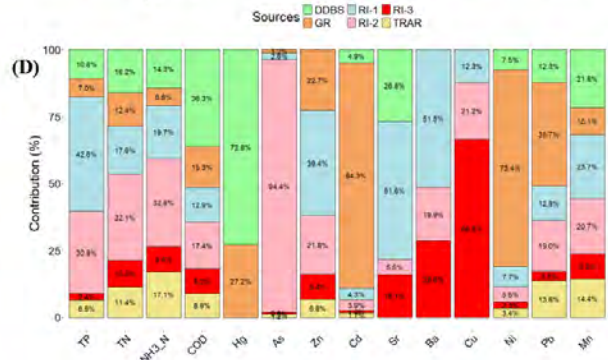
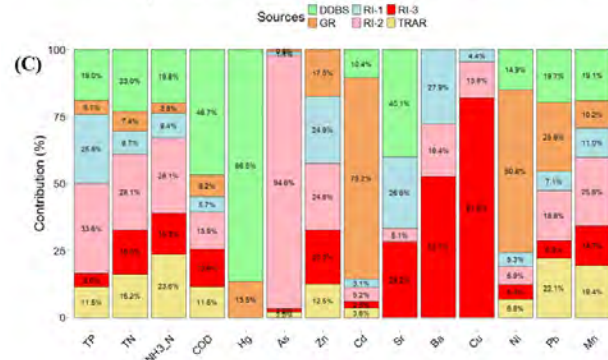
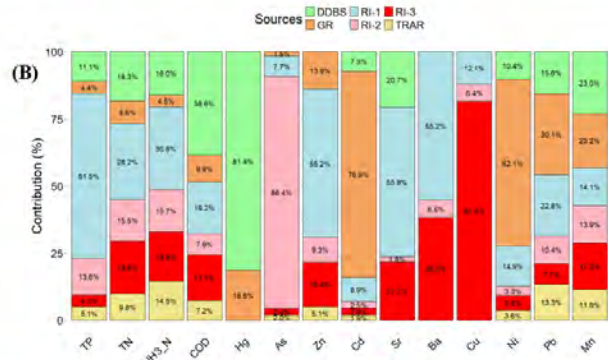
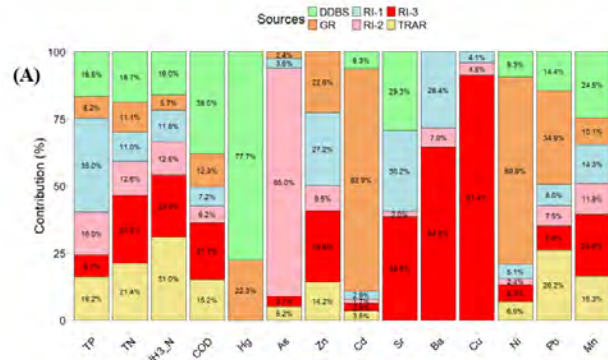


Figure 39. Overall source profile for the monitored and unmonitored sites. The bar plot shows the overall profile of the contaminants from different sources in the monitoring sites (ND1 to D4), and for one unmonitored site; south test well (STW) for June-November, 2023 samples.



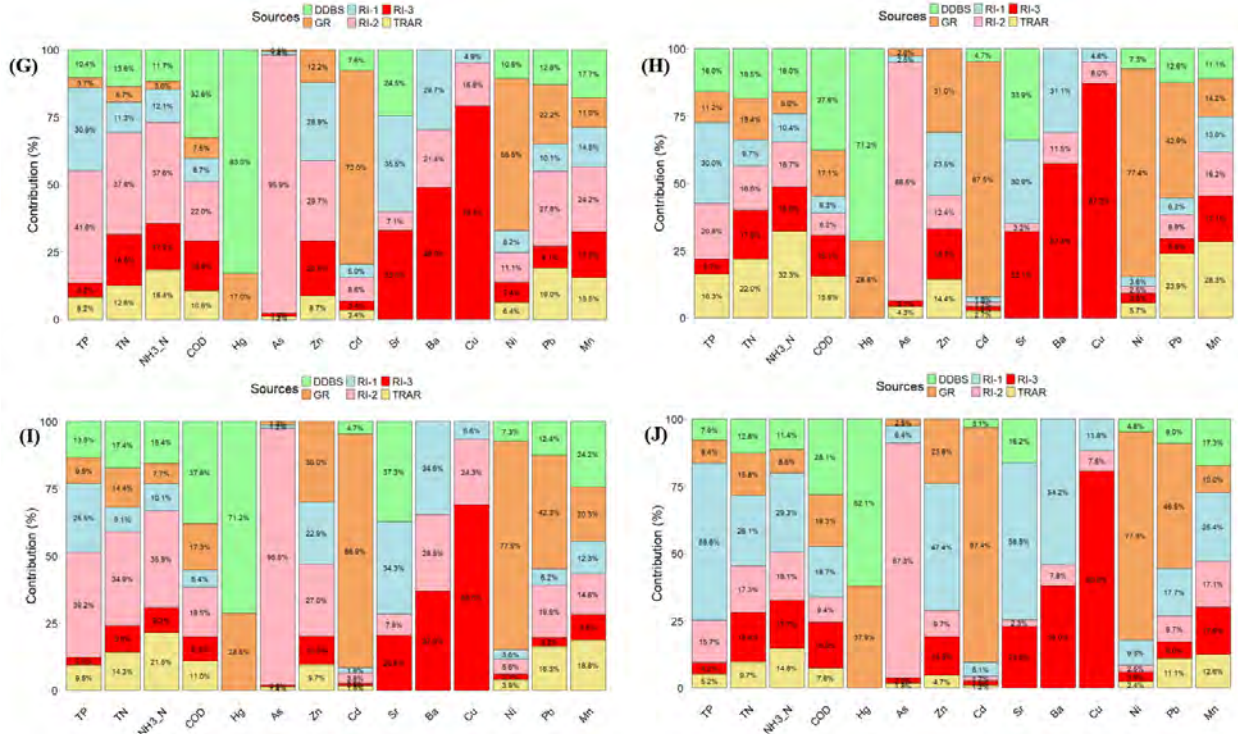


Figure 40. Source contribution for each monitored and one unmonitored sampling site. A to I indicates the monitoring sites, and J is unmonitored site indicated as south test well (STW). **A)** ND1, **B)** ND2, **C)** ND3, **D)** ND4, **E)** ND5, **F)** D1, **G)** D2, **H)** D3, **I)** D4 (ND = Non-drilled, D = Drilled); **J)** STW.

Project 6: Air pollution monitoring and source apportionment in Lake Maurepas airshed

Time series variation. **Figure 41** demonstrates the variation in air pollutants over 15-minute intervals. The dashed red line represents the safe limit declared by the EPA (except for PM4 and PM10). Data is available from January to September 2024 (8 months) and since the project is still ongoing, data for the last quarter is unavailable. In **Figure 41**, PM2.5 and PM10 show a significantly higher trend above the safe threshold. Gases like CO, H₂S, and NO₂ exhibit a similar gradual increase toward the later months. All PM values show a similar upward trend, with a marked increase towards the end of the year. CO₂, however, shows an opposite trend, decreasing toward the later months of the year, while all other gases increase. Moreover, the trend for TVOC in **Figure 41** is unclear and cannot yet be interpreted productively. More data will be needed to provide a clear explanation of its variation (Wong et al., 2004). Most of the gases show a rising trend after April, likely due to the increase in temperature during spring and summer (Elminir, 2005). The overall variation may be caused by several factors, including temperature changes, environmental parameters, and the variation in activities around the lake

that generate these air pollutants (Yu et al., 2015). Therefore, identifying the sources of these pollutants is crucial to explaining the observed variations (Singh et al., 2013).

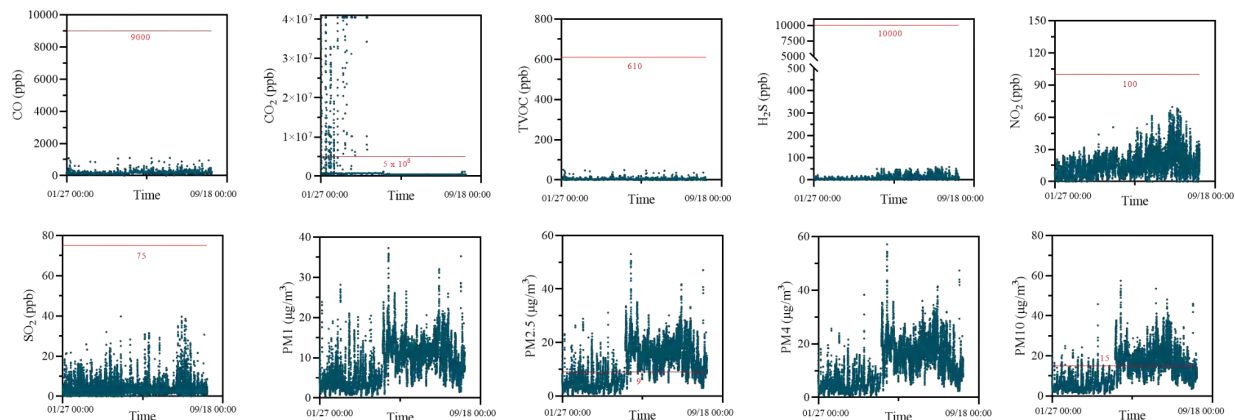


Figure 41. Variation in air pollutants over 15-minute time intervals.

Source apportionment. The source apportionment of air pollutants in Lake Maurepas is currently a work in progress. An initial survey of the literature, combined with considerations of the geolocation characteristics, particularly the nature of nearby industries, has identified several potential source candidates, as outlined below. However, the quantification of contributions and profiles of these potential candidate sources is yet to be completed using the PMF model.

Industrial emissions (oil refineries)

Industrial facilities, including petroleum refineries and chemical plants around Baton Rouge, are significant contributors to pollutants such as SO₂, NO₂, H₂S, and particulate matter. These emissions result from combustion processes and other industrial activities.

Industrial emissions (other)

Chemical plants and other manufacturing facilities are potential sources of pollutants, including SO₂, NO₂, and particulate matter. Other significant pollutants that can be emitted are NO₂, SO₂, PM₁₀, PM_{2.5}, CO, H₂S, and CO₂.

Vehicular traffic emissions

Traffic-related sources, particularly near urban areas and highways, contribute to elevated levels of CO, NO₂, and fine particulate matter. These emissions are primarily associated with gasoline and diesel combustion. Also, this source can generate CO, NO₂, CO₂, PM₁, and PM_{2.5}.

Combustion sources (residential & agricultural)

Biomass burning, residential wood burning, and agricultural fires in surrounding areas can significantly influence particulate matter concentrations, especially during colder months. Potential pollutants are PM₁₀, PM_{2.5}, CO, TVOC

Secondary organic aerosol formation

Organic and inorganic compounds from traffic and industrial sources may undergo chemical transformations in the atmosphere, forming secondary aerosols. Potential pollutants are TVOC, NO₂, PM₁, PM_{2.5}

Biogenic emissions

Natural emissions from vegetation and local wetlands in Louisiana release volatile organic compounds (VOCs), contributing to CO₂ and fine particulates, especially during warmer months. Significant pollutants are CO₂, TVOC, PM₁

Construction and dust resuspension

Urban construction activities and unpaved roads contribute to the release of larger particulate matter, such as PM₄ and PM₁₀, through dust generation and mechanical disruption. Significant pollutants are PM₄, PM₁₀

Discussion/Interpretation

Project 1: Identification of per- and polyfluoroalkyl substances (PFAS) in environmental samples from Lake Maurepas, USA, and their potential health implications

Among the 44 PFAS analyzed (**Table 3**), 25 were detected in either water, sediment, or biological samples collected from Lake Maurepas. Specifically, we detected 13, 12, 12, and 16 PFAS in catfish, blue crab, water, and in sediments respectively (**Table 4; Figure 12**). The undetected PFAS compounds may not be present at measurable levels, may degrade more quickly, or may not accumulate under the lake's environmental conditions. Among the 25 PFAS detected, FOSA-I, PFDA, PFOS (Linear), and PFUnDA were found consistently across all four types of environmental samples. In contrast, PFOA (Linear), PFHxS (Branched), PFHxS (Linear), and PFMPA (PFPeA) were detected only in sediment. Notably, 5:3 FTCA (FPePA), 7:3 FTCA (FHpPA), PFDS, PFTeDA, and PFTrDA were detected only in catfish and blue crab samples, with no detection in water or sediment. **Figure 12** shows the contribution % of each detected PFAS in the environmental samples collected from Lake Maurepas. Both legacy and emerging PFAS were detected in the environmental samples collected from Lake Maurepas. Legacy PFAS, refer to long-chain PFAS compounds that have been widely used in various industrial applications and consumer products since the mid-20th century. These include well-known compounds such as PFOA and PFOS. Legacy PFAS are known for their persistence in the environment and human body, leading to significant concerns about their potential health effects, including developmental, immunological, and endocrine disruption issues. Emerging PFAS, on the other

hand, include shorter-chain alternatives or novel fluorinated compounds that have been developed in response to regulatory pressures to phase out legacy PFAS. Examples of emerging PFAS include compounds like GenX and PFMPA (PF40PeA). While these newer substances were designed to be less harmful and more environmentally friendly, research is ongoing to assess their toxicity, environmental persistence, and bioaccumulation potential. According to the present study, among the 25 detected PFAS in water, sediment, fish, and crab samples, 22 legacy PFAS were identified, while 3 PFAS, including 6:2 FTS, NaDONA, and PFMPA (PF40PeA) could be recognized as emerging PFAS (Brase et al., 2021; Cheng et al., 2023; ITRC, 2023; Manojkumar et al., 2023).

12 PFAS were detected in Lake water including FOSA-1, PFDA, PFOA, PFOS-Linear, PFOS-Branched, PFuDA, NaDONA, PFBA, PFBS, PFHpAPFHxA, and PFPeA. The Σ PFAS detected in water was 70.1 ± 3.96 ng/L. In the present study, the detected PFAS concentrations in Lake water was observed to exceed the reported concentrations in other lakes, particularly the Great Lakes. 16 PFAS were detected in sediments collected from Lake Maurepas. The detected PFAS include 6:2 FTS, FOSA-1, PFDA, PFDoA, PFNA, PFOA-Linear, PFOS-Linear, PFOS-Branched, PFuDA, PFBA, PFBS, PFHpA, PFHxA, PFPeA, PFHxS-Branched, PFHxS-Linear, and PFMPA (PF40PeA). The Σ PFAS detected in sediment was 5.93 ± 0.77 ng/g. Many PFAS detected in sediments have also been previously identified in sediments, particularly from the Great Lakes (Codling et al., 2018; Guo et al., 2016; Li et al., 2024). The concentrations of PFAS in catfish and blue crab tissues shows the extent of contamination in aquatic organisms from Lake Maurepas. In both catfish and blue crab samples, 7:3 FTCA (FHpPA), 6:2 FTS, FOSA-1, PFDA, PFDS, PFNA, PFDoA, PFOA, PFOS-Linear, PFTeDA, PFTrDA, and PFuDA were detected. Additionally 5:3 FTCA (FPePA) was detected only in catfish.

It was interesting to observe that certain PFAS were detected in catfish and blue crab samples, while they were not detected in either the water or sediments. These PFAS included 5:3 FTCA (FPePA), 7:3 FTCA (FHpPA), PFDS, PFTeDA, and PFTrDA. We have identified several possible explanations for this observation. One possible explanation could be related to their habitat and feeding behavior. PFAS are known to bioaccumulate in the tissues of aquatic organisms because of their strong binding capacity (Savoca & Pace, 2021). So, the organisms may accumulate these substances over time through their diet or direct exposure. For example, PFAS may be present in prey organisms (such as smaller fish or invertebrates) that catfish and crabs consume, leading to biomagnification up the food chain. So it is plausible to observe PFAS in the tissues of the organisms without their presence in the water or sediments. It is also possible that these organisms carry PFAS from nearby rivers, including the Blind, Amite, and Tickfaw, which feed into Lake Maurepas. These compounds could then accumulate in their tissues, even when concentrations in the surrounding water or sediment are low. Another possibility could be that the concentrations of these PFAS in water or sediment are below the

detection limits of the analytical methods used, but they are still detectable in the organisms due to differences in the way these substances are distributed within the tissues.

When considering the potential PFAS sources in lakes in literature, atmospheric depositions, contaminated water released by different activities (*i.e.*, wastewater treatment plants), and inputs from tributary rivers were reported as the major sources in lakes from countries like US, Canada and China. It is also important to note that during our preliminary literature search, we observed that many of the PFAS detected in Lake Maurepas have significant potential to cause various diseases and toxicities, including cancers (e.g., breast, liver, kidney, bladder), endocrine disruption, adverse effects on the liver and kidneys, elevated cholesterol levels, and an increased risk of developing diabetes, and more. The potential health impacts of PFAS exposure have been extensively studied, with researchers analyzing both animal models (e.g., rats and mice) and human samples (e.g., blood serum and urine analysis). Epidemiological studies have highlighted significant associations between increased PFAS exposure and various adverse health effects, which are summarized in **Table 5**.

Project 2: Detection and characterization of microplastics in water, sediment and biological samples from Lake Maurepas

MPs' research at Lake Maurepas began in October 2024 and will be conducted monthly. So far, we have finished the examination of the October water sample. The determination of MPs in sediments and biological materials is underway. The concentration of microplastics in the lake's water from several monitoring locations is shown in **Figure 13**. On the other hand, **Figure 14 (a), (b) and (c)** depicts the various colors, shapes, and sizes of microplastics found during the analysis. According to Figure 13, ND1, ND2, and ND3 have the highest MPs concentrations, with 363, 440, and 316 MPs particles per liter, respectively. After these three locations, ND7 showed a comparatively high concentration (233.33). Although other sampling stations showed lower MPs concentrations, they all have concentrations of more than 100 particles per liter. ND1, ND2, and ND3, located near the mouths of Tickfaw, Amite and Blind River respectively, show relatively higher microplastic concentrations compared to other stations. This could indicate significant riverine inputs of microplastics. ND7, situated near the Manchac swamp bridge, also exhibits elevated microplastic levels.

Blue microplastics are the most abundant across all three sampling locations. They consistently make up the largest proportion of total microplastics, with percentages of 50.43%, 61.36%, and 61.00% at ND1, ND2, and ND3, respectively. White microplastics are the second most abundant color. Transparent microplastics are present in smaller but measurable quantities at all locations. Red microplastics are also moderately abundant. Other colors are either absent or negligible across all locations.

Fibers are the most abundant microplastic type across all sampling stations, with fragments as the second most common. Films and foams are the least detected in almost all stations. Fibers dominate in most sampling stations, ranging from approximately 42.86% at ND 6 to 64.81% ND 4. Fragments consistently appear as the second-highest type, ranging from 15.79% (NTW) to 50.53% (ND 3).

The data demonstrates substantial variability in microplastic size distributions across stations. In general, the 100–500 μm size category dominates the microplastic distribution across all samples, consistently representing the largest proportion. The <100 μm size range is the second most prevalent, contributing significantly in some cases but with notable variability. The 500–1000 μm category has moderate representation, typically smaller than the two finer ranges. The largest size category, 1000–5000 μm , consistently makes up the smallest proportion.

Project 3: Mercury in Lake Maurepas and risk assessment of fish and crab consumption

The temporal and spatial variations in Hg levels observed between 2023 and 2024, as well as differences among zones, suggest dynamic Hg contamination patterns in Lake Maurepas. Correlation analysis among Hg concentrations in different sample types—water, sediment, aquatic plants, blue crabs, and catfish—revealed significant interconnections, indicating that Hg levels in water and sediment often influence bioaccumulation in aquatic organisms. Elevated Hg concentrations in sediment, for instance, were associated with higher Hg levels in aquatic plants and benthic organisms like blue crabs, reflecting the key role of sediment as a source of Hg bioavailability. Additionally, Hg in water was linked to Hg in fish tissues, suggesting pathways of exposure through direct water contact or dietary accumulation. Machine learning approaches will be applied to integrate these relationships, enabling risk analysis of Hg exposure by combining environmental parameters, bioaccumulation data, and spatial distributions. These models provided insights into zones and species at higher risk, helping to refine strategies for monitoring and management.

Project 4: Spatial-temporal contaminant spreading analysis in Lake Maurepas in terms of the quality of water and sedimentary mud samples (Gunawardhana et al., 2024)

This study represents the first quantitative and predictive evaluation of physical parameters, contaminants, nutrients, and heavy metals at various sites and depths in Lake Maurepas. By analyzing monthly trends and spatial distributions of these substances throughout the lake, the following key findings were made:

1. The quantitative assessment of water and sediment samples revealed concerning results. With the exception of Hg and $\text{NH}_3\text{-N}$, levels of COD, TN, TP, As, and Pb in the

lake exceeded safety thresholds. Notably, COD concentrations in the lake water exhibited a consistent upward trend during the sampling period.

2. The spatial-temporal analysis demonstrated significant monthly variations in COD, nutrients, and heavy metals, with higher concentrations observed during months of increased rainfall. This pattern likely reflects enhanced pollutant runoff. Elevated pollutant levels were particularly prominent in areas near the inflows from the Tickfaw, Amite, and Blind Rivers, as well as Pass Manchac.
3. The time-series machine learning model developed in this study successfully predicted spatial-temporal patterns of COD, TN, TP, As, and Pb concentrations for December 2023, compensating for missing data. The predictions indicated decreasing trends, suggesting that concentrations in December are not significantly different from those observed in September and October at most sampling sites. This aligns with salinity and specific conductance levels for December.

In summary, pollution hotspots were identified near stream inputs to the lake and Pass Manchac, which connects to Lake Pontchartrain. This study underscores the importance of targeted remediation efforts to reduce pollutant concentrations in these critical areas. It also provides valuable insights for decision-makers regarding the impacts of urban runoff, industrial activities, and agriculture on the lake's water quality over time. While the IDW interpolation method employed in this study proved effective for estimating contaminant concentrations at unsampled sites, it assumes spatial homogeneity among nearby points. This limitation may overlook finer-scale variations, particularly in sparsely sampled regions. Environmental factors such as flow patterns and seasonal shifts in lake dynamics may also introduce uncertainties that the IDW method does not fully capture.

The forest-based predictive model's accuracy was constrained by the relatively small dataset used for training, limiting its generalizability across the lake. Missing or unevenly distributed data points further reduced prediction accuracy in less-sampled regions. Similarly, while LSTM models are well-suited for time-series predictions, their effectiveness depends on the quality and quantity of the data. In this study, the limited dataset may have hindered the model's ability to capture long-term patterns or seasonal cycles accurately. Additionally, unobserved factors influencing contaminant levels, not explicitly accounted for in the dataset, could also affect predictive performance.

Project 5: Quantitative Analysis of Contaminants in Lake Maurepas and Source Identification Using BSMRM

Heavy Metal Distribution. The assessment of heavy metals (HMs) in Lake Maurepas revealed significant depth-related variations, although the variability was less pronounced for metals

such as Pb, Cu, Sr, Ba, and Ni. The study observed that the average concentrations of these metals often exceeded recommended thresholds, particularly for Pb during the months from September to November. River inputs significantly influenced the levels of Ba and Sr, with peak concentrations detected at river confluences. Higher metal concentrations were recorded in the middle and bottom layers, and proximity to the I-55 highway raised concerns regarding contamination from chemical transport and emissions. Overall, the findings suggest that the lake functions as both a sink and a source for organic and inorganic contaminants, with sediment release exacerbating heavy metal concentrations during warmer months.

Source Identification using BSMRM. The source identification of contaminants in Lake Maurepas utilized the Bayesian Statistical Model for the Runoff Matrix (BSMRM), revealing six primary sources of contamination: Transportation-Recreational-Accidental Release (TRAR), Death and Decay of Biological Species (DDBS), three river inputs (RI-1, RI-2, RI-3), and Geological Release (GR). River inputs were found to significantly contribute to elevated levels of TP, TN, and heavy metals such as Cu and As.

At the Tickfaw River connection (ND1), RI-3 accounted for the majority of barium and copper contamination, while GR was responsible for high concentrations of Cd and Ni. Notably, increased mercury levels linked to DDBS highlight bioaccumulation risks in aquatic organisms. The study emphasized the impact of anthropogenic activities, such as industrial discharges and transportation, on contaminant levels, particularly near the I-55 highway and railway lines. Significant nutrient enrichment in the lake suggests a potential risk of eutrophication, necessitating ongoing monitoring of both river inputs and other sources to mitigate ecological and health risks associated with nutrient runoff and heavy metal pollution. Overall, these findings underscore the complex interactions between environmental conditions and human activities, influencing the water quality and ecosystem health of Lake Maurepas.

Project 6: Air pollution monitoring and source apportionment in Lake Maurepas airshed

The time series analysis reveals distinct patterns in pollutant concentrations. It highlights the impact of seasonal and human activities. The elevated PM_{2.5} and PM₁₀ levels above the EPA threshold indicate critical areas of concern which likely stem from industrial emissions and dust resuspension. The observed rise in gases such as CO, NO₂, and H₂S during later months aligns with increased industrial activities and combustion sources. The CO₂ trend deviates, decreasing towards the year's end, which may reflect reduced biogenic emissions or specific industrial activity patterns. Temperature changes and seasonal transitions likely amplify pollutant formation, particularly secondary organic aerosols during warmer months. Unclear trends for TVOCs emphasize the need for extended data collection to discern patterns and

correlations. Source apportionment efforts, guided by PMF, will provide further insights into the proportional contributions of identified sources and enable targeted mitigation strategies.

Future Direction

Project 1: Identification of per- and polyfluoroalkyl substances (PFAS) in environmental samples from Lake Maurepas, USA, and their potential health implications

We plan to analyze and collect data on PFAS-associated diseases and toxicities to quantify the daily intake of various PFAS compounds that have the potential to cause diseases and toxicities, which may result from the consumption of PFAS-contaminated seafood, such as catfish and blue crabs. This study will be extended to develop novel risk assessment models that go beyond traditional factors, exploring new metrics to provide unique insights into PFAS exposure and associated health risks. Given that many PFAS compounds exist as complex mixtures, these novel models will focus on the combined impact of multiple PFAS compounds, examining how their interactions may amplify or mitigate each other's toxicity.

Project 2: Detection and characterization of microplastics in water, sediment and biological samples from Lake Maurepas

Chemical characterization of the detected MPs is ongoing, along with studies on their presence in sediments and biological materials. As there is currently no universal threshold for MPs concentrations, a comparison of our findings with existing literature will be used to assess toxicity levels and potential risks.

Project 3: Mercury in Lake Maurepas and risk assessment of fish and crab consumption

Future work will be focused on expanding the temporal scope of monitoring to include more seasons and extreme weather events to better understand the dynamics of Hg mobilization and bioavailability. Advanced machine learning techniques, such as deep learning models, will be employed to predict Hg distribution under varying environmental scenarios, incorporating factors like precipitation, wind patterns, and industrial activities. Additionally, more detailed species-specific analyses, including trophic transfer studies, can provide a comprehensive understanding of Hg risks throughout the food web.

Project 4: Spatial-temporal contaminant spreading analysis in Lake Maurepas in terms of the quality of water and sedimentary mud samples (Gunawardhana et al., 2024)

Our ongoing research aims to continuously monitor the quality of water and sediment in the lake, with an expanded scope that includes additional compounds. We are also examining biological samples, such as catfish and blue crab, collected at various intervals to evaluate contaminant concentrations, with a particular emphasis on the potential accumulation of heavy

metals. Additionally, we are implementing real-time sensors in the lake to gather big data, significantly improving our ability to forecast and address water quality challenges.

Project 5: Quantitative Analysis of Contaminants in Lake Maurepas and Source Identification Using BSMRM

Our work aims to provide a deeper understanding of how various sources of contamination in the lake influence water quality over time. We plan to conduct a temporal source impact decomposition that will focus on the relative dominance and evolving influence of each identified pollutant source in relation to specific environmental conditions, such as seasonal changes, and anthropogenic factors like industrial discharges and urban runoff. Additionally, we plan to introduce a methodology combining BSMRM with Event Response Analysis and Anomaly Detection (ERAAD) to quantitatively assess the factors influencing the spatiotemporal distribution of HMs and chemicals sources, and to identify pollution risk areas within multiple sampling sites.

Project 6: Air pollution monitoring and source apportionment in Lake Maurepas airshed

As part of future work, this study will focus on advancing source apportionment using the PMF model. Potential source candidates will be validated with quantifying source contributions and source profiles. Additionally, it aims to compare various existing source apportionment methods to evaluate their strengths and limitations, with PMF serving as the benchmark. Furthermore, the study will explore the potential of employing deep learning methods for source apportionment.

Literature Cited

Project 1: Identification of per- and polyfluoroalkyl substances (PFAS) in environmental samples from Lake Maurepas, USA, and their potential health implications

Agency for Toxic Substances and Disease Registry (ATSDR). (2021). *Toxicological profile for perfluoroalkyls*. Atlanta, GA: U.S. Department of Health and Human Services.

Agency for Toxic Substances and Disease Registry (ATSDR). (2024). *What are the health effects of PFAS?* Atlanta, GA: U.S. Department of Health and Human Services.

Ait Bamai, Y., Goudarzi, H., Araki, A., Okada, E., Kashino, I., Miyashita, C., & Kishi, R. (2020). Effect of prenatal exposure to per- and polyfluoroalkyl substances on childhood allergies and common infectious diseases in children up to age 7 years: The Hokkaido study on

- environment and children's health. *Environment International*, 143, 105979. <https://doi.org/10.1016/j.envint.2020.105979>
- Alipour Parvizia, B., Fernando, S., Crimmins, B. S., Hopke, P. K., & Holsen, T. M. (2024). Trends of short- and medium-chain chlorinated paraffin concentrations in top predator fish tissues from the Great Lakes. *ACS ES&T Water*, 4(8), 3433–3442. <https://doi.org/10.1021/acsestwater.4c00264>
- Boafo, Y. S., Mostafa, S., & Obeng-Gyasi, E. (2023). Association of combined metals and PFAS with cardiovascular disease risk. *Toxics*, 11(12), 979. <https://doi.org/10.3390/toxics11120979>
- Bonefeld-Jørgensen, E. C., Long, M., Fredslund, S. O., Bossi, R., & Olsen, J. (2014). Breast cancer risk after exposure to perfluorinated compounds in Danish women: A case–control study nested in the Danish National Birth Cohort. *Cancer Causes & Control*, 25(11), 1439–1448. <https://doi.org/10.1007/s10552-014-0446-7>
- Brase, R. A., Mullin, E. J., & Spink, D. C. (2021). Legacy and emerging per- and polyfluoroalkyl substances: Analytical techniques, environmental fate, and health effects. *International Journal of Molecular Sciences*, 22(3), Article 125. <https://doi.org/10.3390/ijms22030995>
- Buck Louis, G. M., Sundaram, R., Schisterman, E. F., Sweeney, A. M., Lynch, C. D., Gore-Langton, R. E., Maisog, J., Kim, S., Chen, Z., & Barr, D. B. (2013). Persistent environmental pollutants and couple fecundity: The LIFE Study. *Environmental Health Perspectives*, 121(2), 231–236. <https://doi.org/10.1289/ehp.1205301>
- Cheng, H., Jin, H., Lu, B., Lv, C., Ji, Y., Zhang, H., Fan, R., & Zhao, N. (2023). Emerging poly- and perfluoroalkyl substances in water and sediment from Qiantang River-Hangzhou Bay. *Science of the Total Environment*, 875, 162687. <https://doi.org/10.1016/j.scitotenv.2023.162687>
- Codling, G., Hosseini, S., Corcoran, M. B., Bonina, S., Lin, T., Li, A., Sturchio, N. C., Rockne, K. J., Ji, K., Peng, H., & Giesy, J. P. (2018). Current and historical concentrations of poly and perfluorinated compounds in sediments of the Northern Great Lakes—Superior, Huron, and Michigan. *Environmental Pollution*, 236, 373–381. <https://doi.org/10.1016/j.envpol.2018.01.104>

- De Toni, L., Di Nisio, A., Rocca, M. S., Pedrucci, F., Garolla, A., Dall'Acqua, S., Guidolin, D., Ferlin, A., & Foresta, C. (2022). Comparative evaluation of the effects of legacy and new generation perfluoroalkyl substances (PFAS) on thyroid cells in vitro. *Frontiers in Endocrinology*, *13*, Article 915096. <https://doi.org/10.3389/fendo.2022.915096>
- Eaton, A. M. (2024). Fluorotelomer carboxylic acid degradation: Implications for septic systems. *Honors Theses and Capstones*, 796. <https://scholars.unh.edu/honors/796>
- Eve, A. A., Tunc, E., Mehta, D., Yoo, J. Y., Yilmaz, H. E., Emren, S. V., Akçay, F. A., & Erdogan, Z. M. (2024). PFAS and their association with the increased risk of cardiovascular disease in postmenopausal women. *Toxicological Sciences*, *200*(2), 312–323. <https://doi.org/10.1093/toxsci/kfaa101>
- Fakouri Baygi, S., Crimmins, B. S., Hopke, P. K., & Holsen, T. M. (2016). Comprehensive emerging chemical discovery: Novel polyfluorinated compounds in Lake Michigan trout. *Environmental Science & Technology*, *50*(17), 9460–9468. <https://doi.org/10.1021/acs.est.6b01349>
- Fakouri Baygi, S., Fernando, S., Hopke, P. K., Holsen, T. M., & Crimmins, B. S. (2019). Automated isotopic profile deconvolution for high-resolution mass spectrometric data (APGC-QToF) from biological matrices. *Analytical Chemistry*, *91*(24), 15509–15517. <https://doi.org/10.1021/acs.analchem.9b03335>
- Fang, X., Feng, Y., Shi, Z., & Dai, J. (2009). Alterations of cytokines and MAPK signaling pathways are related to the immunotoxic effect of perfluorononanoic acid. *Toxicological Sciences*, *108*(2), 367–376. <https://doi.org/10.1093/toxsci/kfp032>
- Fang, X., Feng, Y., Wang, J., & Dai, J. (2010). Perfluorononanoic acid-induced apoptosis in rat spleen involves oxidative stress and the activation of caspase-independent death pathway. *Toxicology*, *267*(1–3), 54–59. <https://doi.org/10.1016/j.tox.2009.11.004>
- Fang, X., Zhang, L., Feng, Y., Zhao, Y., & Dai, J. (2008). Immunotoxic effects of perfluorononanoic acid on BALB/c mice. *Toxicological Sciences*, *105*(2), 312–321. <https://doi.org/10.1093/toxsci/kfn116>
- Fernando, S., Renaguli, A., Milligan, M. S., Pagano, J. J., Hopke, P. K., Holsen, T. M., & Crimmins, B. S. (2018). Comprehensive analysis of the Great Lakes top predator fish for novel

- halogenated organic contaminants by GC×GC-HR-ToF mass spectrometry. *Environmental Science & Technology*, 52(5), 2909–2917. <https://doi.org/10.1021/acs.est.7b05214>
- Goudarzi, H., Miyashita, C., Okada, E., Kashino, I., Kobayashi, S., Chen, C. J., Ito, S., Araki, A., Matsuura, H., Ito, Y. M., & Kishi, R. (2016). Effects of prenatal exposure to perfluoroalkyl acids on prevalence of allergic diseases among 4-year-old children. *Environment International*, 94, 124–132. <https://doi.org/10.1016/j.envint.2016.05.004>
- Guo, R., Megson, D., Myers, A. L., Helm, P. A., Marvin, C., Crozier, P., Mabury, S., Bhavsar, S. P., Tomy, G., Simcik, M., McCarry, B., & Reiner, E. J. (2016). Application of a comprehensive extraction technique for the determination of poly- and perfluoroalkyl substances (PFASs) in Great Lakes region sediments. *Chemosphere*, 164, 535–546. <https://doi.org/10.1016/j.chemosphere.2016.08.087>
- Huang, M., Jiao, J., Zhuang, P., Chen, X., Wang, J., & Zhang, Y. (2018). Serum polyfluoroalkyl chemicals are associated with risk of cardiovascular diseases in national US population. *Environment International*, 119, 37–46. <https://doi.org/10.1016/j.envint.2018.06.016>
- Interstate Technology Regulatory Council. (2023). *PFAS—Per-and polyfluoroalkyl substances: Chemistry, terminology, and acronyms*. Retrieved from <https://www.itrcweb.org/PFAS>
- Kawabata, K., Matsuzaki, H., Nukui, S., Okazaki, M., Sakai, A., Kawashima, Y., & Kudo, N. (2017). Perfluorododecanoic acid induces cognitive deficit in adult rats. *Toxicological Sciences*, 157(2), 421–428. <https://doi.org/10.1093/toxsci/kfx046>
- Khazaei, M., Guardian, M. G. E., Aga, D. S., & Ng, C. A. (2020). Impacts of sex and exposure duration on gene expression in zebrafish following perfluorooctane sulfonate exposure. *Environmental Toxicology and Chemistry*, 39(2), 437–449. <https://doi.org/10.1002/etc.4645>
- Li, M., Hu, J., Cao, X., Chen, H., Lyu, Y., & Sun, W. (2024). Nontarget analysis combined with TOP assay reveals a significant portion of unknown PFAS precursors in firefighting foams currently used in China. *Environmental Science & Technology*, 58(38), 17104–17113. <https://doi.org/10.1021/acs.est.4c07879>

- Manojkumar, Y., Pilli, S., Rao, P. V., & Tyagi, R. D. (2023). Sources, occurrence, and toxic effects of emerging per- and polyfluoroalkyl substances (PFAS). *Neurotoxicology and Teratology*, 97, Article 107174. <https://doi.org/10.1016/j.ntt.2023.107174>
- Patel, N., Ivantsova, E., Konig, I., Souders, C. L., & Martyniuk, C. J. (2022). Perfluorotetradecanoic acid (PFTeDA) induces mitochondrial damage and oxidative stress in zebrafish (*Danio rerio*) embryos/larvae. *Toxics*, 10(12), Article 776. <https://doi.org/10.3390/toxics10120776>
- Point, A. D., Holsen, T. M., Fernando, S., Hopke, P. K., & Crimmins, B. S. (2019). Towards the development of a standardized method for extraction and analysis of PFAS in biological tissues. *Environmental Science: Water Research & Technology*, 5(11), 1876–1886. <https://doi.org/10.1039/C9EW00765B>
- Raleigh, K. K., Alexander, B. H., Olsen, G. W., Ramachandran, G., Morey, S. Z., Church, T. R., Logan, P. W., Scott, L. L. F., & Allen, E. M. (2014). Mortality and cancer incidence in ammonium perfluorooctanoate production workers. *Occupational and Environmental Medicine*, 71(7), 500–506. <https://oem.bmj.com/content/71/7/500.long>
- Ren, J., Point, A. D., Fakouri Baygi, S., Fernando, S., Hopke, P. K., Holsen, T. M., & Crimmins, B. S. (2022). Bioaccumulation of polyfluoroalkyl substances in the Lake Huron aquatic food web. *Science of the Total Environment*, 819, Article 152974. <https://doi.org/10.1016/j.scitotenv.2022.152974>
- Running, L., Cristobal, J. R., Karageorgiou, C., Camdzic, M., Aguilar, J. M., Gokcumen, O., Aga, D. S., & Atilla-Gokcumen, G. E. (2024). Transcriptomics effects of per- and polyfluorinated alkyl substances in differentiated neuronal cells. *bioRxiv*. <https://doi.org/10.1101/2024.01.26.577438>
- Savoca, D., & Pace, A. (2021). Bioaccumulation, biodistribution, toxicology, and biomonitoring of organofluorine compounds in aquatic organisms. *International Journal of Molecular Sciences*, 22(12), Article 6276. <https://doi.org/10.3390/ijms22126276>
- Steenland, K., Tinker, S., Frisbee, S., Ducatman, A., & Vaccarino, V. (2009). Association of perfluorooctanoic acid and perfluorooctane sulfonate with serum lipids among adults living near a chemical plant. *American Journal of Epidemiology*, 170(10), 1268–1278. <https://doi.org/10.1093/aje/kwp279>

Vieira, V. M., Hoffman, K., Shin, H. M., Weinberg, J. M., Webster, T. F., & Fletcher, T. (2013). Perfluorooctanoic acid exposure and cancer outcomes in a contaminated community: A geographic analysis. *Environmental Health Perspectives*, 121(3), 318–323. <https://doi.org/10.1289/ehp.1205829>

Zhang, S., Wen, Z., Li, X., Lin, L., Zou, C., Li, Y., Wang, Y., & Ge, R. S. (2021). Short-term exposure to perfluorotetradecanoic acid affects the late-stage regeneration of Leydig cells in adult male rats. *Toxicology and Applied Pharmacology*, 433, Article 115777. <https://doi.org/10.1016/j.taap.2021.115777>

Project 2: Detection and characterization of microplastics in water, sediment and biological samples from Lake Maurepas

Alam, M. J., Shammi, M., & Tareq, S. M. (2023). Distribution of microplastics in shoreline water and sediment of the Ganges River Basin to Meghna Estuary in Bangladesh. *Ecotoxicology and Environmental Safety*, 266, Article 115537. <https://doi.org/10.1016/j.ecoenv.2023.115537>

Leistenschneider, C., Wu, F., Primpke, S., Gerdts, G., & Burkhardt-Holm, P. (2024). Unveiling high concentrations of small microplastics (11–500 µm) in surface water samples from the southern Weddell Sea off Antarctica. *Science of the Total Environment*, 927, Article 172124. <https://doi.org/10.1016/j.scitotenv.2024.172124>

Lefebvre, C., Cormier, B., Le Bihanic, F., Magalhães, G. R., Morin, B., Lecomte, S., & Cachot, J. (2024). Temporal distribution of microplastics and other anthropogenic particles in four marine species from the Atlantic coast (France). *Environmental Pollution*, 357, Article 124440. <https://doi.org/10.1016/j.envpol.2024.124440>

Piyawardhana, N., Weerathunga, V., Chen, H. S., Guo, L., Huang, P. J., Ranatunga, R. R. M. K. P., & Hung, C. C. (2022). Occurrence of microplastics in commercial marine dried fish in Asian countries. *Journal of Hazardous Materials*, 423, Article 127093. <https://doi.org/10.1016/j.jhazmat.2021.127093>

Simon-Sánchez, L., Vianello, A., Kirstein, I. V., Molazadeh, M. S., Lorenz, C., & Vollertsen, J. (2024). Assessment of microplastic pollution and polymer risk in the sediment compartment of the Limfjord, Denmark. *Science of the Total Environment*, 950, Article 175017. <https://doi.org/10.1016/j.scitotenv.2024.175017>

Teampanpong, J., Phanchaum, J., Rayaphak, A., & Duengkae, P. (2024). Microplastic accumulation in water from protected areas in Western Forest Complex of Thailand. *Heliyon*, *10*(17), Article e036130. <https://doi.org/10.1016/j.heliyon.2024.e36130>

Project 3: Mercury in Lake Maurepas and risk assessment of fish and crab consumption

Bhattarai, S. (2006). Spatial distribution of heavy metals in Louisiana sediments and study of factors impacting the concentrations (Master's thesis). Louisiana State University and Agricultural and Mechanical College. LSU Scholarly Repository. 10.31390/gradschool_theses.4282

Chen, C. W., Chen, C. F., & Dong, C. D. (2012). Distribution and accumulation of mercury in sediments of Kaohsiung River mouth, Taiwan. *APCBEE Procedia*, *1*, 153–158. <https://doi.org/10.1016/j.apcbee.2012.03.025>

Jaishankar, M., Tseten, T., Anbalagan, N., Mathew, B. B., & Beeregowda, K. N. (2014). Toxicity, mechanism and health effects of some heavy metals. *Interdisciplinary Toxicology*, *7*(2), 60–72. <https://doi.org/10.2478/intox-2014-0009>

Kinuthia, G. K., Ngure, V., Beti, D., Lugalia, R., Wangila, A., & Kamau, L. (2020). Levels of heavy metals in wastewater and soil samples from open drainage channels in Nairobi, Kenya: Community health implication. *Scientific Reports*, *10*(1), Article 8434. <https://doi.org/10.1038/s41598-020-65359-5>

Louisiana Clean Energy Complex. (2024). Retrieved May 20, 2024, from <https://www.airproducts.com/louisiana-clean-energy>

Ma, M., Du, H., & Wang, D. (2019). Mercury methylation by anaerobic microorganisms: A review. *Critical Reviews in Environmental Science and Technology*, *49*(20), 1893–1936. <https://doi.org/10.1080/10643389.2019.1594517>

Raj, D., & Maiti, S. K. (2020). Sources, bioaccumulation, health risks and remediation of potentially toxic metal(loid)s (As, Cd, Cr, Pb, and Hg): An epitomised review. *Environmental Monitoring and Assessment*, *192*(2), Article 108. <https://doi.org/10.1007/s10661-019-8060-5>

Trasande, L., Landrigan, P. J., & Schechter, C. (2005). Public health and economic consequences of methyl mercury toxicity to the developing brain. *Environmental Health Perspectives*, 113(5), 590–596. <https://doi.org/10.1289/ehp.7743>

Ullrich, S. M., Tanton, T. W., & Abdrashitova, S. A. (2001). Mercury in the aquatic environment: A review of factors affecting methylation. *Critical Reviews in Environmental Science and Technology*, 31(3), 241–293. <https://doi.org/10.1080/20016491089226>

Project 4: Spatial-temporal contaminant spreading analysis in Lake Maurepas in terms of the quality of water and sedimentary mud samples

Air Products and Chemicals, Inc. (2024). Project updates USA. Retrieved May 2, 2024, from <https://www.airproducts.com/louisiana-clean-energy/project-updates>

Asmat, A., Hazali, N. A., Nor, A. N. M., & Zuhan, F. K. (2018). Seasonal-spatial of Putrajaya Lake water quality parameter (WQP) concentration using geographic information system (GIS). *International Journal of Engineering and Technology (UAE)*, 7, 176–181. <https://doi.org/10.14419/ijet.v7i3.11.15956>

Baalousha, M., McNeal, S., & Scott, G. I. (2019). An assessment of nonpoint source pollution in stormwater pond systems in coastal South Carolina. *Stormwater Ponds Coastal South Carolina*, 192.

Barazzetti, L., Previtali, M., & Roncoroni, F. (2022). Visualization and processing of structural monitoring data using space-time cubes. In *Proceedings of the International Conference on Computational Science and Its Applications* (pp. 19–31). Springer International Publishing: Cham, Switzerland. https://doi.org/10.1007/978-3-031-10450-3_2

Bargu, S., Hiatt, M., Maiti, K., Miller, P., & White, J. R. (2023). The future of cyanobacteria toxicity in estuaries undergoing pulsed nutrient inputs: A case study from coastal Louisiana. *Water*, 15, Article 3816. <https://doi.org/10.3390/w15213816>

Baustian, M. M., Clark, F. R., Jerabek, A. S., Wang, Y., Bienn, H. C., & White, E. D. (2018). Modeling current and future freshwater inflow needs of a subtropical estuary to manage and maintain forested wetland ecological conditions. *Ecological Indicators*, 85, 791–807. <https://doi.org/10.1016/j.ecolind.2017.10.005>

- Bhattarai, S. (2006). Spatial distribution of heavy metals in Louisiana sediments and study of factors impacting the concentrations (Master's thesis). Louisiana State University and Agricultural and Mechanical College, Baton Rouge, LA, USA.
- Boegehold, A. G., Burtner, A. M., Camilleri, A. C., Carter, G., DenUyl, P., Fanslow, D., Fyffe Semenyuk, D., Godwin, C. M., Gossiaux, D., & Johengen, T. H., et al. (2023). Routine monitoring of Western Lake Erie to track water quality changes associated with cyanobacterial harmful algal blooms. *Earth System Science Data Discussions*, *15*, 3853–3868. <https://doi.org/10.5194/essd-15-3853-2023>
- Burden, D. G., Malone, R. F., & Geaghan, J. (1985). Development of a condition index for Louisiana lakes. *Lake and Reservoir Management*, *1*, 68–72.
- Burlakova, L. E., Hinchey, E. K., Karatayev, A. Y., & Rudstam, L. G. (2018). US EPA Great Lakes National Program Office monitoring of the Laurentian Great Lakes: Insights from 40 years of data collection. *Journal of Great Lakes Research*, *44*, 535–538. <https://doi.org/10.1016/j.jglr.2018.05.017>
- Carlson, D. L., & Swackhamer, D. L. (2006). Results from the US Great Lakes Fish Monitoring Program and effects of lake processes on bioaccumulative contaminant concentrations. *Journal of Great Lakes Research*, *32*, 370–385. [https://doi.org/10.3394/0380-1330\(2006\)32\[370:RFTUGL\]2.0.CO;2](https://doi.org/10.3394/0380-1330(2006)32[370:RFTUGL]2.0.CO;2)
- Cieśliński, R. (2009). Extreme changes in salinity levels in the waters of coastal lakes in Poland. *Limnological Review*, *9*, 73–80.
- Chigira, M., & Oyama, T. (2000). Mechanism and effect of chemical weathering of sedimentary rocks. *Developments in Geotechnical Engineering*, *84*, 267–278. [https://doi.org/10.1016/S0165-1250\(00\)80022-X](https://doi.org/10.1016/S0165-1250(00)80022-X)
- Dökmen, F. (2015). Temporal variation of biological oxygen demand (BOD), chemical oxygen demand (COD), and pH values in surface waters of Gölcük-Kocaeli, Turkey. In *Plants Pollutants and Remediation* (pp. 341–347). https://doi.org/10.1007/978-94-017-7194-8_15
- Gao, K., Beardall, J., Häder, D. P., Hall-Spencer, J. M., Gao, G., & Hutchins, D. A. (2019). Effects of ocean acidification on marine photosynthetic organisms under the concurrent

- influences of warming, UV radiation, and deoxygenation. *Frontiers in Marine Science*, 6, Article 322. <https://doi.org/10.3389/fmars.2019.00322>
- Gunawardhana, T., Rahman, M. A., LaCour, Z., Erwin, E., & Emami, F. (2024). Spatial pattern assessment and prediction of water and sedimentary mud quality changes in Lake Maurepas. *Environments*, 11(12), Article 268. <https://doi.org/10.3390/environments11120268>
- Hassan, B., Qadri, H., Ali, M. N., Khan, N. A., & Yattoo, A. M. (2020). Impact of climate change on freshwater ecosystem and its sustainable management. In H. Qadri, R. Bhat, M. Mehmood, & G. Dar (Eds.), *Freshwater pollution dynamics and remediation* (pp. 105–121). Springer. https://doi.org/10.1007/978-981-13-8277-2_7
- Heidtke, T., Hartig, J. H., Zarull, M. A., & Yu, B. (2006). PCB levels and trends within the Detroit River-Western Lake Erie Basin: A historical perspective of ecosystem monitoring. *Environmental Monitoring and Assessment*, 112, 23–33. <https://doi.org/10.1007/s10661-006-0212-8>
- Ho, L. T., & Goethals, P. L. (2019). Opportunities and challenges for the sustainability of lakes and reservoirs in relation to the Sustainable Development Goals (SDGs). *Water*, 11, Article 1462. <https://doi.org/10.3390/w11071462>
- Huang, J., Huang, Y., & Zhang, Z. (2014). Coupled effects of natural and anthropogenic controls on seasonal and spatial variations of river water quality during baseflow in a coastal watershed of Southeast China. *PLoS ONE*, 9(e91528). <https://doi.org/10.1371/journal.pone.0091528>
- Hunt, A. J., Sin, E. H., Marriott, R., & Clark, J. H. (2010). Generation, capture, and utilization of industrial carbon dioxide. *ChemSusChem*, 3(3), 306–322. <https://doi.org/10.1002/cssc.200900169>
- Ji, G., & Havens, K. (2019). Periods of extreme shallow depth hinder but do not stop long-term improvements of water quality in Lake Apopka, Florida (USA). *Water*, 11(538). <https://doi.org/10.3390/w11030538>

- Karydas, C. G., Gitas, I. Z., Koutsogiannaki, E., Lydakis-Simantiris, N., & Silleos, G. N. (2009). Evaluation of spatial interpolation techniques for mapping agricultural topsoil properties in Crete. *EARSeL eProceedings*, 8, 26–39.
- Khalil, S. M., Forrest, B. M., Lowiec, M., Suthard, B. C., Raynie, R. C., Haywood, E. L., Robertson, Q., & Andrews, J. (2020). Overview of statewide geophysical surveys for ecosystem restoration in Louisiana. *Shore Beach*, 88, 102–109.
- Koski, V., Kotamäki, N., Hämäläinen, H., Meissner, K., Karvanen, J., & Kärkkäinen, S. (2020). The value of perfect and imperfect information in lake monitoring and management. *Science of The Total Environment*, 726, 138396. <https://doi.org/10.1016/j.scitotenv.2020.138396>
- Kushwaha, S. P. S., Khan, A., Habib, B., Quadri, A., & Singh, A. (2004). Evaluation of sambar and muntjak habitats using geostatistical modeling. *Current Science*, 86(10), 1390–1400.
- Li, J., Huang, J. F., & Wang, X. Z. (2006). A GIS-based approach for estimating spatial distribution of seasonal temperature in Zhejiang Province, China. *Journal of Zhejiang University-SCIENCE A*, 7(6), 647–656. <https://doi.org/10.1631/jzus.2006.A0647>
- Louisiana Clean Energy Complex USA. (2024). Retrieved April 28, 2024, from <https://www.airproducts.com/louisiana-clean-energy>
- Lv, Z., Ran, X., Liu, J., Feng, Y., Zhong, X., & Jiao, N. (2024). Effectiveness of chemical oxygen demand as an indicator of organic pollution in aquatic environments. *Ocean Science*, 3, 0050.
- Mance, G. (2012). *Pollution threat of heavy metals in aquatic environments*. Springer Science & Business Media.
- Massarweh, O., Al-Khuzaei, M., Al-Shafi, M., Bicer, Y., & Abushaikha, A. S. (2023). Blue hydrogen production from natural gas reservoirs: A review of application and feasibility. *Journal of CO2 Utilization*, 70, 102438. <https://doi.org/10.1016/j.jcou.2023.102438>
- McCormick, M. J., & Pazdalski, J. D. (1993). Monitoring midlake water temperature in southern Lake Michigan for climate change studies. *Climatic Change*, 25(1), 119–125.

- Montanio, P. A. (2011). *Bayou Dupont marsh and ridge creation CWPPRA project, Fed No. BA-48: Environmental assessment*. Jefferson and Plaquemines Parishes: Barataria, LA, USA. <https://repository.library.noaa.gov/view/noaa/4124>
- Nijmeijer, R., de Haas, A., Dost, R. J. J., & Budde, P. E. (2001). *ILWIS 3.0 Academic: User's guide*. ITC, ILWIS: Enschede, The Netherlands.
- Obolewski, K., Glińska-Lewczuk, K., Szymańska, M., Mrozińska, N., Bąkowska, M., Astel, A., Lew, S., & Paturej, E. (2018). Patterns of salinity regime in coastal lakes based on structure of benthic invertebrates. *PLoS ONE*, 13(e0207825). <https://doi.org/10.1371/journal.pone.0207825>
- Reid, A. J., Carlson, A. K., Creed, I. F., Eliason, E. J., Gell, P. A., Johnson, P. T., Kidd, K. A., MacCormack, T. J., Olden, J. D., Ormerod, S. J., et al. (2019). Emerging threats and persistent conservation challenges for freshwater biodiversity. *Biological Reviews*, 94(3), 849–873. <https://doi.org/10.1111/brv.12480>
- Renaut, R. W., & Owen, R. B. (2023). Lake processes and sedimentation. In *The Kenya Rift Lakes: Modern and Ancient: Limnology and limnogeology of tropical lakes in a continental rift* (pp. 129–160). Springer.
- Schelske, C. L., Coveney, M. F., Aldridge, F. J., Kenney, W. F., & Cable, J. E. (2000). Wind or nutrients: Historic development of hypereutrophy in Lake Apopka, Florida. *Advances in Limnology*, 55, 543–563.
- Schindler, D. W., Bayley, S. E., Parker, B. R., Beaty, K. G., Cruikshank, D. R., Fee, E. J., Schindler, E. U., & Stainton, M. P. (1996). The effects of climatic warming on the properties of boreal lakes and streams at the Experimental Lakes Area, Northwestern Ontario. *Limnology and Oceanography*, 41(5), 1004–1017.
- Seelbach, P. W., Fogarty, L. R., Bunnell, D. B., Haack, S. K., & Rogers, M. W. (2013). A conceptual framework for Lake Michigan coastal/nearshore ecosystems, with application to Lake Michigan Lakewide Management Plan (LaMP) objectives. *U.S. Geological Survey Open-File Report, 2013-1138*, 36 p.
- Shyu, G. S., Cheng, B. Y., Chiang, C. T., Yao, P. H., & Chang, T. K. (2011). Applying factor analysis combined with Kriging and information entropy theory for mapping and evaluating the

- stability of groundwater quality variation in Taiwan. *International Journal of Environmental Research and Public Health*, 8(3), 1084–1109. <https://doi.org/10.3390/ijerph8041084>
- Singer, M. (2011). Down Cancer Alley: The lived experience of health and environmental suffering in Louisiana’s chemical corridor. *Medical Anthropology Quarterly*, 25(2), 141–163. <https://doi.org/10.1111/j.1548-1387.2011.01154.x>
- USGS Coastal and Marine Geology Program USA. (2020–2030). Retrieved April 25, 2024, from <https://pubs.usgs.gov/of/2002/of02-206/biology/pg71fig1.html>
- USGS Earth Explorer USA. (2024). Retrieved April 23, 2024, from <https://earthexplorer.usgs.gov/>
- VanLandeghem, M. M., Meyer, M. D., Cox, S. B., Sharma, B., & Patiño, R. (2012). Spatial and temporal patterns of surface water quality and ichthyotoxicity in urban and rural river basins in Texas. *Water Research*, 46(20), 6638–6651. <https://doi.org/10.1016/j.watres.2012.05.002>
- Vasistha, P., & Ganguly, R. (2022). Water quality assessment in two lakes of Panchkula, Haryana, using GIS: Case study on seasonal and depth-wise variations. *Environmental Science and Pollution Research*, 29(44), 43212–43236. <https://doi.org/10.1007/s11356-022-18635-y>
- Waters, M. N., Schelske, C. L., & Brenner, M. (2015). Cyanobacterial dynamics in shallow Lake Apopka (Florida, USA) before and after the shift from a macrophyte-dominated to a phytoplankton-dominated state. *Freshwater Biology*, 60(8), 1571–1580. <https://doi.org/10.1111/fwb.12589>
- WBRZ-TV (News) Public File. (2024, May 2). Death toll rises to 8 in I-55 pileup caused by super fog. Retrieved from <https://www.wbrz.com/news/death-toll-rises-to-8-in-i-55-pileup-caused-by-super-fog-bridge-will-need-significant-repairs/>
- Wicke, D., Cochrane, T. A., & O’Sullivan, A. D. (2012). Atmospheric deposition and storm-induced runoff of heavy metals from different impermeable urban surfaces. *Journal of Environmental Monitoring*, 14(1), 209–216. <https://doi.org/10.1039/C1EM10643K>

- Wu, Z., Zhang, D., Cai, Y., Wang, X., Zhang, L., & Chen, Y. (2017). Water quality assessment based on the water quality index method in Lake Poyang: The largest freshwater lake in China. *Scientific Reports*, 7, 17999. <https://doi.org/10.1038/s41598-017-18285-y>
- Xu, R., Lu, L., Hu, Y., & Liu, S. (2023). Spatio-temporal characteristics of the impacts of land-use change on carbon emission: A case study of Hangzhou, China. In *Proceedings of the 2023 11th International Conference on Agro-Geoinformatics* (pp. 1–6). IEEE.
- Yang, W., Zhao, Y., Wang, D., Wu, H., Lin, A., & He, L. (2020). Using principal components analysis and IDW interpolation to determine spatial and temporal changes of surface water quality of Xianjiang River in Huangshan, China. *International Journal of Environmental Research and Public Health*, 17(2942). <https://doi.org/10.3390/ijerph17082942>
- Zarco-Perello, S., & Simões, N. (2017). Ordinary Kriging vs inverse distance weighting: Spatial interpolation of the sessile community of Madagascar reef, Gulf of Mexico. *PeerJ*, 5, e4078. <https://doi.org/10.7717/peerj.4078>
- Zhang, X., Rygwelski, K. R., & Rossmann, R. (2009). The Lake Michigan contaminant transport and fate model, LM2-Toxic: Development, overview, and application. *Journal of Great Lakes Research*, 35(1), 128–136. <https://doi.org/10.1016/j.jglr.2008.11.008>
- Zhou, W., Chen, G., Li, H., Luo, H., & Huang, S. L. (2007). GIS application in mineral resource analysis—A case study of offshore marine placer gold at Nome, Alaska. *Computers & Geosciences*, 33(6), 773–788. <https://doi.org/10.1016/j.cageo.2006.11.001>
- Zou, D., Chi, Y., Dong, J., Fu, C., Wang, F., & Ni, M. (2013). Supercritical water oxidation of tannery sludge: Stabilization of chromium and destruction of organics. *Chemosphere*, 93(7), 1413–1418. <https://doi.org/10.1016/j.chemosphere.2013.07.009>

Project 5: Quantitative Analysis of Contaminants in Lake Maurepas and Source Identification Using BSMRM

American Public Health Association (APHA). (2012). *Standard methods for the examination of water and wastewater* (22nd ed.). American Public Health Association.

Baldwin, A. K., Corsi, S. R., De Cicco, L. A., Lenaker, P. L., Lutz, M. A., Sullivan, D. J., & Richards, K. D. (2016). Organic contaminants in Great Lakes tributaries: Prevalence and potential

- aquatic toxicity. *Science of the Total Environment*, 554–555, 42–52.
<https://doi.org/10.1016/j.scitotenv.2016.02.137>
- Bhateria, R., & Jain, D. (2016). Water quality assessment of lake water: A review. *Sustainable Water Resources Management*, 2(2), 161–173. <https://doi.org/10.1007/s40899-015-0014-7>
- Chen, C. Y., Stemberger, R. S., Kamman, N. C., et al. (2005). Patterns of Hg bioaccumulation and transfer in aquatic food webs across multi-lake studies in the Northeast US. *Ecotoxicology*, 135–147. <https://doi.org/10.1007/s10646-004-6265-y>
- Chandrasekhar, R., Satyanarayana, Y., Ramakrishna, C., Vaikunta Rao, L., Kaur, J., & Mehta, S. K. (2023). A case study of the effect of seawater intrusion on the water quality index of the Indian southeastern coastal region. *ACS ES&T Water*, 3(6), 1610–1619.
<https://pubs.acs.org/doi/10.1021/acsestwater.2c00350>
- Dong, G., Hu, Z., Liu, X., Fu, Y., & Zhang, W. (2020). Spatio-temporal variation of total nitrogen and ammonia nitrogen in the water source of the middle route of the south-to-north water diversion project. *Water*, 12(1), 1–13. <https://doi.org/10.3390/w12092615>
- Gunawardhana, T., Rahman, M. A., LaCour, Z., Erwin, E., & Emami, F. (2024). Spatial pattern assessment and prediction of water and sedimentary mud quality changes in Lake Maurepas. *Environments*, 11(12), 268. <https://doi.org/10.3390/environments11120268>
- Hill, D. D., Owens, W. E., & Tchounwou, P. B. (2005). Comparative assessment of the physico-chemical and bacteriological qualities of selected streams in Louisiana. *International Journal of Environmental Research and Public Health*, 2(1), 94–100.
<https://doi.org/10.3390/ijerph2005010094>
- Keddy, P. A., Campbell, D., McFalls, T., Shaffer, G. P., Moreau, R., Dranguet, C., & Heleniak, R. (2007). The wetlands of lakes Pontchartrain and Maurepas: Past, present, and future. *Environmental Reviews*, 15(1), 43–77. <https://doi.org/10.1139/a06-008>
- Park, E. S., Lee, E. K., & Oh, M. S. (2021). Bayesian multivariate receptor modeling software: BNFA and bayesMRM. *Chemometrics and Intelligent Laboratory Systems*, 211, 104278.
<https://doi.org/10.1016/j.chemolab.2021.104280>

- Shaffer, G. P., Gosselink, J. G., & Hoepfner, S. S. (2005). The Mississippi River alluvial plain. In *The world's largest wetlands: Ecology and conservation* (pp. 272–315). Cambridge University Press.
- Stahl, J. B. (1979). Black water and two peculiar types of stratification in an organically loaded strip-mine lake. *Water Research*, 13(5), 467–471. [https://doi.org/10.1016/0043-1354\(79\)90040-X](https://doi.org/10.1016/0043-1354(79)90040-X)
- Steinskog, D. J., Tjøtheim, D. B., & Kvamstø, N. G. (2007). A cautionary note on the use of the Kolmogorov-Smirnov test for normality. *Monthly Weather Review*, 135(4), 1151–1157. <https://doi.org/10.1175/MWR3326.1>
- Su, W., Wu, C., Sun, X., Lei, R., Lei, L., Wang, L., & Zhu, X. (2024). Environmental dynamics of nitrogen and phosphorus release from river sediments of arid areas. *Journal of Arid Land*, 16(5), 685–698. <https://doi.org/10.1007/s40333-024-0099-7>
- World Health Organization (WHO). (2017). *Guidelines for drinking-water quality* (4th ed., incorporating the first addendum). World Health Organization.
- Xue, Y., Ma, Y., Long, G., He, H., Li, Z., Yan, Z., Wan, J., Zhang, S., & Zhu, B. (2023). Evaluation of water quality pollution and analysis of vertical distribution characteristics of typical rivers in the Pearl River Delta, South China. *Journal of Sea Research*, 193, 102380. <https://doi.org/10.1016/j.seares.2023.102380>
- Zhang, H., Zhou, X., Lv, X., Xu, X., Weng, Q., & Lei, K. (2023). Exploration of the factors that influence total phosphorus in surface water and an evaluation of surface water vulnerability based on an advanced algorithm and traditional index method. *Journal of Environmental Management*, 342, 118155. <https://doi.org/10.1016/j.jenvman.2023.118155>
- Project 6: Air pollution monitoring and source apportionment in Lake Maurepas airshed**
- Costabile, F., Bertoni, G., Desantis, F., Wang, F., Weimin, H., Fenglei, L., & Allegrini, I. (2006). A preliminary assessment of major air pollutants in the city of Suzhou, China. *Atmospheric Environment*, 40(33), 6380–6395. <https://doi.org/10.1016/j.atmosenv.2006.05.056>
- Elminir, H. K. (2005). Dependence of urban air pollutants on meteorology. *Science of the Total Environment*, 350(1–3), 225–237. <https://doi.org/10.1016/j.scitotenv.2005.01.043>

- Junninen, H., Niska, H., Tuppurainen, K., Ruuskanen, J., & Kolehmainen, M. (2004). Methods for imputation of missing values in air quality data sets. *Atmospheric Environment*, 38(18), 2895–2907. <https://doi.org/10.1016/j.atmosenv.2004.02.026>
- Ogulei, D., Hopke, P. K., Zhou, L., Pancras, J. P., Nair, N., & Ondov, J. M. (2006). Source apportionment of Baltimore aerosol from combined size distribution and chemical composition data. *Atmospheric Environment*, 40, 396–410. <https://doi.org/10.1016/j.atmosenv.2005.11.075>
- Paatero, P. (1997). Least squares formulation of robust non-negative factor analysis. *Chemometrics and Intelligent Laboratory Systems*, 37(1), 23–35. [https://doi.org/10.1016/S0169-7439\(96\)00044-5](https://doi.org/10.1016/S0169-7439(96)00044-5)
- Paatero, P. (1999). The Multilinear Engine—A Table-Driven, Least Squares Program for Solving Multilinear Problems, Including the n-Way Parallel Factor Analysis Model. *Journal of Computational and Graphical Statistics*, 8(4), 854–888. <https://doi.org/10.1080/10618600.1999.10474853>
- Paatero, P., Eberly, S., Brown, S. G., & Norris, G. A. (2014). Methods for estimating uncertainty in factor analytic solutions. *Atmospheric Measurement Techniques*, 7(3), 781–797. <https://doi.org/10.5194/amt-7-781-2014>
- Paatero, P., & Tapper, U. (1994). Positive matrix factorization: A non-negative factor model with optimal utilization of error estimates of data values. *Environmetrics*, 5(2), 111–126. <https://doi.org/10.1002/env.3170050203>
- Reff, A., Eberly, S. I., & Bhave, P. V. (2007). Receptor modeling of ambient particulate matter data using positive matrix factorization: Review of existing methods. *Journal of the Air & Waste Management Association*, 57(2), 146–154. <https://doi.org/10.1080/10473289.2007.10465319>
- Singh, K. P., Gupta, S., & Rai, P. (2013). Identifying pollution sources and predicting urban air quality using ensemble learning methods. *Atmospheric Environment*, 80, 426–437. <https://doi.org/10.1016/j.atmosenv.2013.08.023>

- Squizzato, S., Masiol, M., Emami, F., Chalupa, D. C., Utell, M. J., Rich, D. Q., & Hopke, P. K. (2019). Long-term changes of source apportioned particle number concentrations in a metropolitan area of the northeastern United States. *Atmosphere*, 10(1), 27. <https://doi.org/10.3390/atmos10010027>
- Venkatram, A. (2002). Accounting for averaging time in air pollution modeling. *Atmospheric Environment*, 36(13), 2165–2170. [https://doi.org/10.1016/S1352-2310\(02\)00200-5](https://doi.org/10.1016/S1352-2310(02)00200-5)
- Wong, D. W., Yuan, L., & Perlin, S. A. (2004). Comparison of spatial interpolation methods for the estimation of air quality data. *Journal of Exposure Science & Environmental Epidemiology*, 14(5), 404–415. <https://doi.org/10.1038/sj.jea.7500338>
- Yu, H.-L., Lin, Y.-C., & Kuo, Y.-M. (2015). A time series analysis of multiple ambient pollutants to investigate the underlying air pollution dynamics and interactions. *Chemosphere*, 134, 571–580. <https://doi.org/10.1016/j.chemosphere.2014.12.007>

V. Education/Outreach
Robert Moreau, PhD
Southeastern Louisiana University,
Turtle Cove Environmental Research Station
Hammond, LA 70402
robert.moreau@selu.edu

Overview

The primary objectives of the Turtle Cove Environmental Research Station are to raise public awareness of the Lake Maurepas Monitoring Project (LMMP) and to ensure all project researchers' needs are met at the Galva Canal Boatshed Complex in Manchac. We proposed to accomplish these objectives in 2023 through expansion of our communication methods, maintaining partnerships with visitors and other organizations, and enhancing our boatshed capabilities. During 2024, our team continued to highlight study findings through our existing education and outreach program, organized a public outreach event through a grant from the National Wildlife Federation (NWF), produced two versions of a project documentary, and developed educational activities with monitoring teams for 2025 which will showcase project field and lab techniques. Turtle Cove staff also assisted researchers with fieldwork, new vessel designs and acquisitions, monitoring buoy logistics, and increased fuel accessibility at the Galva Canal Boatshed. Despite ongoing renovations to the Turtle Cove facility on Pass Manchac, annual visitor numbers increased in 2024. Here, we review our 2024 research, education, and public outreach program data, demonstrate growth in these programs from 2023, and discuss future goals.

Methods

All research, university education, and public outreach events were recorded via shared Google Calendar entries, which included group titles, number of individuals, vessels, and a brief description. These entries were organized by overall category and group type (Table 1), and were used to calculate the annual totals of individuals and user days. User days refers to the number of days a different individual visited or utilized Turtle Cove facilities and resources.

Table 1. Organizational scheme of categories and their associated group types for calendar entries.

Research	University Education	Public Outreach
Turtle Cove	SELU Courses/Lectures	General
SELU Biology Faculty	SELU-Related Field Trips	K-12
Lake Maurepas Monitoring	Outside University Field Trips	Professional Meetings
SELU Interdisciplinary	Workshops	-
Outside Universities	-	-

Any LMMP-related research, university education, or public outreach events were then analyzed separately and compared to overall individual numbers and user days to identify which overall categories and group types received the most project-related information. Additionally, all group types were organized by parish based on the location of a group’s institution or headquarters to visualize the geographic extent of outreach.

Results

Approximately 2,262 individuals and 3,154 user days were recorded in 2024. The research category consisted of 169 individuals over 688 user days; university education consisted of 449 individuals over 710 user days, and; public outreach consisted of 1,644 individuals over 1,756 user days (Figures 1 and 2).

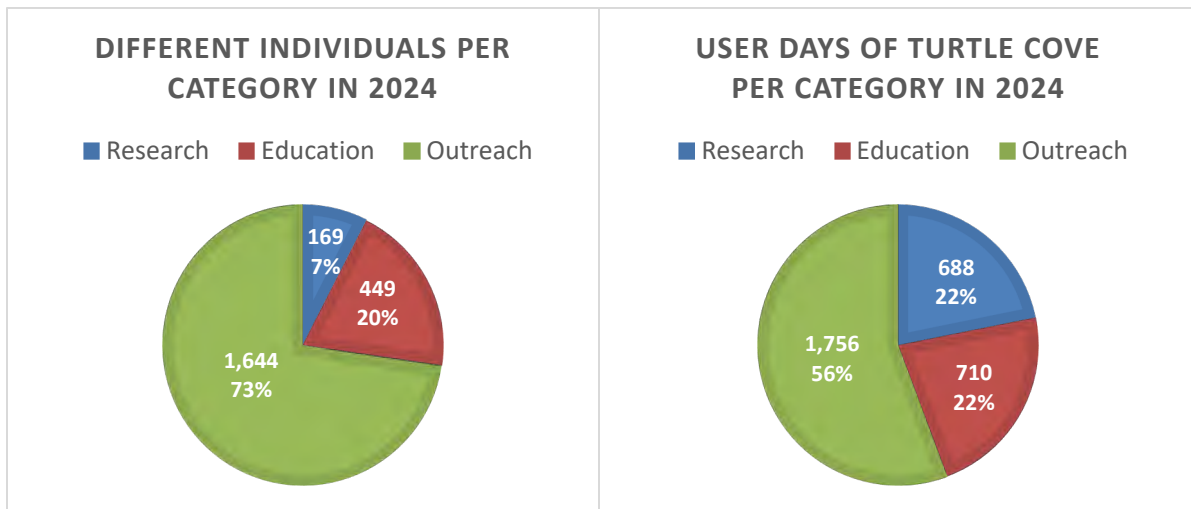


Figure 1. Pie chart showing totals and percentages of different individuals per category in 2024.

Figure 2. Pie chart showing totals and percentages of user days per category in 2024.

LMMP research teams were the highest contributors (74%) to the overall research category, with 58 individuals recording over 506 user days. The overall university education category showed 19 different groups consisting of approximately 300 individuals receiving project-related information through university courses, field trips, and workshops. Additionally, 45 groups consisting of 1,096 individuals recorded under the public outreach category were exposed to the project through community group field trips, K-12 events, and professional meetings. The LMMP university education and public outreach events were attributable to 67% of both overall categories. Southeastern Louisiana University (SELU) courses and K-12 groups contributed the most to these categories, with 184 (61%) individuals and 607 (55%) individuals, respectively (Figures 3 and 4).

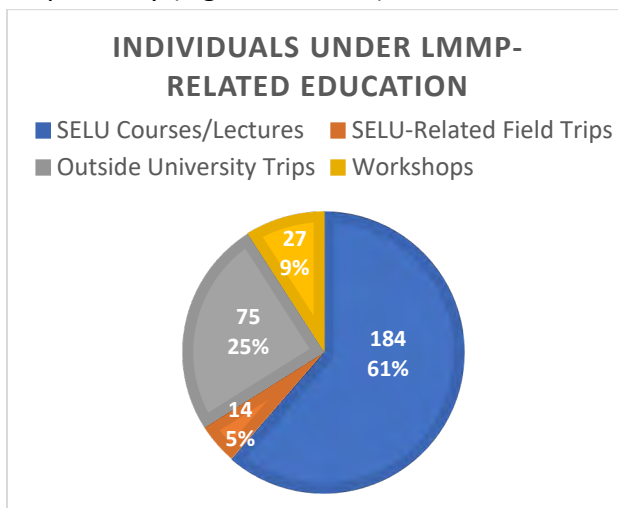


Figure 3. Pie chart showing totals and percentages of individuals recorded under the university education category that received LMMP-related information in 2024.

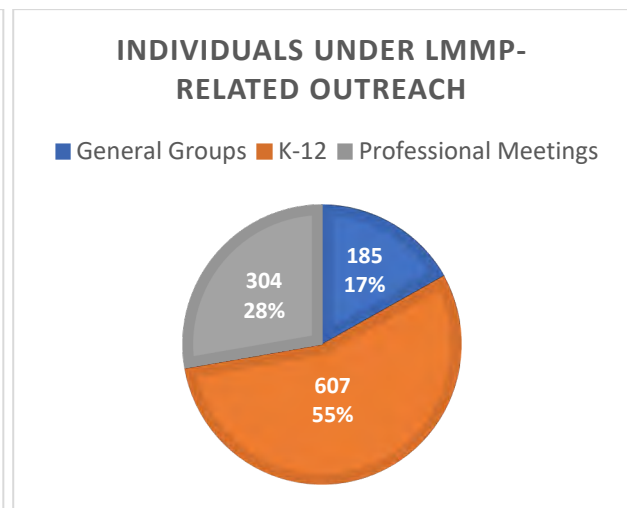


Figure 4. Pie chart showing totals and percentages of individuals recorded under the public outreach category that received LMMP-related information in 2024.

Each LMMP-related category showed an increase in user days from 2023 to 2024 (Figure 5). In total, a 35% increase was calculated across all categories. The research and outreach categories had the highest growth, with approximately 119% and 36% user day increases, respectively.

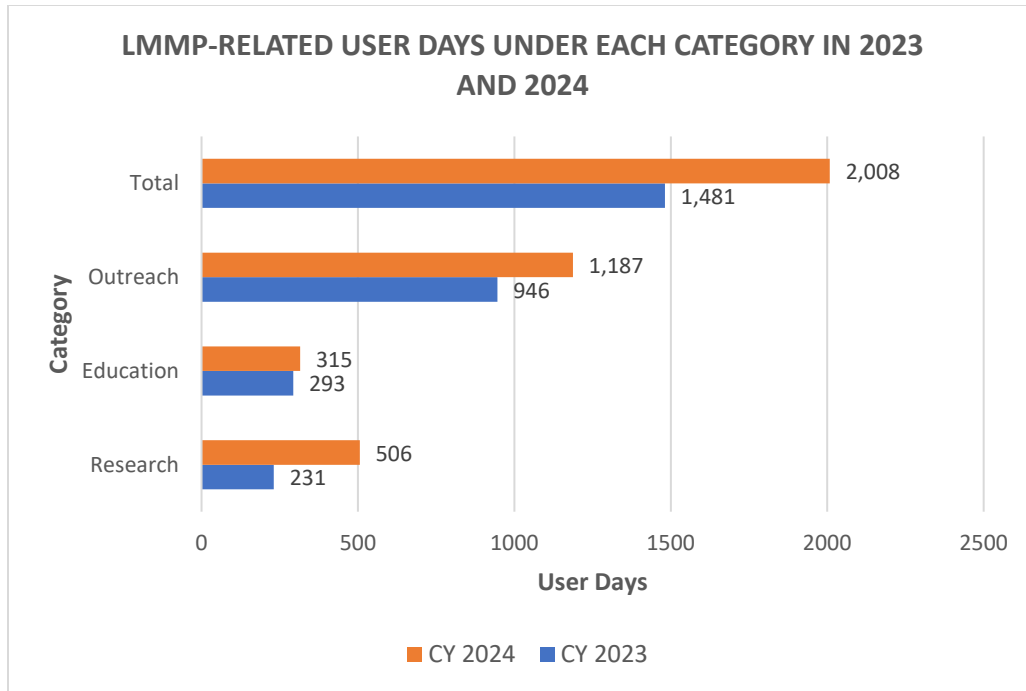


Figure 5. Bar chart showing increases in user days from 2023 to 2024 across each category.

Groups recorded under the university education and public outreach categories that received project information represented approximately eight (8) parishes in Louisiana (Figure 6). Three groups consisting of fewer than 50 individuals from Alabama, Pennsylvania, and Texas were also recorded in 2024.

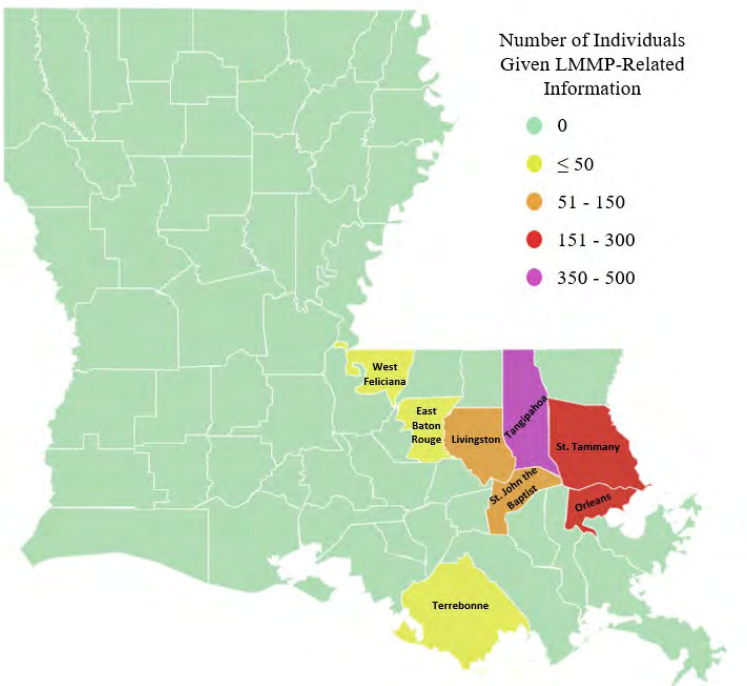


Figure 6. Map showing parishes of origin for university education and public outreach groups that received LMMP information in 2024.

Discussion

The Turtle Cove team met its proposed goals for 2024 and will continue to work toward growing its capabilities in 2025. We provided project-related outreach to 64 groups consisting of 1,396 individuals from 8 parishes and 3 other states. Many of these groups received information through our standard field trips, and some attended events tailored to specifically cover the LMMP, such as the NWF-funded open house event, trips to monitoring buoys, and other lectures led by project director Dr. Kyle Piller at Turtle Cove (Appendix A). Our staff assisted the Wetlands monitoring team with fieldwork and collaborated with them on Coalition to Restore Coastal Louisiana (CRCL) baldcypress tree plantings, which included project discussions with volunteers (Appendix A). Turtle Cove also purchased a 110-gallon fuel tank for the Galva Canal Boatshed, assisted the Aquatics team with funding and acquisition of its landing craft vessel, designed and purchased a mobile hoist (for mainland buoy maintenance/hurricane evacuation storage), and purchased a new motor and accessories for a vessel used by the Wetlands team.

Future Goals

Developing Outreach Events and Expanding Community Engagement Turtle Cove is planning to develop onsite and off-site outreach events with research teams that will offer students and community members opportunities to participate in techniques employed for the LMMP. Specifically, the Aquatics team has proposed to assist Turtle Cove staff with creating events and activities that will showcase trawling, electrofishing, crab trap, and eDNA sampling methods. We also plan to work with the Wetlands team on recruiting volunteers for tree planting events and host another public outreach event similar to the open house in 2025. Additionally, we are awaiting final comments by Air Products officials on two versions (11 and 48 minutes each) of the project documentaries Turtle Cove produced via the Southeastern Channel. These documentaries showcase LMMP researchers' roles as independent monitors and allow for a more multi-media reaching impact on all of our university-community stakeholders, which will greatly increase our outreach capabilities.

Growing the Existing Education and Outreach Program We plan to offer additional field trip options and opportunities for students and community members in 2025, which are expected to bolster visitor numbers. In 2024, we received a grant from the New Orleans Town Gardeners Association for birding-specific outreach. As a result, we will be able to implement and advertise for birding field trips in Manchac via our pontoon boat and canoes. Additionally, we plan to organize a BioBlitz event once repairs to the Turtle Cove facility on Pass Manchac are completed. This event would take place over a few days and allow researchers and volunteers to participate in a biological survey in the Manchac Wildlife Management Area. Turtle Cove will also continue working with the Wetlands team on 2025 CRCL tree plantings.

Galva Canal Boatshed Additions and Improvements Lastly, Turtle Cove will continue to assist researchers with boat designs, maintenance, purchases and logistics. But perhaps most important are our longer-term plans to expand the Galva Canal Boatshed/Classroom Complex with an even larger classroom (proposed for CYs 2026/27), second bathroom and boat launch, and most critically, a 1,000 ft boardwalk that would serve to accommodate education/outreach activities at Galva when inclement weather prohibits use of a boat ride to Turtle Cove. Expansion of the Galva Boatshed facility will greatly improve our ability to provide education and outreach services regardless of marginal weather conditions.

Appendix A

Photograph Log



Photo 1. Dr. Robert Moreau's Tulane and SELU Environmental Management Classes on a Turtle Cove field trip.



Photo 2. NWF-funded LMMP open house event hosted at Middendorff's.



Photo 3. Turtle Cove staff assisting the SELU Wetlands team with fieldwork.



Photo 4. Turtle Cove staff working with the SELU Wetlands team on a CRCL tree planting.